Functional characterisation of natural variants of the hepatitis C virus p7 ion channel protein

Elizabeth Rose Atkins (BA (Hons) Cantab)

Submitted in accordance with the requirements for the degree of Doctor of Philosophy

The University of Leeds
Faculty of Biological Sciences
School of Molecular and Cellular Biology
August 2013

The candidate confirms that the work submitted is her own, except where work which has formed part of jointly authored publications has been included. The contribution of the candidate and the other authors to this work has been explicitly indicated below. The candidate confirms that appropriate credit has been given within the thesis where reference has been made to the work of others.

The chapter within the thesis that has been based on work from jointly-authored publications is chapter 3.

Chapter 3

Li, H., Atkins, E., Bruckner, J., McArdle, S., Qiu, W.C., Thomassen, L.V., Scott, J., Shuhart, M.C., Livingston, S., Townshend-Bulson, L., McMahon, B.J., Harris, M., Griffin, S., & Gretch, D.R. (2012). Genetic and functional heterogeneity of the hepatitis C virus p7 ion channel during natural chronic infection. *Virology*, *423*(1), 30-37.

- Hui Li and others isolated and amplified the patient sequences and performed the sequence analysis in the Gretch lab (University of Washington, Seattle).
- Elizabeth Atkins cloned the p7 sequences into bacterial expression vectors, purified proteins by HPLC and performed liposome assays to measure *in vitro* protein activity.
- Prof. Mark Harris and Dr. Stephen Griffin provided supervision.

Acknowledgements

I would like to thank my supervisors, Mark Harris and Stephen Griffin, for all their help, advice and perseverance. I would also like to thank my tutor Eric Blair for all his support. Particular thanks go to our collaborators in Seattle, Hui Li and David Gretch, and the patients who participated in the original studies, without whom this work would not have been possible.

For their technical and moral support, I would like to thank Iain Manfield for his support with the HPLC, Jon Lippiat for his support with the live-cell imaging and electrophysiology, and Gareth Howell for all his help with microscopy, including building a microscope from spare parts! I also thank Jamel Mankouri and Lucy Freem for their help reviewing the manuscript.

Many thanks also go to my colleagues in the lab; particularly Corine StGelais, Toshana Foster and Laura Wetherill for help/commiserating with the HPLC and liposome work. The rest of you, Carsten, Mair, Lynsey, Cheryl, Barney, Bjorn, Yutaka, Zsofi, Hazel, Doug, Carol, Bruno, Joe, Becky, Hessa, Sian, Diane, Phil, Andy, Sarah and anyone I've missed, you've all been great company. Thanks for all the cake!

I would like to thank all of my friends and family who have supported me throughout, especially my sister Sarah who has been through so much while I was doing this (and I thank her surgeons Mr. Nick Thomas and Mr. Daniel Walsh, and the rest of the neurosurgical team at King's College Hospital for getting her through the last 2 years).

Lastly I would like to thank my flatmate Stephen, whose habit of dressing up in armour made of lino every Sunday and disappearing off to Roundhay Park with his friends to fight monsters with foam weapons, was a welcome reminder that there are stranger things to do than a PhD!

Abstract

The HCV p7 protein is a viroporin that acts to increase endosomal pH to preserve the infectivity of nascent virions. Previous work has identified several key residues in p7 that are critical for its function. A number of compounds have been found to inhibit p7 activity *in vitro* and genotype variation in the p7 sequence is known to have significant effects on p7 inhibitor sensitivity. This study aimed to further our understanding of the role of p7 during HCV infection. The effects of six naturally-occurring p7 variants, within a single genotype, isolated from 5 patients of varying disease severity were investigated.

It was found in *in vitro* liposome assays that the patient polymorphisms caused a wide variation in p7 channel activity. The previously-observed low-pH activation in J4 p7 was also observed in JFH1 p7, but not in H77 p7; this showed a 'V' shaped activation profile, with its lowest activity at pH 6.7 and peak activity at pH 6.2 and 7.4. Four of the patient isolates shared the same activation pattern as H77; two with non-synonymous mutations of S21P and Y31H displaying low-pH activation. In virus, the Y31H mutant was the only Seattle variant to show a significant reduction in the production of infectious virus.

JFH1 intracellular virions have previously been shown to be sensitive to transient exposure to reduced pH, while secreted virions were insensitive to such changes. In this study, it is shown that H77 secreted virions are sensitive to transient reductions in pH, while the Seattle isolate viruses showed reduced pH sensitivity. The Y31H isolate also showed increased sensitivity to the p7 inhibitor rimantadine.

In conclusion, this study found that natural polymorphisms in p7 within a single genotype can cause significant changes in p7 activity. These changes did not show any correlation with the severity of disease in the original patients.

Table of Contents

Table of Figures

List of Tables

Abbreviations:

AmCl – Ammonium chloride

ALT – alanine aminotransferase

APS – Ammonium persulphate

AST – aspartate aminotransferase

ATM – Ataxia telangiectasia mutated, a DNA repair pathway

BLM – Black lipid membrane

CD36 – Cluster of differentiation 36 (also SCARB2)

CD81 – Cluster of differentiation 81 tetraspanin

CF – Carboxyfluorescein

CL2 – Latrophilin 2

CLDN1 – claudin 1

Con1 – Genotype 1B consensus sequence

CQ – Chloroquine

CTL – cytotoxic T-leukocyte

DAPI – 4', 6-diamidino-2-phenylindole

DEPC – diethylpyrocarbonate

DHPC – 1,2-diheptanoyl-*sn*-glycero-3-phosphocholine

DTT – dithiothreitol

ECL – enhanced chemiluminescence

EDTA – ethylenediaminetetraacetic acid

EGFR – epidermal growth factor receptor

ELISA – enzyme-linked immunosorbent assay

EM – Electron microscopy

EMCV - Encephalomyocarditis virus

ER – endoplasmic reticulum

FCCP – Trifluorocarbonylcyanide phenylhydrazone

FFU – Focus forming units

FITC – Fluorescein isothiocyanate

GAG - Glycosaminoglycans

GAPDH – Glutaraldehyde dehydrogenase

GBVA – GB virus A

GBVB – GB virus B

GBVC – GB virus C

GBVD – GB virus D

GT – Genotype

H77 – Genotype 1A full length clone sequence, also H77/JFH1 chimera

HAART – Highly active antiretroviral drug therapy

HCC – Hepatocellular carcinoma

HCV – Hepatitis C virus

HCVpp – Hepatitis C virus pseudoparticles

HDL – High density lipoprotein

HEPES – 4-(2-hydroxyethyl)-1-piperazine ethanesulfonic acid

His-tag – Polyhistidine tag

HMA – Hexamethylene amiloride

HPLC – High performance liquid chromatography

HRP – Horseradish peroxidase

HVR – Hypervariable regions

IAV – Influenza A virus

IDU – Intravenous drug user

IFN – Interferon

IL2 – Interleukin 2

IPTG – Isopropyl β-D-1-thiogalactopyranoside

IRES – Internal ribosome entry site

J4 – Genotype 1B HCV sequence

JFH1 – Japanese fulminant hepatitis 1, genotype 2A

kDa – kiloDalton

LD – Lipid droplet

LDL – Low density lipoprotein

MES – 2-(N-morpholino)ethanesulfonic acid

MSM – Men who have sex with men

*N*NDNJ – *N*-nonyl deoxynojirimycin

*N*NDGJ – *N*-nonyl deoxygalactonojirimycin

OD_{600} – Optical density in a spectrophotometer at 600nm light wavelength

PA – Phosphatidic acid

PAGE – Polyacrylamide gel electrophoresis

PBS – Phosphate buffered saline

PC – Phosphatidylcholine

PFA – Paraformaldehyde

PIPES - Piperazine-N,N′-bis(2-ethanesulfonic acid)

PKR – Protein kinase R

Psi – Pounds per square inch, unit of pressure equivalent to 6.8kPa

PTB – Polypyrimidine tract binding protein

PVDF – Polyvinylidene fluoride

rdPE – Rhodamine-labelled phosphatidylethanolamine

RDRP – RNA-dependent RNA polymerase

Rib - Ribavirin

Rim – Rimantadine

ROI – Region of interest

rpm – Revolutions per minute

SD – Standard deviation from the mean

SDS – Sodium dodecyl sulphate

SEM – Standard error of the mean

SGR – Subgenomic replicon

SP – Signal peptidase

SPR – Surface plasmon resonance

SRBI – Scavenger receptor class B type 1 (also SCARBI)

SVR – Sustained virological response

TBS – Tris-buffered saline

TEMED – Tetramethylethylenediamine

TFA – Trifluoroacetic acid

TLR3 – Toll-like receptor 3

TM – *trans*membrane

TMD – *trans*membrane domain

Tris - Tris(hydroxymethyl)aminomethane

Chapter 1: Introduction

1.1 Viral hepatitis

Viral hepatitis, where a virus primarily infects the liver, can be caused by a number of viruses from different virus families. High numbers of hepatitis cases following blood transfusion were noted after such procedures became common during the 20th century, and the causative agents were sought (Starr, 2000). Most cases are caused by the hepatitis viruses A-E, but it is estimated that up to 20% of cases of viral hepatitis are caused by other agents (Leary *et al.*, 1996).

1.1.1 Hepatitis A

Hepatitis A (HAV) is a non-enveloped virus with a single, positive stranded RNA genome, classified in the *Picornaviridae* family, in the genus *Hepatovirus*. It is transmitted through the faeco-oral route and causes sporadic outbreaks of potentially severe acute hepatitis. The disease typically lasts for 6-8 weeks, with jaundice a common symptom of liver infection. A formalin-inactivated vaccine has significantly reduced the incidence of infection (Martin & Lemon, 2006)

1.1.2 Hepatitis B

Hepatitis B virus (HBV) is a DNA virus of the family *Hepadnaviridae* that can cause a chronic infection of the liver. Transmission of the virus occurs through blood and bodily fluids. Prior to routine screening of blood donations, HBV accounted for a large proportion of cases of post-transfusion hepatitis. In most adult cases, HBV causes an acute infection, with a 1% risk of developing fulminant hepatitis and a 25% risk of developing a chronic infection. Acute HBV infection is slower to progress than HAV, is typically non-cytopathic and shows relatively mild symptoms. Chronic HBV has a risk of long-term liver damage that can cause cirrhosis or hepatocellular carcinoma (Hollinger & Liang, 2001). The virus coat proteins are capable of forming empty virus particles; this property allowed the development of a vaccine based on self-assembled empty particles. Routine vaccination of children against HBV is now performed in over

160 countries, and the incidence rates of acute HBV in the USA fell by 85% between 1990 and 2006 (Liaw & Chu, 2009).

1.1.3 Hepatitis delta virus

Hepatitis delta virus (HDV) is a satellite virus of HBV of the genus *Deltavirus*, with a single stranded negative-sense RNA genome that produces sufficient proteins to replicate the genome and form a viral capsid. HDV requires the envelope glycoproteins from HBV to produce infectious virus particles. The progression of HDV infection is similar to HBV, with transmission via blood and bodily fluids. Patients chronically infected with both HBV and HDV show more rapid progression of liver disease (Polish *et al.*, 1993).

1.1.4 Hepatitis E

Hepatitis E virus (HEV), like HAV, is a small, non-enveloped single-stranded positive sense RNA virus transmitted via the faeco-oral route. It was previously classified in the *Calicivirus* family, but has since been reclassified into the new *Hepevirus* family. HEV is endemic in southeast and central Asia, where it is transmitted through contaminated water. Development of a chronic HEV infection is extremely rare and most acute infections are self-resolving. HEV has an approximate mortality rate of 1%, but this increases in certain at-risk groups including pregnant women (Krawczynski, 1993).

1.1.5 Hepatitis G

Hepatitis G virus (HGV), also known as GB virus C (GBVC), has been classified among the *Flaviridae* family and can chronically infect humans through blood products, vertical transmission and sexual contact. It is a close relative of HCV with ~30% sequence homology and infects hepatocytes, but shows no known pathogenic effects (Stapleton *et al.*, 2004). It is related to GB virus A, one of two viruses (GBVA

and GBVB) originally identified from a patient with acute viral hepatitis after the patient sera was passaged in tamarins.

1.2 Hepatitis C virus

1.2.1 Discovery

Blood transfusion was developed in the early 20th century, and the Second World War saw a large increase in the use of blood products. With this expansion in usage, there was a notable incidence of hepatitis in patients following transfusion (Starr, 2000). Hepatitis A and B were identified and screening methods were developed to prevent contamination of the blood supply, but a third cause was known to exist that could not be identified; this was named chronic non-A non-B hepatitis (Tobler & Busch, 1997). A partial genome of HCV was isolated by the Chiron Corporation in 1989 (Choo *et al.*, 1989). From this partial genome many of the viral proteins were identified, and antigens expressed that allowed the development of an enzyme-linked immunosorbent assay for virus detection (ELISA). This test was used to screen blood donations from 1990 onwards (Tobler & Busch, 1997).

1.2.2 Global prevalence and distribution of HCV

The WHO estimates that the worldwide prevalence of HCV is 3% of the total population. There are seven major genotypes of HCV, with various subtypes, and an uneven geographical distribution (Negro & Alberti, 2011; Lavanchy, 2009). Fig 1.1 shows the genotype distribution and estimated prevalence in each country, where known. Genotype 1A (GT1A) is the most prevalent strain in North America and Europe, followed by GT 1B. GT 2A and 2B are distributed worldwide, but are most prevalent in Japan and northern Italy. GT 3 is the most common strain in the Indian subcontinent. GT 4 is the most common genotype in Africa and the Middle East, and has a high degree of genetic diversity. GTs 5 and 6 are rare, and found in limited

geographical areas: mainly South Africa and the Hong Kong area respectively (Hoofnagle, 2002).

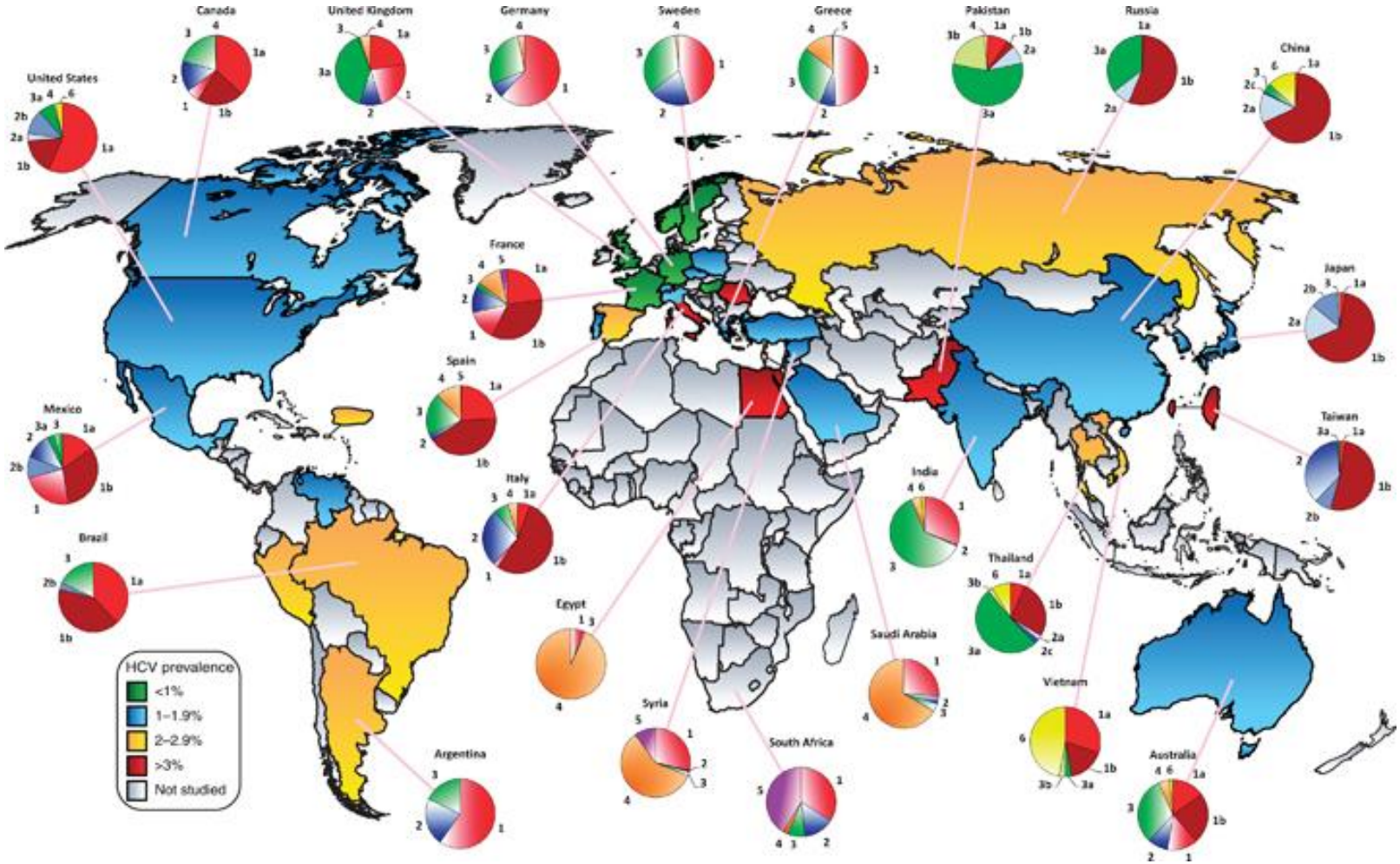

Figure 1.1 Global prevalence and genotype distribution of HCV

HCV prevalence by country is shown where known. Green = below 1% prevalence, blue = 1-1.9%, yellow = 2-2.9%, red = greater than 3%, grey = unknown. Genotype distribution by country is shown in pie charts. Taken from Negro and Alberti, 2011

1.2.3 Transmission, progression and treatment of HCV

1.2.3.1 Transmission

HCV is transmitted through contact with infected blood. In the developed world, the most common risk factor for HCV infection is intravenous drug use (IDU), which is responsible for over 50% of cases. Prevalence of HCV among intravenous drug users can be as high as 60%, with the largest risk factor being the length of time the individual has been injecting drugs (Hope *et al.*, 2001). Whilst the sharing of syringes has declined due to increased awareness of the risk of HIV, HCV may also be transmitted through the shared use of drug preparation equipment, and transmission via intranasal inhalation of cocaine using shared straws has been documented (Clarke & Kulasegaram, 2006).

Historically, blood transfusions were responsible for the majority of HCV cases. Screening of blood donations was initiated as soon as testing was made available in 1990, and transmission via this route has been almost completely eliminated. Transmission to or from healthcare workers via sharp injuries or mucous membrane splash injuries has been well documented, and the risk of infection from a single percutaneous exposure is estimated to be 1.8%. As well as infected blood products, iatrogenic transmission has also been documented from medical devices such as endoscopes (Clarke & Kulasegaram, 2006). In the developing world, safe procedures may not always be followed due to a lack of resources and needles, surgical tools and other equipment may be reused multiple times, increasing the risk of transmission (Shepard *et al.*, 2005). Egypt has the highest known rate of HCV infection in the world as a result of inadequate sterilisation of equipment during treatment for the parasite schistosomiasis during the second half of the 20th century (Strickland *et al.*, 2002).

Tattooing is another potential risk factor, but the increased awareness of HIV has resulted in needles and other paraphernalia no longer being reused between clients,

and thus professional tattooing carries no increased risk of HCV. Non-professional tattooing, especially that carried out in prisons, does carry an increased risk of HCV (Tohme & Holmberg, 2012).

Sexual transmission of HCV is extremely rare, with almost no transmissions documented in discordant heterosexual couples (where one partner is infected and the other is not) (Vandelli *et al.*, 2004). A marginal increase in risk for those with multiple sexual partners has been suggested, but may be attributed to other risk-associated behaviour, including drug use. The only factor significantly known to enhance the risk of sexual transmission is HIV infection, which increases the risk for both HIV+ heterosexual women and HIV+ men who have sex with men (MSM). The statistics on sexual transmission may be complicated by the reliance on self-reporting of intravenous drug use as well as sexual behaviour; one Italian study of discordant heterosexual couples that documented transmission later found that this was due to the sharing of needles between the couple rather than sexual transmission (Tohme & Holmberg, 2010).

Vertical transmission of HCV from mother to child during birth occurs in less than 10% of cases in HIV-negative mothers, which rises in cases of HIV co-infection. A major risk factor for both groups is the level of HCV viraemia, with almost all transmissions occurring in mothers with viraemia levels greater than 10^6 copies per ml (Thomas *et al*., 1998b). HIV+ mothers typically had higher levels of HCV viraemia which may account for some of the increase rate of vertical transmission, but there is still a higher risk of transmission in HIV+ mothers even when HCV viraemia levels are taken into account (Pappalardo, 2003).

Other possible transmission routes have been documented in case studies, but these are likely to be extremely rare. They include traditional shaving techniques, tick bites,

shared use of toothbrushes and biting between children (Clarke & Kulasegaram, 2006).

1.2.3.2 Acute infection

Acute HCV infection has few symptoms, with those reported being mild, such as fatigue (Merican *et al.*, 1993), and often passing entirely undetected. Work in chimpanzees, and the few detected cases of early infections in humans, has found that HCV RNA becomes detectable within days of infection accompanied by up to a 10-fold increase in serum levels of liver aminotransferase enzymes (Hoofnagle, 2002), but seroconversion can take up to 12 weeks (Maheshwari *et al.*, 2008). Clearance of the virus without seroconversion has been documented (Post *et al.*, 2004). At the end of the acute phase of infection, viral RNA drops to very low levels and either becomes undetectable in the case of viral clearance, or a chronic infection develops where the RNA levels increase once again, although typically to a much lower level than during acute infection (Mondelli *et al.*, 2005).

Rarely, acute infection may result in potentially life-threatening fulminant hepatitis. It is of note that the laboratory strain of HCV, Japanese Fulminant Hepatitis 1 (JFH1), originated from a case of fulminant hepatitis in Japan (Wakita *et al.*, 2005).

1.2.3.3 Chronic infection

In approximately 85% of cases HCV will develop into a chronic infection and, once established, spontaneous clearance of the chronic infection is rare (Yokosuka *et al.*, 1999). The initial immune response to the acute infection will generally be effective at reducing the viral load but, as chronic infection becomes established, viral loads increase, although typically to lower levels than usually observed during initial acute infection. HCV infection is largely asymptomatic, with many infections going undetected until the development of liver disease. Analysis of patient data has shown that the risk of developing cirrhosis within 20 years of infection is 10-20% (Seeff,

2002). The viral load and genotype have been shown not to correlate with the level of liver disease, with one exception; genotype 3 HCV displays increased progression to hepatocellular carcinoma (HCC) (Nkontchou *et al.*, 2011).

1.2.3.4 HIV co-infection

The prevalence of HIV and HCV co-infection is linked to blood-borne transmission, with an estimated population of 4-5 million co-infected out of an estimated total of 33.4 million with chronic HCV (Alter, 2006). Those co-infected with HIV often show higher viral titres and are more likely to develop cirrhosis or HCC (Giordano *et al.*, 2004; Soto *et al.*, 1997). Rates of vertical transmission are also increased with HIV co-infection (Pappalardo, 2003). Even with the immunosuppressive effect of HIV infection, some cases of spontaneous clearance of HCV are still observed (Vogel & Rockstroh, 2010). Quasispecies variation in HCV within patients is also reduced when patients are co-infected with HIV, possibly as a result of the reduced selection from the immune system with the overall reduction in immune response due to HIV (Li *et al.*, 2011).

1.2.3.5 Disease progression and pathology

It is thought that the role of HCV in liver pathology is indirect as there is no correlation between viral load and the severity of the disease, with pathology resulting from damage to the liver rather than any direct cytopathic effect of the virus. The only directly cytopathic effect shown for the virus is an association between liver steatosis and GT3 (Kumar *et al.*, 2002). Liver fibrosis is reversible and may recede if HCV treatment achieves a sustained virological response (SVR), but cirrhosis is irreversible. Once the liver has become cirrhotic, it is classified as either compensated, where the liver remains functional; or decompensated, where liver function is impaired. HCC is a rare outcome of HCV infection, but represents a significant healthcare burden.

The link between HCV and HCC is not clear, but some viral proteins have been shown to interact with cellular factors that prevent apoptosis and promote oncogenic signalling, and this may increase the risk of HCC development.

The more advanced the stage of fibrosis, the less likely that treatment will effectively clear the virus. Liver damage as a result of HCV infection is currently the leading cause for liver transplantation in North America and Europe, and thus represents a significant healthcare burden (Keeffe, 2001).

Liver transplantation remains the only option for advanced liver failure caused by HCV. Newly transplanted livers are rapidly re-infected with HCV from reservoirs elsewhere in the body, and the immunosuppression required for transplantation makes clearance of the virus with drug treatment unlikely. Trials are currently underway with newly developed drugs in transplant patients.

1.2.3.6 Diagnosis

HCV is not routinely tested for in the general population, but risk factors such as having been a recipient of blood products prior to the introduction of screening and having been an IDU indicate populations likely to require testing. There are two methods for detecting HCV infection: serological tests detecting the presence of antibodies to the virus, and nucleic acid detection methods that can determine the presence and number of viral RNA genome copies (Krajden, 2000). The serological tests, based on ELISA technology, are dependent on seroconversion. If the person was infected too recently to have seroconverted, or is immunocompromised or immunosuppressed, then this test may generate false negative results. The nucleic acid detection methods, based on RT-PCR technology for the qualitative tests and Q-RT-PCR for the quantitative tests were, until recently, less sensitive than the serological methods but have now equalled them (Ghany *et al.*, 2009). The quantitative methods can be used during on-going treatment to assess the level of

viraemia by measuring the number of infectious units (IUs) in the blood, and can be used to determine if treatment has achieved an SVR. The serological tests, combined with the nucleic acid tests, can be used to determine if the patient is infected with HCV. A positive antibody but negative nucleic acid test can show that the patient was infected but has managed to clear the virus, and a negative serology test with a positive nucleic acid test suggests a patient may only recently have been exposed to the virus and has not yet generated a serological response, or is immunocompromised (Ghany *et al.*, 2009).

1.2.3.7 Treatment

Until recently, treatment of HCV was limited to dual therapy with pegylated interferon (IFN), a cytokine that stimulates the anti-viral response, and ribavirin (Rib), a broad-spectrum nucleoside-analogue anti-viral discovered during screening of nucleoside analogue compounds for activity against viruses (Lau *et al.*, 2002). The treatment is successful if an SVR is achieved where the immune system is able to clear the virus and no virus is detectable by RT-PCR during and after treatment. The efficacy of this therapy varies by genotype. Genotype 1 is the least responsive with an SVR obtained in less than 50% of patients after 48 weeks of drug therapy (Pawlotsky, 2006). The efficacy of the treatment is also affected by the length of time the patient was infected prior to treatment, with those with more advanced liver pathology showing a reduced response to treatment. A number of side effects, such as fatigue and nausea, can additionally lead to early discontinuation of treatment prior to achieving an SVR; this can be particularly problematic among more vulnerable populations such as IDUs.

Two newly developed anti-virals, boceprevir and telapravir, act by inhibiting the viral protease NS3/NS4A. These drugs have been included in the IFN/Rib treatment regimen. Data from clinical trials displayed an improvement in the SVR in patients with genotype 1 HCV from 48% for those on IFN/Rib alone to 70% with telaprevir triple therapy. Boceprevir showed an improvement from an SVR of 40% with standard

IFN/Rib treatment to 67% with boceprevir triple therapy (Poordad *et al.*, 2011). However, both drugs were associated with an increase in the number of reported side effects and showed higher treatment dropout rates compared with standard IFN/Rib therapy (Jacobson *et al.*, 2011; Poordad *et al.*, 2011).

Resistance mutations were also observed during the trial phases, particularly where the drugs were tested as single treatments rather than as triple therapy with IFN/Rib. These resistance mutations were found to still exist in the quasispecies pool several years after protease inhibitor monotherapy, indicating that these mutations do not cause significant impairment of the virus (Susser *et al.*, 2011).

There are also a number of direct-acting antivirals targeted at other HCV proteins currently undergoing clinical trials. These include BMS-790052, a replication-complex inhibitor that acts to inhibit viral replication via a currently unknown mechanism (Gao *et al.*, 2010), and a number of replication inhibitors targeting NS5B, the RNA-dependent RNA polymerase (RdRp) (Legrand-Abravanel *et al.*, 2010).

1.3 Viroporins

1.3.1 Viroporins - a varied group of virus proteins that form channels in membranes

Viroporins are a diverse group of proteins found in many different virus families, including both RNA and DNA viruses, which act to increase membrane permeability. They are small proteins, ranging in size from approximately 60-100 residues. There is poor sequence homology between viroporins from different virus families, but they do share some biochemical and functional characteristics: at least one hydrophobic domain allowing close association with or insertion into membranes. Many viroporins form SDS-resistant oligomers, with structural analysis confirming the homo-oligomerisation into channels. Some viroporins have been shown to be able to substitute or trans-complement one another, but in many cases the additional roles the proteins may have in the virus life-cycle, often mediated by extramembrane domains, may not allow one viroporin to substitute for another. For example, the cytoplasmic domain of influenza A M2 is dispensable for channel formation and function but contains an amphipathic helix that mediates membrane scission of the budding virion (Rossman *et al.*, 2010).

Whilst some viroporins regulate pH in intracellular compartments; some release intracellular calcium ions from storage; and others, primarily those of non-enveloped viruses, disrupt the plasma membrane in order to aid cell lysis and virus release. A classification system for viroporins was recently proposed, shown in Fig. 1.2, classifying the proteins on the basis of the number of membrane-spanning domains and orientation of the protein (Nieva *et al.*, 2012).

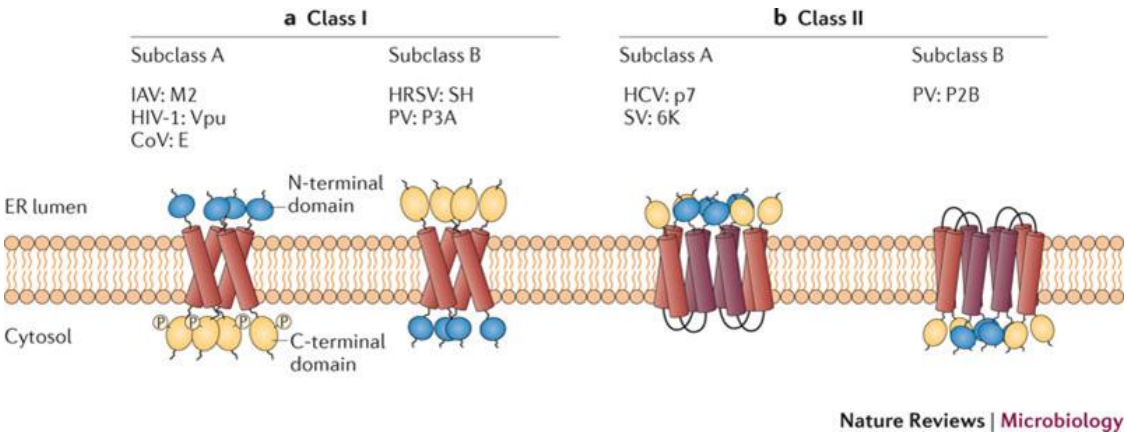

Figure 1.2 Proposed viroporin classification system

Panel (a): Class I viroporins have a single membrane-spanning domain. The A and B subclasses contain proteins that are inserted into the membrane with either a lumenal amino terminus and cytosolic carboxyl terminus (class IA) or a cytosolic amino terminus and lumenal carboxyl terminus (class IB). In addition, class IA members are usually phosphorylated at the C terminus. Known viroporins of each subclass are shown. Panel (b): Class II viroporins form helix–turn–helix hairpin motifs that span the membrane. Subclass A members have lumenal N and C termini, whereas members of subclass B have cytosolic N and C termini. Known viroporins of each subclass are shown. CoV, coronavirus; HCV, hepatitis C virus; HRSV, human respiratory syncytial virus; IAV, influenza A virus; PV, poliovirus. Taken from Nieva *et al*, 2012.

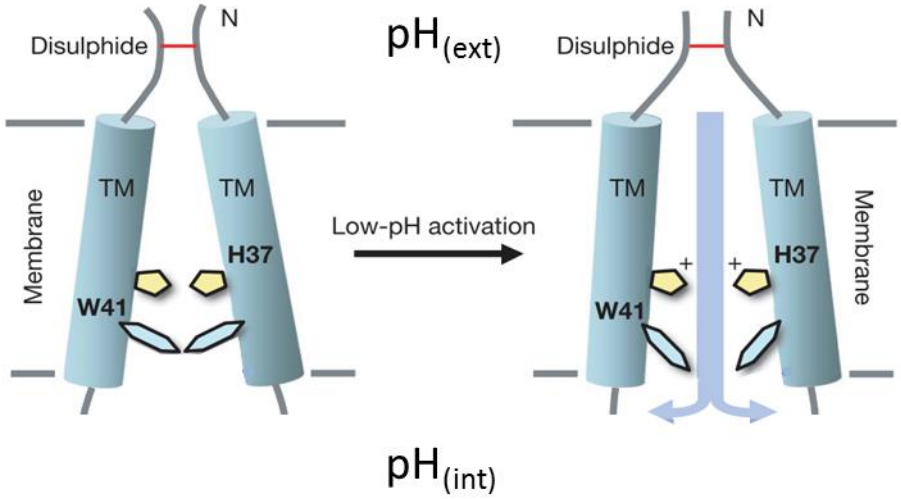

Figure 1.3 IAV M2 gating mechanism

Cartoon of the gating mechanism of IAV M2, depicting two of the 4 TMDs as cylinders with side-chains shown for His37 and Trp41. Protonation of His37 due to a decrease in $pH_{(ext)}$ results in a conformational change in Trp41 that opens the channel and allows proton influx. Adapted from Schnell and Chou, 2008.

1.3.2 Influenza A M2 protein

IAV M2 is a 97-residue integral membrane protein that forms tetramers (Sugrue & Hay, 1991; Lamb *et al.*, 1985), is incorporated into the virion (Zebedee & Lamb, 1988) and has roles in assembly, egress and entry of the virus (Pinto & Lamb, 2006). It has a 23-residue ectodomain, a single *trans*membrane span of 19 residues and a cytoplasmic domain of 55 residues. M2 is expressed abundantly in the cell, with a large proportion of the expressed protein found at the plasma membrane (Lamb *et al.*, 1985). It is also found in other cellular lipid fractions associated with the virus glycoproteins haemagglutinin (HA) and neuraminidase (NA) (Lamb *et al.*, 1985).

The ectodomain is required for incorporation of the protein into the virion (Park *et al.*, 1998), and is exposed at the plasma membrane where binding by monoclonal antibodies restricts the number of infectious virus particles produced (Zebedee & Lamb, 1988). The highly-conserved cytoplasmic domain interacts with the M1 protein during virus particle formation (McCown & Pekosz, 2006). An amphipathic helix in the cytoplasmic domain of M2 has been shown to mediate membrane scission at the neck of the budding virion independently of the ESCRT pathway (Rossman *et al.*, 2010), by inducing membrane curvature (Wang *et al.*, 2012). Both the ectodomain and the cytoplasmic domain show post-translational modifications, with the ectodomain having a disulphide linkage and the cytoplasmic domain palmitoylation and phosphorylation sites. However, none of these modifications significantly affect the ion channel activity of the protein (Holsinger *et al.*, 1995) and none are absolutely required for viral replication. Mutational analysis has shown that the loss of palmitoylation reduces virulence but does not stop virus replication (Grantham *et al.*, 2009), phosphorylation of the cytoplasmic domain is not required for virus infectivity (Thomas *et al.*, 1998a), and the disulphide bonds stabilise M2 but do not affect the replication of the virus either *in vitro* or in animal studies (Castrucci *et al.*, 1997).

The *trans*membrane region of M2 mediates the proton channel activity of the protein, with the minimal truncation of the protein that is still able to form a fully functioning and selective ion channel comprising residues 22-61 (Ma *et al.*, 2009). The proton channel activity of M2 is required at two stages of the virus life cycle. Firstly, it is required during trafficking of HA and NA through the trans-Golgi to prevent endosomal acidification that would cause the HA to undergo a conformational change to the low-pH conformation, which renders the protein unable to mediate membrane fusion during virus entry. Secondly, during virus entry, once the virion has endocytosed into the cell, M2 allows the influx of protons from the acidifying endosome into the virion, destabilising the capsid and allowing the virus to uncoat (Pinto & Lamb, 2006).

The structure of the M2 proton channel has been characterised using X-ray crystallography and NMR techniques. The channel has been shown to have 3 constriction points: valine 27 (V27), histidine 37 (H37) and tryptophan 41 (W41). At neutral pH in solid-state NMR using the TM domain in a cholesterol-rich virus mimetic membrane, the 4 lumenal histidine side groups form a π-stacked ring that breaks the 'water-wire' through the channel lumen.

A cartoon of the IAV M2 gating mechanism is shown in Fig. 1.3. H37 has been shown to act as the proton sensor that mediates both the opening and the proton selectivity of the channel, as mutation of this residue to either glycine or glutamic acid in *Xenopus laevis* oocytes showed channel conductance that was unresponsive to changes in pH, and the H37E mutation was also able to conduct chloride ions (Wang *et al.*, 1995). Solid-state NMR of the TM domain has shown that protonation of a minimum of 2 of the 4 histidine side chains causes the imidazolium groups to repel each other, causing backbone rearrangements that open the pore of the channel and allow the formation of a continuous H-bonded 'water-wire' through the lumen of the channel that allows the transport of protons (Hu *et al.*, 2010). Rather than allowing free flow of aqueous material through the channel, protons may be conducted through

the channel by means of a shuttling exchange across the lumenal protonated histidine residue (Acharya *et al.*, 2010), by ring-flip assisted imidazole deprotonation as the transport mechanism (Hu *et al.*, 2010). This shuttling exchange model explains the high proton selectivity of the channel, and the only other ions to show even partial conductance are, like protons, monovalent cations. W41 acts as a gate, blocking the passage of ions through the lumen of the channel. It interacts with protonated H37 by means of cation-π associations between the imidazole and indole side-groups, and solid state NMR has shown that W41 has increased torsional fluctuations when H37 is protonated at low pH suggesting it is allowing the passage of protons by rotating the indole sidegroup (Williams *et al.*, 2013).

When H37 is unprotonated, W41 forms a gate that blocks entry to the channel from that end, mediating the directionality of proton transport. When pH_{out} is low, the solution has access to H37 and the reduced pH in the water pocket can allow protonation and opening of the channel (Fig. 1.3). With W41 blocking pH_{int}, the reduction of pH on that side of the membrane does not reach H37 in the lumen of the pore due to the blocking effect of the 4 indole rings.

The adamantane drugs amantadine and rimantadine were used to treat IAV infections (Wingfield *et al.*, 1969), and resistance mutations identified M2 as the viral protein affected (Hay *et al.*, 1985). Resistance mutations can arise within 5-7 days of adamantane treatment, mapping to the *trans*membrane region of the protein, and are single nucleotide changes leading to an amino acid substitution at any of 4 sites: residues 26, 27, 30, and 31 (Suzuki *et al.*, 2003). Many influenza strains developed resistance following monotherapy with these drugs (Weinstock & Zuccotti, 2006), and the majority of circulating influenza A strains, including the recent H1N1 swine pandemic, are now resistant (Wang *et al.*, 2009). Structural analysis of amantadine has identified two possible binding sites for the drug: in the lumen of the pore directly blocking the passage of protons through the channel (Stouffer *et al.*, 2008), or on the

lipid side of the channel preventing the structural rearrangements that lead to channel opening (Schnell & Chou, 2008). Further work has identified both arrangements as being possible, but with the pore-binding model showing a higher binding affinity than the lipid-side binding, measured by surface plasmon resonance (SPR) (Rosenberg & Casarotto, 2010).

1.3.3 HIV Vpu protein

HIV Vpu is a 16 kDa, 81-residue integral membrane phosphoprotein that is conserved among HIV1 strains but is not present in HIV2 (Cohen *et al.*, 1988; Strebel *et al.*, 1988). It has a short ectoplasmic domain, an uncleaved leader domain that acts as a *trans*membrane anchor and a longer cytoplasmic domain (Maldarelli *et al.*, 1993). Unlike IAV M2 it is not present in the virion, but it does have two major roles in the virus life cycle. Firstly, it aids the virus in immune evasion by causing the rapid degradation of CD4, a role which is dependent on the phosphorylation of the C-terminal cytoplasmic domain (Paul & Jabbar, 1997), downregulating the expression of MHC class I (Kerkau *et al.*, 1997) and also inhibiting NFκB activation (Bour *et al.*, 2001; Akari *et al.*, 2001). The second major role of Vpu in the virus lifecycle is to improve the efficiency of virus budding (Terwilliger *et al.*, 1989). These two major functions are performed by different domains of the protein. Mutational analysis that scrambled the TM domain but left the cytoplasmic domain intact found that the cytoplasmic domain was responsible for the immune modulations, while truncation analysis found that the TM domain alone enhanced virion release (Schubert *et al.*, 1996). While the C-terminal cytoplasmic domain is not required for oligomerisation of the TM domain, it has been found to stabilise the protein (Ma *et al.*, 2002). Molecular modelling has identified the likely oligomer as a pentamer formed of left-handed helical bundles (Kukol & Arkin, 1999). Structural data has shown a pore structure with a water-filled pore restricted by tryptophan residues at position 22, with serine residues lining the base of the pore (Montal, 2003).

The TM domain of Vpu was found to have ion channel activity in several systems: artificial lipid membranes (Ewart *et al.*, 1996), an *E. coli* permeability assay (Gonzalez & Carrasco, 1998) and in *Xenopus laevis* oocytes (Schubert & Ferrer-Montiel, 1996). The oocyte experiments also identified the channel as being selective for monovalent cations (Schubert & Ferrer-Montiel, 1996). Of the previously-used viroporin inhibitors, it was found that amiloride derivatives, but not amiloride itself or amantadine, were effective at reducing the conductance of the channel *in vitro*, as well as reducing the efficiency of virus budding (Lemaitre *et al.*, 2004; Ewart *et al.*, 2002)

1.3.4 Respiratory syncytial virus SH protein

Human respiratory syncytial virus (hRSV) causes pneumonia in infants. The small hydrophobic (SH) protein is a 64-residue protein with a hydrophobic stretch sufficient for a single span across a membrane. It is redundant for replication of the virus in tissue culture (Bukreyev *et al.*, 1997) but in animal models, including chimpanzees, its deletion results in reduced viral titres (Jin *et al.*, 2000; Whitehead *et al.*, 1999). It has been shown to form pentamers in detergent micelles, with the TM domain forming an α-helix (Gan *et al.*, 2012), and EM visualisation of SH oligomers in membranes found structures consistent with pentamers or hexamers (Carter *et al.*, 2010).

The hypothesised role of the SH protein in the virus lifecycle may be to inhibit TNFα signalling (Fuentes *et al.*, 2007), but it has also been shown to have viroporin activity in black lipid membranes, bacterial permeability assays and liposome assays (Carter *et al.*, 2010; Gan *et al.*, 2008; Perez *et al.*, 1997). The TM domain alone was shown to be selective for monovalent cations, and showed low-pH activation (Gan *et al.*, 2008). Mutation of two histidine residues in SH, one in the TM domain (H22) and one in the C-terminus (H51), found that mutation of both abrogated pH activation, but single mutations of each to alanine still showed some increased activity in response to reduced pH (Gan *et al.*, 2012). There is also a tryptophan at position 15 that has been

suggested to interact with H22 to mediate the pH gating in a manner similar to IAV M2, but this has yet to be investigated further (Carter *et al.*, 2010).

1.3.5 Enterovirus 2B protein

The 2B protein is found in all members of the *enteroviridae* virus family, including poliovirus. It is an approximately 97 residue protein that localises primarily to the ER and Golgi, with a smaller fraction going to the plasma membrane and mitochondria (Madan *et al.*, 2008; de Jong *et al.*, 2003; van Kuppeveld *et al.*, 1997; Sandoval & Carrasco, 1997). Poliovirus 2B has two hydrophobic domains (Agirre *et al.*, 2002), HR1 and HR2, of which the first forms a cationic amphipathic α-helix. Mutation of HR1 has been shown to prevent 2B-induced membrane permeabilisation (Barco & Carrasco, 1998; van Kuppeveld *et al.*, 1997; Aldabe *et al.*, 1996). This membrane permeabilisation is required by the virus for virion release and RNA replication (Van Kuppeveld *et al.*, 1996). The second hydrophobic domain has been shown to stabilise the tetramer via inter-helix interactions. These domains have been shown to fold into α-helices that fold to form a hairpin structure (Martínez-Gil *et al.*, 2011).

Expression of enterovirus 2B has been shown to permeabilise the plasma membrane to allow the usually non-permeant molecule hygromycin B to enter both bacterial and mammalian cells (Aldabe *et al.*, 1996; Lama & Carrasco, 1992). HR2 has tryptophan residues that have been shown to be important for membrane permeability, and may potentially have a role in gating the channel (de Jong *et al.*, 2004).

As part of its uncleaved precursor 2BC, 2B causes the accumulation of vesicles to form replication complexes. Mutation of the loop residues between HR1 and HR2 has been shown to reduce replication of the virus, but does not affect 2B oligomerisation or its ability to permeabilise membranes (de Jong *et al.*, 2004).

1.3.6 Human papillomavirus E5 protein

HPV is a non-enveloped DNA virus with many different strains, and the majority of research has focused on the cancer-causing strains, such as HPV16. The E5 protein of HPV16 is a highly hydrophobic 83-residue protein (Halbert & Galloway, 1988) with a predicted membrane topology of an N-terminus in the ER lumen and C terminus in the cytoplasm, with the hydrophobic part of the protein forming 3 *trans*membrane spans (Krawczyk *et al.*, 2010). It has been shown to be present as a dimer in cervical tissue samples (Kell *et al.*, 1994), and analysis of truncation mutants showed that the hydrophobic regions of the protein were able to interact to form oligomers (Gieswein *et al.*, 2003). E5 localises to the ER, early endosomes, lysosomes and the perinuclear region (Lewis *et al.*, 2008), with overexpression studies often showing a localisation to the Golgi as an artefact.

E5 has been shown to prevent endosomal acidification, a function not necessarily mediated by viroporin activity: E5 has been shown to directly interact with vATPase and thus may be inhibiting the acidification by blocking its function (Straight *et al.*, 1995). The hypothesised role for this is to prevent dissociation of EGFR from its ligand during EGFR trafficking through the acidic late-endosome to lysosome compartments, thus enhancing EGFR signalling, but this is controversial (Suprynowicz *et al*., 2010).

The viroporin activity of E5 was shown in liposome dye-release assays, and it was also shown to form pore structures by electron microscopy (Wetherill *et al.*, 2012). This channel does not show any change in activity in response to changes in pH, and lacks any protonatable histidine residues in the channel lumen. Thus, the primary function of E5 is not thought to be proton conductance but rather release of intracellular calcium stores, thought to be important for some aspects of the virus life cycle.

1.3.7 Alphavirus 6k protein

Alphavirus 6k, present in all members of the alphavirus genus, is a 60-residue protein with a single *trans*membrane span (Melton *et al*., 2002). Low sequence homology in 6k between different members of the genus renders it specific to each virus, as substitution of 6k between viruses abrogates infectivity. It colocalises with the envelope spike proteins in the ER and plasma membrane (Schlesinger *et al.*, 1993), and an acylated form of the protein is present in the virion (Lusa *et al.*, 1991).

6K has been shown not to be required for genome replication, particle formation or the transport of glycoproteins to the plasma membrane (Loewy *et al.*, 1995), but appears to have a role in budding of the virus as 6k-deficient viruses show reduced virus budding (Liljeström *et al.*, 1991). Its role may be to maintain the correct folding of glycoproteins required for budding (Yao *et al.*, 1996).

The viroporin activity of 6k was first shown by an *E. coli* permeabilisation assay (Sanz *et al.*, 1994). Bacterially expressed protein in planar lipid bilayers was shown to have a preference for the conductance of monovalent cations, with a lower conductance of divalent cations (Melton *et al*., 2002). There is a lack of detailed structural analysis, but mutation of a region hypothesised to map to a ring structure inside the channel reduces the cation selectivity of the channel (Melton *et al*., 2002).

1.4 Molecular biology of HCV

1.4.1 Taxonomy

HCV is an enveloped, positive stranded RNA virus classified as part of the family *flaviridae*, in the genus *hepacivirus*. The *flaviridae* family has two further genera, *flaviviruses* and *pestiviruses*. *Flaviruses* are vector-borne and include Dengue virus and Yellow Fever virus. *Pestiviruses* include bovine viral diarrhoea virus and classical swine fever virus (Lindenbach & Rice, 2001). A further genus within this family, *pegivirus*, has been proposed for the GB viruses A, C and D (Stapleton *et al.*, 2011).

A close relative of HCV was recently identified among dogs in two animal shelters in the USA, which showed a 66% sequence homology of the 5' UTR and is estimated to have diverged from HCV between 500-1000 years ago (Kapoor *et al.*, 2011). Given the preliminary name of canine hepacivirus, recent work has also found the virus to be present in horses (Burbelo *et al.*, 2012).

1.4.2 Genotype variation

The six major HCV genotypes and more than 50 subtypes are defined by their genetic variance from one another (Simmonds, 2004; Simmonds *et al*., 1993). One subtype of a seventh genotype has also been identified (Murphy *et al*., 2007). A simplified evolutionary tree in Fig. 1.4 illustrates the divergence between the 7 HCV genotypes (Mandell *et al*., 2009). While there is a high selection pressure to maintain functional regions of the genome, some areas of viral genomes, particularly those coding for the hypervariable regions of the envelope glycoproteins, are very tolerant to mutations. Mutations in one protein under selection pressure from the immune response can result in compensatory mutations in other viral proteins, and over time can lead to the evolution of separate genotypes whose proteins are incompatible in chimeric viruses. Within a subtype, isolated sequences can differ by between 5-15% of nucleotides,

between subtypes within a genotype 10-30% and between genotypes by as much as 30-50% (Hoofnagle, 2002).

HCV also has a high mutation rate within patients, leading to the formation of viral quasispecies. The quasispecies variation ranges between 1-5% of the virus genome (Hoofnagle, 2002).

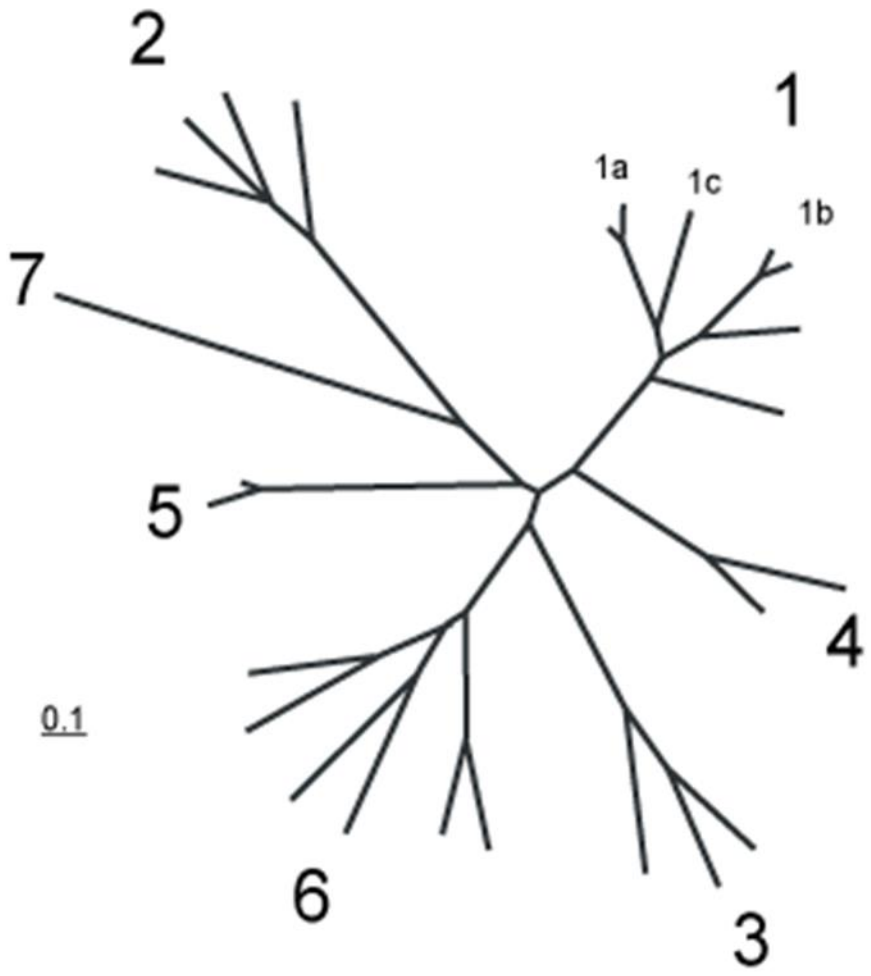

Figure 1.4 Evolutionary divergence of the HCV genotypes

Radial format evolutionary tree showing the genetic relationship between HCV genotypes, evolving from a distant common ancestor. Subtypes are indicated by branches within each genotype group, with limited subtypes shown for simplicity. Scale shown is that of the distance representing nucleotide substitutions per site. Taken from Mandell *et al.* 2009.

1.4.3 Lifecycle

1.4.3.1 Virus entry

The HCV virion binds to a number of cellular receptors that mediate cell entry via the E1-E2 heterodimer. The initial binding of the virion to the cell is to glycosaminoglycans (GAGs), including heparan sulphate. Treatment of cells with heparin inhibits the initial binding of the virion (Morikawa *et al.*, 2007), but does not inhibit entry once the initial binding has occurred (Koutsoudakis *et al.*, 2006).

A number of cellular cofactors have been shown to bind to the virion after initial attachment and mediate cell entry. The first to be identified was cluster of differentiation 81 (CD81), a tetraspanin expressed on a number of cell types (Pileri *et al.*, 1998). CD81 binding was shown to occur after initial attachment of the virion (Cormier *et al.*, 2004). Scavenger receptor class B type 1 (SRBI) is a high density lipoprotein (HDL) internalisation molecule that binds soluble E2. E2 shows a high specificity for SRBI, with the closely related CD36 and mouse SRBI unable to bind E2 (Scarselli *et al.*, 2002). SRBI was shown to bind E2 and HCVpp in a manner indicative of a co-receptor (Bartosch *et al*., 2003c). Claudin1 (CLDN1) is a tight junction component that is highly expressed in the liver and is able to render some non-hepatic cell lines susceptible to HCV infection when ectopically expressed. The kinetics of binding inhibition also indicate that CLDN1 acts at a late stage of virus entry, following CD81 interaction (Evans *et al.*, 2007). Occludin is another tight junction complex protein that is expressed highly in hepatocytes compared with other cells, and ectopic expression in other cell lines results in increased uptake of HCVpp (Ploss *et al.*, 2009). It also shows species specificity, with murine cells rendered infectable by its expression. The low density lipoprotein receptor (LDL-R) has also been shown to be involved in HCV entry, and the internalisation of LDL via clathrin mediated endocytosis to early endosomes is the same predicted path as HCV entry (Thorley *et al.*, 2010). The epidermal growth factor receptor (EGFR) has also been shown to be a

host cell cofactor for HCV entry, by mediating association between CD81 and CLDN-1 (Lupberger *et al.*, 2011). Expression of the HCV-entry cofactors is on the basolateral side of the hepatocytes, with tight-junction involvement. However, this cell polarisation is not required for HCV entry as shown by entry into Huh7 cells, a non-polarised hepatoma cell line.

Once the virion has bound the required co-receptors, it is internalised by clathrin mediated endocytosis and trafficked to early endosomes, where acidification mediates membrane fusion and uncoating of the virus (Hsu *et al.*, 2003).

E2 can also bind to the C-type lectins L-SIGN and DC-SIGN, but binding to these does not cause the virion to enter the cells (Lozach *et al.*, 2004). Instead, these receptors may allow 'capture' of the virions, where the presence of L-SIGN on the liver sinusoidal epithelial cells allows binding of the virion which can then pass from the epithelium to nearby hepatocytes.

A summary of the known receptor proteins involved in the entry pathway is shown in Fig. 1.5.

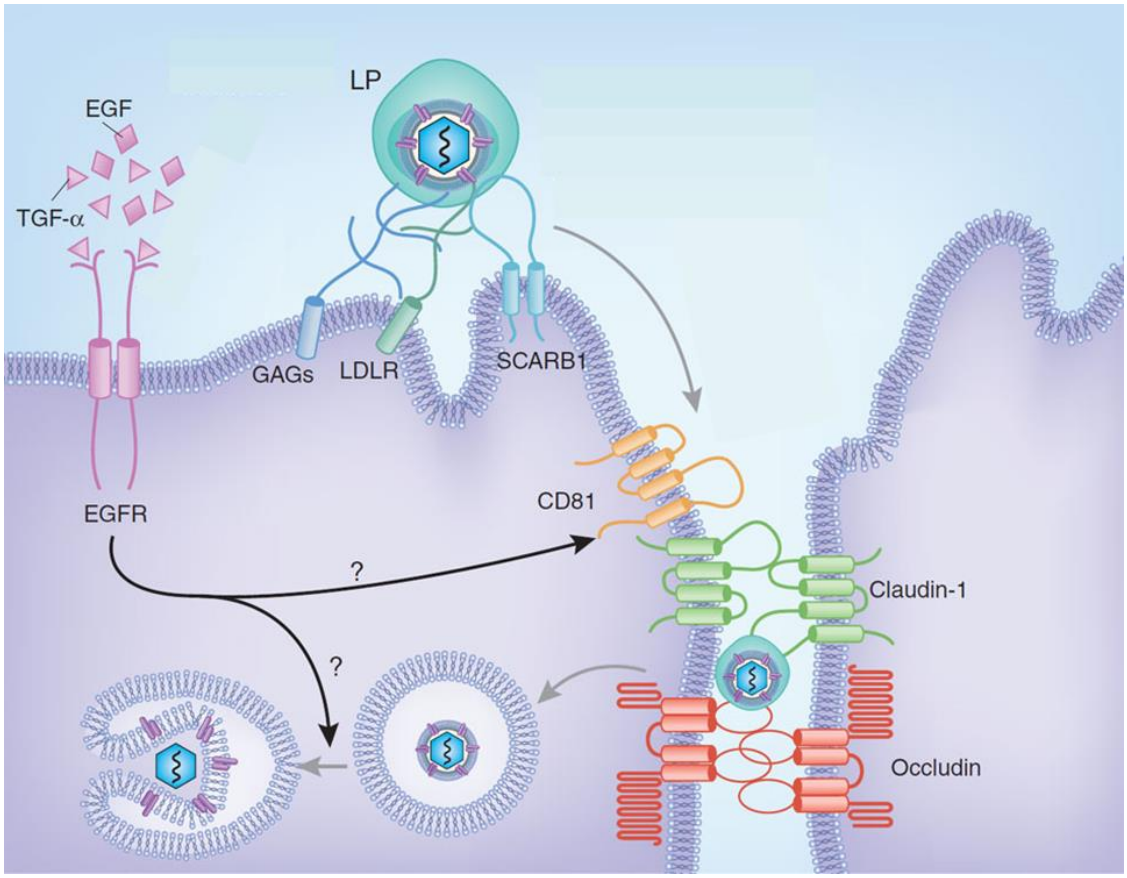

Figure 1.5 HCV Entry

Diagram summarising the known receptors and processes involved in HCV entry into hepatocytes. SRBI is referred to as SCARB1. HCV associates with very-low-density and low-density lipoproteins (LPs) in the bloodstream. It binds the basolateral surface of hepatocytes through glycosaminoglycans (GAGs) and the low-density lipoprotein receptor (LDLR). Engagement by the virus of SCARB1, the tetraspanin CD81 and the tight junction proteins claudin-1 and occludin leads to the clathrin mediated endocytosis of virions. HCV fuses with acidified endosomes and releases its genome into the cytosol. EGFR activation promotes CD81–claudin-1 interactions and membrane fusion, thereby enhancing productive HCV uptake. Taken from (Gerold & Rice, 2011).

1.4.3.2 Viral replication

Once the virus has been uncoated after entry, the genome is thought to undergo several rounds of translation to produce viral proteins that inhibit the cellular immune response and allow the formation of the membranous web replication complexes (Gosert *et al.*, 2003; Egger *et al.*, 2002). The HCV genome is translated to a 3000 amino acid polyprotein that is cleaved by host and viral proteases to produce the ten mature virus proteins, plus an additional 'F' protein translated from a +1 frameshift (Xu *et al.*, 2001; Grakoui *et al.*, 1993). A summary of the translation and cleavage of the polyprotein is shown in Fig. 1.6.

Once viral proteins induce the formation of replication complexes, the RNA-dependent RNA polymerase (RdRp) NS5B can replicate the viral genome via a negative-sense intermediate. The presence of dsRNA in the replication complex could trigger the cellular antiviral response via the RIG-I pathway, but this is blocked by NS3/4a cleavage of MAVS/Cardif, a component of this pathway. Also, HCV has an RNA secondary structure that prevents the binding of host RNAs as an additional means of blocking the activation of dsRNA response pathways (Davis *et al.*, 2008). Analysis of isolated replication complexes found that each contains one negative-sense copy of the genome, with between 2 and 10 positive strands and a high proportion of non-structural proteins NS3-5b with hundreds present per replication complex (Quinkert *et al.*, 2005). The transcribed RNA is then either translated into more viral proteins or packaged into virions.

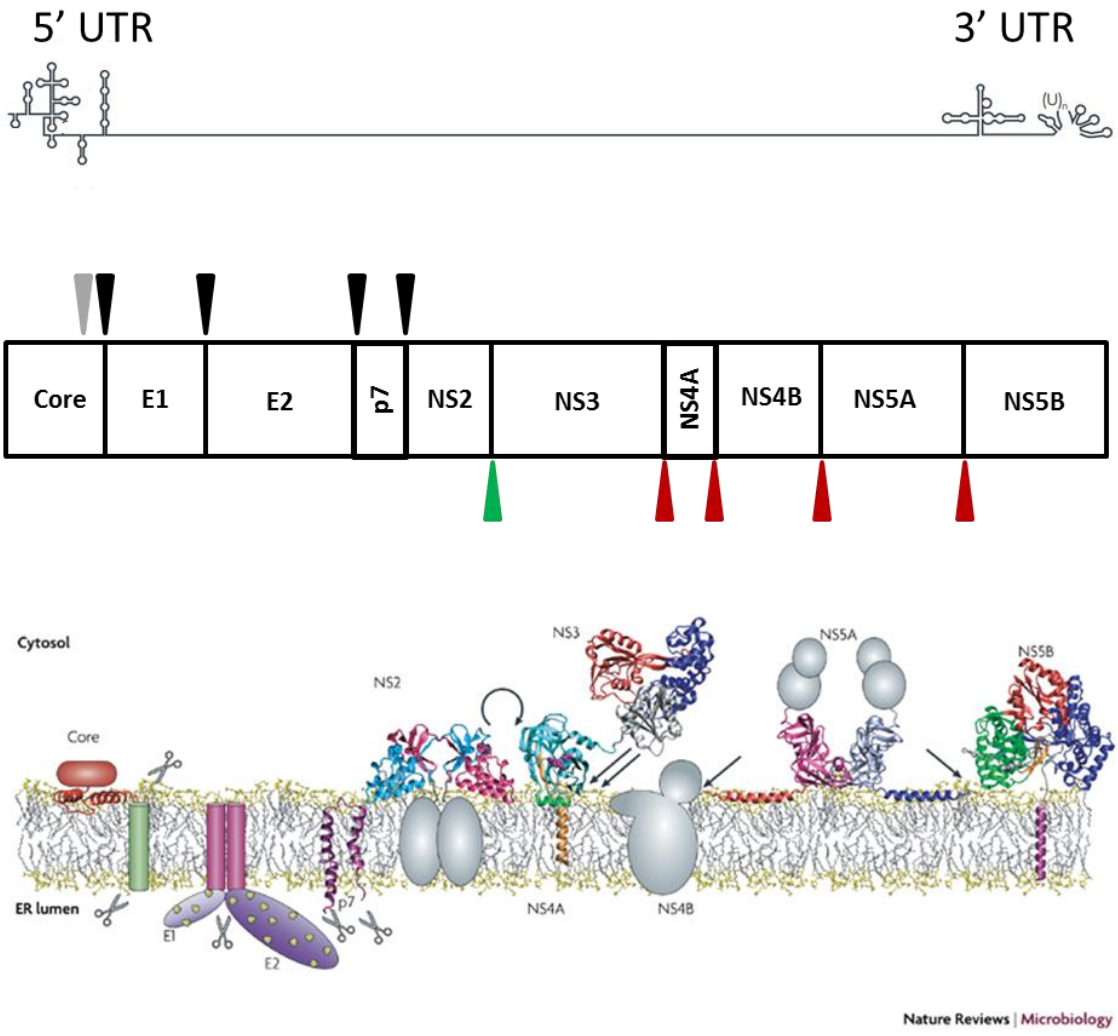

Figure 1.6 Genome organisation and polyprotein processing of HCV

The 9.6kb genome has conserved secondary structure at the 5’ and 3’ UTRs, with the 5’ UTR containing the IRES and the 3’ UTR the transcription initiation site required on the negative strand for positive strand synthesis. The genome is translated to a 3000 amino acid polyprotein. The polyprotein is cleaved by signal peptide peptidase (grey triangle), signal peptidase (black triangle), NS2-3 autoprotease cleavage (green triangle) and NS3/4a protease activity (red triangle) to produce 10 mature virus proteins. The cleaved proteins fold into the structures shown, where these structures are known. Genome and protein structures are taken from Moradpour *et al.* 2007.

1.4.3.3 Virus assembly and egress

The process of HCV assembly and egress is not yet fully understood. For the infectious virions to be assembled, HCV genomes from the replication complexes have to associate with Core protein to form virus capsids. Core has been shown to associate with lipid droplets as a crucial step in the production of infectious virus (Boulant *et al.*, 2006) but it is not known if this is the site at which the virus is packaged. The viral proteins E2, NS2, NS3 and NS5A have been shown to colocalise at lipid droplets at 72 hrs after infection (Jirasko *et al.*, 2010). NS2 and p7 have been shown to be required at an early stage of virus assembly, with the role of p7 at this point not requiring its viroporin function (Jones *et al.*, 2007). The hypothesised role for NS2 and p7 at this stage is to mediate the association of structural proteins with the replication complexes in order to mediate viral assembly (Stapleton *et al.*, 2011; Ma *et al.*, 2011; Jirasko *et al.*, 2010). The envelope glycoproteins remain associated with the ER and adjacent ER-derived membranes, and also interact with NS2.

HCV virions are trafficked through the cis-golgi and the endosomal pathway, mediated by ESCRT proteins (Corless *et al.*, 2010). p7 prevents the acidification of the endosomes in order to maintain the integrity of the envelope glycoproteins (Wozniak *et al.*, 2010).

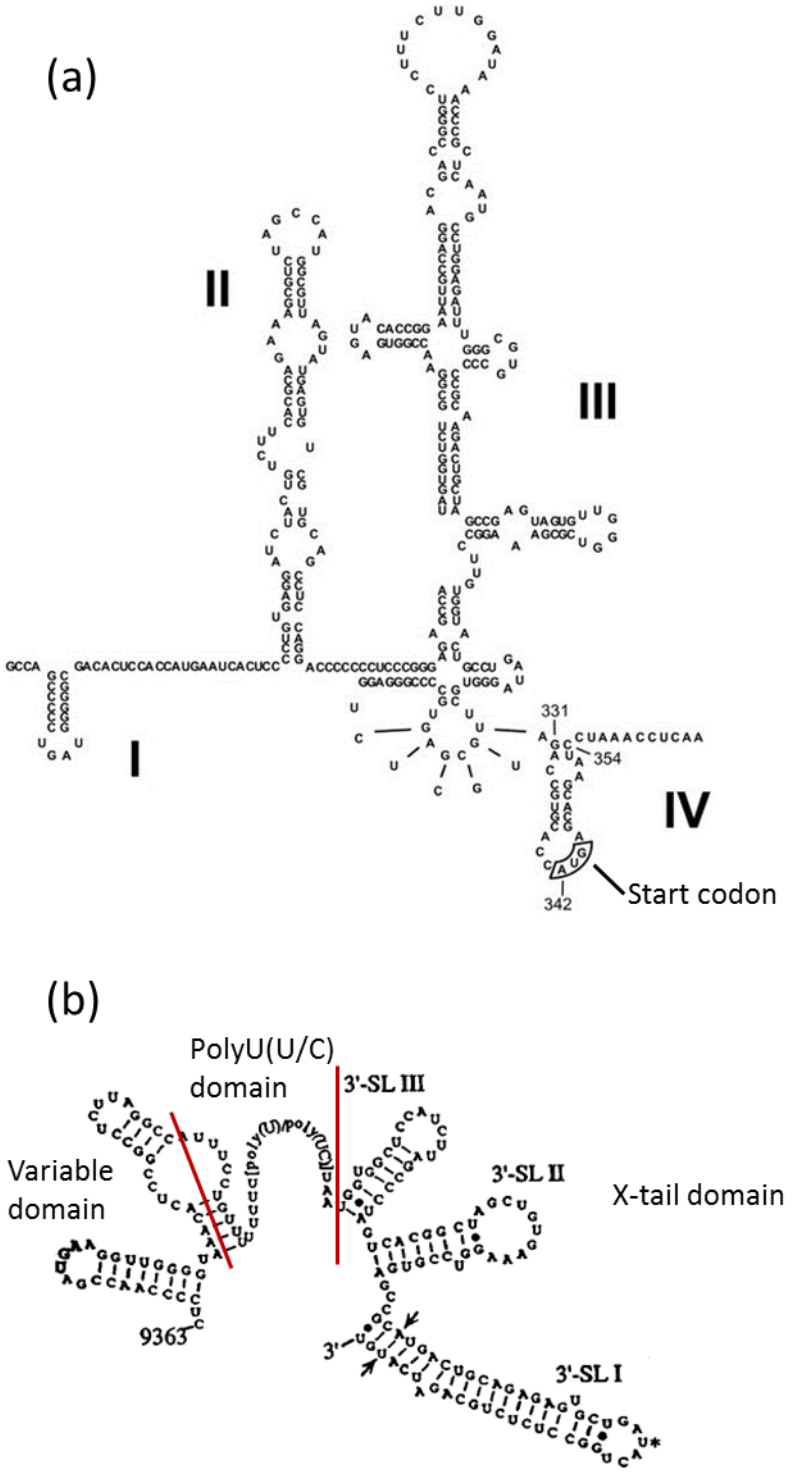

Figure 1.7 Secondary structure of 5' and 3' UTRs

Panel (a) 5' UTR secondary structure, including the IRES and start codon. The 4 stem-loop domains and start codon are labelled. Taken from (Honda *et al.*, 1999). Panel (b) 3' UTR secondary structure, with the variable domain, PolyU(U/C) domain and X-tail with 3 stem-loop structures labelled. Taken from (Kolykhalov *et al.*, 1996).

1.4.4 RNA genome/ Untranslated regions (UTRs)

The genome of HCV is a single-stranded, positive-sense RNA that can be directly translated into the polyprotein, which is cleaved to form the individual HCV proteins. The polyprotein coding sequence is flanked by untranslated regions at the 5' and 3' ends that contain elements important for the replication of the virus.

1.4.4.1 5' UTR

The 5' untranslated region (UTR) of the HCV genome, shown in Fig. 1.7 (a), is a region of 341 nucleotides. It is conserved between HCV genotypes, and has regions of sequence homology with pestiviruses (Han *et al.*, 1991). The 5' UTR shows specific regions of high sequence conservation interspersed with variable regions (Bukh *et al.*, 1992). The 5' UTR is involved in the initiation of both translation of the polyprotein and in genome replication initiation.

Much of the 5' UTR forms the internal ribosome entry site (IRES) of the virus, which initiates protein translation without the need of a 5' cap that cellular mRNAs require for translation initiation. Deletion analysis of the 5' UTR has found that nucleotides 40-370 are required for efficient IRES function, with the initiation codon for protein translation at position 342 (Reynolds *et al.*, 1995). The efficiency of IRES initiation is improved by the presence of the first section of the coding region for Core protein (Reynolds *et al.*, 1995). Deletion of the first 40 nucleotides of the 5' UTR has only a minimal effect on translation (Friebe *et al.*, 2001). The functioning of the IRES has been found to be dependent on a number of structural elements, with mutational analysis showing that preservation of the stem-loop structures is more important than the nucleotide sequence.

The IRES interacts with a number of cellular proteins to facilitate ribosome binding and translation initiation. The translation initiation of HCV differs from the canonical eukaryotic process, needing just two cellular factors, eIF2 and eIF3 to form the pre-

initiation complex (Ji *et al.*, 2004; Pestova *et al.*, 1998). The La antigen, a non-canonical initiation factor, has been shown to bind to the HCV IRES (Costa-Mattioli *et al.*, 2004). A liver-specific micro-RNA, mir122, has been found to greatly enhance virus translation/replication, possibly playing a role in the tissue-distribution of HCV (Jopling *et al.*, 2005). Exogenous expression of mir-122 in the replication non-permissive cell line HepG2 was found to render the cells permissive for HCV replication (Narbus *et al.*, 2011)

The 5' UTR must also interact with viral replication complexes in order to replicate the HCV genome. The first 125 nucleotides of the coding region are sufficient for the initiation of genome replication, but replication is greatly enhanced by the presence of elements within the 5' UTR. In the replicon system, it was found that domains I and II were absolutely required for genome replication and further 5' deletions abolished replication entirely. The addition of domain III increased the colony-forming efficiency 100-fold (Kim *et al.*, 2002).

1.4.4.2 3' UTR

Like the 5' UTR, the 3' UTR is also highly conserved among HCV genotypes (Kolykhalov *et al.*, 1996). The 3' UTR is composed of 3 regions: a short, 40nt variable region immediately after the coding sequence, a polypyrimidine (poly U(U/C)) tract and a 98nt region, known as the X-tail, which forms 3 stem-loop structures, shown in Fig 1.7 (b). The variable region is not absolutely required for genome replication, but its deletion reduces the efficiency of genome replication in the replicon system. Replicons lacking a poly (U(U/C)) tract could only be made viable when this was replaced by a homouridine stretch. No replicons with deletions to any of the stem loop structures of the X-tail were viable (Friebe & Bartenschlager, 2002). Further mutational analysis of the stem-loop structures in the X-tail found that both the nucleotide sequence and the stem-loop structures were required

The 3’ UTR has been found to affect protein translation from the IRES, and thus part of its role may be to interact with the 5’ UTR. Binding of the cellular protein polypyrimidine tract-binding protein (PTB) to the 3’ UTR has been shown to enhance translation of the polyprotein (Ito & Lai, 1997). The 3’ UTR is presumed to act to initiate replication from the minus strand of the HCV replication complex, but this part of the virus lifecycle is, as yet, poorly understood.

1.4.5 Structural proteins

1.4.5.1 Core

Core is the first of the viral structural proteins to be translated, and forms the bulk of the virion. There are two major forms; an immature p23 cleaved from the polyprotein, and a mature p21 form that is cleaved further in the ER by signal peptide peptidase (Targett-Adams *et al.*, 2008; Santolini *et al.*, 1994). A further form, p16, has been observed in GT1 and is the dominant product when the HCV genome is truncated, but it is only observed at much lower levels in longer HCV constructs and is not thought to play a major role in the production of infectious virus (Lo *et al.*, 1994). Core isolated from infected patient sera is exclusively p21, and thus the processed form of the protein is the one that forms the virus capsid (Yasui *et al.*, 1998).

Core is divided into three domains. Domain 1 contains many basic residues and has been shown to be involved in RNA binding and protein-protein interactions. Domain 2 has fewer basic residues and has two amphipathic α-helices linked by a hydrophobic loop. Domain 3 is highly hydrophobic, and has been shown to act as a signal peptide for the correct localisation of the E1 glycoprotein (McLauchlan, 2000).

Core protein forms the virus capsid. Purified Core protein expressed from *E. coli* was found to homo-oligomerise into micelle-like aggregates in aqueous solution in the absence of detergent. Detergent addition led to Core forming stable dimers (Boulant *et al.*, 2005). Deletion studies found that the correct folding of domain 1 was dependent on the presence of the hydrophobic domain 2.

Core has been found to localise to the ER, to punctate structures close to lipid droplets and coating lipid droplets within the cell, with some of the protein localising to the nucleus (Boulant *et al.*, 2008) and to the mitochondria (Schwer *et al.*, 2004). The relocation of Core to the lipid droplets is dependent on the second amphipathic helix of domain 2 (Boulant *et al.*, 2006). Core trafficking is also affected by p7 and NS2 in a

strain-specific manner, with p7-NS2 of the high-titre Jc1 chimera showing a large degree of localisation to the ER, and reduced LD distribution compared with JFH1 (Boson *et al.*, 2011).

NS5A protein has also been found to interact and colocalise with Core at the surface of lipid droplets, and it is hypothesised that its role here may be to associate HCV genomic RNA with the Core protein in order to facilitate virion assembly (Shi *et al.*, 2002).

A fraction of the Core protein is phosphorylated, and a mutant possessing an extra phosphorylation site showed increased trafficking to the nucleus, indicating that phosphorylation of Core protein may cause its nuclear distribution (Lu & Ou, 2002). Core has been found to suppress transcription from the p53 promoter and reduce p53 expression in mammalian cell transfection studies, possibly contributing to the reported transforming capability in mouse studies (Ray *et al.*, 1997), and may thus contribute to the risk of HCV infection resulting in HCC.

In mouse studies using chimeric vaccinnia viruses, it was found that the presence of Core was sufficient to impair the immune response, leading to reduced function of cytotoxic T-leukocytes (CTLs), and reduced production of IFN-γ and interleukin 2 (IL2) (Large *et al.*, 1999). A transgenic mouse line expressing Core in T-cells using the CL2 promoter found that there was increased T-lymphocyte cell death and a reduced immune response in the mice and, surprisingly, also found high levels of liver pathology with infiltration of apoptotic T-lymphocytes into the liver tissue.

1.4.5.2 F protein

The frameshift (F) protein was discovered in 2001 (Xu *et al.*, 2001; Walewski *et al.*, 2001). It is formed by a ribosomal shift during the translation of Core protein. Antibodies to F protein are found in advanced cases of chronic HCV (Komurian-Pradel *et al.*, 2004), and acute cases (Morice *et al.*, 2009). Initially it was thought to

have a role in the virus lifecycle, and it is known to be expressed *in vivo* as antibodies have been detected in patient sera. The protein has been shown to be unstable (Roussel *et al.*, 2003) and it is not yet known if it is necessary for virus infection in cell culture. High levels of antibodies against F protein have been found in patients with HCC however, which may indicate a role for F protein in pathogenesis (Dalagiorgou *et al.*, 2011)

1.4.5.3 E1 and E2

E1 and E2 are the Type 1 envelope glycoproteins that are incorporated into the virion and mediate virus entry. Following cleavage from the viral polyprotein, they associate in the ER to form heterodimers (Deleersnyder *et al.*, 1997), and this association is dependent on the C-terminal *trans*membrane domains (TMDs) of both proteins (De Beeck *et al.*, 2000). E1 requires the presence of E2 in order to fold correctly, but E2 folding is independent of E1 (Boo *et al*., 2012; Michalak *et al*., 1997). A number of ER chaperones including calnexin, calreticulin and BiP also bind to E1 and E2 heterodimers, but only calnexin has been found to be involved in correct protein folding (Choukhi *et al.*, 1998). Both E1 and E2 possess-terminal signal sequences that are required for their correct membrane association (Cocquerel *et al.*, 2002; Michalak *et al.*, 1997).

Heterodimerisation of E1 and E2 is a crucial step for virus infectivity. Within the ER, dimerisation occurs through non-covalent bonds. During virus assembly, a number of cysteine residues present in each protein are able to form disulphide bridges, linking the proteins covalently. These cysteine residues are highly conserved across all genotypes in both glycoproteins (Wahid *et al.*, 2013).

E2 is the primary glycoprotein involved in virus entry. It has been found to bind to CD81, SRBI, claudin and occludin. Recently E1 has been identified as binding to ApoE and ApoB lipoprotein receptors (Mazumdar *et al.*, 2011).

E2 possesses hypervariable regions (HVR), where the majority of quasispecies variation within patients is concentrated. These regions map to areas of the proteins that are accessible to antibody binding, suggesting there is a high selection pressure on these regions during chronic infection. The HVR1 of E2 is involved in virus attachment and entry, and antibody-neutralisation of this region with patient or chimpanzee sera renders the virus unable to infect cells (Owsianka *et al*., 2005; Bartosch *et al*., 2003a).

1.4.6 p7

p7 is discussed in detail in section 1.5.

1.4.7 Non-structural proteins

1.4.7.1 NS2

NS2 is a 217 residue membrane-anchored protein (Santolini *et al.*, 1995), with at least one *trans*membrane domain and a cytosolic C-terminal domain. The cytosolic domain is a protease which, in conjunction with the first section of NS3, displays autoprotease activity in a zinc dependent manner. This is required for correct protein folding (Pallaoro *et al.*, 2001; Pieroni *et al.*, 1997). The N-terminal *trans*membrane region of NS2 is dispensable for protease activity, as shown by expression of minimal NS2/3 constructs in *E. coli* (Thibeault *et al.*, 2001). NS2 contains the catalytic domain for NS2-3 autocleavage, with the Zn^{2+} binding domain of NS3 acting as a cofactor (Schregel *et al.*, 2009). The structure of the catalytic domain of NS2 has been shown to be a dimer with two active sites acting in tandem (Lorenz *et al.*, 2006). The HCV subgenomic replicon shows that NS2 is not required for replication of the HCV genome (Lohmann *et al.*, 1999). However, it is absolutely required for virus assembly. NS2 has been shown to interact with E2, p7, NS3 and NS5A (Popescu *et al.*, 2011). Mutations in Core, E1, E2, p7 and NS5A reported to abolish viral assembly also changed the subcellular localisation of NS2 (Popescu *et al.*, 2011). Based on its direct

interactions with these viral proteins, NS2 is thought to act as a linker between the structural and non-structural proteins, linking the replication complexes to viral assembly (Popescu *et al.*, 2011).

Alterations in the p7 sequence preceding NS2 cause significant disruption to NS2 localisation and function. The NS2-NS5A interaction was disrupted by both deletion of p7, or alanine mutations of the two basic loop residues of p7 (Tedbury *et al.*, 2011). Mutations in the protease active site of NS2 have been shown to affect RNA replication, but this is likely due to the inhibition of NS2/3 cleavage (Dentzer *et al.*, 2009). NS2 is phosphorylated at Serine 168 (S168) which targets NS2 for proteasomal degradation (Franck *et al.*, 2005). Mutation of this site significantly impairs the production of infectious virus (Yi *et al.*, 2009). The S168A mutation did not affect the localisation of Core, NS3 or NS5A, and intracellular particles with a buoyant density similar to infectious virus were produced, indicating that S168 of NS2 is required at a post-assembly state of virus maturation (Yi *et al.*, 2009). NS2 has also been shown to inhibit IFNβ promoter activity independently of other HCV proteins, via an as-yet unknown mechanism (Kaukinen *et al.*, 2006).

1.4.7.2 NS3

NS3 is a 72 kDa, 483-residue protein that non-covalently associates with NS4A as a cofactor. It has an N-terminal half that is a chymotrypsin-like serine protease (Hahm *et al.*, 1995; Eckart *et al.*, 1993), which cleaves the downstream viral proteins NS4A, NS4B, NS5A and NS5B from the polyprotein (Bartenschlager *et al.*, 1994; Tomei *et al.*, 1993). The C-terminal half of the protein acts as an RNA helicase during replication of the viral genome (Gwack *et al.*, 1996; Kim *et al.*, 1995).

The crystal structure of NS3 shows two 6-stranded β-barrels with a trypsin-like fold and a tetrahedrally coordinated zinc binding site, with the catalytic triad of the enzyme lying between the two β-barrel domains (Love *et al.*, 1996). Addition of a minimal

NS4A cofactor peptide shows that it is incorporated into a β-sheet of the enzyme core (Kim *et al.*, 1996).

NS3 is cleaved from NS2 by an autoprotease activity dependent on the catalytic domain of NS2 and the Zn^{2+} binding domain of NS3 (Schregel *et al.*, 2009). No uncleaved NS2/3 can be detected without the use of protease inhibitors or inhibitory mutations.

NS3/4a also inhibits several pathways of the cellular immune response (Breiman *et al.*, 2005). NS3/4A cleaves TRIF, an adapter protein in the TLR3 pathway that can activate both IRF3 and NFκB transcription factors (Li *et al.*, 2005); and Cardif/MAVS, an adapter downstream of the RIG-I signalling pathway (Horner *et al.*, 2012; Kaukinen *et al.*, 2006). By cleaving these two proteins, the virus is able to significantly reduce the cellular antiviral response and prevent extracellular signalling to the immune system via IFN-β (Kaukinen *et al.*, 2006).

The RNA helicase function of NS3 is dependent on the C-terminal 466 residues and remains when the protease domain is truncated (Kim *et al.*, 1995). Helicase activity is dependent on the presence of ATP and Mg^{2+} ions (Frick *et al.*, 2007; Kim *et al.*, 1995), and has been shown to proceed in an 'inchworm' like fashion, unwinding a stretch of nucleotides before pausing (Dumont *et al.*, 2006; Serebrov & Pyle, 2004). The crystal structure of the helicase domain shows a 3 domain-structure with an oligonucleotide binding-groove between domains 2 and 3 (Kim *et al.*, 1998). While NS4A is not required for the RNA helicase function of NS3, its presence has been shown to increase RNA binding and ATP hydrolysis efficiency (Beran *et al.*, 2009).

NS3 has also been found to interact with DNA repair pathways including ATM (ataxia-telangiectasia mutated), reducing the DNA repair response after cell irradiation. This reduction in repair mechanisms may contribute to the risk of development of HCC (Lai *et al.*, 2008).

1.4.7.3 NS4A

NS4A is a 54-residue membrane protein that acts as a cofactor for the NS3 viral serine protease. Truncation analysis has shown that the functional domain required for NS3 binding is a central portion comprising residues 21-32, which is sufficient for NS3/4a protease function in cell-free systems (Tomei *et al.*, 1996; Lin *et al.*, 1995). In addition to its crucial role as a cofactor for NS3 protease function, NS4A has also been found to promote ATP hydrolysis in the NS3 helicase domain. Residues in the C-terminal acidic domain of NS4A mediate this cofactor activity, shown by mutational studies that drastically reduce ATP-coupled RNA binding and duplex unwinding (Beran *et al.*, 2009). The N-terminal 21-residue *trans*membrane α-helix of NS4A has been shown to be involved in intramembrane protein-protein interactions during the assembly of functional replication complexes (Brass *et al.*, 2008).

The C-terminal 19 residues contain acidic residues that allow pH-dependent folding into an α-helix. Mutation of these residues reduces the hyperphosphorylation of NS5A and reduces the efficiency of the NS5B replicase. These residues have been postulated to act as a regulatory electrostatic switch that regulates the hyperphosphorylation of NS5A and viral replication (Lindenbach *et al.*, 2007).

NS4A has also been shown to accumulate on mitochondria and render cells prone to mitochondria-mediated apoptosis (Nomura-Takigawa *et al.*, 2006). Whilst this effect may be balanced by the anti-apoptotic effects of other HCV proteins, NS4A may be partially responsible for the increased cytopathic effect observed in HCV infected cells in culture.

1.4.7.4 NS4B

NS4B is a 27 kDa highly hydrophobic integral membrane protein (Hügle *et al.*, 2001), predicted to comprise an N-terminal amphipathic domain, a central 4-span *trans*membrane region and an amphipathic helical C terminal domain (Gouttenoire *et*

al., 2010a). The N and C termini were thought to be oriented towards the cytoplasm due to their availability for NS3/4A proteolytic cleavage, but a fraction of NS4B shows post-translational translocation of the N-terminal amphipathic domain into the ER lumen (Lundin *et al.*, 2003). This fraction is reduced when coexpressed with NS5A which may modulate this translocation by a direct or indirect association (Lundin *et al.*, 2006). NS4B shows some oligomerisation, thought to be mediated by the amphipathic α-helix AH2, which becomes a *trans*membrane domain following N-terminal translocation to the cytosol, (Gouttenoire *et al*., 2010b). The central hydrophobic domain, comprising the hypothesised 4 α-helical *trans*membrane spans, can act as both a membrane anchor and an ER-targeting domain (Gouttenoire *et al.*, 2009).

NS4B has been show to localise to the ER where it colocalises with the other non-structural proteins (Hügle *et al.*, 2001). It induces membrane rearrangements to form the membranous web, a membrane-bound matrix of vesicles on which HCV replication complexes form (Gosert *et al.*, 2003; Egger *et al.*, 2002). Mutations which abolish this rearrangement, such as those to the N-terminal amphipathic domain, have been shown to abolish virus replication (Lundin *et al.*, 2006).

1.4.7.5 NS5A

NS5A is a multifunctional protein that is involved in both virus replication and assembly. NS5A also acts to modify the cell environment to make it more conducive to viral replication. It is a phosphoprotein that can exist in a basally phosphorylated p56 or a hyperphosphorylated p58 form, and localises to the virus replication complexes, directly binding to NS5B and co-localising with other non-structural proteins in the replication complexes (Macdonald & Harris, 2004). NS5A has 3 domains separated by low complexity sequences. The first domain is an amphipathic α-helix, which mediates membrane association of the protein. Mutation of the amphipathic domain has been shown to impair HCV replication (Elazar *et al.*, 2003; Brass *et al.*, 2002). It also contains a zinc-binding domain that is required for the

functioning of the protein (Tellinghuisen *et al.*, 2004). Domain I also mediates NS5A dimer formation, for which two differing structures have been determined (Love *et al.*, 2009; Tellinghuisen *et al.*, 2005). The second and third domains are natively unstructured (Hanoulle & Verdegem, 2009; Liang *et al.*, 2007), although domain III has a slight propensity to partially fold into an α-helix (Verdegem *et al.*, 2011).

NS5A has been shown to interact with the viral polymerase NS5B to enhance viral replication (Macdonald & Harris, 2004). All 3 domains are involved to some extent in RNA binding (Foster *et al.*, 2010), preferentially binding the polypyrimidine tract of the 3' UTR, as well as the 3' region of the negative strand (Huang *et al.*, 2005). Domain III enhances RNA replication but is not required for it (Hughes *et al.*, 2009). It is, however, absolutely required for virus assembly (Tellinghuisen *et al.*, 2008).

NS5A is involved in the modulation of cell signalling pathways to block the cellular antiviral response and enhance virus replication. NS5A has been shown to suppress the induction of IFN within the cell (Aizaki *et al.*, 2000). Mutations in NS5A have been shown in some studies to correlate with an increased response to IFN-treatment (Enomoto *et al.*, 1995, 1996), but this has been disputed (Brillet *et al.*, 2007). It has also been shown to block the action of a pro-apoptotic K^+ channel (Mankouri *et al.*, 2009) maintaining the survival of infected cells in response to oxidant stress, inhibit p38 and Ras-ERK signalling and activate PI3 kinase-AKT signalling (Macdonald *et al.*, 2005). The majority of NS5A protein interactions are mediated by a conserved polyproline motif (Macdonald & Harris, 2004) that interacts with SH3 domain-containing host cell proteins.

1.4.7.6 NS5B

NS5B is a 65 kDa RNA-dependent RNA-polymerase (RDRP) that replicates the viral genome. It is anchored to cell membranes by a C-terminal 21-residue *trans*membrane domain (Ivashkina *et al.*, 2002), truncation of which does not affect the *in vitro* activity

of the RDRP domain, but does result in the protein being soluble and monodispersed (Ferrari *et al.*, 1999). NS5B is localised to the ER and ER-associated membranes modified by NS4B, and the *trans*membrane anchor is both necessary and sufficient for this localisation (Schmidt-Mende *et al.*, 2001).

The RDRP structure has been determined, with an active site showing a number of conserved motifs found in other viral RDRPs, such as the GDD domain (Lesburg *et al.*, 1999; Yamashita *et al.*, 1998). Mutation of the GDD residues renders the virus unable to replicate. The active site shows a high specificity for the X-tail of the 3'UTR (Zhong *et al*., 2000b, 2000a), and this specificity is mediated by a conserved 'thumb' like domain, deletion of which allows nonspecific dsRNA to bind to the active site (Hong *et al.*, 2001).

NS5B has been shown to associate with a number of other proteins, both viral and cellular, in order to form the RNA replication complex, including the cellular RNA helicases elF4A and p68 (Goh *et al.*, 2004; Kyono *et al.*, 2002). The viral helicase NS3 is able to associate with NS5B, and NS4B has also been shown to associate with both of these proteins in a possibly inhibitory role (Piccininni *et al.*, 2002). NS5A modulates the activity of NS5B, and mutations that abolish their association also impair RNA replication (Shimakami *et al.*, 2004). NS5B has no proofreading ability, and comparative sequencing of HCV in patients and inoculated chimpanzees estimated an error rate of between $1.44x10^{-3}$-$1.92x10^{-3}$ per base per year (Bartenschlager & Lohmann, 2000). This high error rate is responsible for the observed quasispecies variation found in HCV patients.

1.4.8 Experimental systems for HCV

1.4.8.1 Animal models

Animal models for HCV are limited: the only primate species susceptible to HCV infection are chimpanzees (*Pan troglodytes*). Early work, prior to the identification of HCV, found that sera from patients with non A, non B post transfusion hepatitis was able to infect chimpanzees and cause elevated ALTs and hepatitis-associated liver histology changes (Shimizu *et al.*, 1979; Alter *et al.*, 1978; Tabor *et al.*, 1978). As well as exposure to infectious patient sera, chimpanzees can also be infected by injection of HCV RNA directly into the liver, allowing assessment of the *in vivo* replication ability of specific HCV mutations (Sakai *et al.*, 2003). However, while there are a number of uses for chimpanzees in HCV research, there are a number of important clinical differences when compared with the disease in humans. In humans it is estimated that 85% of those exposed to HCV will develop a chronic infection; in chimpanzees this figure is estimated to be between 30-40% (Lanford *et al.*, 2001). They are also long lived and, with the higher clearance rate, few chimpanzees will sustain a chronic infection for sufficient number of years for the potential development of cirrhosis and hepatocellular carcinoma.

Chimpanzees are a protected species and their use as a HCV model system is therefore extremely limited, with only a very small number of individual animals used. Thus, experiments using chimpanzees may be highly prone to differing effects based on the genetic variation between the hosts.

GB virus B (GBV-B) is another member of the *flavivirus* family and has a similar genome organisation to HCV. It is able to cause an acute, self-limiting infection in tamarins (Schlauder *et al.*, 1995; Karayiannis *et al.*, 1989) and has thus been used as a model for HCV. The lack of chronic infection limits its uses as a model for HCV, but

examination of the differences between the viruses may shed light on what causes the differences between acute and chronic infections.

The development of mouse models for HCV has produced some promising results. Transplantation of human hepatocytes into immune deficient mice renders them vulnerable to infection, but the immune deficiency results in no liver damage occurring, thus limiting their use as a model for HCV infection (Bissig *et al.*, 2010; Mercer *et al.*, 2001). Engineering the expression of human receptors CD81 and occludin into murine cells (Ploss *et al.*, 2009) and mice (Dorner *et al.*, 2011) rendered them permissive to HCV entry, but viral protein expression could not be detected indicating that murine cellular factors may be blocking HCV replication. The most physiologically-relevant mouse model so far produced is one transplanted with both human hepatocytes and immune cells, which shows signs of hepatitis and fibrosis following HCV infection (Washburn *et al.*, 2011).

1.4.8.2 HCV pseudoparticles

Before the development of an infectious virus clone, the expression of HCV pseudoparticles (HCVpp) was the only means of studying the entry mechanism of the virus. These particles are a hybrid of the lentivirus murine leukaemia virus with the envelope glycoproteins E1 and E2 of HCV, generated by co-transfection of expression constructs for the constituents into a producer cell line (Bartosch *et al*., 2003b). The virus pseudoparticles generated can then enter permissive cells.

Virus-like particles (VLPs) can also be generated using a baculovirus expression system, which found that Core, E1 and E2 are sufficient to generate VLPs that can enter permissive cells (Baumert *et al.*, 1998)

The pseudoparticle systems were used to identify cell receptors that interact with E1 and E2, such as CD81, SRBI, Claudin and Occludin (Ploss *et al.*, 2009; Evans *et al.*, 2007; Cormier *et al.*, 2004; Scarselli *et al.*, 2002).

1.4.8.3 Subgenomic replicon

The subgenomic replicon contains the minimal viral RNA sequence required for replication of the genome. The bicistronic construct was made using the GT1B consensus sequence (Con1), with the HCV IRES driving translation of neomycin phosphotransferase to allow colony selection, followed by an EMCV IRES driving expression of the NS3-5B region of the HCV genome (Lohmann *et al.*, 1999), a schematic of which is shown in Fig 1.8 (a). Following transfection of the construct into the Human hepatoma 7 (Huh7) cell line, cells harbouring the replicon were selected using geneticin. Inclusion of NS2 was found to reduce RNA replication (Lohmann *et al.*, 1999). Sequencing of the replicon following serial passage found a number of culture-adaptive mutations that increased replication; two in NS3, one in NS4B and four in NS5A (Krieger *et al.*, 2001). This culture-adapted replicon was given the name FK5.1. However, when these culture adaptations were engineered into RNA used to infect chimpanzees, it was found that the RNA was no longer able to establish an infection. Thus, mutations that improve RNA replication may be harmful to the virus if the assembly of infectious virions becomes impaired (Bukh *et al.*, 2002).

Further adaptations to the replicon, such as creating a chimeric 5' UTR with poliovirus also increased replication efficiency (Friebe *et al.*, 2001). An Huh7-derived cell line, Huh7.5, created by serial passage of FK5.1 harbouring cells which were cured with interferon, were found to be more permissive for replicon RNA replication due to a defect in the dsRNA-detecting RIG-I signalling pathway (Blight *et al.*, 2002). This cell line was also found to be permissive for replication of GT1A replicons (Blight *et al.*, 2003), where previous attempts in Huh7 cells had not been successful (Blight *et al.*, 2000). Further modifications to the replicon included replacement of the neomycin phosphotransferase gene with firefly luciferase, allowing RNA replication after transfection to be measured (Krieger *et al.*, 2001).

Creation of a GT2A replicon using JFH1 produced a replicon capable of forming colonies at 60X the rate of FK5.1, and the replicon was also found to have efficient replication without culture adaptations (Kato *et al.*, 2003). A JFH1 luciferase replicon for transient replication assays had a replication rate 200X greater than FK5.1 (Targett-Adams & McLauchlan, 2005). The advantage of these systems is that, without culture adaptations that can impair the infectivity of the virus, the replication observed is more likely to be physiologically relevant to HCV virus replication.

1.4.8.4 JFH1 infectious clone

The infectious cell culture system for HCV was developed using a genotype 2a isolate from a patient with fulminant hepatitis, Japanese Fulminant Hepatitis (JFH1), cultured in the replication-permissive cell line Huh7 (Lindenbach *et al.*, 2005; Wakita *et al.*, 2005; Zhong *et al.*, 2005). This system is able to produce virus at an infectivity of 10^4 focus forming units per ml (FFU/ml) (Zhong *et al.*, 2005), and was able to infect chimpanzees, although the resulting infection was shorter in duration and had lower pathogenicity than that caused by the original JFH1 patient sera (Kato *et al.*, 2008; Zhong *et al.*, 2005).

A number of JFH1 chimeras have been developed in order to investigate how genotype variation affects viral replication. In order to replicate, most of these chimeras require the replicative machinery (NS3-5B) of JFH1 but will tolerate the Core-NS2 region of other HCV isolates. One such chimera, Jc1, has the Core-NS2 region of GT2A J6, and can produce titres as high as 10^5 FFU/ml, the highest thus far observed with HCV in culture (Pietschmann *et al.*, 2006). A full-length GT1A, H77S, was found to be able to replicate in cells and to produce a limited amount of virus, but production of infectious virus was at very low levels when compared with JFH1 (Yi *et al.*, 2006). A chimera of this isolate with JFH1 produced higher levels of infectious virus, showing some adaptive mutations that enhanced particle production (Yi *et al.*, 2007). These chimeras allow the effect of changes in the structural proteins on virus

infectivity to be investigated, and provide a much more relevant model of viral entry than the previously used pseudoparticle systems. a simplified diagram of full-length JFH1 and its chimeras H77 and Jc1 is shown in Fig. 1.8.

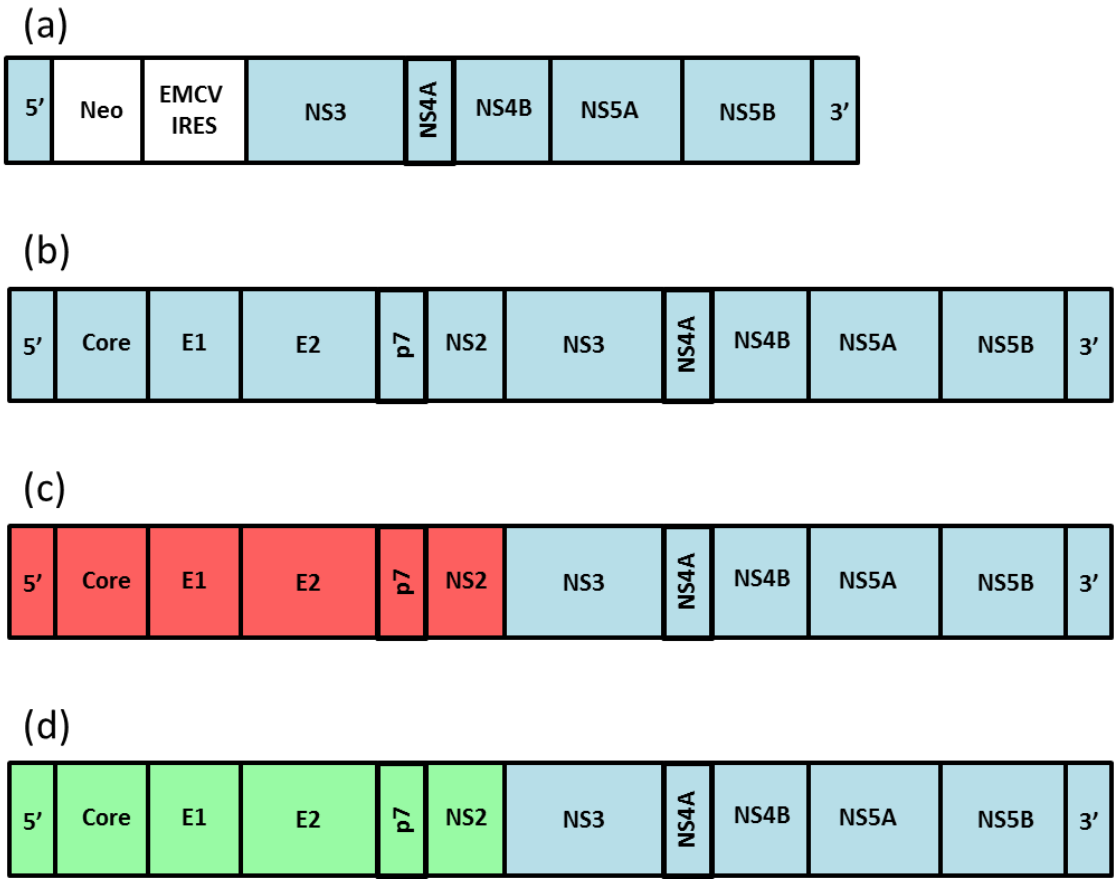

Figure 1.8 Genome structure of HCV replicon and virus constructs

Organisation of HCV constructs used to investigate the virus lifecycle.(a) Subgenomic replicon, containing the HCV IRES followed by the neomycin phosphotransferase gene (Neo), the encephalomyocarditis virus IRES (EMCV IRES), and the non-structural proteins NS3-5B of the HCV sequence. (b) Full-length JFH1 sequence. (c) Chimeric construct containing the Core-NS2 region from the GT1A H77 isolate. (d) Chimeric construct Jc1 containing the Core-NS2 region from GT2A J6.

1.5 p7

1.5.1 Discovery

p7 was the last HCV protein to be identified. The other nine proteins were characterised by the use of expression constructs and *in vitro* translation, and it was noted that cleavage of the E2-NS2 region was slower than for other linkages in the polyprotein. E2 also undergoes glycosylation during processing which increases its molecular weight (Grakoui *et al.*, 1993), and in combination with the presence of uncleaved E2-p7 may have indicated multiple forms of E2 rather than the existence of an additional viral protein. Further analysis of the E2-NS2 linker region found a second cleavage site, but at the time this was ascribed to generating two different forms of E2 (Mizushima *et al.*, 1994). Further investigations into the E2-NS2 region using a series of c-myc tagged C-terminal truncations identified a 7 kDa protein, p7, after immunoprecipitation (Lin *et al.*, 1994). A high proportion of uncleaved E2-p7 was also observed, indicating lower cleavage efficiency than found for other HCV proteins.

1.5.1.1 Cleavage from the HCV polyprotein

As with the preceding structural proteins in the polyprotein, cleavage of p7 from E2 and NS2 was shown to be mediated by host signal peptidase (SP), as the presence of microsomal membranes was sufficient for protein cleavage. The SP cleavage of the p7 junctions in the ER is slower than for the preceding structural proteins, leading to the presence of uncleaved E2-p7-NS2, E2-p7 and p7-NS2. Mutations upstream of p7 in E2 have been found to increase the rate of cleavage and so the limited cleavage rate may well be a viral mechanism to limit the availability of the fully cleaved proteins (Isherwood & Patel, 2005). However, work in the JFH1 virus system has confirmed that none of these uncleaved p7 products are required for virus replication, as insertion of an additional IRES at either end of p7 does not significantly affect the production of infectious virus particles (Jones *et al.*, 2007).

1.5.1.2 Topology and localisation

Early sequence analysis identified two possible *trans*membrane domains (TMDs), with a predicted topology of the N and C termini of the protein being oriented towards the lumen of the channel, with two basic residues present in the cytosolic loop (Carrère-Kremer *et al.*, 2002). This topology was confirmed by overexpression of N or C termini myc-tagged constructs that reached the plasma membrane, with the myc tag detectable by immunofluorescence without permeabilisation of the cell (Carrère-Kremer *et al.*, 2002).

Initial overexpression studies to determine the localisation of p7 found that it localised to the ER, the mitochondria and the plasma membrane (Carrère-Kremer *et al.*, 2002). However, in more physiologically relevant systems, trafficking to the plasma membrane is not observed, and the apparent mitochondrial localisation was in fact ER positive sites surrounding the mitochondria (Griffin *et al.*, 2005). JFH1 p7, when tagged with eGFP or HA epitopes, showed no localisation to mitochondria or the plasma membrane (Haqshenas *et al*., 2007b). The ER is the primary localisation of p7, with no association found with the Golgi by immunofluorescence (Vieyres *et al.*, 2013). IAV M2, the prototype viroporin which forms a proton conductive channel, localises to the *trans*-Golgi to prevent acidification that can lead to conformational changes in the envelope glycoproteins (Ciampor *et al.*, 1992). The presence of p7 in endosomes, while not detectable by immunofluorescence, can be seen indirectly by its effect on raising endosomal pH, which is blocked by the p7 inhibitor rimantadine (Wozniak *et al.*, 2010).

1.5.1.3 p7 as a viroporin

The viroporin activity of p7 was identified by ion channel recordings performed using GST-tagged bacterially expressed protein in the black lipid membrane (BLM) system. Channel activity could be blocked by the M2 inhibitor amantadine (Griffin *et al.*, 2003). Chemically synthesised p7 also displayed channel activity in this system (Pavlović *et*

al., 2003). High throughput assays of p7 function were then developed using a liposome based dye-release assay, using the self-quenching fluorescent dye carboxyfluorescein, that could be used to measure activity levels of the protein *in vitro* under a variety of conditions (StGelais *et al.*, 2007).

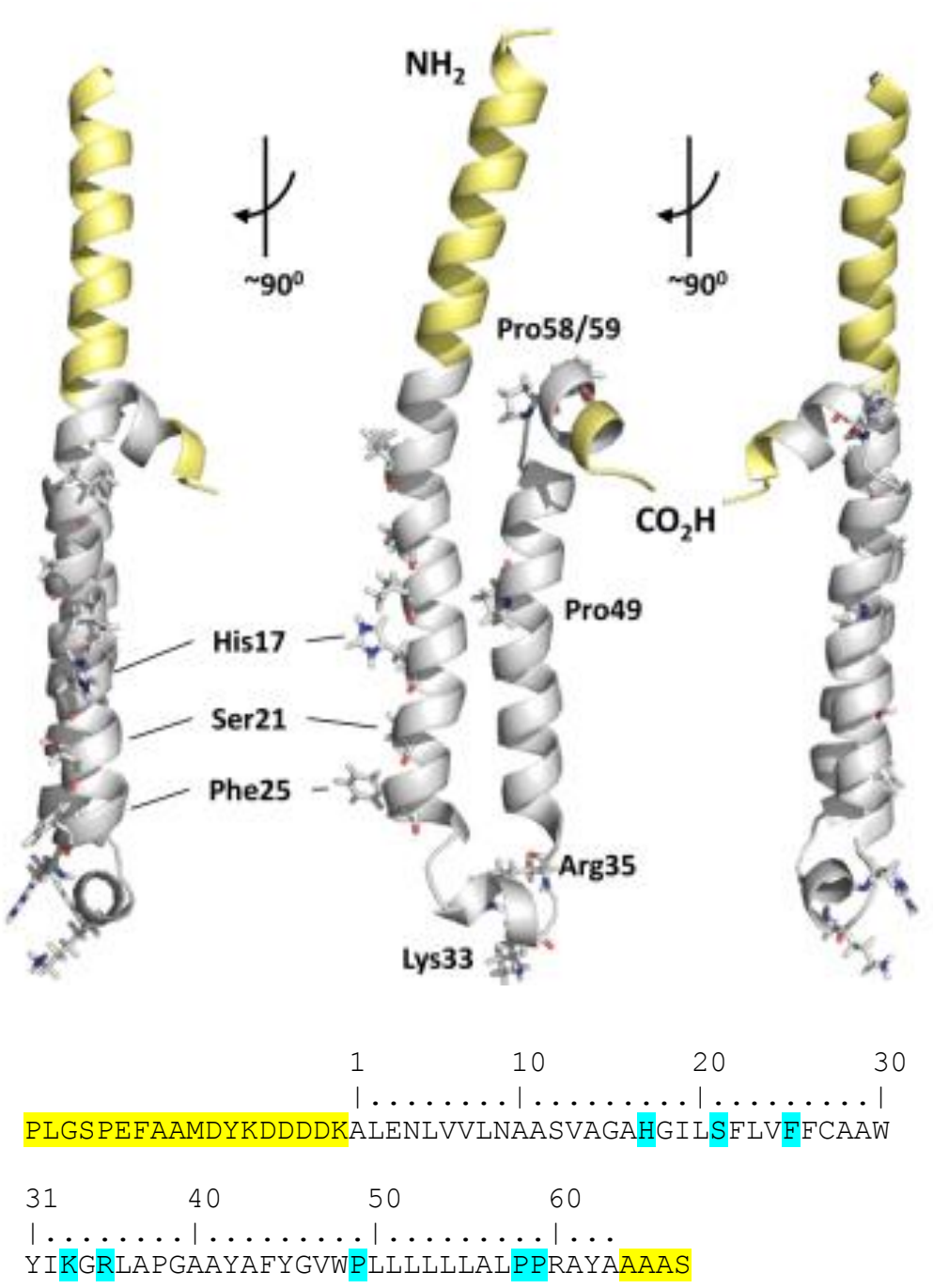

Figure 1.9 J4 p7 monomer structure

Cartoon NMR structure of the GT1B J4 p7 monomer in solution in methanol, including the N-terminal FLAG tag and 4 additional residues on the C terminus, with the sequence shown below. The extra residues at the N and C terminus are coloured yellow in the structure cartoon and in the sequence, and annotated residues in the structure cartoon are highlighted in blue in the sequence below. Three copies are shown in vertical rotation, and proline residues P49, P58 and P59 are highlighted. TMD 1 shows a straight helix containing the lumenal residues H17, S31 and F25, followed by a short loop domain containing the two conserved basic residues K33 and R35, and TMD2 with a slight kink at P49 before a sharp turn at the C-terminus caused by P58 and P59. Top image taken from Foster *et al*, 2014.

1.5.2 Structure

1.5.2.1 Structural analysis

p7 is a 63 amino-acid protein with a high proportion of hydrophobic residues. *In silico* analysis of the p7 sequence predicted a mostly alpha-helical secondary structure (Patargias *et al.*, 2006) with helical wheel plots of both *trans*membrane domains predicting that the helices were amphipathic (Clarke *et al.*, 2006). The overall structure of the monomer was predicted to be a helix-loop-helix structure (Carrère-Kremer *et al.*, 2002). A number of solution and solid state NMR studies have been performed to establish the structure of p7. While none of these studies have, at this time of writing, produced a complete atomic structure of full length p7, they have shown details of the α-helical secondary structure and inter-helix interactions. Other structural analysis techniques, such as circular dichroism (CD) spectroscopy and electron microscopy, have also provided details of the protein architecture. Biochemical analysis confirmed the topology of p7 as an integral membrane protein with both N and C termini present on the same side of the membrane, providing evidence for a hairpin protein structure (Carrère-Kremer *et al.*, 2002).

The helix-loop-helix structure has been confirmed by NMR in GT1B J4 (Fig 1.9). A slight kink in TMD1 occurred at H17, showing a possible constriction point in the channel (Cook & Opella, 2011). A further, hydrophobic constriction point in the channel at F25 was hypothesised to play a role in maintaining the closed position of the channel and possibly contribute to its cation selectivity (Montserret *et al*., 2010). This hypothesis may be supported by biochemical data, as mutations of phenylalanine residues in TMD1 of GT1B J4 p7; F22, 25 and 26 to alanine, and the point mutation F25A, all produce highly active channels (Foster *et al.*, 2011; StGelais *et al.*, 2009).

It had previously been hypothesised from *in silico* modelling that TMD2 would have some degree of tilt relative to TMD1 (Patargias *et al.*, 2006). NMR data showed that in

GT1B J4 p7 both of the TMDs are tilted in the membrane, with TMD1 and 2 showing tilt angles of 10° and 25° respectively from the bilayer normal (Cook & Opella, 2010).

It was found that *in vitro* synthesised GT1B p7, with a C27A mutation to prevent disulphide bond formation, in a variety of membrane mimetic conditions showed a mostly alpha-helical structure by CD spectra in all tested conditions, and solution NMR in 50% trifluoroethanol/water confirmed the presence of these helices. As well as those TMD alpha helices already predicted, a further helix was found in the N-terminal domain of the protein (Montserret *et al*., 2010). However, no inter-helix interaction by long-range NOE was detected under these conditions indicating that the protein did not fold into full tertiary structure. A recent study of the GT1B J4 p7 monomer structure in methanol (Foster *et al*., 2014) has modified the previously generated *in silico* structures, shifting the position of the cytosolic loop and showing interactions between the TMDs, confirming the hairpin structure (Fig 1.9).

Early theoretical analysis hypothesised that p7 required at least 5 subunits to form a functioning channel (Pavlović *et al.*, 2003). Evidence for oligomerisation of the protein came from chemical crosslinking studies. These studies showed that HepG2 cells transfected with a p7 expressing plasmid produced a p7 antibody-reactive band on western blot of a size consistent with a hexamer (Griffin *et al.*, 2003). Crosslinking was also used to show channel structures by electron microscopy, with crosslinking of bacterially expressed GST-p7/GST-His-p7 fusion proteins in microsomal membranes showing possible hexamer or heptamer channel structures (Griffin *et al.*, 2003). Later work by the same group found both hexamers and heptamers were formed in liposome membranes (Clarke *et al.*, 2006), although other studies under different experimental conditions using chemically synthesised protein and different lipids found that only hexamers were present (Luik *et al.*, 2009). These hexamers, consisting of GT2A p7 in micelles of the detergent DHPC, showed a flower-petal like channel structure at a resolution of 16 Å, where the wide ‘petals’ were formed by the

N and C terminal tails of the protein, confirmed by gold-particle immunolabelling (Luik *et al.*, 2009). It is possible that both heptamers and hexamers may coexist under *in vivo* conditions as functional channels. Consistent with this, *in silico* analysis of both possible oligomer structures indicates that both hexamers and heptamers are capable of forming functional channels (Chandler *et al.*, 2012).

Recent work has indicated that the composition of the membrane environment also has a strong effect on p7 structure (Whitfield *et al.*, 2011). This could have potentially high significance. While the majority of p7 within a cell accumulates within the ER, the functioning of the protein may well change as it is trafficked through different cellular compartments. It is possible that p7 may not function as an ion channel until it is required during the latter stages of viral assembly or egress.

1.5.2.2 N and C terminal tails

The N and C termini show a high degree of conservation with the first and last 3 residues absolutely conserved between HCV genotypes. These residues adjacent to the cleavage site are absolutely required for signal peptidase cleavage. While these regions do not play a direct role in the viroporin activity of p7, they may act to stabilise the oligomer.

The N and C terminal tails of the protein are thought to act as signal sequences for p7 cleavage. They may also be responsible for genotype-specific interactions with other HCV proteins, as chimeras between GT1A H77 and GT2A J6 p7 found that the *trans*membrane domains could be exchanged between genotypes and still produce infectious virus in chimpanzees, but not the terminal tails of the protein (Sakai *et al.*, 2003). This genotype specificity could indicate that these regions are responsible for interactions with other viral proteins, unrelated to the viroporin activity of the channel.

1.5.2.3 Basic loop

The cytosolic basic loop between the two TMDs at positions 33-35, consisting of two positively charged residues of arginine or lysine separated by a single glycine, has been shown to be crucial to the functioning of the protein and for infectivity of the virus (Griffin *et al.*, 2004). These residues are highly conserved, with only arginine or lysine ever present at these positions. Initial mutations generated in HCV RNA injected into chimpanzees found that these residues were required for infectivity *in vivo* (Sakai *et al.*, 2003). *In vitro*, mutation of both residues to alanine, K33A R35A, in J4 p7 abrogates p7 function and it was found to no longer form an integral membrane protein, as the mutant p7 could be dissociated from liposome membranes when washed with sodium bicarbonate (StGelais *et al.*, 2009).

The equivalent mutation in the JFH1 system, R33A R35A, was found to abolish the infectivity of the virus and cause a significant reduction in Core release, with no significant effects on genome replication. The double loop mutant did show a small recovery of virus infectivity when the infected cells were treated with the vATPase inhibitor Bafilomycin A, which raises endosomal pH and may partially compensate for the loss of p7 viroporin function (Wozniak *et al.*, 2010). The less-severe mutation R33Q R35Q also caused complete abrogation of both Core release and infectivity, and single mutations of each arginine residue displayed a significant drop of 1 $\log_{10}$ in the production of infectious virus (Jones *et al.*, 2007). However, mutation of the basic loop has also been shown to disrupt the processing of the downstream NS2 protein, indicating that the loss of viral infectivity as a result of these mutations may be due to the disruption of correct polyprotein processing, rather than a specific ion channel defect (Tedbury *et al.*, 2011).

1.5.2.4 Channel lumen

The nature of the p7 channel lumen dictates ion conductance, and specificity. Work in BLMs found that p7 has a high specificity for cations, with a relative conductance rate

11 times higher for cations than for anions (Montserret *et al*., 2010). Analysis of the channel pore identified a number of luminal residues affecting channel characteristics. The passage of cations through this pore is dependent on this local environment, with some residues possessing side-chains that protrude into the channel, restricting the flow of ions. Other residues, whether polar or hydrophobic in character, will affect the hydrophilicity of the pore and thus aid or hamper the passage of ions.

In vitro studies of the GT1B J4 p7 have included alanine mutations to all the residues thought to line the lumen of the pore. Of these mutations, S21A and C27A had only a minimal effect on channel activity, whereas mutation of H17 to alanine showed a significant drop in activity (StGelais *et al.*, 2009). It is worth noting, however, that GT1A H77 p7 does not show a loss in activity with the H17A mutation in the BLM system (Chew *et al.*, 2009).

The presence of H17 in the lumen of the channel has been demonstrated biochemically in the H77 isolate, through the use of copper ions to chelate the histidine residue and block ion flux through p7 in a BLM system (Chew *et al.*, 2009). Structural modelling *in silico* of p7 of other genotypes has also shown orientation of H17 to the channel lumen (Foster *et al*., 2011; StGelais *et al*., 2009). J4 p7 has been shown *in vitro* to have an increased level of activity in response to reduced pH (StGelais *et al.*, 2007).

While hydrophilic residues in the channel lumen are required for the conductance of aqueous ions, a number of hydrophobic residues are also present. Structural data from NMR experiments predict a constriction point at F25, where the large, hydrophobic side chain may form a barrier to the passage of ions forming part of a gating mechanism. This hypothesis is supported by mutational analysis of p7 where mutations F22, 25 and 26 to alanine, and the single F25A mutation, were shown to produce p7 channels with enhanced activity in liposome dye release assays (Foster *et*

al., 2011; StGelais *et al.*, 2009). The F25A mutant was later also found to confer resistance to iminosugar inhibitors (Foster *et al.*, 2011)

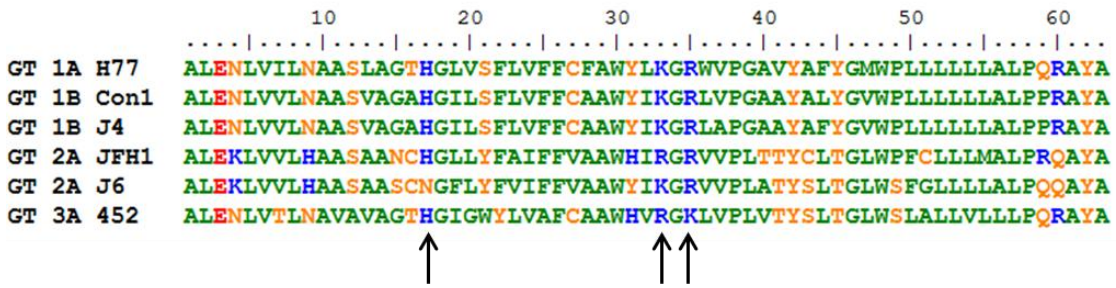

Figure 1.10 Inter-genotype sequence variation in p7

p7 amino acid sequence for 6 isolates from commonly used laboratory HCV strains; H77 from GT1A, Con1 and J4 from GT1B, JFH1 and J6 from GT2A and 452 from GT3A. Residues with hydrophobic side chains are shown in green, residues with polar side chains in orange, residues with charged acidic residues shown in red, and residues with charged basic side chains shown in blue. Black arrows indicate the frequent histidine at position 17, and the conserved basic residues arginine and lysine at positions 33 and 35.

1.5.2.5 Genotype variation

The primary sequence of p7 across HCV genotypes identifies a number of highly conserved residues (Fig 1.10). The N and C termini show a high degree of conservation, owing to the need to maintain the recognition sequence for signal peptidase cleavage of p7 from E2 and NS2. In many cases, the variations between genotypes show synonymous mutations, most commonly where hydrophobic residues are replaced with other hydrophobic residues. The two basic residues in the loop domain at positions 33 and 35 are interchangeable between arginine and lysine.

However, substitution of the hydrophobic residues, while not changing the overall hydrophobicity of the protein, may have other consequences. It has been shown that in genotype 1b HCV, the L20F mutation observed in clinical trials of the p7 inhibitor amantadine (Mihm *et al.*, 2006) was confirmed *in vitro* to confer resistance to adamantanes (Foster *et al.*, 2011). Similarly, an F25A mutation in GT1B J4 p7 and GT2A JFH1 p7 confers resistance to iminosugar inhibitors (Foster *et al.*, 2011). Thus, while synonymous mutations within and between genotypes may not significantly alter the biophysical properties of the protein, they can have significant effects on p7 drug sensitivity, representing sites of resistance mutations during drug treatment.

Other residues display notable differences between genotypes. Of particular interest are the residues hypothesised to play a role in p7 gating with particular focus on H17. This histidine residue may act as a pH sensor within the lumen of the channel, with its protonation state determining the open or closed state. While H17 is conserved between many HCV genotypes, it is not universal, with J6 p7 possessing an asparagine at this position. *In vitro* J6 p7 is less active than GT1B J4 p7, but when the structural proteins of J6 are substituted into the JFH1 virus system, the chimera shows the highest production of infectious virus of any HCV viral construct. Whilst sequence variation between J6 and JFH1 in other viral proteins exists, it is interesting

that the mutation of a conserved p7 residue does not significantly impact the infectivity of the virus.

1.5.2.6 Hypothesised gating mechanism

The gating mechanism for influenza A M2 viroporin has been well established, with a substantial amount of structural data available (Manor *et al.*, 2009; Huang *et al.*, 2008; Tang *et al.*, 2002). In brief, H37 of IAV M2 acts as a proton sensor, as histidine is unprotonated at neutral pH but becomes protonated at acidic pH, with a pKa of 6.5. Once protonated, the change in electrostatic potential of the channel results in a shift in the gating residue W41, this opens the channel to allow proton flux.

There are clearly a number of differences between M2 and p7. p7 is formed of 6 or 7 subunits with a second TMD to stabilise the oligomer, compared to M2 which has only 4 subunits with a single TMD span across the membrane. However, the increased activity of p7 in response to low pH (StGelais *et al.*, 2007) would indicate that some form of pH activation is taking place.

A similar motif to IAV M2, HXXX(W/Y) can be found in some HCV isolates. In IAV M2 these helix-adjacent residues act as the gating mechanism, with the protonation of H37 under acidic conditions causing a change in the electrostatic potential that causes a shift in the position of the gate residue W41 that opens the channel (Kass & Arkin, 2005). However, this motif is not universally conserved in HCV with many isolates having serine at position 21 (Meshkat *et al.*, 2009). (Fig. 1.10, Fig. 3.1).

1.5.2.7 Non-lumenal TMD residues

Mutagenesis of a number of other residues has also identified other important structural elements of p7. A conserved proline in TMD2, P49, introduces a kink in the helix. Mutation of this residue to alanine shows a slight reduction in channel activity at 5 μM compared with wild-type J4 p7, but when assayed at higher concentration shows much higher activity than WT J4 p7 (StGelais *et al.*, 2009).

A glycine, G39, near the start of TMD2, has also been mutated to alanine. This was found to cause a 60% reduction in channel activity (StGelais *et al.*, 2009). However, it is worth noting that this residue is only conserved within genotype 1, with other genotypes possessing a leucine at this position.

Alanine mutations targeting a series of leucines in TMD2, L50-55, also hypothesised to be involved in oligomerisation, caused only a slight reduction in channel activity, and conferred increased resistance to amantadine (StGelais *et al.*, 2009). This region shows some sequence divergence between J4 p7, with L50-55, and JFH1 p7, with FCLLLM, and so this poly-leucine motif may be required for amantadine binding.

1.5.3 Role of p7 in the virus lifecycle

1.5.3.1 Prevention of endosomal acidification during virus assembly and egress

The prototype viroporin, IAV M2, has two roles within the virus life cycle: it prevents acidification of cellular compartments during the maturation and assembly of the envelope glycoproteins HA and NA, and is incorporated into the virion where, on entry into a cell, it allows the influx of protons, a trigger allowing the virus to uncoat and release its genome to initiate replication. However, other viroporins have been shown to play differing roles in the virus lifecycle; viroporin 2B of poliovirus acts to destabilise the plasma membrane and thus aid the release of the unenveloped virion (Agirre *et al.*, 2002).

p7 has been shown to have a higher level of activity *in vitro* in response to reduced pH, but has also been shown to conduct other cations (Premkumar *et al.*, 2004). There was some doubt on the importance of p7 in the prevention of endosomal acidification in the HCV lifecycle as the mature virions, unlike IAV, are not inactivated by exposure to low pH. However, it has since been shown that nascent, intracellular HCV virions are sensitive to reduced pH. It was also shown that p7 is highly effective in preventing the acidification of endosomal compartments, and this effect could be

inhibited by the addition of p7 inhibitors. A p7 mutant deficient in virus production could be partially rescued by the addition of the endosomal vATPase inhibitor bafilomycin (Wozniak *et al.*, 2010).

The prototype viroporin IAV M2 is incorporated into virions, but many other viroporins are not. Studies using HCV pseudoparticles have shown that p7 is dispensable for HCV entry (Hsu *et al.*, 2003; Bartosch *et al.*, 2003b).

1.5.3.2 Non-viroporin activity

While the primary role of p7 in the virus lifecycle is likely to be the prevention of compartmental acidification during virus assembly and egress, it is known to interact with a number of other viral proteins independently of its viroporin activity. NS2, in particular, has been shown to be affected by alterations in p7, with its absence or mutation of the basic loop residues to alanine altering NS2 localisation. In GT1B, the culture adapted replicon FK5.1 was given the additional sequence of NS2, or p7-NS2 with the preceding signal peptide sequence from E2. In the absence of p7, the NS2 protein did not show the usual reticular staining pattern and was fully soluble in detergent, indicating decreased membrane association. NS2 also no longer interacted or localised with NS5A (Tedbury *et al.*, 2011).

p7 was also shown to strongly affect the localisation pattern of NS2 in different virus isolates. Interestingly, the change in NS2 localisation differed between wild-type JFH1 and the GT2A chimera Jc1 (Boson *et al*., 2011).

Other viral proteins shown to interact with p7, primarily by co-immunoprecipitation, include Core, E2, NS3 and NS5A (Popescu *et al.*, 2011). Thus, while p7 has been shown to not be required for replication, it may play a role in the switch between replication and assembly. As the majority of p7 distributes to the endoplasmic reticulum, where acidification of the compartment is not yet likely to have a significant impact on the infectivity of the resulting virions, its role early in the life cycle may be

the correct conformation and localisation of other viral proteins. The changes in lipid composition between different cellular compartments may also play a role in this functional switching between the activities of the protein (Whitfield *et al.*, 2011), although, as yet, any viroporin activity of p7 in the ER has not been demonstrated.

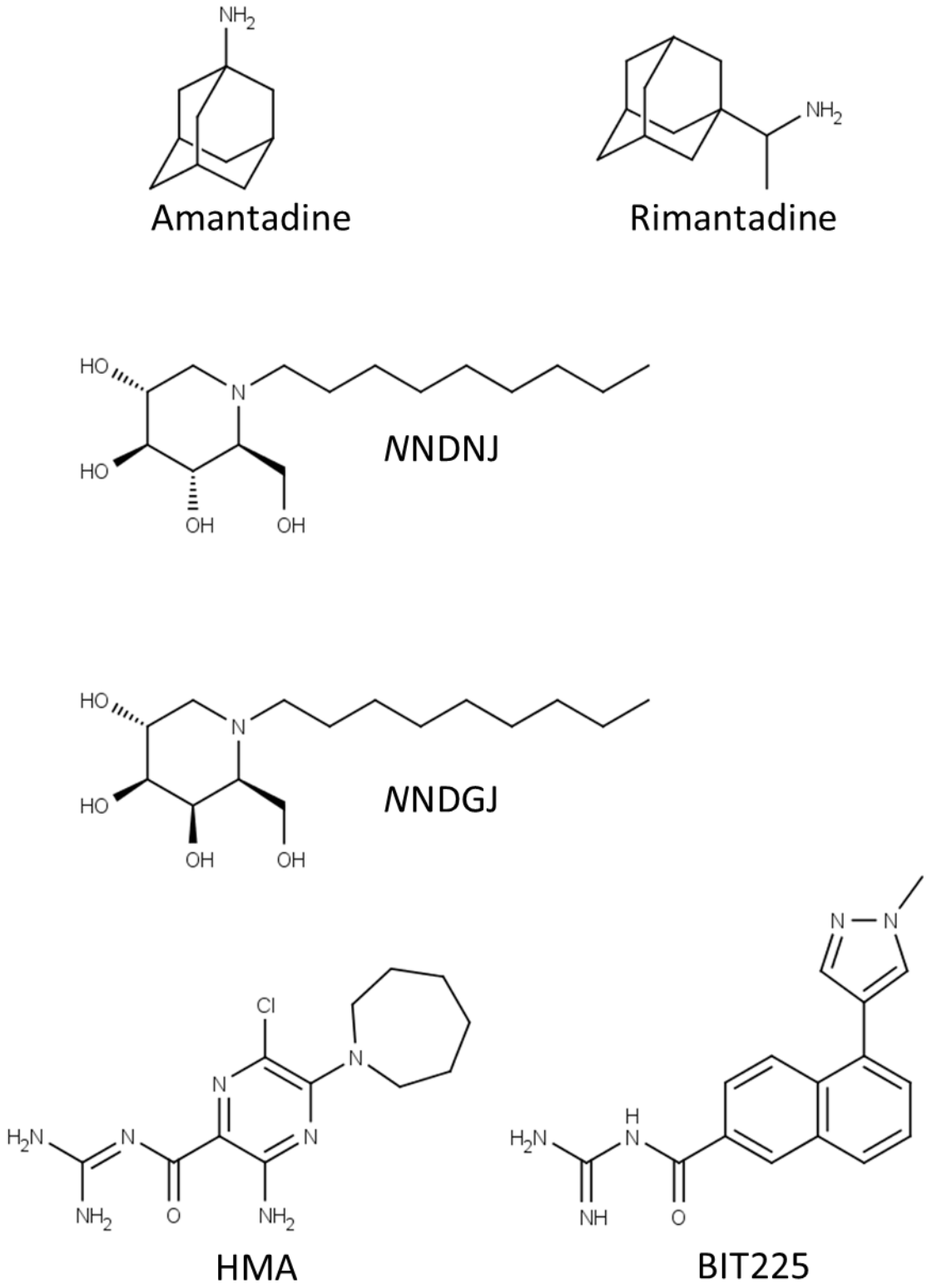

Figure 1.11 p7 inhibitor structures

Structures of the adamantanes amantadine and rimantadine, the iminosugars *N*-nonyl deoxynojirimycin (*N*NDNJ) and *N*-nonyl deoxygalactonojirimycin (*N*NDGJ), and the amilorides hexamethylene amiloride (HMA) and BIT225.

1.5.4 Inhibitors of p7

1.5.4.1 Adamantanes

The adamantanes, amantadine and rimantadine, are the oldest antiviral drugs and were originally developed against influenza virus (Wingfield *et al.*, 1969). The structures are shown in Fig. 1.11. A method was established to express tagged p7 in bacteria and purify it by reverse-phase high performance liquid chromatography (HPLC), allowing the initial studies of the function of p7 to be performed. The BLM studies showed that amantadine, an inhibitor of the prototype viroporin IAV M2, also inhibited p7 ion channel activity (Griffin *et al.*, 2003). Later studies found that another drug from the same family, rimantadine, was also effective (StGelais *et al.*, 2007).

The efficacy of the adamantanes varies between genotypes, both *in vitro* and in chimeras of the JFH1 virus. GT1b J4 p7 showed sensitivity to both amantadine and rimantadine, while JFH1 showed resistance to amantadine but was still sensitive to rimantadine. GT1A H77 p7 showed lower sensitivity to both adamantanes (Griffin *et al.*, 2008).

Clinical trials using these drugs observed few anti-viral effects. This may be due to a number of factors: amantadine was the most commonly used adamantane in trials but has been shown *in vitro* to be less effective against GT2A p7, and the use of a single virus-specific drug in combination with IFN/Rib treatment is likely to result in rapid escape mutations as observed with HIV monotherapy, prior to the advent of highly active antiretroviral drug therapy (HAART). A possible escape mutation, L20F, in GT1B was identified during one such clinical trial with amantadine (Mihm *et al.*, 2006).

In silico modelling identified a putative adamantane binding site in the pore of p7 (Patargias *et al.*, 2006), similar to a previously identified site in IAV M2 (Cady *et al.*, 2010). Later work from more detailed oligomer computer models based on the known monomer structure identified a second site with a higher predicted binding affinity, this

time in the membrane side of the channel, comprising a leucine-rich binding pocket. When the L20F mutation was modelled into this pocket, a reduction in the predicted binding efficiency of adamantine was observed. Subsequent analysis using bacterially expressed protein in NMR experiments to measure changes in rimantadine binding found that the L20F mutant showed no shift that would indicate drug binding, and so it is likely that this mutation blocks rimantadine binding (Foster *et al.*, 2011). Recent work developing compounds to bind to this leucine-rich pocket has identified a number of potential leads that can possibly overcome the L20F escape mutation (Foster *et al*., 2011).

1.5.4.2 Iminosugars

Chemically synthesised GT1A H77 p7 in the BLM system was used to identify a new family of p7 inhibitors, the iminosugars n-nonyl deoxynojirimycin (*N*NDNJ) and n-nonyl deoxygalactonojirimycin (*N*NDGJ) (Pavlović *et al.*, 2003). The structure of the iminosugars includes a long alkyl-chain that is thought to intercalate between monomers and prevent the formation of a functioning channel, shown in Fig. 1.11. NNDNJ has been shown to prevent oligomerisation of GT1B p7 in DHPC (Foster *et al.*, 2011).

Iminosugars also display different levels of activity against different genotypes, with genotype 3A showing the least sensitivity to the drug (Griffin *et al.*, 2008). A comparison of the sequence variation between the genotypes identified a possible resistance polymorphism at position 25, where genotype 3a had an alanine instead of phenylalanine. Further investigation of this polymorphism through introducing the F25A mutation into JFH1 found that this mutation was sufficient to confer iminosugar resistance, with only a minimal effect on the production of infectious virus observed (Foster *et al.*, 2011).

1.5.4.3 Amilorides

Hexamethylene amiloride (HMA) has been shown to block p7 activity *in vitro* in BLMs (Premkumar *et al.*, 2004) and in the liposome system. However, at concentrations inhibitory to p7 function, HMA showed cytotoxic effects meaning its effects on JFH1 could not be assessed (S. Griffin, unpublished observations).

The amiloride analogue BIT225 was identified from a pool of antiviral compounds using a bacterial survival assay, where p7 expression is induced in bacteria in the presence of potential inhibitors. As p7 expression in bacterial cells results in cell lysis, inhibitors can be identified by an increase in cell survival times. BIT225 was then tested for p7 inhibition in planar lipid bilayers, and was found to efficiently inhibit ion channel activity. It also displayed good antiviral activity against the HCV-related BVDV (Luscombe *et al.*, 2010). The structures of both amiloride compounds are shown in Fig. 1.11.

1.6 Aims of this project

Genotype variations have been shown to affect the activity and inhibitor sensitivity of p7. This project sought to answer the question of how patient-derived, naturally occurring p7 polymorphisms within a single genotype affected p7 activity, drug resistance and the production of infectious virus. A number of methods were used to answer this question: previously characterised *in vitro* liposome based dye release assays, cloning of the p7 sequences into a chimeric virus to investigate the effects on the production of infectious virus, and the development of cell-based assays to study the effect of p7 on cellular endosomal pH.

Chapter 2: Materials and methods

2.1 Antibodies:

Primary Antibody	Supplier	Monoclonal/ polyclonal	Species	Experimental Dilution
1055 terminal bleed serum	Custom, Glaxo-Smith-Kline	Polyclonal	Rabbit	1:7000
2716	In-house	Polyclonal	Rabbit	1:1000
FLAG	Sigma-Aldrich	Monoclonal	Mouse	1:20,000
GST	Serotec	Monoclonal	Mouse	1:1000
NS5A	In house	Polyclonal	Sheep	1:5000
Core	In house	Polyclonal	Sheep	1:5000
NS2	Dr. G Haqshenas, Monash University	Polyclonal	Rabbit	1:5000
AP33 (E2)	Dr. A. Patel, University of Glasgow	Monoclonal	Mouse	1:2000
AB8245 (GAPDH)	Abcam	Monoclonal	Mouse	1:30,000

Table 2.1 Primary antibodies

Secondary antibody	Supplier	Monoclonal/ polyclonal	Species	Experimental Dilution
Anti-mouse HRP linked	Sigma-Aldrich	Polyclonal	Goat	1:10,000
Anti-rabbit HRP linked	Sigma-Aldrich	Polyclonal	Goat	1:10,000
Anti-sheep HRP linked	Sigma-Aldrich	Polyclonal	Donkey	1:10,000
Alexa-Fluor 594 anti-sheep	Invitrogen	Polyclonal	Donkey	1:500

Table 2.2 Secondary antibodies

2.2 Bacterial culture methods

2.2.1 Bacterial strains

Escherichia coli DH5α Genotype: F-, *Φ80dlacZΔM15*, *endA1*, *recA*, *hsdA1*, (r_k^-, m_k^+), *supE44*, *thi1*, *deoR*, *gyrA96*, *relA1*, (ΔlacZYA-argF), U169, λ-, were purchased from Life Technologies Inc. *Escherichia coli* BL21-(DE3) Genotype: F-, *ompT*, *hsdSB*, (r-, mB-), *gal*, *dcm*, (DE3), were purchased from Novagen Ltd.

All bacterial cultures were grown in Luria-Bertani (LB) broth (10 g/L NaCl, 5 g/L yeast extract, 10 g/L tryptone, pH 7.5), supplemented with 100 µg/ml ampicillin or 50 µg/ml kanamycin where appropriate. For bacterial colony production, agar was supplemented with the appropriate selection antibiotic, poured onto single-vented plates and stored at 4 °C until required. Bacteria were plated out or streaked onto the agar and incubated overnight at 37 °C unless otherwise stated.

2.2.2 Plasmids

pGEX-6P-1 (GE Healthcare) was used for the expression of GST-FLAG-p7 fusion proteins in BL21 DE3 cells, and carries an ampicillin resistance marker. pET24a containing histidine-tagged human rhinovirus serotype 14 3C protease was supplied by Arie Geerlof, University of Oxford, and carries a kanamycin resistance marker.

The JFH1 full length virus construct was supplied by Dr Takaji Wakita, National Institute of Infectious Diseases, Tokyo, Japan, (Wakita *et al.*, 2005) and carries an ampicillin resistance marker. The H77/JFH1 chimera HJ3-5 was supplied by Prof. Stanley Lemon, University of North Carolina, USA, (Yi *et al.*, 2007) and carries an ampicillin resistance marker.

pCDNA3.1+ (Invitrogen) carries an ampicillin resistance marker.

pLXV-IRES-mCherry (Clontech) containing IAV M2 and IAV M2 (A30P) were supplied by Ann Wozniak, University of Kansas, USA (Wozniak *et al.*, 2010) and carry an ampicillin resistance marker.

VAMP-pHluorin was originally constructed by Prof. Gero Miesenbock (Miesenbock *et al.*, 1998), University of Oxford, and was supplied by Dr Jonathan Lippiat, University of Leeds.

The subgenomic replicon FK5.1 was originally supplied by Prof. Ralf Bartenschlager, University of Heidelberg, and cloning of NS2 and SPp7-NS2 into this replicon was

performed by Dr. Phillip Tedbury, University of Leeds. Cloning of the JFH1 replicons was also performed by Dr. Tedbury. All contain an ampicillin resistance marker.

pBF+ is an amphibian expression vector containing the 5' and 3' UTRs of the *Xenopus* β-globin gene flanking the multiple cloning site. It was supplied by Dr Jonathan Lippiat, University of Leeds, and carries an ampicillin resistance marker.

2.2.3 Preparation of competent bacterial cells

Cells were prepared according to the Inoe method (Sambrook *et al.*, 1989). Bacterial cultures (250 ml) were grown overnight at 18 °C. Once the cells reached an optical density of 0.55 at OD_{600nm} they were harvested at 6000 xg and resuspended in 80 ml of ice-cold Inoe transformation buffer (55 mM $MnCl_2$, 15 mM $CaCl_2$, 250 mM KCl, 10 mM PIPES (pH 6.7)). The bacteria were pelleted again by centrifugation and resuspended by swirling in 20 ml of ice-cold Inoe transformation buffer. DMSO (1.5 ml) was added and the culture aliquoted and snap-frozen in liquid nitrogen. Competent bacteria were stored at -80 °C.

2.2.4 Transformation of bacterial cultures

For each transformation, 100 µl of competent cells were thawed on ice, added to 10–50 ng of DNA and gently mixed and incubated on ice for 30 minutes. The cells were transferred to a 42 ˚C water bath for 45 seconds (heat shocked) and placed on ice for a further 1 minute. LB medium (100 µl) was then added to the cells and they were placed in a 37 ˚C shaking incubator for 1 hour. The cells were plated onto pre-warmed 2YT-agar plates (containing appropriate selection antibiotics) with a sterile glass spreader. The inoculated plates were placed in a 37 ˚C incubator and grown overnight.

2.2.5 Preparation of bacterial cultures for protein expression:

A single colony was picked from freshly transformed BL21 cells and a 5 ml culture grown overnight in LB broth containing the appropriate antibiotic (100 µg/ml ampicillin or 50 µg/ml kanamycin). Overnight cultures were diluted 1:100 into 400 ml LB broth

and grown at 30 °C in a shaking incubator at 180 rpm until the OD_{600} reached 0.6, at which point a 1 ml pre-induction sample was taken for reference. IPTG was then added to the bacterial culture to a final concentration of 1 mM and cells incubated for a further 4 hrs. A second, post induction sample was taken prior to harvesting at 4 hrs and the OD normalised to that of the pre-induction sample. Cells were pelleted at 6000 xg for 15 minutes and the supernatant removed. Bacterial pellets were either immediately progressed to the lysis and inclusion body prep or resuspended in 5 ml PBS and frozen at -20 °C for later use. The pre and post induction reference samples were run on SDS-PAGE gels and coomassie-stained to visualise protein expression.

2.3 DNA methods

2.3.1 Polymerase chain reaction (PCR)

2.3.1.1 Primers

Oligonucleotide primers were designed with a minimum of 15 complementary bases to the sequence to be amplified. Any additional desired sequence (FLAG-tag, restriction endonuclease cleavage sites etc.) were added to the design. Primers were ordered from either MWG or Sigma-Aldrich and dissolved in dH_2O to a concentration of 100 pmol/µl and stored at -20 °C.

2.3.1.2 Cloning PCR

Polymerase chain reaction (PCR) was performed using Pfu Turbo (Stratagene) according to the manufacturer's instructions. Reactions were assembled in thin-walled 0.1 ml PCR tubes with the following: 5 µl 10x Pfu buffer (200 mM Tris-HCl (pH 8.8), 20 mM $MgSO_4$, 100 mM KCl, 100 mM $(NH_4)_2SO_4$, 1% Triton X-100, 1 mg/ml nuclease-free BSA), 0.5 µl of a dNTP mix (25 mM 2'-deoxyadenosine 5'-triphosphate, 25 mM 2'-deoxycytidine 5'-triphosphate, 25 mM 2'-deoxyguanosine 5'-triphosphate, 25 mM 2'-deoxythymidine 5'-triphosphate), 10-20 ng template DNA, 50 pmol of each primer (see primer sequences in Appendix 1), 1.25 units of Pfu Turbo polymerase,

and an appropriate volume of dH_2O to give a total volume of 50 µl. Thermocycling reactions were set for 2 minutes of denaturation at 90 °C, followed by 10 cycles of denaturation (90 °C, 1 minute), annealing (45 °C, 1 minute) and elongation (70 °C, 1 minute per kb), followed by another 20 cycles with the annealing temperature raised to 55 °C, and a final elongation step of 72 °C for 1 minute. The PCR product was assessed by gel electrophoresis and purified by phenol-chloroform extraction.

2.3.1.3 Overlap PCR

Overlap PCR was used during virus cloning to extend beyond the p7 sequence to a suitable restriction endonuclease site. Chimeric primers incorporating the terminal sequence of p7 and the start of the H77 NS2 sequence were used to generate PCR products, which were purified and combined in a 1:1 molar ratio for the second round of PCR, with 5' and 3' primers added. The full length product for virus cloning was then analysed by gel electrophoresis to verify the desired length, before continuation of the cloning.

2.3.1.4 Colony screening PCR

Colony screening PCR was performed to screen for bacterial colonies following transformation. A reaction mixture of 10X ThermoPol buffer (20 mM Tris-HCl (pH 8.8), 10 mM $(NH_4)_2SO_4$, 10 mM KCl, 2 mM $MgSO_4$, 0.1% TritonX100) (NEB), 50 pmol of each primer, dNTPs to the same concentration as the cloning-PCR reactions, 1.25 units of Taq polymerase (NEB) and dH_2O was made up to 50 µl in thin-walled 0.1 ml PCR tubes. Single colonies were picked and inoculated onto agar plates containing suitable antibiotic and then pipetted up and down in the PCR reaction mixture. Thermocycler reactions were set up with an initial denaturation step (90 °C, 1 minute), followed by 30 cycles of denaturation (90 °C, 45 seconds), annealing (45 °C, 45 seconds) and elongation (72 °C, 0.5 minute per kb), with a final elongation step (72 °C, 1 minute). Products were analysed by gel electrophoresis.

2.3.2 Phenol-chloroform extraction of DNA

This method was used for removal of protein contamination from DNA samples, which can potentially interfere with DNA modification or transfection experiments. PCR products were made up to a volume of 200 µl and then thoroughly mixed with an equal volume of phenol-chloroform isoamyl alcohol 25:24:1 (v/v) (Sigma Aldrich) pH 8.0. This was centrifuged (16,000 xg, 10 minutes) and the upper, aqueous layer carefully transferred to a fresh tube avoiding the protein interface. An equal volume of chloroform was added, and centrifuged as above. The aqueous layer was then transferred to a fresh tube and 0.1 volumes of 3M sodium acetate (pH 5.2) and 2.5 volumes absolute ethanol added. The mixture was then incubated at -80 ˚C for 30 minutes, and the DNA pelleted by centrifugation, washed with ice-cold 70% ethanol and dried. The DNA pellet was then dissolved in dH_2O and the DNA quality examined by agarose gel electrophoresis.

2.3.3 Determination of DNA concentrations

DNA concentration was determined by absorbance at 260 nm on a Nanodrop (Thermo-Scientific), with absorbance at 280 nm also measured to detect any protein impurities in the DNA preparation.

2.3.4 Restriction endonuclease digestion

Restriction digests were carried out using NEB restriction endonucleases with the exception of MauBI (Fermentas). Reactions were set up according to the manufacturer's instructions, with a minimum of 1 unit of enzyme per 1 µg of DNA. Screening digests were performed for 1 hr at 37 °C, and digests for cloning ligations for 16 hr.

2.3.5 TAE Agarose gel electrophoresis

Agarose powder was diluted into 1 X TAE buffer (40 mM Tris, 40 mM glacial acetic acid, 1 mM EDTA, pH 8) at 0.5% (w/v) for large plasmids, or 2% (w/v) for small PCR

or restriction digest fragments. The agarose mixture was heated until dissolved, and allowed to cool before the addition of 0.5 µg/ml ethidium bromide. The gels were poured into the casting mould (Biorad); well combs inserted and allowed to set. The gel was placed in the running tank (Biorad) and immersed in 1 X TAE buffer. DNA samples were mixed with Orange-G loading buffer (5% glycerol (v/v), 1 mM EDTA, 0.01% Orange G, 1 X TAE) and loaded into the wells. Electrophoresis was performed at 8 V/cm until the Orange G dye-front migrated to the end of the gel. Hyperladder I (Bioline) size markers were used to estimate the size of DNA fragments. DNA was imaged on a UV-transilluminator (Syngene).

2.3.6 Gel-extraction of DNA fragments

DNA bands were excised from agarose gels and placed in a 1.5 ml microcentrifuge tube. The DNA was extracted by freeze thawing and mashing the gel slice using a sterile pipette tip. An equal w/v of phenol (pH 8) (Sigma-Aldrich) was added and the sample vortexed for 1 min. The samples were then frozen at -80 °C for 20 minutes then thawed at 37 °C for 1 min, then centrifuged at 16,000 xg for 20 minutes. The top aqueous phase was then transferred to a fresh microcentrifuge tube and ethanol precipitated as described in section 2.3.2.

2.3.7 Ligation

T4 DNA Ligase (Invitrogen) was used for all DNA ligations. Estimations of the quantity of vector and insert DNAs were made from the intensity of bands upon agarose gel electrophoresis by comparison with standard DNA markers. Typical ligation reactions comprised a 3:1 molar ratio of vector: insert DNA in 1X T4 ligase buffer with 1 unit of ligase. The reaction was performed overnight at 14 °C. The ligation mix was then transformed into DH5α *E. coli*, plated on agar plates containing appropriate selective antibiotic and resulting colonies screened for the presence of insert by either colony PCR or restriction endonuclease digestion of the purified plasmid.

2.3.8 Small-scale preparation of plasmid DNA

DNA for screening analysis was prepared using the alkaline lysis method (Sambrook *et al.*, 1989). Single colonies were picked and grown in 5 ml of LB broth, containing the appropriate antibiotic overnight at 37 °C. Cultures were pelleted at 4000 xg and the supernatant removed.

Bacterial pellets were resuspended in 100 µl of solution 1 (50 mM Tris HCl (pH 8.0), 50 mM glucose, 10 mM EDTA), then lysed with 100 µl of solution 2 (0.2 M sodium hydroxide, 1% (w/v) SDS) and incubated for 5 min. The lysis reaction was terminated and cellular debris precipitated by the addition of solution 3 (3 M potassium acetate (pH 5.2)), and the sample centrifuged at 16,000 xg for 5 minutes to remove the precipitate. The aqueous solution was then transferred to a fresh tube and the DNA ethanol-precipitated, air-dried and resuspended in an appropriate volume of dH_2O.

DNA for sequencing was prepared using the Qiagen Spin Miniprep kit according to the manufacturer's protocol. Bacterial pellets were resuspended in 250 µl of buffer P1, lysed with 250 µl of buffer P2 and neutralised in 350 µl of buffer N3. The reactions were centrifuged at 16,000 xg for 10 minutes to pellet the precipitates and the supernatants loaded onto Qiagen spin columns. The DNA was then washed with buffers PB and PE before elution with dH_2O. The isolated DNA was diluted to a concentration of 50 ng/µl and sequenced by GATC Biotech.

2.3.9 Large-scale preparation of plasmid DNA

Larger quantities of DNA were prepared using Qiagen Midi- or Maxi-prep kits according to the manufacturer's instructions. For midipreps, 50 ml of LB broth containing the appropriate antibiotic were inoculated with a single colony and incubated overnight at 37 °C in a rotary shaker. For maxipreps, 250 ml cultures were inoculated with a 5 ml overnight starter culture picked from a single colony and grown for 10 hours. Bacteria were pelleted at 6000 xg. The bacterial pellets were

resuspended in an appropriate volume of buffer P1, and lysed in buffer P2 at room temperature for 5 min. Chilled buffer P3 was then added to neutralise the reaction, and the plasmid preps incubated on ice for 15-20 min. The precipitate was pelleted by centrifugation at 21,000 xg for 30 min, and transferred to a fresh tube and centrifuged as above. Qiagen-tips were equilibrated with buffer QBT and the lysates loaded. The column-bound DNA was then washed twice with buffer QC before elution with buffer QF. An appropriate volume of isopropanol was added and precipitated DNA was pelleted by centrifugation at 4000 xg for 1hr at 4°C. The pellet was washed with 70% ethanol, air-dried, and dissolved in dH_2O.

2.4 Protein purification

2.4.1 Preparation of 3C protease:

pET24a containing His-tagged 3C protease from rhinovirus was a kind gift from Arie Geerlof (University of Oxford). Bacteria were transformed and a 5 ml overnight culture inoculated (1:100) into a 400 ml culture in a shaking incubator at 37 °C until an OD_{600} of 0.6 was achieved. Protein expression was induced with 1 mM IPTG for 4 hours and cells harvested by centrifugation at 6000 xg. Bacterial pellets were resuspended in lysis buffer (PBS supplemented with protease inhibitors Aprotinin, Leupeptin, Pepstatin A and AESBF (Pefabloc)) and sonicated on ice for 20 seconds with 20 seconds rest, for 10 cycles. The lysates were cleared by centrifugation at 21,000 xg and the supernatant filtered through a 0.45 micron filter (Millipore). A HiTrap column (GE Healthcare Lifesciences) was charged with nickel and equilibrated with Buffer A (20 mM Na_3PO_4 (pH 8), 0.5 M NaCl, 10 mM imidazole) prior to loading the protein. The filtered supernatant was loaded onto the column and washed with buffer A, with all flow through from the column stored for analysis. The protein was then eluted in Buffer B (20 mM Na_3PO_4, 0.5 M NaCl) with increasing concentrations of imidazole (0.1 M- 0.5 M) and 1 ml stored at each step. Samples from each flow-through, wash

and elution step were analysed by SDS-PAGE followed by coomassie staining. Elution fractions containing the desired protein band were pooled and dialysed into 4 L of storage solution (50 mM Tris-Cl (pH 8), 150 mM NaCl, 10mM EDTA, 1 mM DTT, 20% glycerol) at 4 °C. The dialysis solution was changed once and left at 4 °C overnight. The dialysed protein was then aliquoted and frozen at -80 °C until use.

2.4.2 Expression of GST-fusion constructs

GST-FLAG-p7 plasmids were transformed into BL21 *E. coli* and a single colony grown in a 5 ml overnight starter culture. This starter culture was diluted (1:100) into 400 ml of LB and incubated in a shaking incubator at 30 °C until an OD_{600} of 0.6 was achieved. A 1 ml sample of the uninduced bacterial culture was taken for analysis. Protein expression was induced by the addition of 1 mM IPTG and the culture incubated with shaking at 30 °C for a further 4 hrs. A further 1 ml sample of the bacterial culture was taken and the concentration by OD_{600} normalised to that of the pre-induction sample. The bacterial culture was harvested by centrifugation at 6000 xg for 15 min, the supernatant removed and the bacterial pellet either stored at -20 °C until use or directly progressed to French Press lysis and inclusion body preparation.

2.4.3 French Pressure Cell lysis of bacterial cells:

Bacterial pellets were resuspended in a total volume of 30 ml lysis buffer (PBS supplemented with protease inhibitors: leupeptin 1 µg/ml, pepstatin A 1 µg/ml, aprotinin 2 µg/ml, 0.2 mM AEBSF (Pefabloc), 1 mM EDTA). The French Pressure Cell (Thermo-Fisher Scientific) was chilled at 4 °C and the bacterial solution placed in the chamber. The lysate was subjected to a piston pressure of 1000 psi, equivalent to an internal shear pressure around the valve of 40,000 psi. The lysate was passed through the French Press twice and stored on ice after lysis. A 50 µl sample of the lysate was taken for SDS-PAGE analysis.

2.4.4 Inclusion body preparation and cleavage

The inclusion bodies were pelleted at 3300 xg for 45 min, and the supernatant decanted and stored. The pellet was then resuspended in 100 mM ammonium acetate, and the inclusion bodies pelleted at 3300 xg for 15 minutes and a sample of the supernatant stored. The inclusion body pellets were then washed in Tris-NaCl (50 mM Tris, 150 mM NaCl, pH 7) and pelleted as above. The inclusion bodies were resuspended in cleavage buffer (50 mM Tris, 150 mM NaCl, 1 mM DTT, 1 mM EDTA, pH 7) and a pre-cleavage sample stored for analysis. 3C protease was then added (volume added dependent on the activity of the batch of 3C protease) and the cleavage reaction incubated on a rotating disc overnight at 4 °C. The following morning, a sample of the cleavage reaction was stored and the inclusion bodies pelleted again for 15 minutes at 3300 xg. A sample of the supernatant was also taken at this stage. The pellets were resuspended in Tris-NaCl (50 mM Tris, 150 mM NaCl, pH 7) to a small total volume (typically 4 ml) and solubilised by the addition of 10% solution N-lauroylsarcosine (Aldrich) in Tris-NaCl (50 mM Tris, 150 mM NaCl, pH 7) to a final concentration of 0.5%. The solubilised protein was cleared of any remaining insoluble matter by centrifugation at 16,000 xg. The supernatant was then transferred to a High Performance Liquid Chromatography (HPLC) loading vial and stored at 4 °C. Reference samples taken throughout the bacterial lysis, inclusion body preparation and cleavage steps were analysed by SDS-PAGE to ensure that the protein had been purified and cleaved as expected.

2.4.5 High Performance Liquid Chromatography (HPLC)

Reverse-phase HPLC was carried out on a Dionex HPLC system incorporating a PDA-100 photodiode array detection unit, an ASI-100 automated sample injector, a P680 HPLC pump and an automated fraction collector. Reverse phase buffers were made up as follows: Buffer A 95% H_2O, 5% acetonitrile, 0.1% trifluoroacetic acid (TFA); Buffer B 20% H_2O, 80% acetonitrile, 0.1% TFA. The buffers were filtered

through a 0.1 micron Nalgene filter prior to loading onto the HPLC system. The HPLC columns used, either a Phenomenex Jupiter C4 300 Å 10 mm x 250 mm or 30 mm x 250 mm, were equilibrated into Buffer A. The solubilised protein was placed in the autosampler. Gradients were run by increasing the percentage of Buffer B from 0-55% over the first 3 minutes, then from 55-80% from minutes 3-30, then 80-100% for minutes 30-31, staying at 100% for minutes 31-35, returning back to 0% buffer B for minutes 35-40 and running at 0% buffer B for minutes 40-45 in order to re-equilibrate the column in preparation for the next run. If particular proteins showed poor peak separation with this programme, the programme was altered to extend the gradient during the peak separation stages. Spectroscopy for the column eluents was read at wavelengths of 215 nm and 280 nm, to detect peptide bonds and side chain absorbance respectively. Each protein peak detected in the HPLC eluent was collected during the first run, after which only the region in which the p7 peak eluted was collected. 100 µl samples were taken from the peak fractions and dried in a Genvac rotary evaporator overnight. The samples were run on SDS-PAGE and assessed by western blot analysis to ensure separation of the peak fractions.

2.4.6 Determination of purified FLAG-p7 concentration by A_{280} absorption in methanol

Purified FLAG-p7 was dissolved in methanol and the absorbance (A_{280}) measured in a spectrophotomer using quartz cuvettes. The concentration was determined using the Beer-Lambert equation, where:

$$A = \varepsilon c l$$

The absorbance A, at A_{280}, is the product of the extinction coefficient ε, the concentration in moles per litre, c, and the length of the path through which the light travelled (the width of the cuvette, 1 cm), l. The extinction coefficient was calculated for each p7 protein purified using the ProtParam tool on the ExPASy Bioinformatics

Resource Portal, provided by the Swiss Institute for Bioinformatics (www.expasy.com). The coefficients are shown in Table 3.2.

2.4.7 Tris-Glycine Polyacrylamide Gel Electrophoresis:

All SDS-PAGE work was carried out using the BioRad Mini-Protean II system. 30% acrylamide was purchased from VWR International. Tris-glycine gels were prepared to the following recipes: 12-15% (v/v) acrylamide, 0.35M Tris-Cl pH 8.8, 0.5% (w/v) SDS, 0.1% (w/v) APS, 0.2% (v/v) TEMED. The plates were assembled and gels poured to three quarters of the height of the front plate and a layer of water saturated butanol added to ensure that the surface of the resolving gel was level. Once the resolving gel had polymerised, the butanol was removed and the surface washed with distilled water. The stacking gel was made to the following recipe: 5% acrylamide (v/v), 0.175 M Tris pH 6.8, 0.2% (w/v) SDS, 0.7% (w/v) APS, 0.36% (v/v) TEMED. The stacking gel was poured into the top of the plates and combs (10 or 15 wells) inserted. Protein samples were denatured in 2X Laemmli buffer (100 mM Tris-Cl pH 6.8, 4% (w/v) SDS, 15% (v/v) glycerol, 10 mM DTT, 0.01% (w/v) Bromophenol blue) and heated for 5 minutes at 95 °C.

2.4.8 Tris-Tricine Polyacrylamide Gel Electrophoresis:

Tris-tricine gels were made to the following concentrations: Resolving gel 10% acrylamide, 1 M Tris pH 8.45, 10.5% glycerol, 0.1% SDS (w/v), 0.06% APS, 0.13% (v/v) TEMED. Stacking gel: 4% acrylamide, 0.75 M Tris-Cl pH 8.45, 0.75% SDS (w/v), 0.6% APS (w/v), 0.3% TEMED (v/v). Cathode buffer (0.1 M tricine, 0.1 M Tris, 0.1% SDS) was poured into the top tank, and anode buffer (0.2 M Tris-Cl, pH 8.9) added to the bottom tank. Samples were denatured as above and gels were run at 100 V for 100 minutes until the dye front reached the bottom of the gel.

2.4.9 Coomassie staining of SDS-PAGE gels:

SDS-PAGE gels were soaked in Coomassie stain (0.1% (w/v) Coomassie Brilliant Blue, 10% (v/v) acetic acid, 45% (v/v) methanol, 45% (v/v) H_2O) for a minimum of 1 hr. Excess stain was removed by soaking in destain solution (10% (v/v) acetic acid, 45% (v/v) methanol, 45% (v/v) H_2O) for a minimum of one hour until protein bands were visible.

2.4.10 Western Blotting:

Proteins from SDS-PAGE gels were transferred to Polyvinylidene fluoride (PVDF) membranes using a semi-dry transfer unit. PVDF was activated by soaking in methanol, and blotting paper was soaked in transfer buffer (25 mM Tris, 192 mM glycine, 20% methanol (v/v)) and rolled to remove residual trapped air. PVDF was placed on top of one sheet of blotting paper and each gel placed on the PVDF, making sure no air was trapped between the layers. The second layer of blotting paper was placed on top and the sandwich pressed to remove trapped air. The transfer rig was set at 15 V for one hour, with a maximal current of 500 mA. PVDF membranes were then removed and blocked in 10% dried skimmed milk (w/v) in TBS-T (Tris-buffered saline, 0.1% Tween-20) for one hour on a rotary shaker at room temperature. The blots were then placed in 5% skimmed milk in TBS-T with the appropriate primary antibody (see section 2.1) and labelled overnight at 4 °C on a rotary shaker. Membranes were then washed for 5-10 minutes in TBS-T three times and labelled with the appropriate HRP conjugated secondary antibody in 5% skimmed milk in TBS-T for one hour at room temperature. The membranes were washed four times in TBS-T. ECL solution was prepared by mixing equal volumes of ECL 1 (100 mM Tris-Cl pH 8.5, 0.3 mM p-coumaric acid and 25 mM luminol) and ECL 2 (100 mM Tris-Cl pH 8.5 and 0.01% H_2O_2). 1 ml of ECL solution was added to each membrane. When blots showed weak staining with standard ECL solutions, ECL Plus (GE Healthcare) was used as per the manufacturer's instructions. Excess ECL was

removed by rinsing in dH_2O and the membranes sealed in clear plastic. Membranes were exposed to photographic film under darkroom conditions and developed using a Konica SR0101 processor.

2.5 *In vitro* liposome assays

2.5.1 Liposome preparation

Liposomes were prepared as described previously (StGelais *et al.*, 2007). Carboxyfluorescein buffer (50 mM 5(6)-carboxyfluorescein, 10 mM HEPES, 10 mM NaCl, 134 mM NaOH), while stated to be pH 7.4 in the original buffer recipe (Rex & Schwarz, 1998), when tested was found to be pH 7.0. Phosphatidic acid (PA, 10 mg/ml), phosphatidylcholine (PC, 10 mg/ml) and rhodamine-labelled phosphatidylethanolamine (rPE, 1 mg/ml) in chloroform solution were purchased from Avanti Polar Lipids and stored at -20 °C. Lipids were pipetted into a glass test tube using glass syringes (Hamilton Ltd.) with 1:1 ratio of PA: PC to a total of 1 mg of lipid with 5 µg of rPE as a label. The lipids were dried into a film on the bottom of the test tube and further dried under vacuum for 2 hrs. The lipids were then resuspended in carboxyfluorescein buffer, the tube filled with argon, sealed with parafilm, and resuspended by vigorous shaking at room temperature overnight.

The lipid suspension was extruded using an Avanti Polar Lipids extrusion kit, using 0.4 µm pore size filters. The extruder was warmed to 37 °C and the extrusion performed at this temperature. A 5 µl sample of the lipid suspension was taken and stored for later comparison. The lipid suspension was passed through the filter a minimum of 15 times. The liposome mixture was added to a 2 ml ultracentrifuge tube and the liposomes pelleted at 100,000 xg for 15 minutes. The supernatant was then removed and the pellet resuspended in assay buffer (107 mM NaCl, 10 mM HEPES, pH 7.4), and centrifuged as above. The wash step was repeated a further 2 times to

remove any unincorporated carboxyfluorescein. After the final spin, the liposome pellet was resuspended in 0.5 ml of assay buffer and the rhodamine absorbance compared with the pre-extrusion sample. The concentration of the liposomes was calculated as a proportion of the total lipid remaining after extrusion. Liposomes were stored at 4 °C.

2.5.2 Real-time dye-release assay

The liposomes were diluted in assay buffer in a 96-well black fluorescence plate (Greiner Bio One) to a final concentration of 50 μM. Purified p7 protein was resuspended in methanol and added to wells to no greater than 5% methanol (v/v). The pore-forming bee-venom peptide melittin was included as a positive control, and total dye release induced with the addition of 0.5% Triton X100 (v/v). The release of carboxyfluorescein was measured using a FluoStar platereader with excitation and emission wavelengths of 485 nm and 520 nm respectively. Fluorescence values were measured every 30 seconds over a period of 30 minutes. Initial dye release rates were calculated from the curve gradient over the first 5 minutes.

2.5.3 Liposome pH assay

The liposome pH assay was adapted from previously described methods (StGelais *et al.*, 2007). As the liposomes displayed high background dye release in the previously-used citrate-phosphate buffers, an alternative protocol was developed using liposome assay buffers titrated to different pH points. The liposomes were pelleted at 100,000 xg for 15 minutes and resuspended in liposome assay buffer at pH 7.4, 6.7 and 6.2. 200 μl reactions were prepared including methanol and triton X100 controls, and FLAG-p7 incubated with the liposomes for 15 minutes. The reactions were then transferred into 0.2 ml ultracentrifuge tubes and spun at 160,000 xg for 20 min. At the end of each spin, 100 μl of supernatant was removed and placed in a 96-well fluorescence plate. The Triton-X100 controls were measured and the pH 6.7 and 6.2 samples restored to full fluorescence by the addition of 1 M Tris-Cl (pH 8). Equal

volumes of 1 M Tris-Cl were added to each of the other samples at each pH, and the fluorescence of each well measured on the platereader.

2.6 RNA synthesis

2.6.1 Preparation of DEPC-treated solutions

Water and phosphate-buffered saline (PBS) used for RNA experiments was treated with diethylpyrocarbonate (DEPC) to a final concentration of 0.1% (v/v) to remove RNase activity. The solutions were then placed overnight in a 37 °C shaker and autoclaved to sterilise the solutions.

2.6.2 Preparation of DNA template

RNA templates were linearised by restriction endonuclease digest with either ScaI or XbaI (New England Biolabs), and if necessary, DNA overhangs were removed by treatment with Mung Bean Nuclease (New England Biolabs). The linearised DNA was purified by phenol-chloroform extraction and resuspended in DEPC-treated water.

2.6.3 RNA synthesis and clean-up

Surfaces and equipment were treated with RNase-Zap (Ambion) prior to RNA preparation. RNA was synthesised using the Promega T7 RiboMax Express Large Scale RNA Production System. The reactions were assembled according to the manufacturer's instructions and incubated for 30 minutes at 37 °C, after which DNAse was added to digest the template. The reactions were then purified by phenol-chloroform extraction as detailed in section 2.3.2, using acidic phenol-chloroform isoamyl-alcohol (pH 4) (Sigma-Aldrich).

Xenopus mRNA transcripts were generated using the SP6 mMachine mMessage system (Ambion) according to the manufacturer's instructions and purified as above.

2.6.4 RNA agarose gel electrophoresis

RNA transcripts were analysed for purity and degradation by denaturing 3-(N-morpholino) propanesulfonic acid (MOPS) formaldehyde gel electrophoresis. 1% (w/v) agarose was heated in 1 X MOPS buffer (0.04 M MOPS, 0.01 M sodium acetate, 1 mM EDTA in DEPC-treated H_2O) until dissolved, and allowed to cool before the addition of 6.5% (v/v) formaldehyde. The gel was poured into the casting mould; a well-comb inserted, allowed to set and immersed in 1 X MOPS buffer in a gel tank. RNA samples were prepared by the addition of 10 µl RNA loading buffer (56% (v/v) formamide, 10% v/v formaldehyde, 6% glycerol, 0.025% (w/v) bromophenol blue and 10 g/ml ethidium bromide in MOPS buffer) to 1 µl of RNA transcript or RNA ladder (Ambion) and heated at 65 °C for 10 minutes. Gels were run at 80 V for 1 hr, and the RNA imaged on a UV transilluminator (Syngene).

2.6.5 RNA quantification

RNA was quantified by measurement of the absorbance at 260 nm on a NanoDrop (Thermo Scientific). The 260:280 nm ratio was measured to assess RNA purity.

2.7 Cell culture

2.7.1 Routine cell passage

Huh-7 cell lines were cultured in DMEM supplemented with 10% FCS, 1% non-essential amino acids, 2 mM L-glutamine, 100 IU/ml penicillin, and 100 µg/ml streptomycin at 37 °C in a humidified 5% CO_2 incubator. Media for virus work was supplemented with 25 mM HEPES (GIBCO, pH 7.4, sterile) for additional buffering against acidic metabolites. Huh7 and Huh7.5 cells were maintained at sub-confluent levels for up to 20 passages. Subgenomic replicon-harbouring cell lines were maintained in DMEM supplemented with 250 µg/ml G418.

2.1.1 Transfection of cell lines

Cells were plated out onto 6 well plates for protein analysis at a density of 2 x 10^5 per well, and onto 8-well microscopy slides (Ibidi) for live cell imaging at a density of 1 x 10^4 per well. One day prior to transfection, Huh-7 cells were seeded (2 × 10^5) into six-well plates. Cells were transfected using 5 µl polyethylenimine (PEI) (Polysciences Inc.) with 1 µg DNA per well of a 6-well plate in 0.5 ml Opti-Mem (Gibco). For 8-well microscopy slides, the transfection reagents were mixed in the same proportions and 100 µl were added to each well. Cells were incubated for a minimum of 16 hrs before detection of protein expression. Where 6-well plates were harvested for protein analysis, cells were washed twice in PBS, lysed in 200 µl of GLB and removed from the 6-well plate using a cell scraper.

2.8 Virus work

2.8.1 Electroporation of Huh7 cells

Huh7 cells were pelleted at 1000 xg and washed by resuspension in DEPC-PBS 3 times prior to resuspension in DEPC-PBS at a concentration of 1.5x10^7 cells per ml. 6x10^6 cells were transferred into an electroporation cuvette and 10 µg of RNA added. The cells were electroporated at 950 µF, 270 V. Following electroporation, the cells were diluted into warm media and pipetted to preventing clumping of cells. All equipment was sterilised in 5% virkon after use (w/v). The electroporated cells were moved into the CL3 facility, and media changed 4 hours post-electroporation.

2.8.2 Harvesting of extracellular and intracellular virions

Extracellular virus was harvested from the media of virus electroporated cells and stored at 4 °C. Virus supernatants were clarified by centrifugation at 1000 xg for 5 minutes to remove cell debris. To assess intracellular virus infectivity, cells were

harvested using the following protocol. Cells were washed 3 times in PBS, and resuspended in 1 ml of PBS using a cell scraper. The cells were then pelleted at 1500 xg and resuspended in an appropriate volume of PBS. A sample of the infected cells was pelleted and lysed in Glasgow lysis buffer (GLB) (10 mM PIPES (pH 7.2), 120 mM KCl, 30 mM NaCl, 5 mM $MgCl_2$, 1 Triton X-100, 20% glycerol, leupeptin 1 g/ml, pepstatin A 1 g/ml, aprotinin 2 g/ml, 0.2 mM AEBSF (Pefabloc), 1 mM EDTA, 5 mM NaF, 2 mM Na_3VO_4, 5 mM $Na_4P_2O_7$) for western blot analysis. The cells were then subjected to 5 rounds of freeze-thaw lysis using a 37 °C water bath and a dry-ice/ethanol mixture. Lysed cells were centrifuged at 1000 xg to remove cell debris.

2.8.3 Measurement of infectious viral titres

$8x10^3$ Huh7 cells were seeded into each well of a 96-well flat bottom clear plate and allowed to grow overnight. These plates were then taken into the CL3 facility. For the assessment of extracellular virus infectivity, the media was removed and replaced with virus supernatants harvested from electroporated cells. Virus supernatants were diluted 10-fold and serially diluted into subsequent wells in triplicate. For intracellular virus infectivity assays, 50 µl of PBS containing harvested intracellular virus was added to the first well, and serially diluted into subsequent wells. Following 48 hrs of infection, cells were washed twice in PBS and fixed in 4% PFA (4% (w/v) paraformaldehyde in PBS) for 20 minutes, after which the plates were removed from the CL3 facility. Cells were then washed in filtered PBS, and permeabilised with 0.1% Triton in PBS (v/v). Cell were blocked in 10% FBS in PBS (blocking media) for 30 minutes and labelled with sheep anti-NS5A antibodies diluted in blocking medium for 1hr. Cells were stained with AlexaFluor594 Donkey α-Sheep secondary antibodies, with 3 PBS washes between each stage. Cells were viewed on a Nikon eclipse T5100 fluorescence microscope at 20X magnification and focus forming units (FFU) counted.

2.8.4 Virus infectivity time course

For the assessment of the time course of virus infection, Huh7 cells were electroporated, and each electroporation divided into 3 T25 vented flasks (Sarstedt). The media of each flask was then replaced at 4 hours post-electroporation. Virus supernatants were harvested at 24, 48 and 72 hours post electroporation and virus infectivity of the supernatants assayed as above.

2.8.5 pH sensitivity assay

The following methods were adapted from (Wozniak *et al.*, 2010). HEPES/MES buffer (20 mM HEPES, 20 mM MES, 133.5 mM NaCl, 2 mM $CaCl_2$, 4 mM KCl, 1.2 mM $MgSO_4$, 11 mM glucose) was prepared to pH 3.3, pH 3.9, pH 6.0 and pH 7.4, so that when mixed 1:1 (v/v) with PBS at a later stage of the experiment it would generate a pH gradient of 4.0, 5.2, 6.2 and 7.4. Extracellular virus was collected and concentrated by centrifugation through a sucrose cushion pellet at 150,000 xg using an AH650 rotor in a Sorvall ultracentrifuge and resuspended in PBS. Intracellular virus was prepared by freeze-thaw lysis of harvested cells into a suitable volume of PBS, followed by removal of cell debris by centrifugation at 1000 xg for 5 minutes. Virus samples, both extracellular and intracellular, were then mixed 1:1 with the HEPES/MES buffers to generate the pH gradient, and incubated at 37 °C in a waterbath for 10 minutes. On removal from the waterbath, those at acidic pH were neutralised by the addition of 1 M NaOH to a final pH of 7.4. The infectivity of the virus was then titred.

2.8.6 Temperature sensitivity assays

Previous studies have demonstrated that that secreted JFH1 HCV virions are steadily inactivated at 54 °C over a period of 40 minutes (Song *et al.*, 2010). To determine the temperature sensitivity of collected virus supernatants, media from electroporated cells was collected 48 hr post-electroporation and stored at 4 °C until required. This media was then aliquoted to the appropriate volume and placed in a waterbath at

54 °C. At each 5 minute timepoint, the supernatants were removed from the waterbath and placed immediately on ice to reduce the temperature. The supernatants were then titred to measure the reduction of infectivity over time in response to high temperature.

2.9 Microscopy

2.9.1 Fluorescence microscopy

Whole-cell fluorescence microscopy was carried out on an Axiovert 135 microscope with a monochromatic excitation unit controlled by Openlab software. Cell media was removed and replaced with HEPES cell buffer (10 mM HEPES, 133.5 mM NaCl, 2 mM $CaCl_2$, 4 mM KCl, 1.2 mM $MgSO_4$, 1.2 mM NaH_2PO_4, 11 mM glucose, pH 7.4) prior to imaging. For Lysosensor Yellow/Blue DND-160 (Invitrogen) staining, cells were incubated in 5 μM Lysosensor in cell imaging buffer for 30 minutes and washed 3 times in HEPES cell buffer before imaging. Alkalinising chemicals were added to the cells in cell media for 2 hrs prior to imaging, and were present in all subsequent wash and stain solutions. Where p7 inhibitor compounds were used, they were diluted in cell imaging buffer, added after the final wash step and incubated for 5 minutes prior to imaging.

For confocal microscopy, labelled cells were viewed on an inverted Zeiss 510-META laser scanning confocal microscope under an x40 objective lens (numerical aperture = 1.40). pHluorin was excited using an argon laser fitted with 488 nm filters, and emission read at 530 nm.

Images were analysed using ImageJ software, where appropriate using macros to identify regions of interest (ROI). The macro used is detailed in Appendix 2.

Fluorescence intensity in the ROIs was measured using ImageJ, and data were then analysed using Microsoft Excel.

2.10 Electrophysiological methods

All electrophysiological procedures were carried out by Dr Jonathan Lippiat.

2.10.1 Removal and preparation of *Xenopus laevis* oocytes

Female *Xenopus laevis* frogs were anaesthetized by immersion in 2% 3-aminobenzoic acid (pH 7.2 with Tris and HCl) for 45 minutes. The frogs were then killed by cervical dislocation and pithing, in full accordance with Home-office Schedule 1 guidelines. Ovarian lobes were then removed via a mid-line incision (Stuhmer & Parekh, 1995). The ovarian lobes were broken into small fragments with forceps and separated into single cells via two 60 minute incubations in 1 mg ml^{-1} collagenase dissolved in OR-Mg solution (NaCl 82 mM, $MgCl_2$ 2 mM, HEPES 0.5 mM, KCl 0.2 mM; pH 7.4). The cells were washed between collagenase incubations five times with OR-Mg solution (first wash) and 8 times (second wash) prior to transferring the now single cells into ND-96 solution (NaCl 9.6 mM, $MgCl_2$ 0.1 mM, HEPES 0.5 mM, $CaCl_2$ 0.18 mM, KCl 0.2 mM; pH 7.4). Dumont stage V and VI oocytes were then selected for injection.

2.10.2 cRNA microinjection of *Xenopus laevis* oocytes

Prior to injection, glass capillaries were sterilised by baking at 200 ºC for at least 4 hours. Sterile glass capillaries were pulled into very fine tipped pipettes and then broken to the desired length and diameter with a pair of flame-sterilized forceps. 50 nl of cRNA was then injected into the light hemisphere of each oocyte using a Pneumatic Pico-Pump pressure injection system (WPI). Successfully injected and healthy oocytes were incubated at 18 ºC for 24 hrs in ND-96 solution.

2.10.3 Electrophysiological recordings from *Xenopus laevis* oocytes

The Gene Clamp 500 amplifier (Axon Instruments) was used for electrophysiological recordings. Both current and voltage outputs from the voltage-clamp amplifier were displayed on a Takronix 5113 dual beam storage oscilloscope (using D.C. coupled 5A22N and 5A21N amplifiers). The signals were fed via a CED 1401 analogue interface to a computer running the CED on-line analysis software (version 6). The current signal was low-pass filtered at 1 kHz by the amplifier and sampled at 4 kHz.

The oocyte was placed into the chamber perfused with high potassium Ringer solution (90 mM KCl, 1 mM $MgCl_2$, 1.8 mM $CaCl_2$, 5 mM HEPES (pH 7.4)) at a rate of ~ 2 ml min^{-1}. The perfusion was maintained through the chamber via removal of excess solution via a suction tube connected to a peristaltic pump. The electrode holders containing the current and voltage electrodes were filled with 3 M KCl and mounted onto head stages either side of the oocyte chamber and the bath electrode submerged in the bath solution. The electrode resistances were adjusted between 0.3 and 1 MΩ for the current electrode and between 0.3 and 2 MΩ for the voltage electrode via gentle tapping of the tips with tissue paper. To minimize the interference the current and voltage electrodes were separated with a copper shield once the oocyte had been impaled and the whole apparatus was assembled inside a Faraday cabinet placed on an air-table, both of which were earthed to the circuit ground. Both electrodes were offset to 0 mV and gently inserted into the oocyte. The oocyte was then left 10 minutes to allow the membrane potential to stabilise with healthy oocytes displaying membrane potentials of ~ -30 to -70 mV. The amplifier was then set to clamp and the gain and stability on the amplifier adjusted to maximize the square wave of the voltage trace with small capacitance for the current trace.

Results were processed using Origin Pro software (Origin Lab).

Chapter 3: *In vitro* functional analysis of naturally-occurring variations in p7.

3.1 Introduction: How do naturally occurring p7 polymorphisms in a patient cohort affect protein function?

p7 is essential for HCV infectivity in culture (Jones *et al*., 2007; Steinmann *et al*., 2007) and for virus replication in chimpanzees (Sakai *et al.*, 2003). While some residues are highly conserved, there are regions of sequence variability across HCV genotypes. Fig. 3.1 (a) shows a consensus sequence derived from analysis of all genotypes and subtypes, with variants at each position listed below in order of decreasing frequency (Steinmann *et al*., 2007). Experimental infection of chimpanzees with inter-genotypic chimeric viruses indicated that the N and C termini of the protein show genotype specificity, possibly linked to interactions with other HCV proteins (Sakai *et al.*, 2003). Other variations are less significant; homologous substitutions where residues are replaced by those with similar properties, such as substitution of hydrophobic residues within the TMDs and the interchangeability of arginine and lysine at positions 33 and 35 in the basic loop domain are common variants between HCV isolates.

A major role of p7 in the virus life cycle is to prevent endosomal acidification during virion secretion/production, in order to preserve the infectivity of nascent virions (Wozniak *et al.*, 2010). The prototype viroporin IAV M2 has a well characterised structure and gating mechanism, with the protein forming tetramers with high specificity for directional proton conductance, where the channel only opens in response to reduced external pH (Pinto & Lamb, 2006). The gating mechanism responsible involves two key residues, His37 and Trp41, which are adjacent in the channel lumen. Protonation of the His37 residues in the channel lumen results in σ-π interactions with the Trp41 side chain that cause a conformational change that opens the channel. This conformational change is blocked by amantadine (Okada *et al.*, 2001).

Previous work in this laboratory has developed methods to study the activity of p7 using *in vitro* methods (StGelais *et al.*, 2007; Clarke *et al.*, 2006). In brief, to avoid the toxicity of native p7 expression in bacterial cells, it is expressed as a GST-fusion protein that forms inclusion bodies. These inclusion bodies are purified and the GST-tag cleaved using rhinovirus 3C protease. The protein can then be solubilised with detergent and purified by reverse-phase HPLC. After this purification, the HPLC solvents are evaporated, and the desiccated protein stored until required. The protein is soluble in methanol and folds into a monomeric conformation, with channel activity measurable *in vitro* using a liposome dye-release assay (Foster *et al*., 2011; StGelais *et al*., 2007). The liposomes contain carboxyfluorescein (CF) at a self-quenching concentration; on the addition of a pore-forming peptide such as bee venom peptide melittin (Rex & Schwarz, 1998) or membrane-disrupting detergent such as Triton X-100, the dye is released and diluted into the surrounding media, allowing it to fluoresce. The addition of p7 to liposomes causes a rapid initial release of CF which gradually tails off at a point below the maximum level of dye release as measured by Triton X-100 liposome lysis, as liposomes are present in excess. This activity is titratable, with higher concentrations of p7 resulting in faster initial rates of dye release and higher endpoint levels. CF is also quenched when the pH is reduced below pH 7.4, and so using liposomes to investigate p7 activity requires the use of an endpoint assay where the dye release is allowed to occur at reduced pH, and the pH restored to 7.4 prior to fluorescence readings. It was determined that GT1B J4 p7 shows a 2-fold increase in activity when the pH is reduced to pH 6.2 (StGelais *et al.*, 2007).

These methods were used to assess differences in p7 activity and drug response between a number of different genotypes (Griffin *et al.*, 2008), as well as the effect of targeted mutagenesis on the activity of J4 p7 (StGelais *et al.*, 2009).

p7 from different HCV genotypes also showed distinctive responses to drug treatment, with GT1B J4 p7 showing sensitivity to two adamantane drugs, amantadine and

rimantadine, GT1A H77 p7 showing low sensitivity to both adamantanes, and GT2A JFH1 p7 only showing sensitivity to rimantadine. Given the effect of amantadine on IAV M2 to 'lock' the channel into the closed conformation (see section 1.3.2), differences in the adamantane sensitivity between HCV genotypes may indicate possible changes in channel gating. Previous mutagenic analysis of GT1B J4 p7 identified a number of residues important for p7 function, including a histidine residue at position 17 that may have a role in gating the channel, analogous to the His37 proton-sensor of IAV M2 (Wang *et al.*, 1995).

Targeted mutagenesis and the variation between genotypes have revealed many variants in p7 activity, but p7 alterations also exist within individual patients as a result of virus quasispecies. It is possible therefore that the high mutation rate inherent to HCV will result in changes in the p7 amino acid sequence with both functional and structural consequences, tolerated within the evolutionary constraints of maintaining viral fitness. Our collaborators at the University of Washington, Seattle, have worked with HCV patients with a particular focus on measuring quasispecies mutation rates and natural, functional variants of HCV that arise in response to selection pressure from variation between hosts (Li *et al.*, 2011). Our collaboration focused on one particular study assessing changes in p7 sequences in 27 newly-diagnosed patients infected with a single HCV GT (1A). These patients had varying disease profiles; some had mild disease with little or no liver fibrosis (Ishak fibrosis score 0-1), and others had severe disease and more advanced liver fibrosis (2-3). A number of the patients were also co-infected with HIV. The frequency of mutations within p7 in the patient quasispecies was determined prior to treatment, and from each patient serum sample 12 p7 clones were amplified by RT-PCR. The genetic diversity of these sequences was analysed, with specific residues showing a high degree of conservation and others showing greater mutability. Those who were co-infected with HIV showed a lower degree of sequence variability.

Six isolates were identified with a number of non-synonymous mutations (Li *et al*., 2012a). Fig 3.1 (b) shows an alignment of the much-studied GT1B J4 p7 with the GT1A prototype H77, and the deviations of the Seattle patient isolates from H77 p7 shown below. Two of the isolates came from patients with mild disease (M) with low levels of liver fibrosis, whilst the remaining 4 isolates were derived from 3 patients with more severe disease (S), showing advanced liver fibrosis. The majority of mutations were synonymous with respect to amino acid composition, including substitutions of the hydrophobic residues leucine, isoleucine and valine at position 7 and the replacement of arginine with lysine at position 35 in Seattle isolates M1 and M2. Table 3.1 summarises the patient data for these isolates and highlights the non-synonymous mutations.

Variant ID	Short name	Amino acid change	Host characteristics	
			Fibrosis stage	HIV status
M220_4	M1	S21P, P38S, A40T	1	Negative
M234_1	M2	H17R	0	Positive
S235_1	S1	Y31H	3	Negative
S056_167	S2	H17N, F44C	3	Negative
S630_175	S3-1	T16A	3	Negative
S630_180	S3-2	T16A, R35G, V41T	3	Negative

Table 3.1 Details of Seattle patient isolates

The original identification numbers for each isolate with their abbreviations, significant mutations, fibrosis stage by Ishak score and HIV status. The isolates are referred to by their abbreviated names throughout.

A number of notable non-synonymous mutations were found in each isolate, including several within *trans*-membrane domain (TMD) 1 that we predicted may change the

character of the channel lumen, based both on previous functional data (StGelais *et al.*, 2009) as well as our recently solved monomeric 1b NMR structure (Fig. 1.9).

M1 has a mutation of a highly conserved lumenal serine, S21P. Previous work showed that a J4 p7 S21A mutation did not significantly impair channel activity *in vitro* (StGelais *et al.*, 2009), making it possible that this amino acid position may not be functionally significant. However, changing the serine to a proline may introduce a kink in TMD1 that could affect the activity of the protein. Proline is also more hydrophobic than the polar serine, and thus may also change the balance between hydrophobicity and hydrophilicity within the channel lumen.

The hypothesised pH-sensor residue, H17, is altered in two of the isolates; the H17N polymorphism in S2 also occurs in some GT2A p7 sequences, including the J6 infectious clone, but the H17R mutation in M2 is a much less common variant at this position (Steinmann *et al*., 2007). H17N removes a ionisable residue from the channel, with the potential to alter the hydrophilicity of the channel lumen and thus affect the activity of the protein; as a polar molecule, asparagine is more hydrophilic than unprotonated histidine as calculated by hydropathy analysis (Kyte & Doolittle, 1982). The H17R mutation substitutes a larger residue which, unlike histidine, is protonated at neutral pH. The addition of this larger, charged residue to the lumen of the channel might be expected to cause a significant change in p7 activity. It is of note that the H17A mutation in the JFH1 virus system, which has an additional histidine at position 31, only reduces infectivity by 1 $\log_{10}$, and a H17E mutation shows no impairment in infectivity (Meshkat *et al.*, 2009).

S1 has an Y31H mutation, introducing a second histidine. This polymorphism is also present in JFH1 p7, and while it is not in the lumen of the channel, the NMR structure shows that it is likely to reside close to the entrance of the pore, potentially allowing it to exert influence as a second pH sensor. Mutation of the H31 residue in the JFH1

virus system to Y, F or L only showed a 0.5 $\log_{10}$ drop in infectivity for the H31F mutant, and no significant reductions for H31Y or H31L (Steinmann *et al*., 2007).

The T16A change in both S3-1 and S3-2 does not occur at a luminal residue, but it is adjacent to the His17 residue and alanine is also present in GT1b p7 sequences, including J4. Other variants found at this position include serine, cysteine, glutamine and asparagine (Steinmann *et al*., 2007).

S3-2 has an R35G mutation of one of the two basic loop residues; mutation of both these residues to alanine loses all p7 activity *in vitro* (StGelais *et al.*, 2009). The loop domain has been shown to be crucial to infectivity (Sakai *et al.*, 2003), and short peptide analysis found that this region was highly membranotropic with the basic residues at positions 33 and 35 possibly interacting with the heads of negatively-charged phospholipids (Pérez-Berná *et al.*, 2008). Mutations of these residues in the JFH1 virus system also have a major impact on the production of infectious virus. Single mutations of either residue to the non-charged but polar residue glutamine causes a greater than 1 $\log_{10}$ drop in infectivity, and mutation of both residues to either glutamine or alanine results in a complete loss of virus infectivity (Steinmann *et al*., 2007). However, in the J6/JFH1 chimera Jc1 the R33Q R35Q mutant is reduced by 2 $\log_{10}$ compared with a 3 $\log_{10}$ drop for the R33A R35A mutant. The mutation of only one of these residues may still allow the remaining residue to fulfil the function of the basic loop domain, hypothesised to be required for correct orientation of the channel. A double alanine mutation in J4 p7 in the *in vitro* liposome assay results in the protein associating with, but not fully integrating into membranes, as it can be washed off with a high pH bicarbonate solution (StGelais *et al.*, 2009).

In this chapter, the consequences of the sequence variations in the patient isolate p7s were investigated using the previously-developed *in vitro* liposome assays to measure the activity of these isolates. Previous work had also shown that J4 p7 showed

increased activity at reduced pH (StGelais *et al.*, 2007), as does the prototype viroporin IAV M2 and, given that the hypothesised pH sensor residue His17 was altered in two of the Seattle isolate p7s, the activity in response to reduced pH should also be investigated. As the isolates came from patients with both mild and severe disease, as rated by fibrosis level, it is also of interest to see if there is any correlation between p7 activity *in vitro* and with the severity of disease.

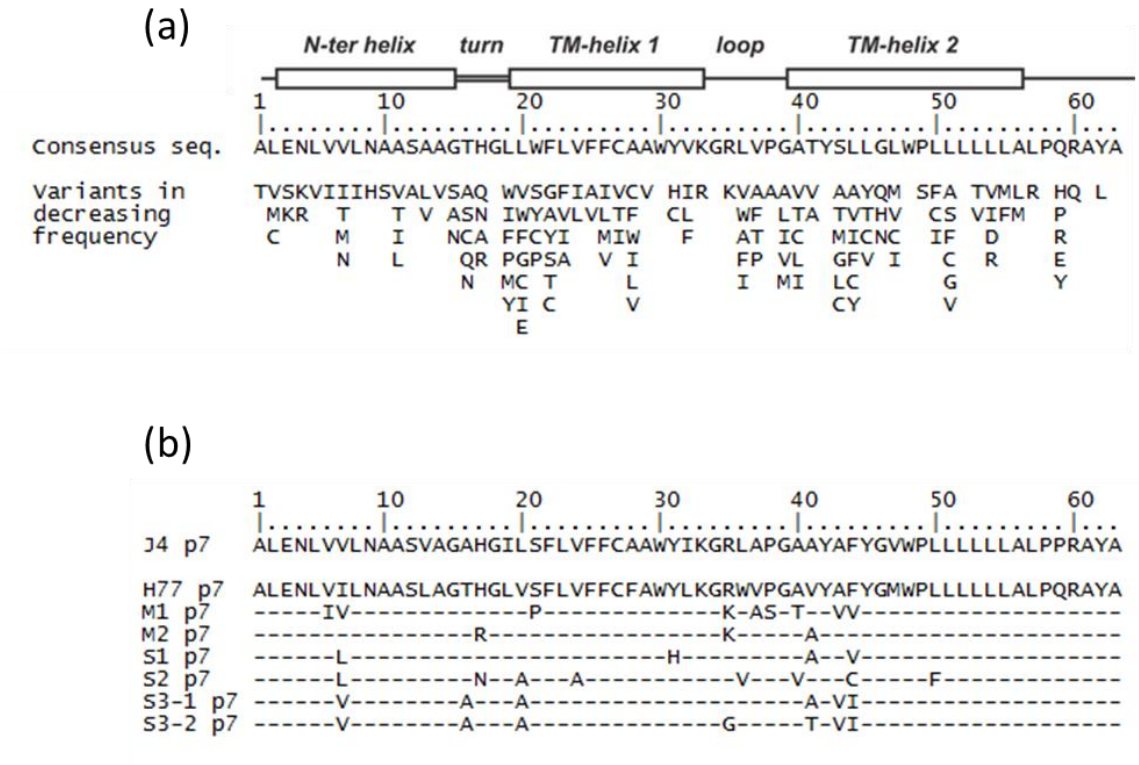

Figure 3.1 Sequence variation of p7 across genotypes, and patient isolate sequences

Panel (a): Consensus sequence from 26 p7 sequences from all major HCV genotypes and subtypes, adapted from Steinmann *et al* 2007. Variants from this consensus sequence at each position are listed in decreasing order of frequency. Panel (b): J4 and H77 prototype p7 sequences with 6 GT1A Seattle patient isolates below, with sequence variants from H77 shown. Conserved residues between H77 and the Seattle patient sequences are represented by dashes.

3.2 Results

3.2.1 Cloning of Seattle patient isolate sequences into pGEX-6p1 for bacterial expression

The patient isolate sequences were sent from Seattle as cDNA. These segments were then amplified by PCR, using primers that incorporated *Eco*RI and *Not*I restriction sites and an N-terminal FLAG tag. The primers used are listed in Appendix 1. Fig. 3.2 is a map of the pGEX-6p-1 vector, showing the 3C protease cleavage site and the restriction sites used for cloning.

The PCR products and vector were digested and ligated, the ligation reaction transformed into bacteria, and plasmids from resulting colonies screened by restriction digest. Successful cloning was confirmed by dsDNA sequencing. Successful constructs were transformed into BL21 *E. coli* and protein expression induced and purified as previously described (see methods sections 2.2.5 and 2.4) (StGelais *et al.*, 2009).

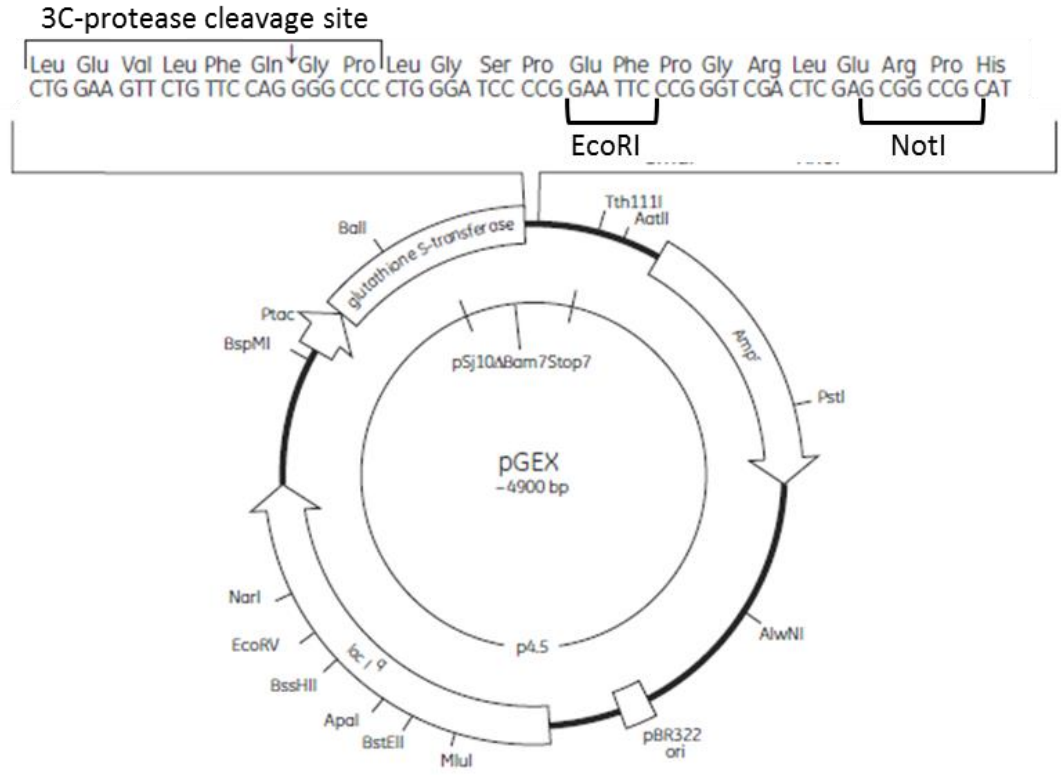

Figure 3.2 Schematic of the pGEX-6p-1 plasmid

Plasmid map of the pGEX-6p-1 plasmid showing the 3C protease cleavage site and the multiple cloning site, with restriction endonuclease cleavage sites EcoRI and NotI highlighted. Image copyright: GE Healthcare

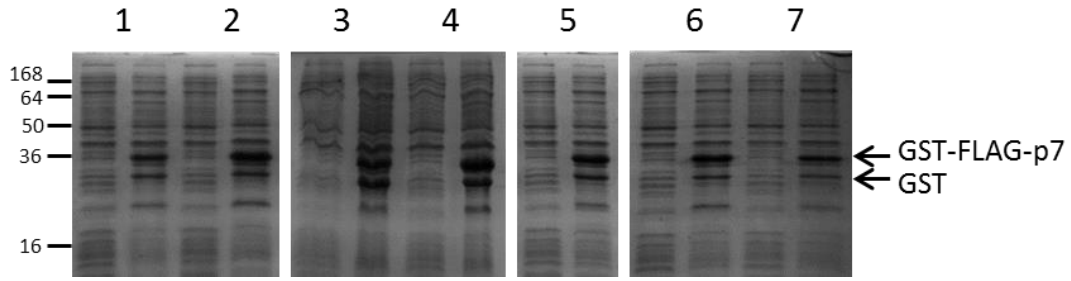

Figure 3.3 Coomassie stain showing bacterial expression of H77 GST-FLAG-p7 and GST-FLAG-p7 constructs of all 6 patient isolate p7 sequences

Bacterial culture samples were taken before induction and 4hrs after induction of expression with 1mM IPTG. Post induction samples were normalised to the optical density of the pre-induction samples, the bacteria harvested by centrifugation and resuspended in Laemmli buffer. Samples were run on SDS-PAGE gels and stained with Coomassie Brilliant Blue. Samples are shown in the following order: 1. H77, 2. M1, 3. M2, 4. S1, 5. S2, 6. S3-1, 7. S3-2, with both the uninduced and induced samples shown. Induced expression of GST-FLAG-p7 proteins appears at 36 kDa, with a smaller band appearing below, matching the size of GST alone.

3.2.2 Expression and purification of HCV genotype 1a FLAG-p7 proteins

3.2.2.1 Protein expression

Cloned plasmids were transformed into BL21 *E. coli* and bacterial cultures grown. Protein expression was induced using the galactose analogue IPTG, and the cultures grown for a further 4 hours before the bacteria were harvested by centrifugation. Samples were taken before induction and before harvesting, with the latter normalised to the optical density at OD_{600} of the pre-induction samples. These samples were then run on SDS PAGE and stained with Coomassie Blue to show protein expression, shown in Fig. 3.3. GST-FLAG-p7 proteins can be seen at 36 kDa in the induced lane for each construct, with a smaller band at ~28 kDa corresponding to GST alone.

3.2.2.2 Purification of prototype genotype 1a FLAG-p7 from the H77 isolate.

The GT1A prototype H77 was expressed and purified as described previously (Griffin *et al.*, 2008; Clarke *et al.*, 2006). Bacterial cultures expressing the protein were harvested and the cells lysed by pressure lysis using a French Press. The insoluble inclusion bodies were then purified by centrifugation and resuspension in various wash buffers to remove cell debris and unwanted protein. The purified protein was then cleaved overnight using His-tagged rhinovirus 3C protease, which results in approximately 50% cleavage efficiency of inclusion body resident protein (Fig. 3.4). The cleaved protein was then solubilised in N-lauroylsarcosine and purified by reverse-phase HPLC. The chromatogram shown in Fig. 3.4 shows the peak separation of the solubilised proteins, with FLAG-p7 the last peak to be eluted from the column. The purity of the peak fractions was tested by western blot, and p7 peak fractions from multiple HPLC runs pooled and desiccated under vacuum.

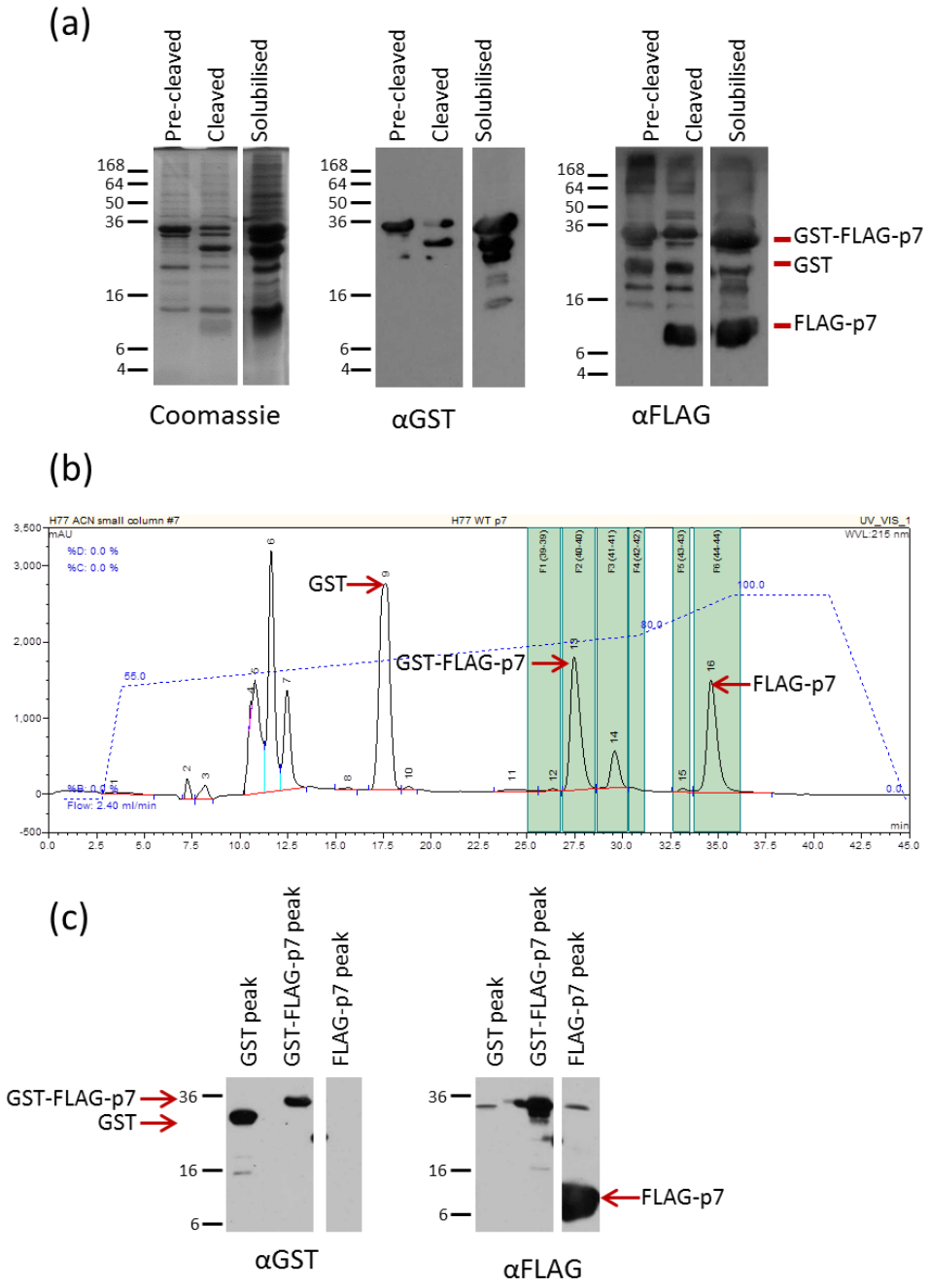

Figure 3.4 Purification of H77 FLAG-p7 by inclusion body preparation and reverse-phase HPLC

Panel (a) shows the inclusion body protein cleavage by 3C protease and solubilised protein, with samples from each stage run on 15% Tris-Glycine SDS-PAGE gels and either stained with Coomassie or assessed by western blot analysis with GST and FLAG antibodies. Panel (b) shows the HPLC elution peaks as measured by the absorbance at wavelength 215 nm, with the peaks shown generated by Dionex Chromeleon Software. Regions shaded green represent the fraction collection of peaks for the specific run shown, and the blue dashed line shows the percentage of Buffer B used to generate the reverse-phase gradient. Protein elution peaks for GST, GST-FLAG-p7 and FLAG-p7 are shown by the red arrows. Panel (c) shows the analysis of eluted peaks by 15% Tris-glycine SDS-PAGE followed by western blot with GST and FLAG antibodies, with GST, GST-FLAG-p7 and FLAG-p7 bands shown by red arrows.

3.2.2.3 Patient isolate p7 sequences exhibit altered retention times during HPLC purification

The patient isolate p7 sequences were expressed and purified in the same manner as H77 p7. However, some differences were seen in the column retention times for the p7 peaks of the Seattle FLAG-p7s, shown in Table 3.2. In reverse-phase HPLC, a reduction in retention time would indicate a reduction in hydrophobicity of the protein, as a less hydrophobic mixture of HPLC solvents is required to elute the protein from the column. Mutations that cause non-synonymous changes in residues in a protein as small as p7 are likely to result in changes to the physical properties of the protein. These changes can be predicted using the ProtParam tool on the ExPASy website, which analyses the amino acid sequence and predicts many physical properties of the protein, such as the molecular weight, the grand average of hydropathy (GRAVY) score and the extinction coefficient for absorbance at 280 nm. The values calculated for H77 FLAG-p7 and the Seattle p7s are listed in Table 3.2. The GRAVY score for each protein, where the higher the number the more hydrophobic the protein is, was used to estimate if any of the sequence variations would cause a change in column retention likely to require a change in the HPLC program parameters.

While these predicted values may explain some of the shifts in HPLC retention times for the different proteins, they do not explain all observations. H77 and M1 are predicted to have similar scores for both molecular weight and hydrophobicity, yet there is a 4-minute reduction in retention time for M1 (Table 3.2). Two isolates that show a lower GRAVY score than H77, M2 and S1, vary in their retention times; M2 has reduction of 2 minutes, while S1 has a 10 minute reduction in retention time that required a reduction in the gradient in the HPLC programme to ensure adequate peak separation, with an extension of the time taken for the gradient between the 55-80% buffer B phase of the program (See materials and methods section 2.4.5). S2 has a slightly higher GRAVY score than H77, which would be predicted to extend the

column retention, but in fact the retention time showed a reduction by 4.5 minutes. S3-1 had a higher GRAVY score than H77 but the retention time was similar with a difference of only 0.5 min, while S3-2 with the highest GRAVY score showed a slight increase in the retention time by 1.5 minutes.

FLAG-p7 protein	MW (Da)	Grand average of hydropathicity (GRAVY)	Extinction coefficient (M^{-1} cm^{-1})	HPLC retention time (minutes)
JFH1	8509	0.548	17210	N/A
J4	8203.6	0.732	18450	N/A
H77	8444.9	0.63	23950	34.5
M1	8398.8	0.629	23950	31.5
M2	8407.8	0.589	23950	32.5
S1	8342.7	0.583	22460	24.5
S2	8296.7	0.645	18450	30
S3-1	8352.8	0.654	23950	34
S3-2	8283.7	0.675	23950	36

Table 3.2 Physical properties of the FLAG-p7 proteins calculated by ProtParam, and HPLC retention times

Theoretical values for the physical and chemical properties of the FLAG-p7 proteins were calculated by inputting each amino acid sequence into the ProtParam tool of the ExPASy Bioinformatics Resource Portal. HPLC retention times were taken from the first run for each FLAG-p7 protein using the standard program, before any changes were made to the HPLC gradients to ensure peak separation.

3.2.2.4 Purified proteins show changes in electrophoretic mobility

After the removal of the HPLC solvent, the concentrations of each of the purified proteins were checked by resuspension in methanol and measurement of the absorbance at 280 nm (A_{280}). The ProtParam tool was used to calculate the predicted extinction coefficient for each of the isolate proteins and the concentration determined using the Beer-Lambert law (see Materials and Methods, section 2.4.6).

Once the concentration of each of the proteins was established, 5 μg of each protein per gel was run on SDS-PAGE gels, which were either stained with Coomassie brilliant blue stain or transferred to PVDF membrane for western blot, with results shown in Fig 3.5. The FLAG blot (Fig. 3.6 (c)) shows very strong antibody binding making correct identification of the FLAG-p7 proteins difficult, but the GST blot (Fig. 3.5 (b)) shows minimal contamination of the S2, S3-1 and S3-2 purified proteins by uncleaved fusion protein, and no fusion protein in the other purifications. The Coomassie stain (Fig 3.5 (a)) clearly shows the monomeric purified proteins, but there are some slight size variations. This has been seen before with targeted mutagenesis of GT1B p7 (StGelais *et al.*, 2009), and is hypothesised to be due to the minor changes in protein size and hydrophobicity caused by the sequence variations.

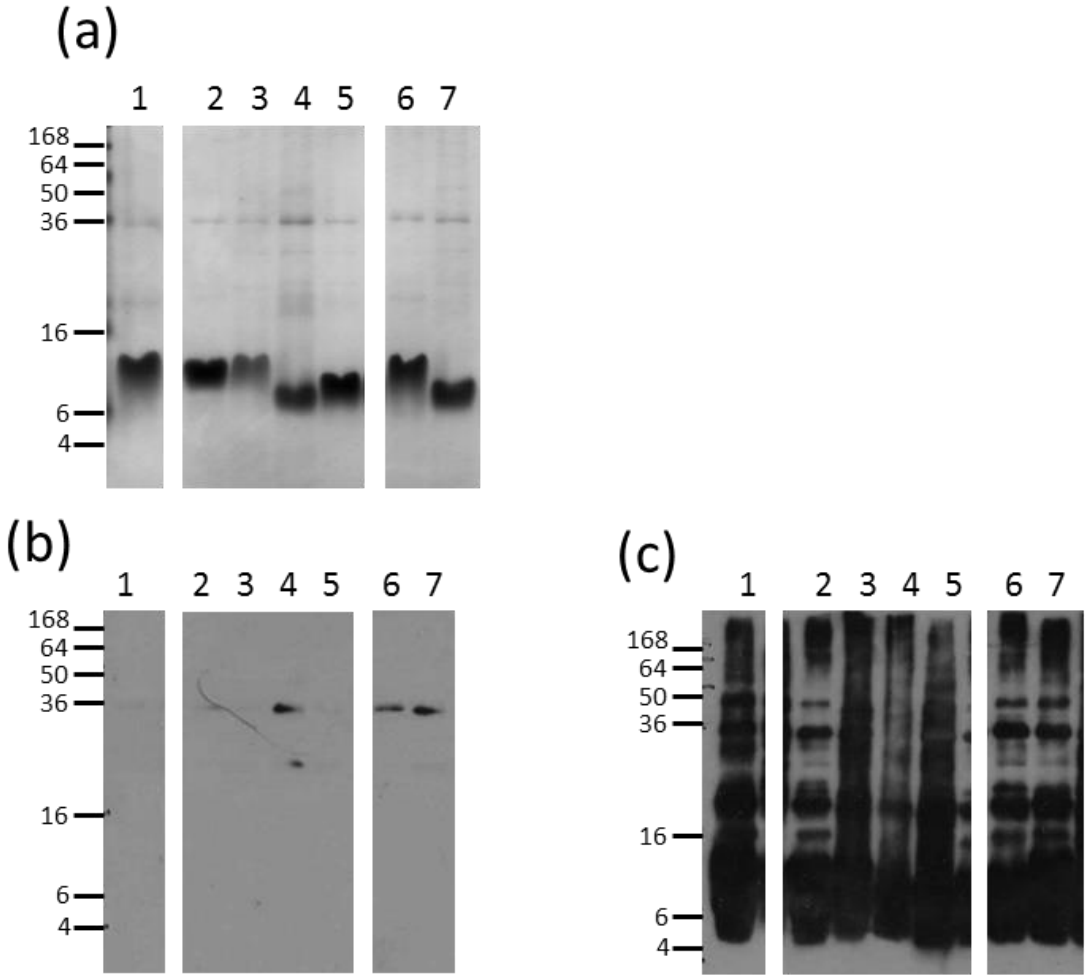

Figure 3.5 Coomassie stain and western blots of purified FLAG-p7 proteins following desiccation.

Protein samples were resuspended in Laemmli buffer, heated at 95 °C and 5 µg of each protein run on 15% Tris-glycine SDS-PAGE gels. The gels were then either stained with Coomassie Brilliant Blue or transferred to PVDF membrane and probed by western blot for FLAG and GST proteins. For all panels, the lanes are: 1. H77 FLAG-p7, 2. M1 FLAG-p7, 3. M2 FLAG-p7, 4. S2 FLAG-p7, 5. S1 FLAG-p7, 6. S3-1 FLAG-p7, 7. S3-2 FLAG-p7. Panel (a) shows the Coomassie stain, panel (b) shows the α-GST western blot, and panel (c) shows the α-FLAG western blot.

3.2.3 Patient derived FLAG-p7 proteins show wide variation in activity levels compared to prototype sequences

To investigate how the naturally-occurring patient variations affected the activity of p7, the FLAG-p7 proteins were tested in the liposome dye release assays (StGelais *et al.*, 2007). On addition of a pore-forming protein, CF is released from the liposomes, where it is present at self-quenching concentration, to the surrounding media allowing it to fluoresce. Each protein was tested in duplicate. The p7 proteins were added last, and the plate immediately measured. The rate of fluorescence increase as the dye was released from the liposomes was measured every 30 seconds over a period of 30 minutes. The rate of dye release over the first 5 minutes was also calculated. The results are shown in Fig 3.6.

J4 FLAG-p7 was included as a control, but the principle relevant comparison for patient isolate sequences was with the genotype 1a prototype H77 FLAG-p7. The result that initially stands out is the S2 isolate, which shows a very high reaction rate and endpoint, with an initial reaction rate three times that of H77 and an endpoint twice as high, with a p-value on the initial rate of less than 0.05. M2 and S3-2 show similar rates to H77 and do not have p-values below 0.05. M1, S1 and S3-1 all show initial reaction rates that are lower than H77 and have p-values less than 0.01. S1 also shows a reaction rate only moderately higher than the background control of the protein-carrier methanol alone.

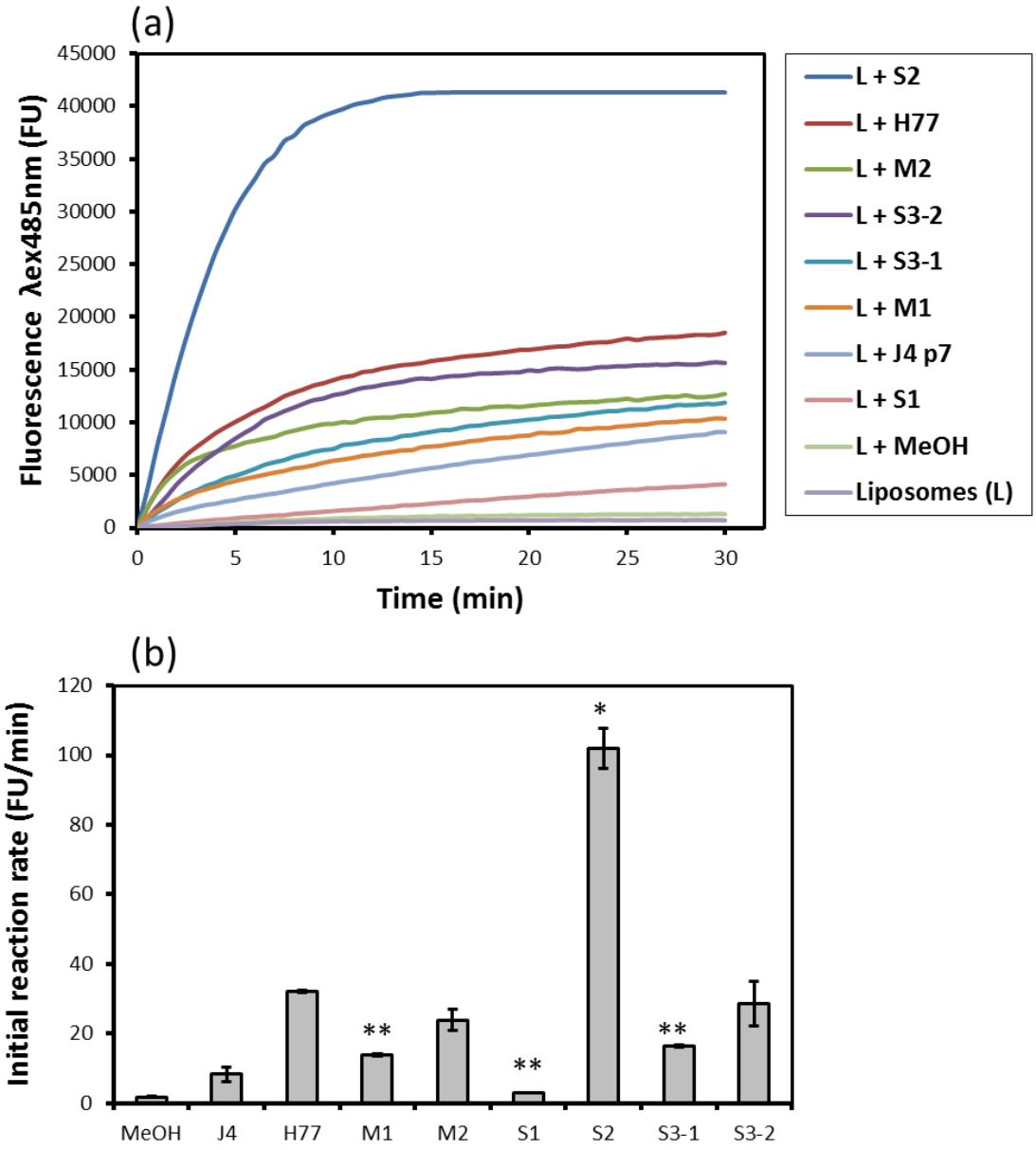

Figure 3.6 Liposome assay showing total fluorescence over time and initial reaction rates for J4, H77 and Seattle patient isolate FLAG-p7s

FLAG-p7 proteins were resuspended in methanol and mixed with 50 μM liposomes prepared as described in section 2.5.1. Carboxyfluorescein release was measured by fluorimetry at excitation and emission wavelengths of 485 nm and 520 nm respectively, at 37 °C for 30 min. Panel (a): Carboxyfluorescein release over time. Panel (b): Initial rates calculated from the first 5 minutes of the curves shown in panel (a). Results were performed in duplicate and error bars represent standard deviation between the duplicates.

3.2.4 Do prototype and patient genotype 1a p7 proteins exhibit differential pH responsiveness?

3.2.4.1 J4 FLAG-p7 displays increased activity at reduced pH_{ext} in a liposome based assay.

In addition to the liposome activity assay, an endpoint assay to measure changes in p7 activity in response to changes in external buffer pH (pH_{ext}) was also developed (StGelais *et al.*, 2007). Briefly, liposomes were pelleted and then resuspended in citrate-phosphate buffers at different pH values. These liposomes were then incubated with p7 protein, followed by removal of the remaining liposomes by ultracentrifugation, and the fluorescence of the released carboxyfluorescein restored by the addition of Tris-Cl (1M, pH 8.0) buffer to restore neutral pH. This showed that J4 p7 showed increased activity in response to reduced pH_{ext} in this system, as does the prototype viroporin IAV M2 (Stephen Griffin, unpublished observations).

Previous work with J4 p7 showed a 2-fold increase p7 activity when the pH_{ext} was reduced from 7.4 to 6.2 (StGelais *et al.*, 2007). With the modified pH assay, the results shown in Fig 3.7 indicate that activity at pH 6.7 shows a 15% increase compared with the activity at pH 7.4, and the activity at pH 6.2 is 175% higher, an increase of almost 3-fold in activity.

3.2.4.2 H77 displays a different pH-activity profile to prototype controls from other HCV genotypes.

Two other HCV genotype prototypes, JFH1 and H77 p7 were then also investigated for their response to low pH. H77 is the prototype GT1A sequence, and thus makes the closest comparison for the patient isolate sequences. JFH1 is the GT2A isolate that is able to replicate in cell culture, and thus is the best-characterised isolate to have been studied with full rounds of virus replication. Like the S1 patient isolate sequence, JFH1 has a second histidine at position 31, which may lie just outside the

entrance to the channel pore, and so the effect of this additional histidine residue in proximity to the pore in both p7 proteins was also worthy of investigation.

The results are shown in Fig 3.7. JFH1 showed a similar profile to J4 p7, but with a much higher increase in activity. At pH 6.7, the activity increases by 43% compared with the activity at pH 7.4, and at pH 6.2 the activity increases by 700%, 8-fold higher activity than at pH 7.4.

However, H77 showed a different activation profile. At pH 7.4, H77 activity was 54% higher than the J4 p7 control at the same pH. At pH 6.7, the activity dropped 60% to just below the activity of J4 p7 at pH 7.4, then at pH 6.2 the activity rebounded to 48% higher than the activity of J4 p7 at pH 7.4. This pattern formed a V-shaped activity profile.

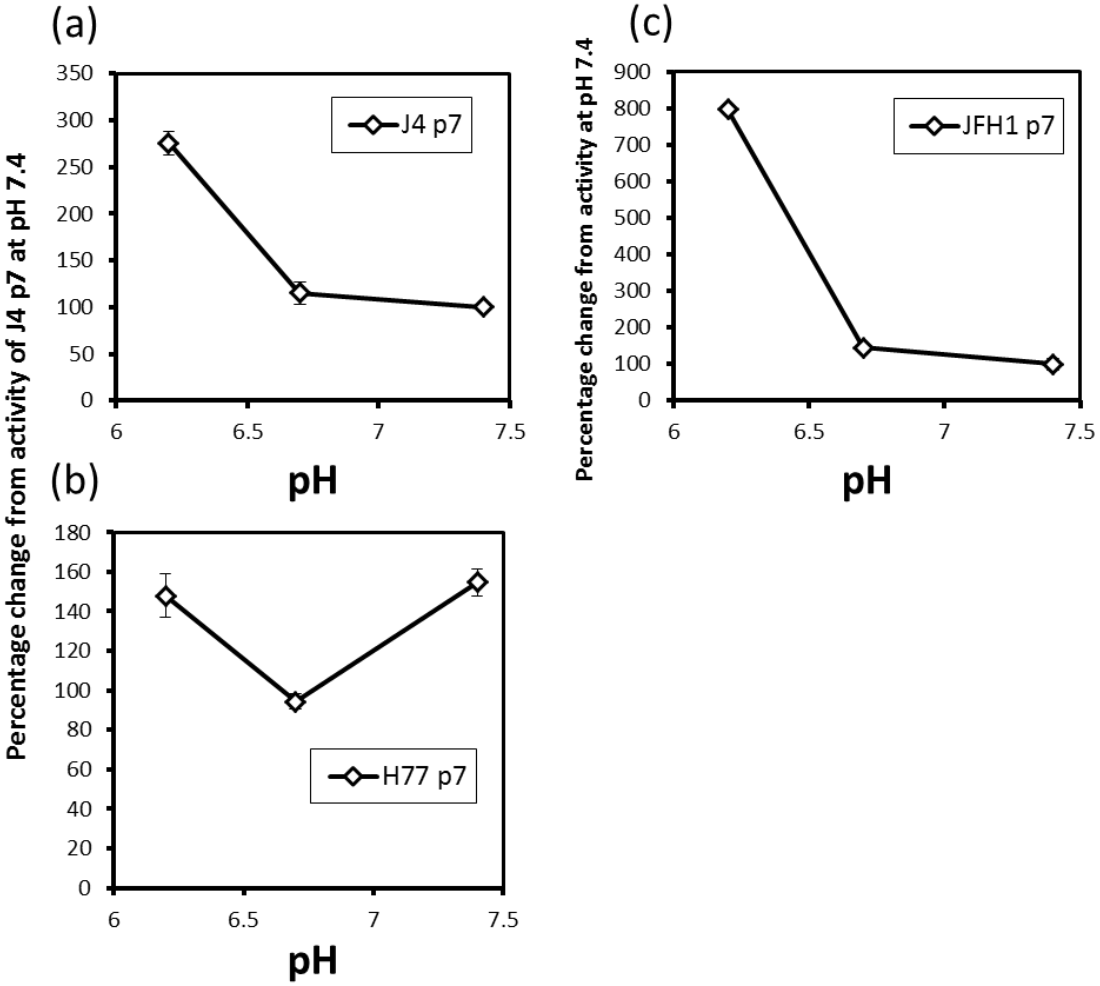

Figure 3.7 Liposome pH assay for prototype FLAG-p7 proteins

Liposomes were pelleted by ultracentrifugation and resuspended in liposome assay buffer at pH 6.2, 6.7 and 7.4. Liposomes at 50 µM were incubated with 10 µg FLAG-p7 protein in methanol for 15 minutes then ultracentrifuged to pellet the remaining liposomes. Controls with methanol alone for background and 0.5% (v/v) triton-X100 for complete dye release were also included. Supernatants were removed to a fluorescence plate and the fluorescence of the triton-X100 controls at pH 6.2 and 6.7 restored by the addition of 1 M Tris-Cl pH 8. The same volume of Tris-Cl pH 8 was then added to the methanol controls and FLAG-p7 wells to restore their full fluorescence. Panel (a) shows the results for J4-FLAG-p7, with the methanol backgrounds subtracted from the fluorescence released by FLAG-J4-p7. Results were normalised to the fluorescence release at pH 7.4. Panel (b) shows the results for H77-FLAG-p7, with the methanol only controls subtracted and J4-FLAG-p7 at pH 7.4 controls included allowing normalisation to this value. Panel (c) shows the pH assay for JFH1-FLAG-p7, with the methanol-only controls subtracted. As no J4-FLAG-p7 control was used in this experiment, JFH1-FLAG-p7 is normalised to its dye release at pH 7.4.

3.2.4.3 Activity profiles of the Seattle isolate p7s in response to reduced pH

The pH activity of the Seattle patient isolates was then investigated, to see how the sequence variations might affect the pH activity profiles of p7. Of particular interest were the M2 and S2 with alterations from His17, and S1 with a second histidine residue at position 31.

Two of the Seattle patient isolate sequences, M1 with an S21P variation and S1 with an Y31H mutation displayed a switch in the channel gating to the low-pH activated phenotype. Shown in Fig 3.8, M1 activity at pH 7.4 was 65% that of the J4 p7 control, with a slight increase at pH 6.7 to 68%, then at pH 6.2 the activity increased to 154% that of the J4 p7 control at pH 7.4. S1 showed the lowest activity at pH 7.4 at 36% that of the J4 p7 control, which increased to 42% at pH 6.7 and 125% at pH 6.2.

The isolates M2, S2, S3-1 and S3-2 all showed a similar V-shaped pH activation profile to H77 p7, with the lowest activity at pH 6.7 and higher activities at pH 7.4 and 6.2, shown in Fig 3.9. M2 showed an activity of 165% that of the J4 p7 control at pH 7.4, then dropped to 120% at pH 6.7 and increased again to 141% at pH 6.2. S2 showed the highest activity rate, starting at 199% of the J4 p7 control at pH 7.4, then dropping to 144% at pH 6.7 and increasing to 188% at pH 6.2. S3-1 started at 135% of the J4 p7 control at pH 7.4, dropping to 110% at pH 6.7 and increasing to 154% at pH 6.2. S3-2 showed similar activity to J4 p7 at pH 7.4, only 4% higher than the J4 p7 control, dropping to 82% at pH 6.7 and increasing to 90% at pH 6.2.

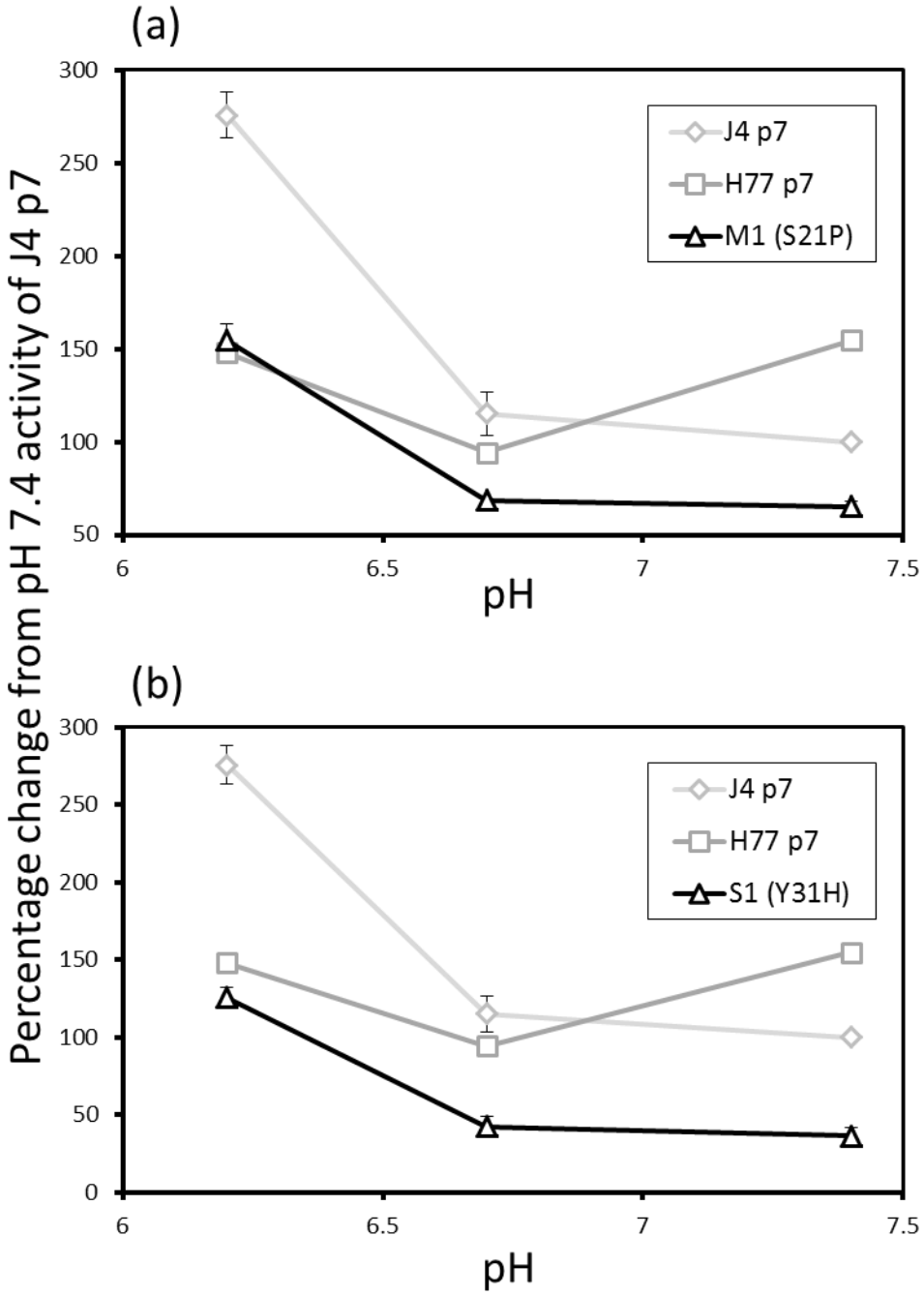

Figure 3.8 Seattle FLAG-p7 proteins M1 and S1 show low-pH activation

Panel (a) shows the pH activity profile for M1, with its S21P polymorphism, and Panel (b) shows the pH activity profile for S1, with its Y31H polymorphism. Activity profiles for J4-FLAG-p7 and H77-FLAG-p7 are shown in pale grey (J4 FLAG-p7) and dark grey (H77 FLAG-p7).

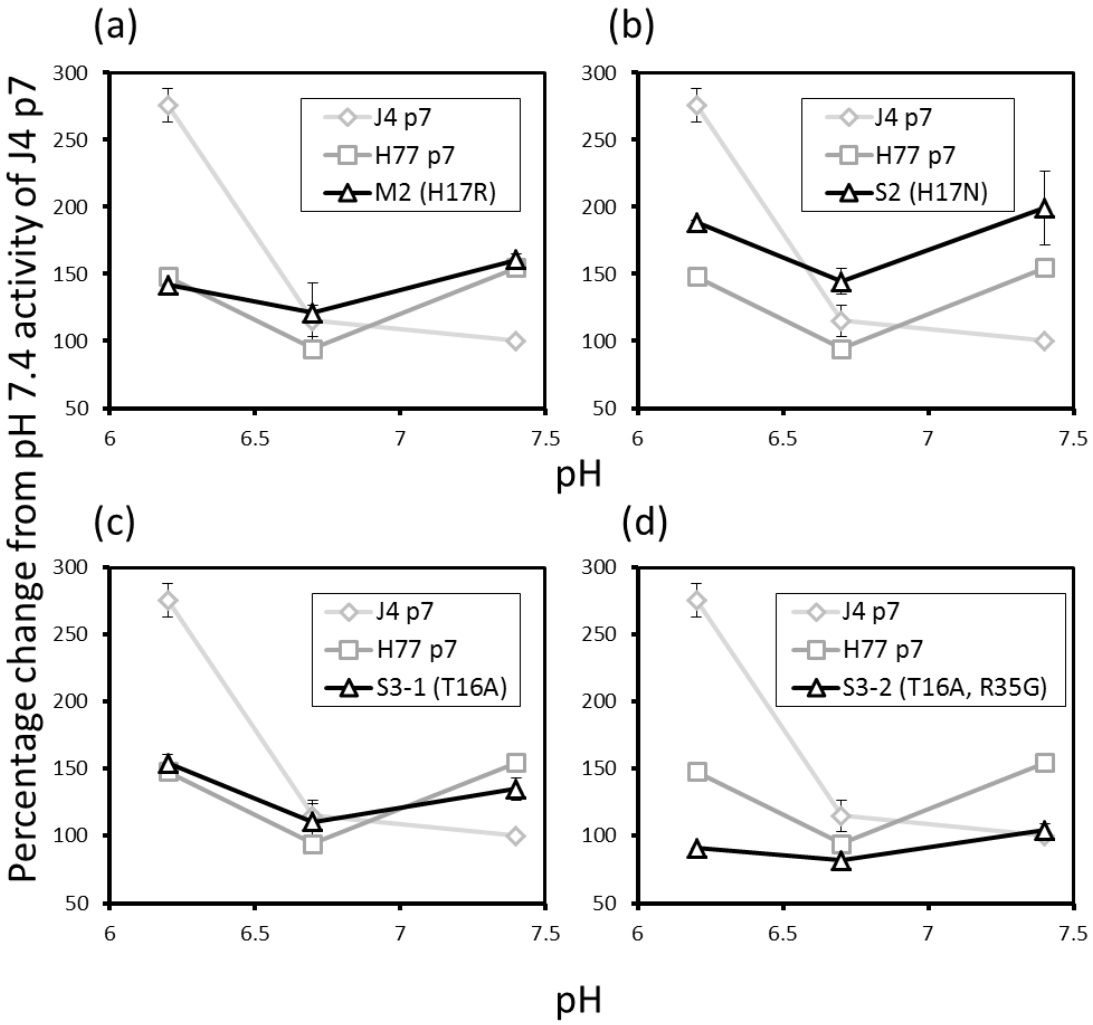

Figure 3.9 Seattle FLAG-p7 proteins displaying a V-shaped pH response profile, but at varying activity levels

pH activity assays for the remaining Seattle FLAG-p7s M2, S2, S3-1 and S3-2. Activity profiles for J4-FLAG-p7 and H77-FLAG-p7 are shown in pale grey (J4 FLAG-p7) and dark grey (H77 FLAG-p7). Panel (a) shows M2 (H17R), panel (b) shows S2 (H17N), panel (c) shows S3-1 (T16A) and panel (d) shows S3-2 (T16A, R35G)

3.3 Discussion

The functional variants of HCV p7 derived from patients allow the investigation of how far the p7 sequence can change, and what effect these changes may have on p7 activity. This initial work focused on using the previously developed bacterial expression system and *in vitro* liposome dye release assay to investigate the activity (StGelais *et al.*, 2007). The real-time dye release assay had been previously used to measure variation in p7 activity levels and drug responses between different genotypes (Griffin *et al.*, 2008), and the effect of targeted mutagenesis on J4 p7 (StGelais *et al.*, 2009).

3.3.1 Predicted changes in protein hydropathy cannot wholly explain changes in HPLC column retention times

The changes in column retention times for the Seattle patient isolates cannot wholly be explained by the changes in protein hydrophobicity as calculated using the ProtParam tool. S1, predicted to be the most hydrophilic, does show a major 10 minute reduction in retention time when compared with H77, but M2 with a predicted hydropathy score almost as low only showed a 2 minute reduction in retention time. Of the 3 isolates predicted to be more hydrophobic than H77, S2 showed a 4.5 minute reduction in retention time, S3-1 showed a 0.5 minute reduction and S3-2 showed a 1.5 minute increase. There are two possible reasons for this mismatch between predictions and results. Firstly, the GRAVY score is calculated using a cumulative score of all the amino acids present, and whether or not they are hydrophobic or hydrophilic, without reference to whatever residues are adjacent. Also, these numbers are based on the amino acid properties at neutral pH, and so the physical properties of the protein may have been changed by the low pH conditions of the HPLC buffers which contain 0.1% TFA, a strong acid used as an ion pairing agent in HPLC solvents. Secondly, it has previously been observed for N-lauroylsarcosine when comparing its retention times between two different sized columns that its retention time was

dependent on the number of column volumes of buffer that had passed through the column, rather than the specific hydrophobicity of the buffer concentrations at the elution point (T. Foster, unpublished observations). Such shifts in elution times between different columns have not however been observed for any of the protein peaks.

3.3.2 Seattle p7 variations result in very different activity levels in a real-time dye release assay at pH 7.4

Of the two mutants with His17 substitutions, M2 with an H17R mutation and S2 with an H17N mutation; only S2 showed a significantly higher activity than H77 p7 activity at pH 7.4. The H17R mutation, adding a residue to the channel that is permanently protonated at neutral pH, could be predicted to result in a more open channel conformation. However, the H17N mutation results in a 3-fold increase in channel activity under standard conditions, whilst the H17R mutant does not show activity that is significantly different from that of H77 p7. The same variant in the genotype 2a J6 p7 was previously found to result in a slightly higher endpoint than the GT2A JFH1 p7 in the same *in vitro* system, with initial dye release rates at ~100 FU/min for both (StGelais, 2008). However, in virus studies the Jc1 chimera containing the structural proteins of J6 with the non-structural proteins of JFH1 produces a higher number of infectious virus particles (Pietschmann *et al.*, 2006), although differences in the other structural proteins may also play an important role in the increase in viral titres. Substitution of J6 p7 alone into JFH1 was also found to increase production of infectious virus, but not to the same extent as seen with the Jc1 chimera (Steinmann *et al*., 2007).

Three of the isolates showed significant reductions in activity compared with H77 under standard conditions. Of these, two isolates showed several mutations from the H77 sequence. S1 showed the greatest reduction in activity and possessed an Y31H mutation. This severe reduction in activity is surprising as the Y31H mutation is

relatively common across HCV genotypes, and thus would not be expected to cause such a significant drop in p7 activity. Based on the J4 p7 NMR structure model the residue at position 31 does not map to the lumen of the channel, and so would not necessarily be predicted to block the channel directly. However, it is close enough to the cytosolic entrance to the channel lumen that it is feasible that it could be acting as a second sensor, restricting the channel further than the single histidine at position 17 is able to do.

S3-1, with an A16T mutation, may have affected the position of the adjacent His17 in the channel lumen and thus have changed the ability of p7 to allow the movement of molecules through the channel.

The relatively high activity of S3-2 with its R35G mutation is unexpected, given that loop mutations have previously been shown to significantly decrease virus infectivity if the mutation is to anything other than a basic residue (Steinmann *et al*., 2007). The low levels of bacterial expression could also indicate a degree of malfunction in the protein, as previously observed with the K33A R35A mutation (StGelais *et al.*, 2009). This double-alanine loop mutation was also found to be unable to fully insert into membranes. However, as R35G is a single polymorphism, of one of two basic loop residues, the single arginine at position 35 may maintain the structural requirements for the basic loop.

3.3.3 Naturally occurring patient variants result in a switch in p7 gating phenotype

The pH of the carboxyfluorescein buffer inside the liposomes (pH_{int}) was pH 7, while the assay buffer external to the liposomes (pH_{ext}) was pH 7.4; pH 6.7 is the closest of the 3 external pH points measured. As the pH gradient is increased in either direction from this midpoint then H77 p7 activity increases. The pH changes of p7 activity between the different genotypes in response to pH was unexpected – there are 12

amino acid differences between the GT1A H77 p7 and GT1B J4 p7, compared with 26 differences between J4 p7 and the GT2A JFH1 p7 and 29 between H77 and JFH1. The role of His17 in H77 p7 may also not be as clear as for J4 p7; in J4 p7 the H17A mutation results in a severe reduction in p7 activity in the liposome assay, while in H77 p7 the same mutation in black lipid membranes, an alternative *in vitro* system, does not result in any loss of protein activity (Chew *et al.*, 2009). Thus, while His17 in H77 p7 has been shown to be present in the lumen of the channel using copper-chelation in the BLM system that blocks channel activity (Chew *et al.*, 2009), it may well not be acting as a pH sensor and/or gate. H77 p7 may already have a wider channel lumen, meaning any restriction caused by the lumenal histidine residue is insignificant to p7 function.

It is likely that low-pH activation of the p7 channel requires a histidine residue in or close to the lumen of the channel, so the phenotypic switch to low-pH activation cannot occur in the two isolates with no histidine residues. The remaining two isolates, S3-1 and S3-2 that do have His17 may just be too similar to H77 p7 to have a different phenotype.

Very few mutations were required for this switch in phenotype to pH-gated activity: the non-synonymous change for M1 was S21P and for S1, Y31H. Both isolates are far closer in overall sequence to H77 than they are to either J4 or JFH1. The S21P mutation may cause a change in the structure of transmembrane domain 1, introducing a kink in the alpha-helix that may constrict the channel to the point where the protonation-state of His17 can change the activity of the channel. Proline is also more hydrophobic than the polar serine, and thus may also change the characteristics of the channel pore lumen

The introduction of a second histidine through the Y31H mutation in the S1 isolate introduces a second possible sensor or gating residue; it may well be the case that for

this isolate the protonation-state of His17 is insignificant for channel opening but His31 is significant. It is notable that the increase in activity is more similar to that of J4 p7 than of JFH1: JFH1 also has a histidine at position 31 but shows a much higher proportionate increase in activity. With JFH1 p7 it is possible that both histidine residues are acting to gate the channel and thus the proportionate activity change on reduction of pH is considerably higher.

3.4 Conclusions

Naturally occurring variants in the p7 sequence cause changes in activity levels observed *in vitro*. There is no correlation between p7 activity and disease severity seen in the patients with the few samples tested. There is, however, a change in the channel gating phenotype observed in M1 and S1, with the non-synonymous variations S21P and Y31H respectively being sufficient to alter the pH-activation profile to that found in other genotypes.

Chapter 4: The effect of naturally-occurring variations in p7 on the production of infectious virus.

4.1 Introduction

The genotype 2a JFH1 infectious virus system was developed in 2005 (Wakita *et al.*, 2005). Until recently JFH1 and its chimeras were the only HCV constructs to efficiently produce infectious virions, and so other genotypes have been studied by the use of chimeric constructs with structural proteins substituted into the JFH1 system. The GT1A chimera HJ3-5, which contains the Core-NS2 sequence of H77 and NS3-5B of JFH1 shows the highest production of infectious virus of any GT1A chimera yet created (Yi *et al.*, 2007). HJ3-5 is referred to throughout this chapter as the H77 chimera or H77 for simplicity. A replication-null mutant JFH1-GND, henceforth referred to as GND, has a GDD-GND mutation in the viral RNA dependent RNA polymerase NS5B that renders it unable to replicate its genome, and is used as a control.

Previous studies have identified genotype-specific effects of p7, with the lumenal tails of the protein mediating non-viroporin activity (Sakai *et al.*, 2003). Substitution of p7 from the high-titre Jc1 (J6/JFH1) chimera into JFH1 has been shown to increase infectious virus titres (Steinmann *et al*., 2007), while substitution of GT1B p7 into JFH1 resulted in delayed virus release (Haqshenas *et al*., 2007a).

Following the initial characterisation of the Seattle isolate p7 activity *in vitro*, the p7 sequences were substituted into the H77 chimera. While variations in other viral proteins are likely to have occurred in the original patient isolate viruses, the substitution of p7 alone allows any changes in the production of infectious virus to be directly ascribed to the variations in the p7 sequence. It is possible that some changes may result in changes to p7 protein processing, particularly in the case of S3-2 where the R35G variant may impair p7-NS2 processing, as shown in the GT1B SPp7 replicon with the K33A R35A loop mutation (Tedbury *et al.*, 2011) and with the equivalent mutation in the JFH1 virus (Steinmann *et al*., 2007). Thus, viral protein expression was also analysed by western blot analysis.

The change in gating phenotype observed *in vitro* may affect the production of infectious virus. Previous work found that nascent JFH1 virions displayed reduced infectivity when transiently exposed to reduced pH, while secreted virions had undergone a maturation process that rendered them insensitive to the same conditions (Wozniak *et al.*, 2010). The difference in gating phenotype between JFH1 and H77 may lead to changes in virion pH sensitivity and the maturation process. Thus, the Seattle p7 viruses that displayed a low-pH activation gating phenotype may also show changes in virion pH sensitivity.

Substantial variations in p7 inhibitor sensitivity have previously been observed between p7 from different genotypes (Griffin *et al.*, 2008), and some resistance mutations to inhibitors identified. These include the L20F mutation that renders GT1B less sensitive to amantadine (Foster *et al.*, 2011; Mihm *et al.*, 2006), and F25A that confers resistance to *N*NDNJ (Foster *et al.*, 2011; StGelais *et al.*, 2009). Changes in gating phenotypes shown *in vitro* may also alter the sensitivity of M1 and S1 to p7 inhibitors when compared with H77 and the other Seattle variants. In addition, for all isolates, the synonymous, hydrophobic substitutions may also have effects on inhibitor binding; the L20F substitution in GT1B is synonymous, but significantly reduces adamantane binding.

This chapter aimed to characterise the role of p7 in the pathogenicity of the Seattle patient isolates, by cloning the sequences into the H77 chimera and investigating the effects of the p7 polymorphisms on the production of infectious virus. The changes in pH-gating phenotype observed *in vitro* may also have an effect on the role of p7 in preventing endosomal acidification during virus assembly and egress, and the effect of transient exposure to reduced pH on the H77 chimera and the Seattle isolates was also investigated. Finally, p7 inhibitors have previously been found to have genotype-specific effects on virus production, and the effect of the Seattle isolate polymorphisms on inhibitor sensitivity was also investigated.

4.2 Results

4.2.1 Cloning of virus constructs

Examination of the sequence of the GT1A/JFH1 chimera pJ3-5 identified two unique restriction sites, MauBI and AfeI, up- and downstream of the p7 sequence. Three of the patient isolate p7 sequences, M1, M2 and S1, had sufficient flanking sequence to use simple PCR to amplify the cloning insert sequence required. The S2, S3-1 and S3-2 sequences comprised only the coding region for p7 and none of the flanking sequences. In order to generate the flanking sequences incorporating the restriction sites, a long forward primer (for sequences see Appendix 1) was used for the 5' end. The 3' flanking sequence required was longer, and overlap PCR using the H77 NS2 sequence as a template for the missing 3' section was used to generate this section (Fig. 4.1). Incorporation of the patient isolate p7s into the pHJ3-5 plasmid was confirmed by commercial sequencing using the short forward and reverse primers flanking the p7 sequence.

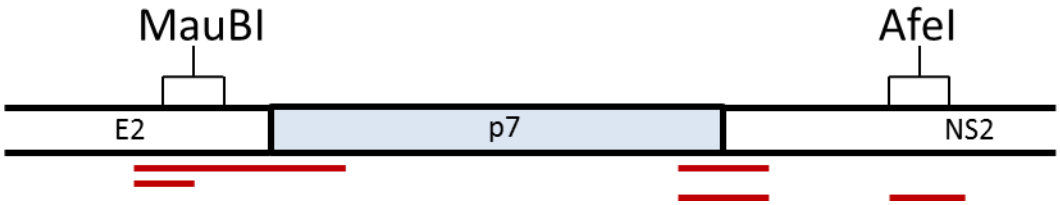

Figure 4.1 Cloning strategy for insertion of Seattle patient isolate p7s into the HJ3-5 chimera

Diagram showing the restriction endonuclease sites MauBI and AfeI close to the p7 coding region of the H77-JFH1 chimera HJ3-5. The sequence of the H77 chimeric virus was analysed for the presence of restriction endonuclease cleavage sites using pDRAW32, and MauBI and AfeI sites identified in proximity to the p7 coding region. Primers were designed to allow amplification of the sequence. For M1, M2 and S1, the cDNA had sufficient flanking sequence for a simple PCR amplification. For S2, S3-1 and S3-2, a long forward primer and overlap PCR of the region downstream of p7 had to be used to generate sufficient sequence to reach the restriction endonuclease sites.

4.2.2 Effects of patient isolate p7s on viral titres

4.2.2.1 Genotype prototypes JFH1 and H77 show expected viral titres

Initial work established the infectivity levels of the prototype viruses, JFH1 and H77. After optimisation of the timecourse of virus infectivity, JFH1, H77 and the replication-null mutant GND were assayed for their infectivity every 24 hrs for a period of 72 hrs. This timecourse was also used to compare the infectivity of the patient isolates. Secreted virus was harvested by removal of the cell media, and intracellular virus was harvested by freeze-thaw lysis of the infected cells. The results are shown in Fig. 4.2 (a) and Fig. 4.3 (a). As expected, the GND mutant did not produce infectious virus, whilst both parental strains secreted infectious virus; with JFH1 titres of 1.1 x 10^4 focus forming units per ml (FFU/ml) at 24 hrs, 2.3 x 10^4 FFU/ml at 48 hrs and 3.8 x 10^4 FFU/ml at 72 hrs. The H77 virus showed similar infectious titres at 24 and 48 hrs (7.6 x 10^3 FFU/ml and 2.6 x 10^4 FFU/ml respectively). At 72 hrs however, the infectious titres dropped to 5.5 x 10^3 FFU/ml.

The intracellular virus (Fig. 4.3 (a)) showed consistently higher values for the H77 chimera, which produced 1.9 x 10^3 FFU/ml at 24 hrs compared with 1.1 x 10^3 FFU/ml for JFH1. At 48 hrs the separation was higher; 1 x 10^4 FFU/ml for H77 and 1.8 x 10^3 FFU/ml for JFH1. At 72 hrs however, the infectivity of the H77 intracellular virus dropped to 2.9 x 10^3 FFU/ml, while JFH1 increased to 4.2 x 10^3 FFU/ml. The overall ratios of secreted: intracellular virus, (Fig. 4.4 (a)) shows that at each timepoint, JFH1 has a higher ratio of intra-to extracellular infectivity, indicating a greater efficiency of virus release. The most efficient release of virus was observed at 24 hrs for the H77 chimera and at 48 hrs for JFH1. For both viruses, the cell media showed signs of acidification at 72 hrs. The loss of H77 chimeric virus infectivity when the media becomes acidified is investigated further in section 4.3.2.

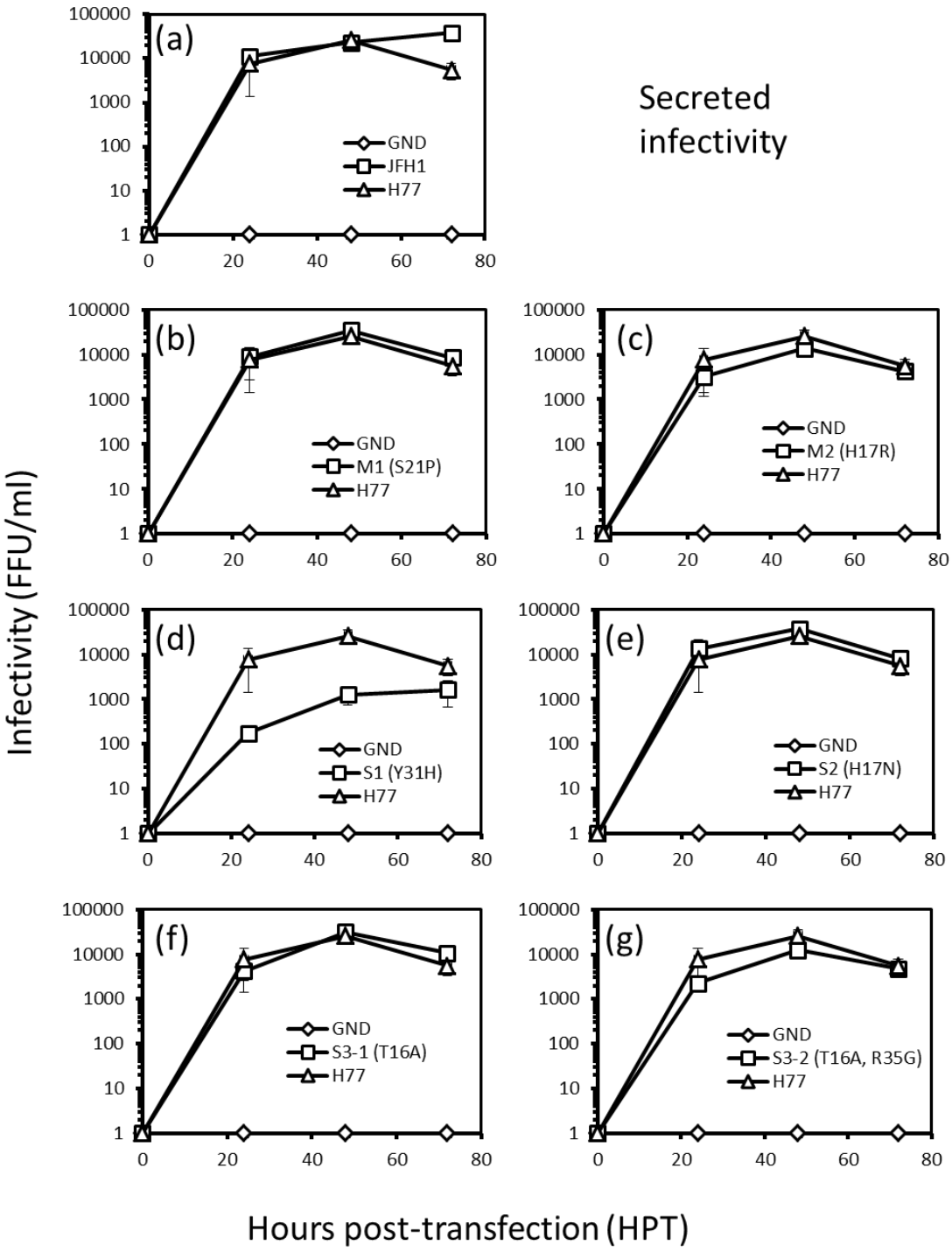

Figure 4.2 Infectivity of secreted virus over 72hr

Infectivity of secreted virus for JFH1, the replication-null mutant JFH1-GND, the H77/JFH1 chimera (H77) and the H77/JFH1 chimera with the p7 sequence substituted for the Seattle patient isolate p7 sequences. Secreted virus was harvested by the removal of media from infected cells. Infectivity was assessed by focus forming assay, where virus was serially diluted into a titre plate and allowed to infect cells for 48 hours. The infected cells were fixed and stained, then the foci counted. Each panel shows the GND and H77 controls, with the following additions: Panel (a) JFH1, (b) M1 (S21P), (c) M2 (H17R), (d) S1 (Y31H), (e) S2 (H17N), (f) S3-1 (A16T), (g) S3-2 (A16T, R35G). Experiments were performed in triplicate. Error bars = standard error of the mean (SEM)

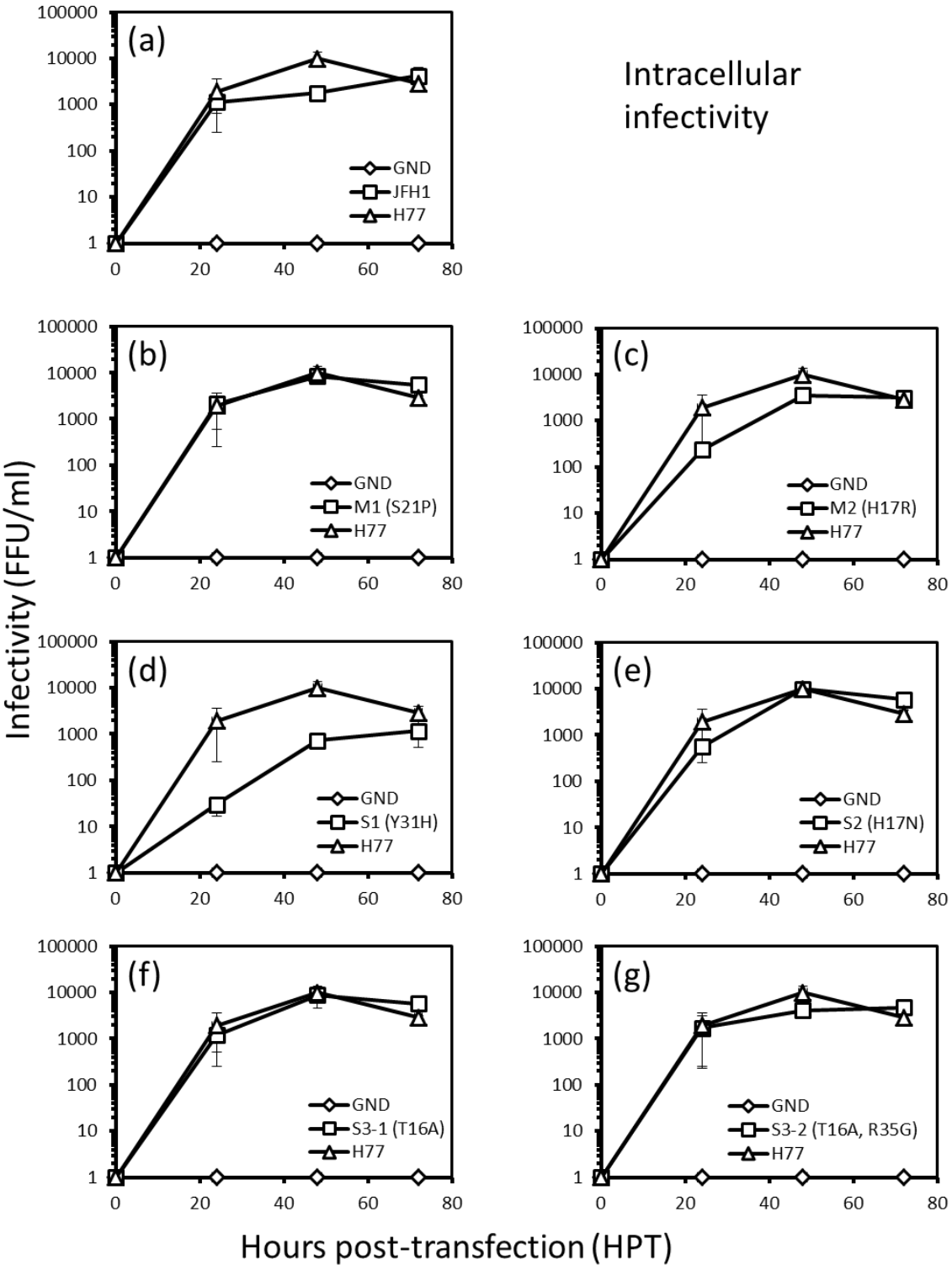

Figure 4.3 Timecourse of intracellular virus infectivity over 72hr

Intracellular infectivity of JFH1, JFH1-GND H77 and the H77/JFH1 chimera with substituted p7 sequences. For each Seattle patient isolate, intracellular virus was harvested by freeze-thaw lysis and infectivity assessed by focus forming assays 48 hrs post-infection. Each panel shows the GND and H77 controls, with the following additions: Panel (a) JFH1, (b) M1 (S21P), (c) M2 (H17R), (d) S1 (Y31H), (e) S2 (H17N), (f) S3-1 (A16T), (g) S3-2 (A16T, R35G). Experiments were performed in triplicate. Error bars = SEM

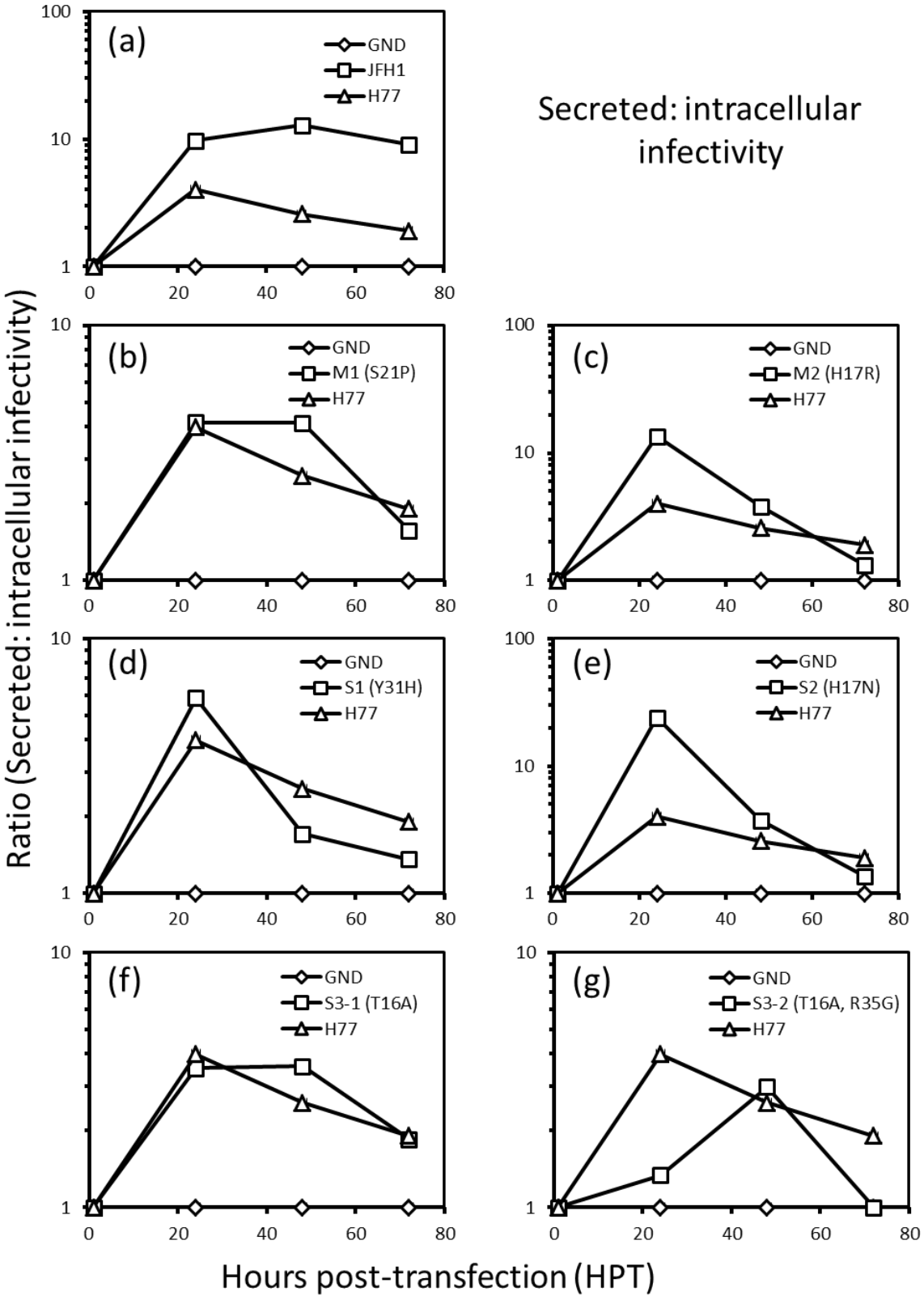

Figure 4.4 Ratio of secreted: intracellular virus over 72hr

Ratio of secreted: intracellular virus was calculated from Figs. 4.2 and 4.3. Each panel shows GND and H77 controls, with the following additions: Panel (a) JFH1, (b) M1 (S21P), (c) M2 (H17R), (d) S1 (Y31H), (e) S2 (H17N), (f) S3-1 (A16T), (g) S3-2 (A16T, R35G).

4.2.2.2 Seattle isolate p7s produce infectious virus

To investigate the effects of the Seattle variations on the production of infectious virus, the cloned Seattle isolate p7 viruses were analysed in the same manner as the parental strains.

M1 with its significant S21P mutation showed slightly higher extracellular titres than H77, with 8.9 x 10^3 FFU/ml at 24 hrs, 3.5 x 10^4 FFU/ml at 48 hrs and 8.5 x 10^3 FFU/ml at 72 hrs (Fig 4.2 (b)) The intracellular infectivity (Fig. 4.3 (b)) was also close to H77 (2.1 x 10^3 FFU/ml at 24 hrs, 8.4 x 10^3 FFU/ml at 48 hrs, and 5.5 x 10^3 FFU/ml at 72 hrs). The secreted: intracellular ratio at 24 hrs was similar for both, M1 4.1 and H77 4.0, but the slight increase in secreted viral titres and decrease in intracellular titres at 48 hrs results in a higher intra/extracellular infectivity ratio at 48 hrs (M1= 4.1 vs. H77 = 2.5).

M2 (H17R) shows reduced extracellular titres compared to H77 (3.1 x 10^3 FFU/ml at 24 hrs, 1.3 x 10^4 FFU/ml at 48 hrs and 4.2 x 10^3 FFU/ml at 72 hrs) (Fig. 4.2 (c)). The intracellular titres were also lower, (2.3 x 10^2 FFU/ml at 24 hrs, 3.6 x 10^3 FFU/ml at 48 hrs and 3.1 x 10^3 FFU/ml at 72 hrs (Fig. 4.3 (c)). The lower intracellular infectious titres increased the secreted: intracellular ratio to a peak of 13.4 at 24 hrs compared with 4.0 for H77 at the same timepoint.

S1 (Y31H) is the sole Seattle isolate that in virus shows a significant reduction in the production of infectious virus. (Fig. 4.2 (d)), The S1 secreted infectious titres were 1.7 x 10^2 FFU/ml at 24 hrs, 1.2 x 10^3 FFU/ml at 48 hrs and 1.6 x 10^3 FFU/ml at 72 hrs. The intracellular titres were also reduced (3.0 x 10^1 FFU/ml at 24 hrs, 7.3 x 10^2 FFU/ml at 48 hrs and 1.2 x 10^3 FFU/ml at 72 hrs). This is the only GT1A virus that did not show a drop in virus titres at 72 hrs. Interestingly, whilst both secreted and intracellular virus titres were considerably lower than for any other GT1A chimeric virus tested, the secreted: intracellular ratio was slightly higher at 24 hrs than for H77,

(5.8 for S1 vs. 4.0 for H77), suggesting that the release of infectious virus progeny may be more efficient for S1.

S2 (H17N) shows an increase in secreted viral titres compared with H77 (Fig. 4.2 (e)), (1.3 x 10^4 FFU/ml at 24 hrs, 3.7 x 10^4 FFU/ml at 48 hrs and 8.0 x 10^3 FFU/ml at 72 hrs). When intracellular virus infectivity was assessed (Fig. 4.3 (e)), a reduction in virus titres at 24 hrs (5.6 x 10^2 FFU/ml) was observed, but the intracellular infectious virus titres increased to similar levels to H77 intracellular titres at 1 x 10^4 FFU/ml at 48 hrs, before dropping to 5.8 x 10^3 FFU/ml at 72 hrs. The increase in secreted virus and decreased intracellular virus at 24 hrs resulted in a high secreted: intracellular ratio of 24.0 at 24 hrs, which decreased to 3.7 at 48 hrs, higher than H77 (that displayed a ratio of 2.5 at 48 hrs) (Fig. 4.4 (e)). The high ratio at 24 hrs and increased infectivity at 48hrs compared to H77 may indicate more efficient virus release for S2.

S3-1 (A16T) displayed lower secreted infectious titres than H77 (4.2 x 10^3 FFU/ml at 24 hrs) but increased higher than H77 at 48 hrs (3.1 x 10^4 FFU/ml), before dropping to 1.0 x 10^4 FFU/ml at 72 hrs (Fig 4.2 (f)). The intracellular titres (Fig 4.3 (f)) were lower than H77 at 24 and 48 hrs, (1.2 x 10^3 FFU/ml and 8.8 x 10^3 FFU/ml respectively), dropping to 5.8 x 10^3 FFU/ml at 72 hrs. The ratio of secreted: intracellular virus was only slightly lower than H77 at 24 hrs: (3.5 vs. 4.0), but the ratio increased at 48 hrs to 3.6 vs. H77 which decreased to 2.5 (Fig. 4.4 (f)) suggesting that a higher efficiency of virion release is maintained during the later stages of infection.

S3-2 (A16T, R35G) showed a reduction in virus infectivity over time, with titres of 2.3 x 10^3 FFU/ml at 24 hrs, 1.2 x 10^4 FFU/ml at 48 hrs and 4.7 x 10^3 FFU/ml at 72 hrs (Fig 4.2 (g)). The intracellular titres were also lower than H77 at 24 and 48 hrs, with titres of 1.7 x 10^3 FFU/ml and 4.1 x 10^3 FFU/ml respectively. Unusually, the intracellular titres did not decrease at 72 hrs, but further increased to 4.7 x 10^3 FFU/ml. The secreted: intracellular ratio is low at 24 hrs at 1.3, but increases at 48 hrs to 3.0 before

dropping to 1.0 at 72 hrs. This shift in the peak ratio could indicate a delay in the release of infectious virus progeny from S3-2 infected cells.

4.2.2.3 Assessment of the expression of virus proteins of the Seattle patient isolate p7 viruses

To investigate any effects of the Seattle p7 variations on viral protein expression and polyprotein cleavage, samples of the infected cells were harvested for intracellular virus as in Fig. 4.3, and assessed for virus protein expression by western blot analysis (Fig 4.5). Expression of the viral proteins p7, NS2, E2, Core, and NS5A were assessed, and the cellular protein GAPDH probed as a loading control. The blots for E2, p7 and NS2 were carried out to assess if polyprotein processing around p7 was affected by the sequence variations. Core and NS5A blots were performed to assess general viral protein expression, and to investigate the correlation between the release of infectious virus and levels of structural and non-structural proteins within the cell. The GAPDH blots were carried out to check the health of the infected cells, and to ensure that any reductions in infectious virus production were not due to cytotoxic effects. Samples for p7 and NS2 western blots were run on Tris-tricine gels, as they were previously found to show good band resolution for small proteins, as well as reduced background staining for one of the antibodies used in this study (the 1055 TB antibody for GT1B p7). All other blots were run on Tris-glycine gels; 10% for E2, 12% for Core, NS5A and GAPDH. As expected, the GND virus showed no viral protein expression. The consistent levels of GAPDH expression confirmed the Huh7 cells were healthy. JFH1 shows the expression of viral proteins at all 3 timepoints, while H77 and the Seattle viruses display only show minimal NS5A expression at 24 hrs, with no detectable expression at 24 hrs for any of the other viral proteins. The expression of viral proteins at 48 hrs is often noticeably higher than at 72 hrs, indicating that the acidification of the media may be reducing viral protein expression as well as the production of infectious virus.

The 2716 p7 antibody for JFH1 p7 was found to be cross-reactive with H77 p7. As this antibody was originally raised against the N-terminal 13 residues of JFH1 p7, the H77 and Seattle p7 expression levels cannot be directly compared to each other due to sequence variation in this region (Fig. 3.2). While M1 shows low apparent expression levels, this could also be due to sequence variations at position 6 and 7 (V6I I7V). M2 possesses an identical sequence to H77 in this region, and the p7 expression levels were comparable with H77. S1 and S2 are also identical in this N-terminal region with an I7L variant, and S1 shows lower p7 expression levels than S2. S3-1 and S3-2 are also identical in this region with an I7V variant, and S3-2 shows very low p7 expression levels when compared with S3-1.

The NS2 sequence is identical between the H77 and Seattle viruses, but variations in its expression levels between the viruses were observed. H77, M2 and S3-1 all show slightly lower expression levels than M1, S1, S2 and S3-2. E2, also identical between the viruses, also shows some variations, with S1 and S3-2 showing higher E2 levels, possibly indicating an intracellular accumulation of E2, due to reduced virus export, or improper E2 folding.

Core levels also show some variation, with S1 showing lower expression levels. This could correlate with the reduced production of infectious virus for S1, as reduced Core expression will limit the amount of infectious virus that can be produced. NS5A does not show a significant variation in expression between the viruses, indicating that the changes in p7 do not influence NS5A expression/stability. GAPDH also shows no variation between the viruses or the GND control, showing that the viruses have not increased any virus specific cytopathic effects, and that the acidification of the media that most likely impacted the H77 and Seattle viruses at 72 hrs, did not affect the overall health of the infected cells.

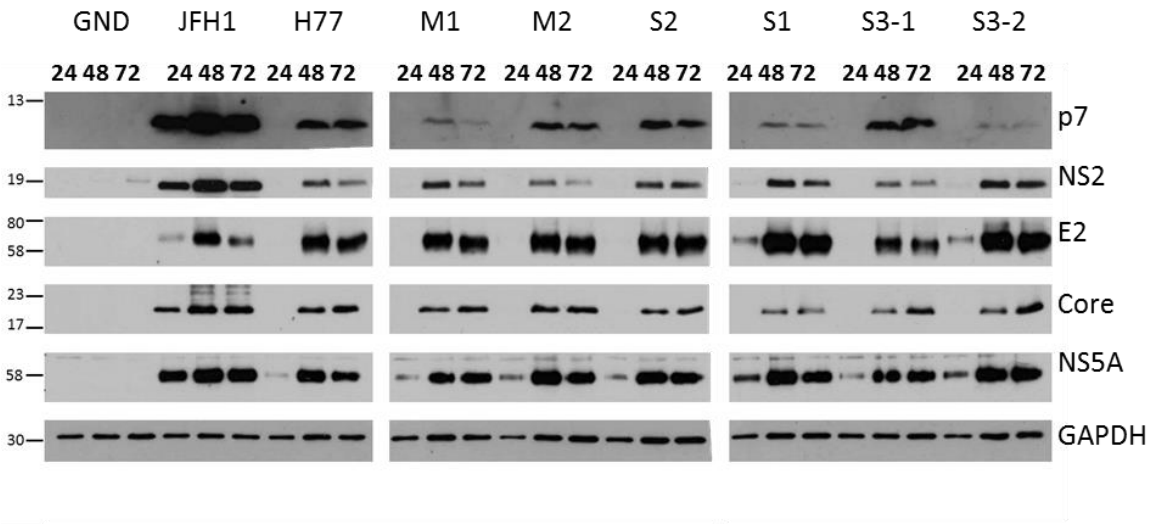

Figure 4.5 Expression of viral proteins over 72 hrs

Infected cells were harvested and assessed for virus protein expression by Western blot analysis. Western blots for p7 and NS2 were run on 10% Tris-tricine SDS-PAGE gels, E2 blots on 10% Tris-glycine SDS-PAGE gels and Core, NS5A and GAPDH blots were run on 12% Tris-glycine SDS-PAGE gels. All gels were transferred to PVDF membranes using the standard protocol. For each virus, 24, 48 and 72 hr timepoints are shown.

4.2.3 Exposure to low pH impairs genotype 1a viral infectivity

Both H77 and the Seattle patient chimeras showed a consistent loss of virus infectivity at 72 hours. This loss is most likely due to the build-up of metabolites such as lactic acid in the cell media, which is sufficient to cause a reduction of extracellular pH. The effect of exposure of GT1A virions to low pH was therefore investigated. Previous work in JFH1 identified that intracellular virus particles were rendered non-infectious by transient exposure to low pH, whilst secreted virions appeared to have undergone a maturation step during virus assembly/release that rendered them resistant to pH-mediated inactivation (Wozniak *et al.*, 2010). The transient pH reduction protocol used in these studies was adapted and optimised, and the results are shown in Fig 4.6. The relative insensitivity of secreted JFH1 particles to transient exposure to low pH was reproduced, with a drop of only 25% in infectivity when the pH was reduced to 4.0, compared to an 85% reduction of infectivity in intracellular particles. H77, as hypothesised, displayed a loss in infectivity following exposure to low pH of both secreted and intracellular virions, with secreted virions showing a 49% loss of infectivity at pH 6.2, 69% at pH 5.2 and 78% at pH 4.0, which were statistically significant differences from JFH1 at all 3 reduced pH values. The loss of infectivity of intracellular virus was also greater for H77 than JFH1, with JFH1 showing an 85% loss of infectivity at pH 4.0, while H77 showed a 97% loss.

As p7 is not thought to be present in the HCV virion, the effect of low pH exposure on the infectious virions is most likely mediated by the envelope glycoproteins E1 and E2 that control acid-dependent fusion during virus entry. If this is the case, then the secreted Seattle isolate p7 viruses would be predicted to show the same pH sensitivity as the H77 chimera, as the structural proteins are identical between these viruses.

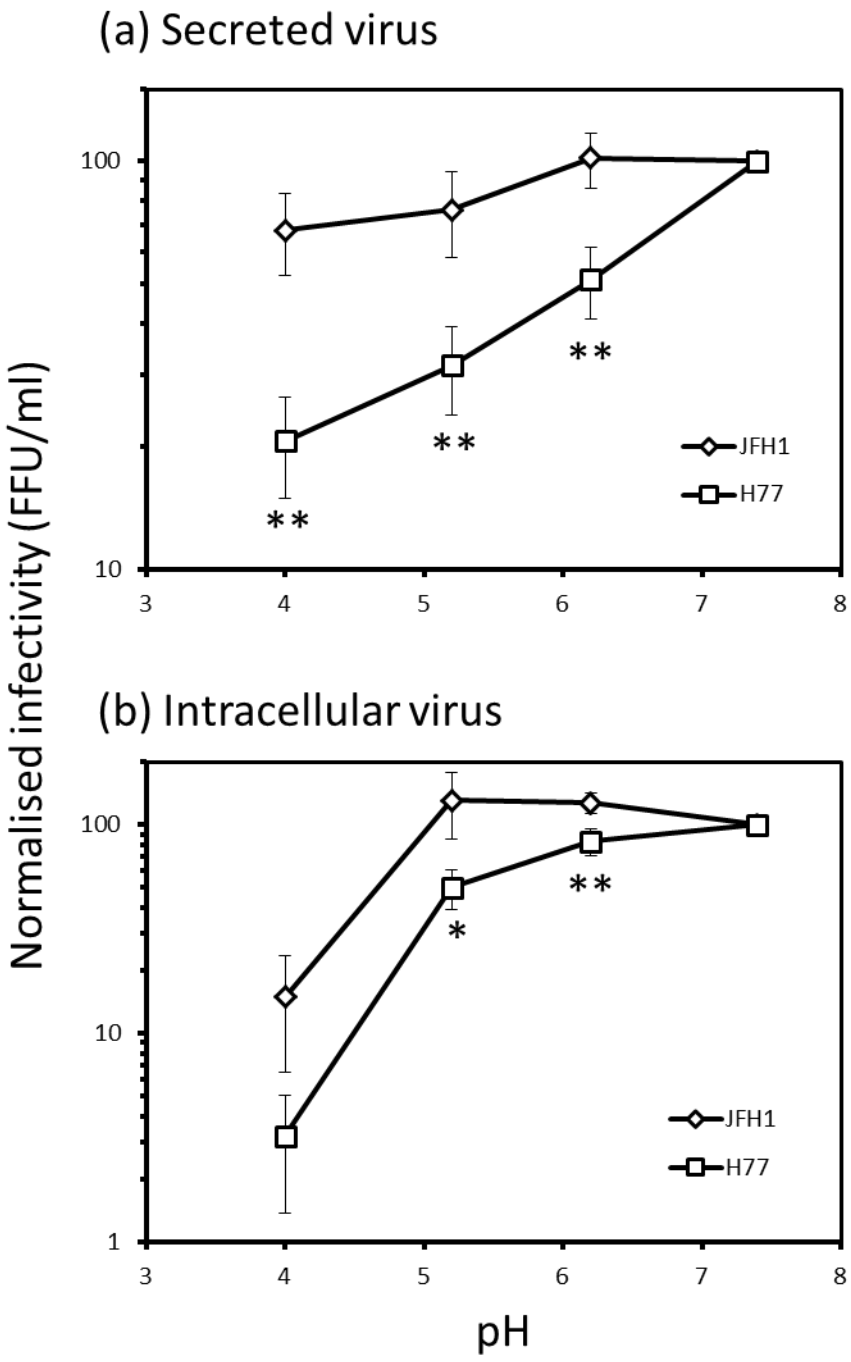

Figure 4.6 Infectivity of JFH1 and H77 viruses after transient exposure to reduced pH.

Secreted virus was concentrated by sucrose-cushion centrifugation and resuspended in PBS. Intracellular virus was harvested by freeze-thaw lysis of infected cells in PBS. Virus in PBS was then mixed 1:1 with HEPES-MES buffers to produce a final pH of 4, 5.2, 6.2 and 7.4 at 37 °C for 10 minutes. Samples were restored to neutral pH using 1 M NaOH. Samples were titred for infectivity by focus forming assays. Experiments were performed in triplicate and normalised to the infectivity at pH 7.4. Error bars = SEM. A Student T test was used to compare each pH point, * = p≤ 0.05, ** = p≤ 0.01.

4.2.4 Seattle isolates M1, S1 and S2 show apparent secreted virion pH sensitivity closer to JFH1 than H77

Due to the marked differences in pH sensitivity of JFH1 and H77 virions, the effect of any changes in the M1, S1, and S2 Seattle patient isolates were assessed for their pH sensitivity as in Fig. 4.6. If the virion pH sensitivity is mediated entirely by the structural proteins, then no differences would be expected to be observed between the parental H77 and the Seattle patient isolate viruses. M1 and S1 both display a low-pH activation profile *in vitro*, and while S1 had low viral titres compared with the other viruses, it was also the only GT1A virus that did not show a drop in the infectivity of secreted virus at 72 hr during the timecourse of infection.

All 3 of the Seattle viruses tested showed a pH sensitivity pattern that was closer to that of JFH1 than H77 (Fig 4.7). Due to limited time, only one experiment was performed, and this resulted in low statistical significance for some data-points. While M1 shows a similar pattern to JFH1, it did not show statistically significant differences with H77 at each pH point. S1, however, did show statistically significant differences from H77 at all 3 of the reduced pH points. S2 also showed statistically significant differences from H77 at all the reduced pH points, but at pH 4.0 it also displayed significant differences from JFH1, showing intermediate pH sensitivity between JFH1 and H77.

The intracellular virus pH sensitivity, however, showed levels closer to that of H77 than JFH1, although fewer of the data-points showed any statistical significance. Once again, M1 did not show a statistical significance. However, the data-points at pH 6.2 and 5.2 are close to those of H77, whilst the sensitivity to pH 4.0, was similar to that of JFH1. For S1, the pH sensitivity again matched that of H77, and at pH 6.2 shows a statistically significant difference from the JFH1 value. S2, which showed an intermediate sensitivity for secreted virus at pH 4.0, showed a reduction in infectivity at pH 6.2 that was significantly greater than both JFH1 and H77.

Thus, while these were initial experiments and were not repeated to the same extent as the JFH1 and H77 virus pH assays shown in Fig. 4.6, the changes in pH sensitivity from H77 may indicate that the pH sensitivity of the virion is mediated by more than genotype variations in the envelope glycoproteins. These data point to a role of changes in p7 affecting the glycoprotein maturation process that is hypothesised to render secreted JFH1 virions insensitive to transient reductions in pH.

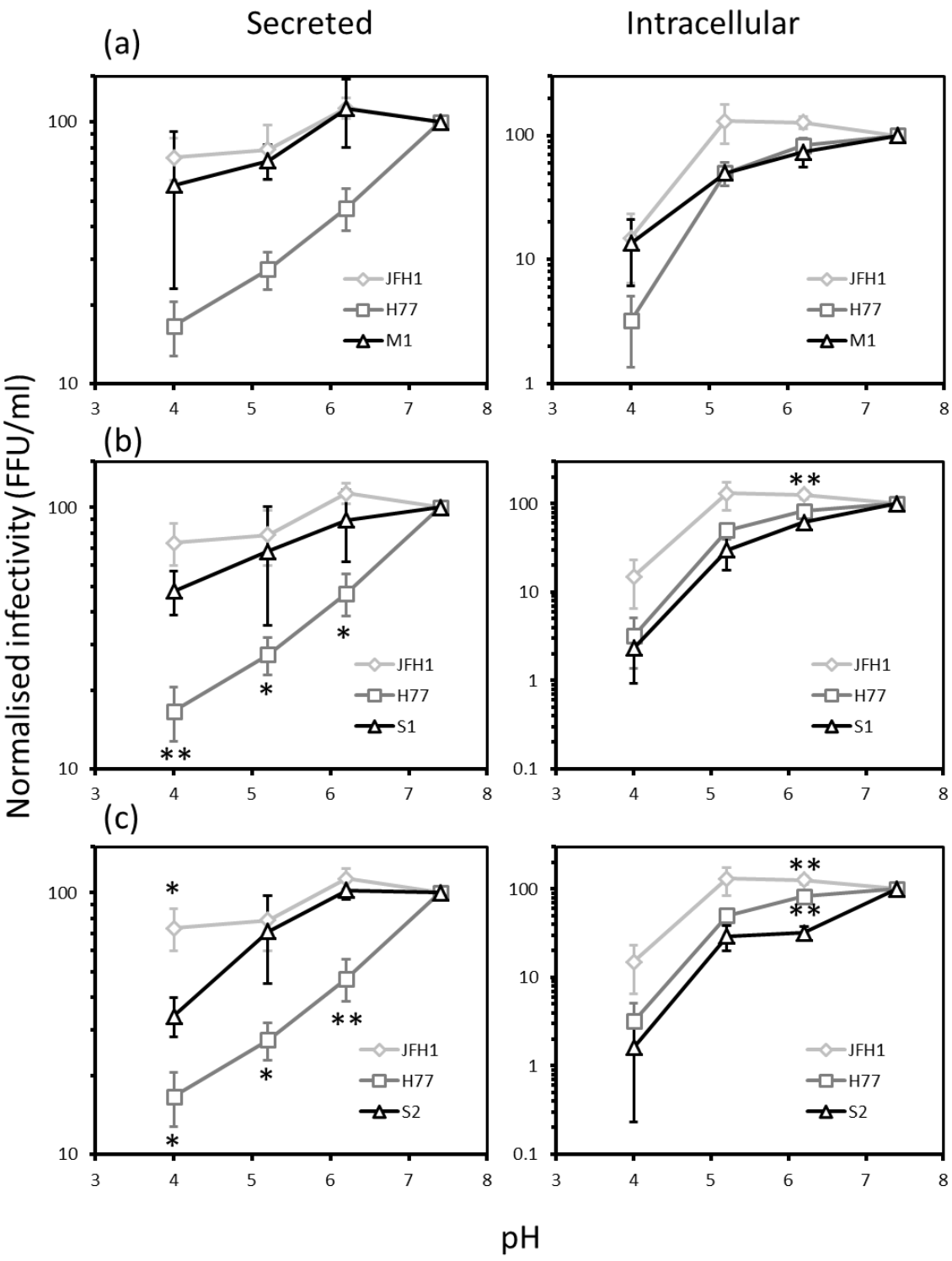

Figure 4.7 Infectivity of M1, S1 and S2 H77 viruses after transient exposure to reduced pH

Secreted virus from M1, S1 and S2 viruses were concentrated and assessed for sensitivity to pH as in Fig. 4.6. Experiments were performed in duplicate and normalised to the infectivity at pH 7.4. Error bars = SD. A Student T test was used to compared the parental virus to the Seattle virus, * = p≤ 0.05, ** = p≤ 0.01.

4.2.5 JFH1 and H77 show similar sensitivity to temperature

One possible reason why GT1A virus particles display greater sensitivity to transient exposure to low pH may be due to a greater overall instability of the viral particles, perhaps due to weaker non-covalent associations between Core protein units in the capsid, or between E1 and E2 heterodimers. One relatively simple way to test the stability of virions is to assess their thermal stability. JFH1 particles have been shown to be rendered non-infectious by exposure to high temperature; 54 °C was sufficient to reduce infectivity to undetectable levels over a period of 40 minutes (Song *et al.*, 2010). Thus, to assess their thermal stability, JFH1 and H77 virions were exposed to temperatures of 54 °C and samples removed at 5 minute intervals over a period of 1 hour. The infectivity of these samples was then assessed by focus forming assays. The results are shown in Fig 4.7.

The relative infectivity of each virus stock was normalised to the T=0 timepoint for each virus isolate. After 5 minutes of high temperature treatment, H77 showed a 55% drop in infectivity, compared with a 34% drop for JFH1. At T=10, JFH1 infectivity had dropped a further 30%, while H77 remained constant. For the remainder of the timecourse the percentage of JFH1 infectivity remained below that of H77. Taken together, these data suggest that the enhanced sensitivity of the H77 virions to decreased pH was not due to the H77 virions possessing lower stability than their JFH1 counterparts.

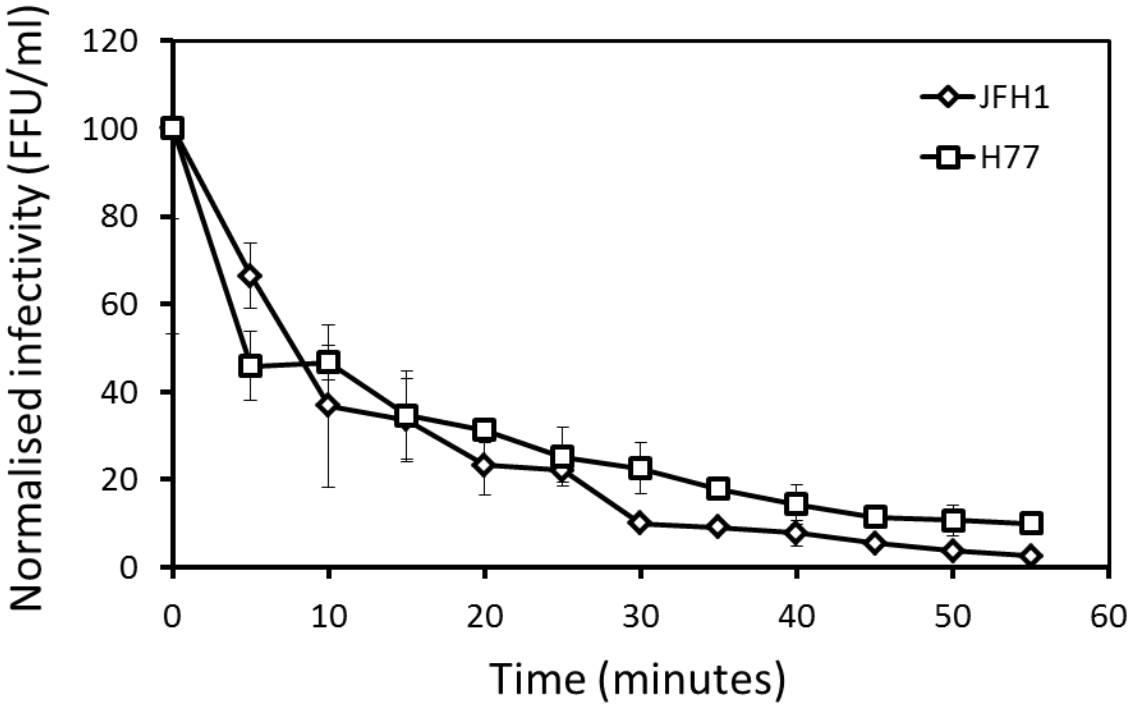

Figure 4.8 Thermostability of JFH1 and H77 viruses

Secreted JFH1 and H77 virus were incubated at 54 °C and assessed for infectivity by focus forming assay. Experiments were performed in triplicate and normalised to the initial levels of infectivity. Error bars = SEM.

4.2.6 M1 and S2 show H77-like responses to p7 inhibitors, S1 shows high sensitivity to rimantadine

Previous work comparing the effect of p7 inhibitors on HCV genotypes found a number of phenotypes. H77 was found to be resistant to adamantanes, JFH1 was sensitive to rimantadine but not amantadine, Jc1 (J6) was sensitive to all characterised p7 inhibitors, as was J4, and the GT3A p7 452 was resistant to *N*NDNJ. The *in vitro* work with the Seattle patient isolate p7s showed that M1 and S1 had low-pH activation phenotypes more typical of J4 or JFH1 than H77. Thus, whether the change in gating phenotype also mediated an alteration to p7 inhibitor sensitivity was investigated. Due to time constraints, only selected Seattle viruses were investigated; these included M1 and S1 due to their low-pH activated gating phenotypes, and S2 due to its high activity and the Jc1-like H17N variation.

To assess the effects of p7 inhibition on the production of infectious virus for M1, S1 and S2 isolates, Seattle viruses were incubated in media containing rimantadine and *N*NDNJ at 20, 40 and 80 μM from 4-48 hrs post-transfection. The results for rimantadine are shown in Fig. 4.9. As expected, JFH1 showed greater sensitivity to rimantadine than H77, with a 48% drop in infectivity at 20 μM, 64% at 40 μM and 67% at 80 μM. H77 showed only a slight response to rimantadine, with an 18% drop in infectivity at both 20 μM and 40 μM, and at 80 μM increased to 5% higher than the no-drug control. This increase in infectivity may be due to the basic nature of rimantadine adding an extra buffering effect to the media, preventing the acidification that impacts on H77 infectivity. Of the Seattle p7 viruses, M1 and S2 both followed the same pattern as H77, with M1 showing a 15% drop at 20 μM rimantadine, 17% at 40 μM and an increase above the no-drug control of 26% at 80 μM. S2 displayed a 21% drop at 20 μM and 40 μM, increasing to 5% below the no-drug control at 80 μM. S1, however, displayed increased sensitivity to rimantadine with a 45% drop at 20 μM, 46% at 40 μM and 53% at 80 μM.

The results for *N*NDNJ are shown in Fig. 4.10. Both JFH1 and H77 viruses were sensitive to *N*NDNJ, with JFH1 showing greater sensitivity than H77. JFH1 displays a 63% drop in infectious virus production at 20 μM, 78% at 40 μM and 91% at 80 μM, while H77 has a 26% drop at 20 μM, 47% at 40 μM and 71% at 80 μM. Again, M1 and S2 show a similar sensitivity to H77, with M1 showing a 29% drop at 20 μM, 52% at 40 μM and 74% at 80 μM, and S2 showing a 33% drop at 20 μM, 46% at 40 μM and 76% at 80 μM. S1 showed greater sensitivity to *N*NDNJ than both H77 and JFH1, with a 91% drop at 20 μM, 95% at 40 μM and 98% at 80 μM. It is thus possible that the changes in p7 inhibitor sensitivity are due to the synonymous hydrophobic residue substitutions in p7 sequence.

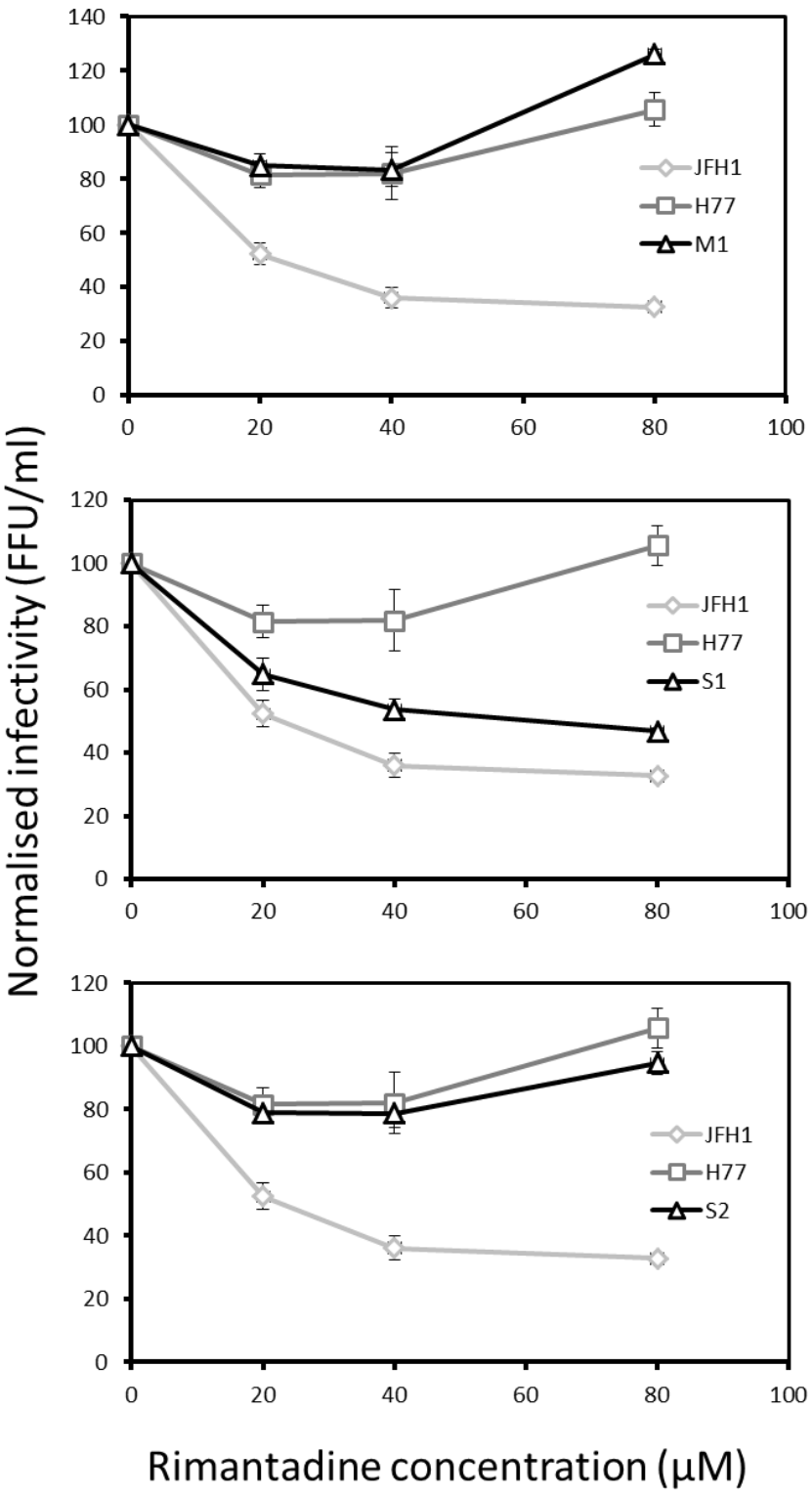

Figure 4.9 Effect of rimantadine on JFH1, H77, M1, S1 and S2 viruses

Virus electroporations were aliquoted into 12-well plates. 4 hrs post-electroporation, infected cells were treated with rimantadine (20-80 µM) for a further 48 hrs. Secreted virus was harvested and virus infectivity titred. Experiments were performed in triplicate. Error bars = SE of the mean.

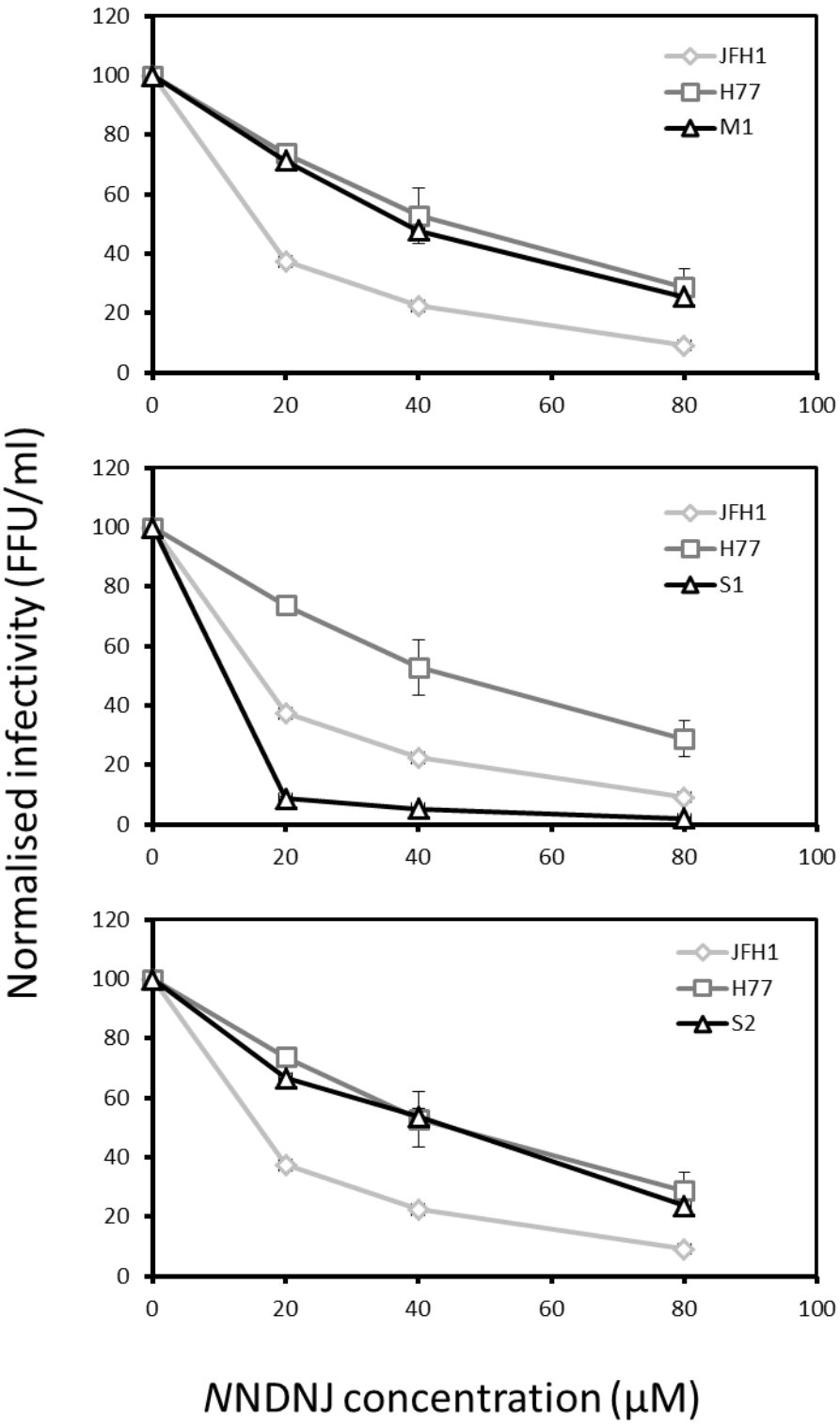

Figure 4.10 Effect of *N*NDNJ on JFH1, H77, M1, S1 and S2 viruses.

Virus electroporations were aliquoted into 12-well plates. 4 hrs post-electroporation, infected cells were treated with *N*NDNJ (20-80 µM) for 48 hrs. Secreted virus was harvested and virus infectivity titred by focus forming assay. Experiments were performed in triplicate. Error bars = SEM

4.3 Discussion

The substitution of p7 sequences between viral constructs has previously been used to identify p7-specific effects on the production of infectious virus (Steinmann *et al*., 2007; Sakai *et al*., 2003). While the lumenal tails of p7 have been shown to display genotype specific effects, substitution of p7 into the same genotype where the lumenal tails are identical or closely conserved, should rule out effects on polyprotein cleavage at the E2-p7-NS2 junctions and protein-protein interactions. The Seattle patient isolate sequences were thus substituted into a H77 chimera to assess the effects of their sequence variations on the overall production of infectious virus. In the course of this work, genotype-specific differences in pH sensitivity of the virus particles were identified.

While the major virus system for HCV is entirely based on JFH1 and its chimeric derivatives, this does have advantages when comparing the effect of an individual protein on the production of infectious virus. As pHJ3-5 is a chimera of H77, the RNA replication machinery, with the exception of its interactions with the structural proteins, cannot be implicated in any loss of infectivity. By substituting the Seattle patient isolate p7 sequences into the H77/JFH1 chimera, any possible compensatory mutations that occurred in the full virus of the patient isolate can be ruled out, and any overall change in the production of infectious virus can be attributed to differences in p7 function. As these sequences were derived from patients, and thus originated from infectious viruses, the problems of any non-specific effects of the mutations, such as the effect of mutation of the basic loop residues causing the incorrect processing of NS2, can also be ruled out. The N and C terminal lumenal tails of each p7 are also unchanged in the patient isolates when compared with the H77 sequence. As these regions mediate the non-viroporin activity of p7, it is likely that any effects on the production of infectious virus are due to changes in the viroporin activity of p7.

4.3.1 Effects of Seattle variations on infectious virus production

High levels of p7 activity are hypothesised to enhance the protection of nascent virions against the exposure to a reduced endosomal pH during virus assembly and release. However, this may also lead to enhanced cytopathic effects as any perturbation of normal endosome activity would also be enhanced. Low levels of p7 activity, or changes in the gating phenotype, could result in a reduced production of infectious virus when the substituted Seattle patient isolates are present. This may be due to the virions in this study consisting of the structural proteins of H77 with no compensatory mutations that may have occurred in the original Seattle isolates to compensate for changes in p7 activity. This would include the protection from endosomal acidification.

The two isolates that showed a low-pH activation profile *in vitro* displayed very different phenotypes in virus. M1 showed comparable titres to H77, while S1 showed a ~1.5 $\log_{10}$ drop for secreted virus and a ~1 $\log_{10}$ drop for intracellular virus. Thus, the change in gating phenotype alone cannot account for specific changes in the production of infectious virus.

M1 showed comparable expression levels of all H77 viral proteins, with the exception of p7: the apparent low p7 expression levels may simply be a result of the antibody specificity, as two residue variations between M1 and H77 are present in the N terminal 13 residues targeted by the antibody (V6I and I7V).

M2, with its H17R variant, showed slightly lower activity than H77 p7 *in vitro* although the differences were not found to be statistically significant. The viral titres were lower for M2 than for H77 for both secreted and intracellular virus, with the lower intracellular titres resulting in an increase in the secreted: intracellular ratio. Thus, while virus titres may be reduced, it is possible that the changes in p7 increased the efficiency of virus release. The western blot results showed comparable expression

levels of Core, E2 and NS5A, but with slightly reduced NS2 levels. Mutations of p7 in a GT1B replicon containing p7 and NS2 were previously shown to have variable effects on NS2 levels, with H17A showing no impact on NS2 expression, while G39A caused a reduction. The K33A R35A mutation displayed a complete loss of NS2 (Tedbury *et al.*, 2011). This suggests that the reduction in NS2 levels, in this study, were most likely due to the changes in p7. The reduced levels of NS2 may explain the reduction in infectious virus production observed.

S1 p7, with its Y31H variation, showed the greatest reduction in viral titres of all the Seattle patient isolate viruses. S1 showed the lowest p7 viroporin activity *in vitro* and when the pH was reduced to 6.2 its activity never exceeded that of H77. The reduced p7 activity, in addition to the lack of activity shown at pH 7.4, may account for this isolate p7 displaying a significant effect on viral infectivity.

Despite the high activity of the S2 isolate observed in *in vitro* liposome assays, it displayed no phenotype in virus systems, with the virus timecourse displaying only a modest increase in the production of infectious virus in comparison with H77. Jc1, which has the highest production of infectious virus of any HCV construct yet created, also possesses an H17N variation, and substitution of Jc1 p7 alone into the JFH1 background has previously been shown to increase titres by ~1.5 $\log_{10}$. While S2 only shows a slight increase in comparison (42% higher than H77 at 48 hrs) this sequence variation may enhance the production of infectious virus. Previous work with Jc1 p7 (J6 p7) showed *in vitro* activity levels in liposome assays below that of J4 and JFH1 p7 (Griffin *et al.*, 2008), meaning the high level of *in vitro* activity shown by S2 cannot be directly correlated with the H17N variation.

S3-2 showed slightly reduced viral titres when compared with H77 and with its close partner S3-1. As the major mutation in this isolate is in one of the two basic loop residues, this result was surprising. Previous work in JFH1 found that single mutations

to either of the two loop residues to the polar glutamine rather than the hydrophobic alanine, resulted in a 1 $\log_{10}$ drop in the production of infectious virus The double-alanine loop mutation in both JFH1 and a GT1B replicon containing p7 has previously been shown to perturb E2-p7-NS2 processing, with uncleaved E2-p7-NS2 found in virus (Steinmann *et al*., 2007) and no detectable NS2 in the replicon (Tedbury *et al.*, 2011). Despite this, the R33Q R35Q mutation in virus did not show a defect in p7 processing (Steinmann *et al*., 2007). Thus, while it is surprising that the R35G variant in S3-2 only caused a slight drop in the production of infectious virus, previous work shows that protein processing may not be affected. The presence of at least one charged basic residue may still allow this region to mediate membrane insertion of p7, and the lower activity shown *in vitro* may mean enhanced endosomal p7 accumulation is required to raise the endosomal pH to similar levels to WT p7, maintaining the stability and infectivity of virions. This may account for why, unlike the other Seattle isolates, S3-2 shows a peak secreted: intracellular ratio at 48 hrs rather than 24 hrs.

S3-1 and S3-2, which originated from the same patient and are the most closely matched pair of all the Seattle isolate p7s, show some interesting variations in protein expression levels. The Core and NS5A levels are closely matched, but S3-1 shows lower levels of NS2 and E2, and higher levels of p7 than S3-2. The R35G mutation, while not showing a severe impact on viral titres, as might have been expected based on all previous work involving mutations to the basic loop residues, clearly has major effects on protein levels. No detectable uncleaved precursors were found by western blot so these effects are unlikely to be due to polyprotein processing defects.

All Seattle patient isolate viruses showed expression of the viral proteins p7, NS2, E2, Core and NS5A by western blot, but there were some variations evident. Some of the variations observed for p7 may be accounted for by the specificity of the antibody, as it was originally raised against the N-terminal 13 residues of JFH1. However, as some of the H77 and Seattle p7 sequences are matched in the first 13 residues it is possible

to perform a comparison of p7 expression. M1 shows low apparent p7 levels, but possesses two residues that differ from H77 (V6I and I7V) and so this may be attributed to reduced antibody binding. M2 is identical to H77 in this region, and the expression levels are comparable. S1 and S2 however, are identical in their sequences for the first 13 residues and do show reduced expression for S1 – combined with the lower expression levels observed for Core protein. This reduced expression may account for why the titres are much lower for S1 than for any of the other Seattle isolate viruses.

The variations in E2 levels shown between the different viruses seem to have a reverse-correlation with the production of infectious virus – the viruses with the lowest titres show the highest levels of E2. With the lower *in vitro* activity of both of these p7s, the E2 levels could be explained by an accumulation of non-functional E2 protein, possibly as a result of reduced p7 viroporin activity. This is unlikely to be due to polyprotein processing defects, however, as no uncleaved proteins were detected for any of the Seattle isolate p7 viruses.

4.3.2 Secreted H77 virions are more sensitive to transient exposure to reduced pH than JFH1

The persistent reduction in infectivity of secreted H77 virus and all but S1 of the Seattle isolate viruses at 72 hrs suggested that experimental conditions at this timepoint were causing the reduction in infectivity. At the 72 hr timepoint, the cell media displayed signs of acidification, with the phenol red fading to an orange colour. This acidification is due to the accumulation of cell metabolites, most likely lactic acid as many tumour cell lines primarily use glycolysis for respiration (Moreno-Sánchez *et al.*, 2007). JFH1 secreted virions have previously been shown to be insensitive to transient exposure to reduced pH, while the intracellular virions were sensitive to intracellular pH (Wozniak *et al.*, 2010). This assay was adapted to compare the relative pH sensitivity of JFH1 and H77 virions. The observed increased pH sensitivity

of secreted H77 virions may provide a reason why H77 p7 shows higher activity at pH 7.4 *in vitro*; with more sensitive virions, p7 may have to act earlier in the virus life cycle and prevent even slight alterations to endosomal acidification

The drop in infectivity also seen with the intracellular H77 virus and many of the Seattle p7 viruses may be accounted for by an effect shown in section 5.2.3. An endosome-targeted pH sensor protein fused to the endosomal protein VAMP2 (Miesenbock *et al*., 1998) was shown to be highly responsive to external buffer pH in Huh7 cells, and so the acidification of the media may also result in acidification of intracellular compartments, thus overriding any ability of p7 to raise endosomal pH.

4.3.3 Virions from Seattle variants M1, S1 and S2 show possible intermediate pH sensitivities

If the virion pH sensitivity were mediated entirely by the structural proteins that form the virion, particularly the E1 and E2 envelope glycoproteins that mediate acid-dependent membrane fusion (Hsu *et al.*, 2003), then it would be expected that the virions produced by the Seattle p7 viruses would be identical to those produced by the parental H77 chimera. However, as this was not the case it raises the intriguing possibility of p7 mediating a process of virus maturation that renders the virions resistant to transient exposure to reduced pH. Another possibility is that p7 could be present in the virions in very low numbers, and the variations in p7 may affect the resistance of the virions to reduced pH. p7 has never been detected in virions, so this possibility can be considered unlikely.

However, these experiments were not repeated due to reasons of time and so further repeats would be advisable before it can be stated with certainty that the changes in p7 have altered the pH sensitivity of the virions, as the initial timecourse assays showed that all Seattle viruses but S1 had reduced infectivity at 72 hrs.

4.3.4 JFH1 and H77 virus particles show similar thermal stability

A possible explanation for the greater sensitivity of H77 virions to transient reductions in pH could be that the virion components Core, E1 and E2 formed less stable interactions than in JFH1 virions. If the non-covalent associations between these proteins were weaker, then it would be expected that H77 virions would be heat inactivated more quickly than JFH1. The thermal inactivation of JFH1 virus infectivity had previously been shown over a 40 minute period at 54 °C (Song *et al.*, 2010), and so secreted virions were tested at this temperature. It was found that JFH1 and H77 virions had no major differences in the speed at which they were heat inactivated. Thus, the pH-sensitivity of the secreted virions is not dictated by the overall stability of the virus particles.

4.3.5 p7 inhibitor sensitivities changed in S1 (Y31H)

4.3.5.1 S1 (Y31H) shows an increased sensitivity to rimantadine, M1 and S2 are comparable to H77

The increased sensitivity of S1 to rimantadine is surprising when the sequences of H77, M1 and S2 are compared. Of the 3 Seattle isolate viruses tested, S1 has the least total deviation from the H77 sequence, with a single non-synonymous variant Y31H, and three synonymous changes I7L, V41A and F45V. This compares with 9 variant residues between M1 and H77, and 8 variants between S2 and H77. The mutations previously found to confer adamantane resistance in J4 p7 were L20F (Foster *et al.*, 2011), and amantadine resistance with L50-55A (StGelais *et al.*, 2009). S1, like H77 has a valine at position 20 and no alterations to L50-55. A leucine-rich binding pocket was identified in J4 p7 as the rimantadine binding site (Foster *et al.*, 2011), but the sole additional leucine residue in S1 is at position 7, predicted to lie in the N-terminal lumenal tail rather than adjacent to other leucine residues in the TMDs. Also the same I7V variant is present in S2, which showed no increased sensitivity to rimantadine. Thus, the increase in rimantadine sensitivity observed does not conform

to any known precedent in previously-studied p7 resistance mutations, and may be due to its gating phenotype.

M1 also shows a low-pH activation profile, but no sensitivity to rimantadine. M1 has just under half the initial rate of H77 at pH 7.4 in the liposome assay, while the very low activity of S1 at pH 7.4 may indicate that the S1 channel is almost completely inactive at this pH. The Y31H variation may cause this low channel activity, both as an additional barrier to ion passage through the channel, and as a relatively hydrophobic residue at pH 7.4.

4.3.5.2 S1 shows greater *N*NDNJ inhibition

*N*NDNJ was included as a control drug that inhibits both JFH1 and H77 p7. However, S1 p7 viruses possessed an enhanced sensitivity to this drug on the production of infectious virus. F25A is known to confer *N*NDNJ resistance (Foster *et al.*, 2011), but both H77 and all the Seattle variants also have phenylalanine at this position and so this cannot explain the increased sensitivity to *N*NDNJ observed. One possibility is that the low levels of p7 expression with S1 when compared with S2 could mean that there are proportionately fewer p7 channels present in the cell. This may enhance the effectiveness of *N*NDNJ on the production of infectious virus.

4.4 Conclusions

All the Seattle isolate p7 sequences were able to produce infectious virus when cloned into an H77 chimeric background, although S1 resulted in a significant drop in viral titres. The R35G variant in S3-2 caused only a slight drop in viral titres, and a delay in virus release shown by the peak in the secreted: intracellular ratio at 48 hrs rather than 24 hrs. Once again, no differences were observed between the ‘mild’ M and ‘severe’ S isolates. H77 virions are more sensitive to transient exposure to reduced pH.

Chapter 5: The development of cell based assays to measure p7 activity.

5.1 Introduction

p7 has been shown to increase the pH of intracellular compartments. Blocking this process using p7 inhibitors significantly reduces virus infectivity (Wozniak *et al.*, 2010). Whilst live cell imaging is an effective method to characterise the cellular effects of p7 during virus infection, the use of live cell microscopy on cells infected with the JFH-1 infectious clone presents a number of challenges. As no fluorescence microscope was available in the CL3 facility during the course of this study, cell based p7 assays suitable for a CL2 containment microscope required development. p7 alone and in the context of subgenomic replicons has previously been expressed in a number of cell-based systems.

Intracellular pH can be measured using a number of techniques. Lysosensor yellow-blue DND-160 (Lysosensor Y/B) (Invitrogen Molecular Probes) was used in previous studies to determine that p7 raised endosomal pH, and that this effect could be blocked by the p7 inhibitor rimantadine (Wozniak *et al.*, 2010). Fig. 5.1 shows the excitation (a) and emission (b) spectra for Lysosensor Y/B, with excitation peaks at 340 and 380 nm, and a major emission peak at 540 nm, with increased tailing towards 400 nm as the pH is increased. Previous work used dual excitation at 340 and 380 nm with emission readings taken at 440 and 525 nm respectively, and compared the ratio of these emission readings to a standard curve of Lysosensor Y/B in free solution to determine vesicular pH (Wozniak *et al.*, 2010).

Other investigations of intracellular pH have made use of a pH-sensitive GFP, ratiometric pHluorin, targeted to specific cellular compartments by tagging with appropriate cellular proteins of known specific endosomal distribution (Miesenbock *et al.*, 1998). pHluorin was developed by targeted mutagenesis of fluorophore-adjacent residues to histidine, the only residue with a pKa in the physiological pH range, followed by random mutagenesis with selection for fluorescence and protein stability. This resulted in a single histidine substitution (S202H), and 8 compensatory mutations

for ratiometric pHluorin. Fig. 5.2 shows the excitation spectra for both native GFP and ratiometric pHluorin, both showing excitation peaks at 400 and 470 nm, with the emission read at 508 nm. Native GFP shows a slight reduction in excitation as the pH is reduced, but ratiometric pHluorin shows alterations in the ratio between the peaks (strongest peak = 400 nm at pH 7.5, at pH 5.5, strongest peak = 470 nm). VAMP2-tagged pHluorin has previously been used to specifically measure endosomal pH as VAMP2 is known to distribute to sorting endosomes, late endosomes, or lysosomes (Smith & Lippiat, 2010).

As it was not possible to use the full length virus for live-cell imaging, a number of p7-expression constructs were considered and tested. p7-containing replicons were previously generated (Tedbury *et al.*, 2011), although the function and localisation of p7 in these replicons (where p7 is dispensable for replication) was not determined. A p7-NS5B replicon represents the most physiologically-relevant system to assess p7 cellular functions, where infectious live-virus cannot be used. To allow the investigation of the effect of p7 on intracellular pH through live cell imaging techniques, bicistronic constructs that express both SPp7 and mCherry as a marker protein were generated, as both pHluorin and Lysosensor Y/B display spectra emission in the green fluorescence wavelength while mCherry can be viewed at red emission wavelengths.

A third cell-based system for measuring p7 activity is through two-electrode voltage clamp of *Xenopus laevis* oocytes. Rather than using fluorescent proteins or compounds to measure intracellular vesicle pH, the whole-cell two-electrode voltage clamp technique allows the measurement of ion flow across the cell, following the injection of oocytes with mRNA encoding JFH-1 p7 and subsequent ion channel formation in the oocyte plasma membrane. This system is widely used for measuring the activity of mammalian ion channels. Also, oocyte electrophysiology was successfully used to characterise many of the properties of the prototype viroporin, IAV M2. While this system has less physiological relevance to the normal p7 viroporin activity to increase endosomal pH, it can allow the detailed analysis of channel conductance.

In this chapter, three techniques were utilised to measure p7 function in cellular assays. Lysosensor Y/B and ratiometric pHluorin were used to measure the effect of p7 on vesicular pH, and electrophysiological recordings allowed a detailed analysis of p7 channel function, as previously performed with IAV M2.

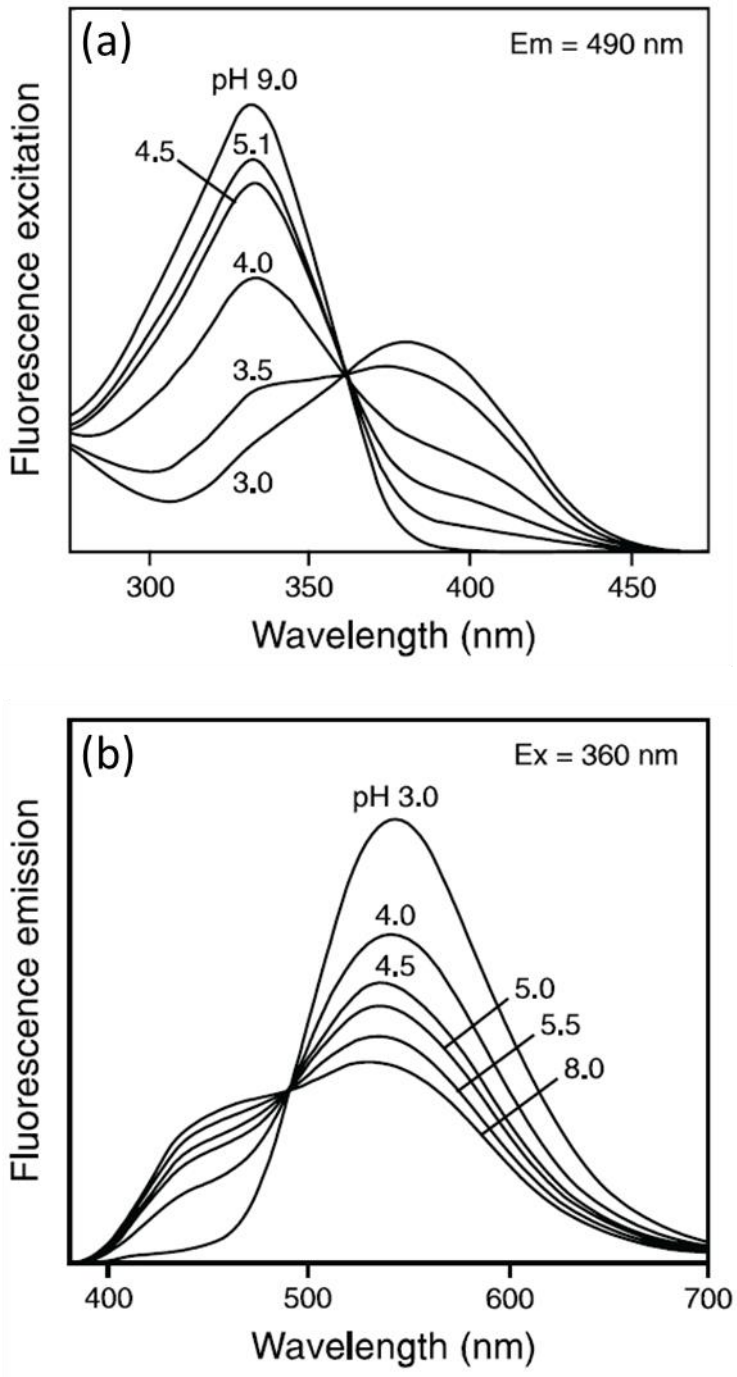

Figure 5.1 Excitation and emission spectra of Lysosensor Yellow/Blue DND-160

Panel (a) shows the excitation spectrum of Lysosensor Y/B between 275 nm and 475 nm with the emission measured at 490 nm. Panel (b) shows the emission spectrum of Lysosensor Y/B between 380 nm and 700 nm with excitation at 360 nm. Lysosensor in free solution was titrated to the indicated pH for each spectrum. Image copyright: Invitrogen Molecular Probes.

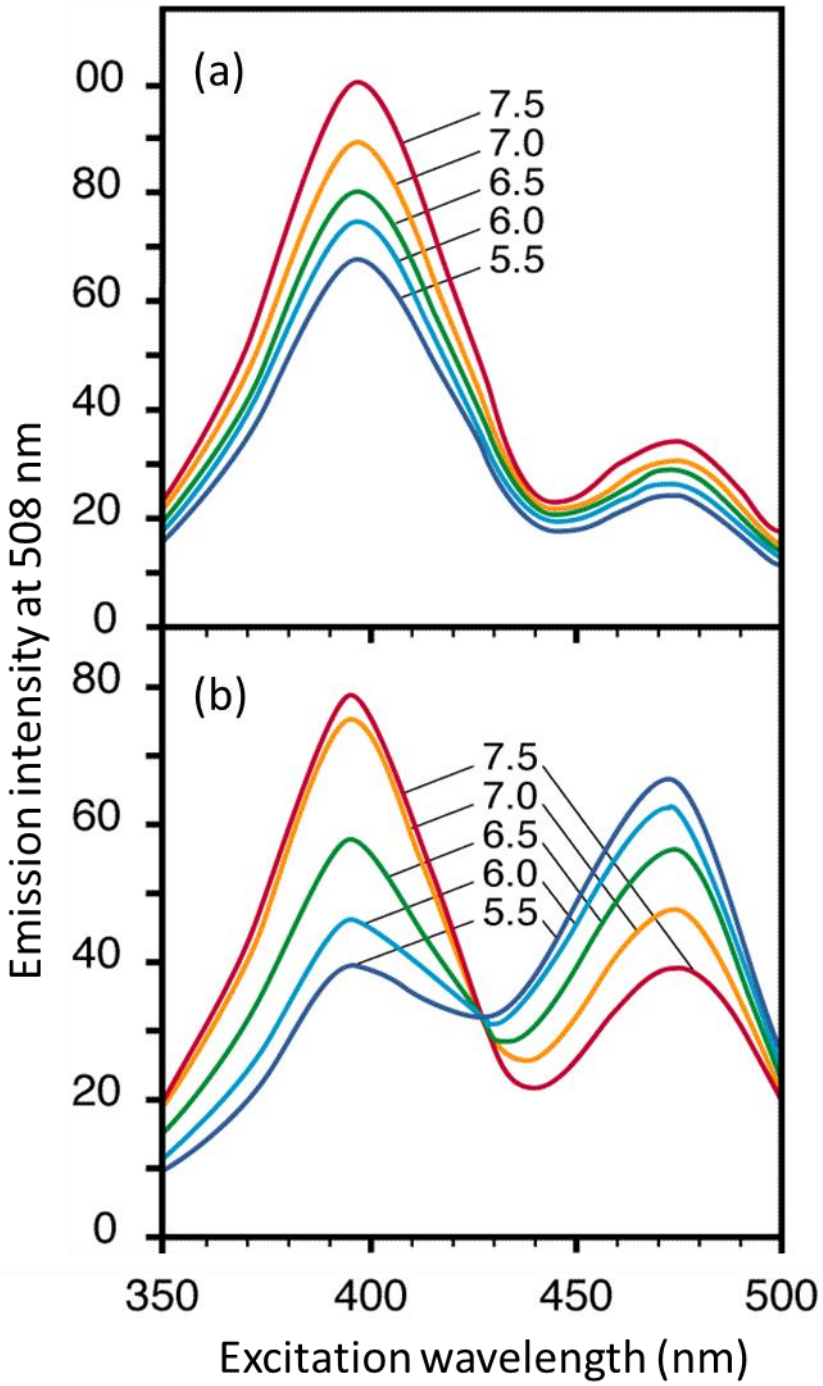

Figure 5.2 Excitation spectrum of GFP and ratiometric pHluorin between pH 5.5 and 7.5

The excitation spectrum of (a) GFP and (b) ratiometric pHluorin between wavelengths 350 and 500 nm, with emission read at 508 nm. GFP and Ratiometric pHluorin in free solution were titrated to the indicated pH points and results normalised to native GFP at pH 7.5. Taken from Miesenbock *et al*., 1998.

5.2 Results

5.2.1 Live-cell imaging optimisation

Both pHluorin and Lysosensor yellow/blue require the use of light wavelengths at or below 400 nm. It was found that ordinary tissue-culture dishes led to high background fluorescence at these wavelengths. Alternative systems were tested including glass-bottomed 2 cm dishes (Iwaki), but these experiments were both time-consuming and low throughput. More high-throughput assays were attempted, utilising glass-bottomed 96-well plates (Iwaki), but these displayed poor cell adhesion, even after poly-lysine treatment of the glass surface prior to cell seeding. After testing a number of options, 8-well microscopy slides (Ibidi) were determined as the most suitable for subsequent assays. These slides allowed the best compromise for the experimental conditions under investigation and maintained the health of cells, allowing an effective number of images to be taken to give high N numbers for statistical significance, that could be captured in a reasonable timeframe before the fluorophores became bleached or, in the case of Lysosensor, trafficked out of the endosomal pathway. All fluorescence experiments herein were performed with 8-well slides, with the exception of the initial flow chamber pHluorin experiments which were carried out in fluorodishes (WPI) that could be fixed firmly to the confocal microscope.

5.2.2 Lysosensor Y/B

5.2.2.1 Lysosensor calibration

Lysosensor Y/B has previously been used to measure the effect of p7 on intracellular pH. Previous recordings were performed on a confocal microscope with excitation wavelengths of 340nm and 380nm, with emission wavelengths read at 440nm and 510nm respectively (Wozniak *et al.*, 2010). These conditions could not be replicated with the facilities available, meaning a new system was developed that was able to approximate these conditions. A whole-cell fluorescence microscope was attached to a monochromator that was able to generate an excitation wavelength between 250-

750 nm. Appropriate filters and dichroic mirrors were added to the system to allow measurements of blue (440 nm), green (530 nm) and red (615 nm) emission wavelengths. Initial work with Lysosensor Y/B found that an excitation wavelength of 340nm produced a high background level of fluorescence; whilst a single excitation wavelength at 380nm produced a small but recordable signal in the blue emission channel. As the ratio between green/blue emissions was required for the ratiometric measurement of pH, the midpoint excitation wavelength of 360 nm – where the excitation spectra shown in Fig. 5.1 converge – was found to produce sufficient blue signal above the background levels to allow accurate readings to be performed.

The pH dependent behaviour of Lysosensor Y/B was next established using this system. The dye was diluted to 100 nm in HEPES cell buffer at a range of pH values, and a curve of the ratiometric change in response to changes in pH was generated. An equation relating the Lysosensor Y/B ratio at each pH value was then generated from this curve (Fig 5.3). If experimental conditions were altered, this curve had to be re-determined in order to allow an accurate pH calculation in each experiment.

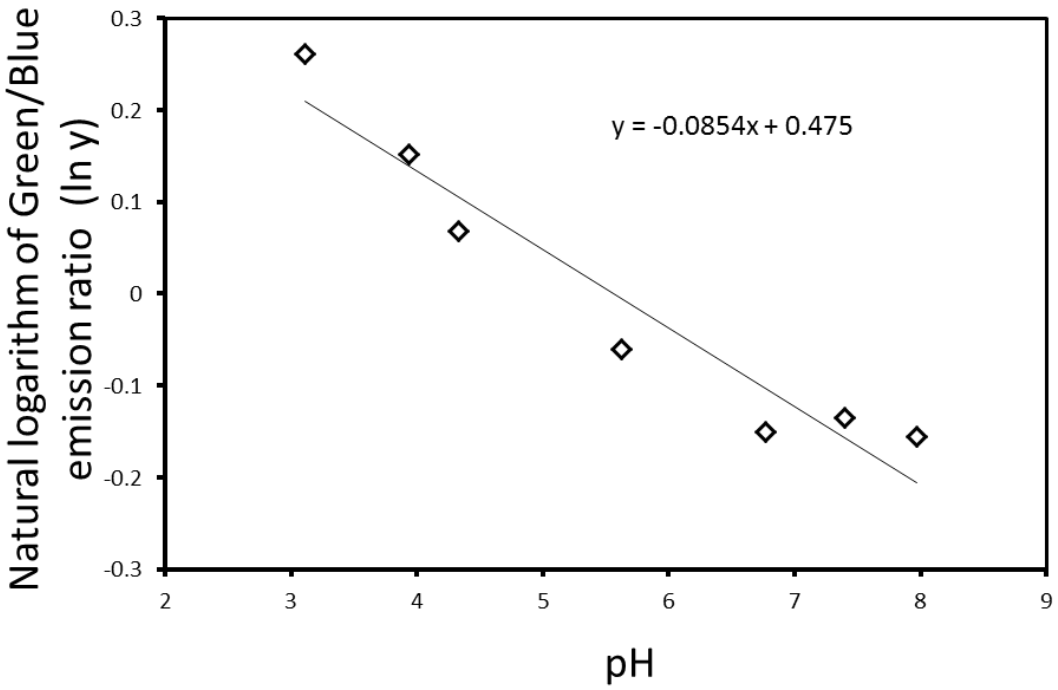

Figure 5.3 Control curve for Lysosensor Y/B ratios in response to changes in pH

Lysosensor Y/B at 10nm in free solution in HEPES cell buffer was titrated to the pH points shown and fluorescence readings taken at emission wavelengths of 420 nm and 530 nm with excitation at 360 nm. Fluorescence intensity was measured using Image J analysis software, and the 530 nm signal divided by the 420 nm signal to generate the Green/blue ratio. Microsoft Excel was used to calculate the natural log of the Green/blue emission ratio, a linear regression line calculated and the equation shown to allow the calculation of pH values from green/blue ratio. Ratios were taken from 10 images for each data point. Error bars = SD

5.2.2.2 Positive control and p7 inhibitor concentration calibration

Lysosensor Y/B has been previously used to show that p7 prevents endosomal acidification (Wozniak *et al.*, 2010). In order to assess the correct function of the Lysosensor Y/B, compounds previously shown to alkalinise endosomes were used as positive controls. Bafilomycin A (BafA) is an inhibitor of the cellular vATPase that drives protons into the lumen of endosomes, the inhibition of which prevents endosomal acidification and has previously been used with Lysosensor Y/B (Wozniak *et al*., 2010). Chloroquine (CQ) is a drug originally used to treat malaria, which preferentially accumulates in acidic cellular compartments and increases their pH (Homewood *et al.*, 1972). Ammonium chloride (AmCl) and chloroquine (CQ) are both lysomotropic amines, which are membrane permeable until protonated in the low pH of lysosomes and other acidic cellular compartments (Dijkstra *et al.*, 1984). Sodium bicarbonate ($NaHCO_3$) has also previously been used to induce endosomal alkalinisation (Jamel Mankouri, unpublished observations).

Each of these drugs was tested at their characterised inhibitory concentrations (Fig. 5.4 (a)). AmCl is not shown, as it was found to either inhibit lysosensor uptake or cause cell death, meaning no Lysosensor Y/B staining was visible. BafA at 100 pM showed no effects on cellular pH compared to untreated controls. CQ and $NaHCO_3$ both influenced the lysosensor ratios, and these two compounds were taken forwards into subsequent experiments (Fig. 5.4 (b)). This second experiment found that, of the two compounds, CQ was the most effective at inducing a change in the lysosensor ratio. Further calibrations with CQ titration over a range of 2-20 μM showed a dose-dependent effect on endosomal pH (Fig. 5.4 (c))

To assess the effects of p7 inhibition on intracellular pH, a reversible effect on the Lysosensor ratio would be expected with the specific p7 inhibitor rimantadine. It was first important to investigate any non-specific effects of rimantadine on the Lysosensor Y/B ratio, as rimantadine is a basic compound that, in high enough concentrations, could non-specifically elevate endosomal pH. Consistent with this, 100 μM rimantadine

increased the measured endosomal pH from 3.8 to 5.6. At lower concentrations known to maintain p7 inhibition, (50 μM) rimantadine displayed a lesser effect, increasing the endosomal pH from 3.8 to 4.7 (Fig. 5.5).

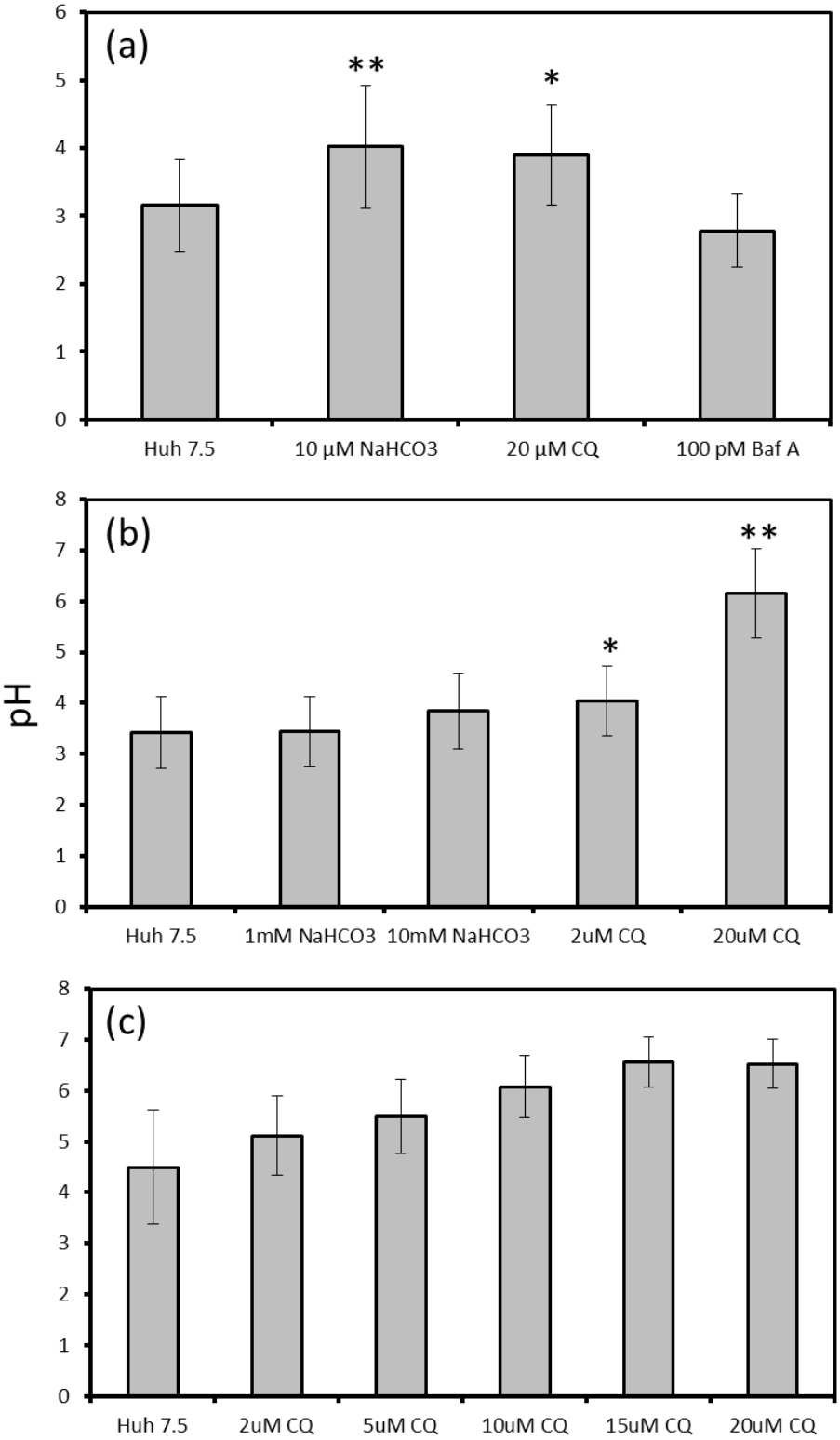

Figure 5.4 Positive controls for Lysosensor calibration

Panel (a): Huh 7.5 cells were incubated with 20 µM chloroquine (CQ), 10 µM sodium bicarbonate ($NaHCO_3$) and 100 pM bafilomycin A (Baf A) to test their ability to alkalinise endosomal compartments. Chemicals were applied for 2 hours prior to imaging, with cells also incubated with 2 µM Lysosensor Y/B for 30 minutes before immediate imaging. Panel (b). Chloroquine and sodium bicarbonate were tested further. Panel (c): titration of chloroquine from 2 µM to 20 µM. For all data-points N = 20 cells. A Student T test was used to compare all chemicals with the cell-only control, * = $p \leq 0.05$, ** = $p \leq 0.01$

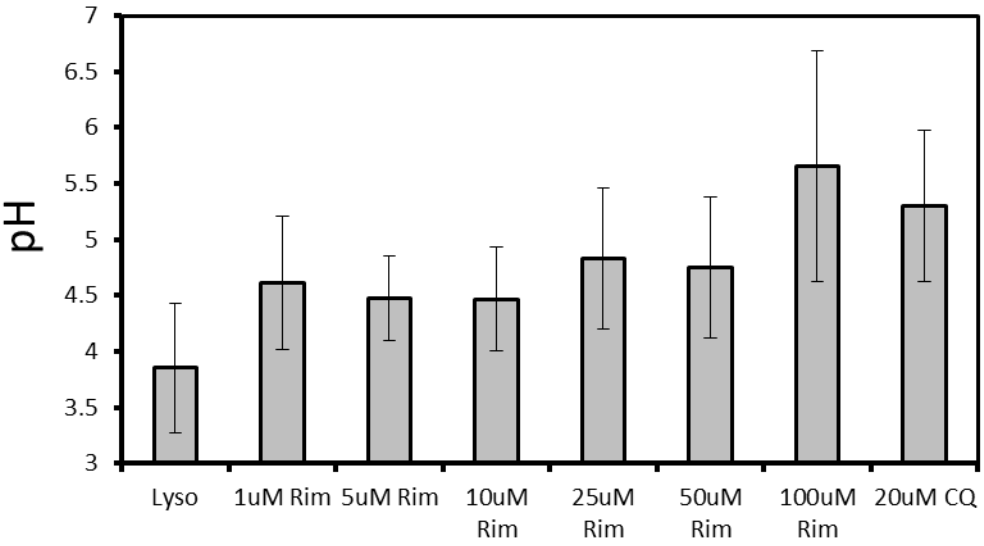

Figure 5.5 Effect of the p7 inhibitor rimantadine on vesicular pH

Huh 7.5 cells were incubated with 1-100 μM rimantadine for 2 hrs minutes prior to Lysosensor Y/B imaging. Fluorescence intensity was measured using ImageJ, data processed and pH values calculated using Microsoft Excel.

5.2.2.3 SPp7-NS5B replicons

Live-cell imaging could not be performed on virus-infected cells as no suitable microscopes were available for use in the CL3 facility. The next most physiologically relevant system was the SPp7-NS5B subgenomic replicon (SGR). The SGR does not typically include p7, as it is not required for genome replication, but previous work had developed a number of replicons containing NS2-5b and SPp7-5b, in both a GT1B background (Con1/FK5.1) and JFH1 (Tedbury *et al.*, 2011). The preceding signal peptide from E2 was found to be required, as without it the replicon was not functional (Phillip Tedbury, unpublished observations).

These replicons were developed to study NS2 localisation and function, and p7 expression was not characterised at the time. Analysis of the two replicons found that p7 expression was not detectable in the Con1/FK5.1 replicon, but could be detected by western blot analysis in the JFH1 SPp7-5B system (Fig. 5.6 (a)). The effect of p7 expression on vesicular pH was therefore analysed using Lysosensor Y/B comparing the vesicular pH of naive Huh 7.5 cells to that of the JFH1 SPp7-5b replicon, with the JFH1 NS2-5B replicon included as a control for any non-specific effects of the replicon on endosomal pH.

The results, shown in Fig. 5.6 (b), show the vesicular pH of untransfected Huh 7.5 was averaged at 4.4, with the positive control CQ increasing the endosomal pH to 7.3. Cells harbouring the NS2-5B SGR displayed a lower endosomal pH than untransfected cells (pH 3.8) that increased to pH 5.1 following treatment with 50 μM rimantadine. Both these data-points showed statistically significant differences to the normal endosomal pH of Huh 7.5 cells. The SPp7-5B replicon-harbouring cells showed a pH of 4.1, increasing to 4.9 following treatment with 50 μM rimantadine. Neither of these two data-points showed statistically significant differences to Huh 7.5 cells. These results indicate that despite the p7 expression detected by western blot, p7 fails to increase endosomal pH in replicon harbouring cells.

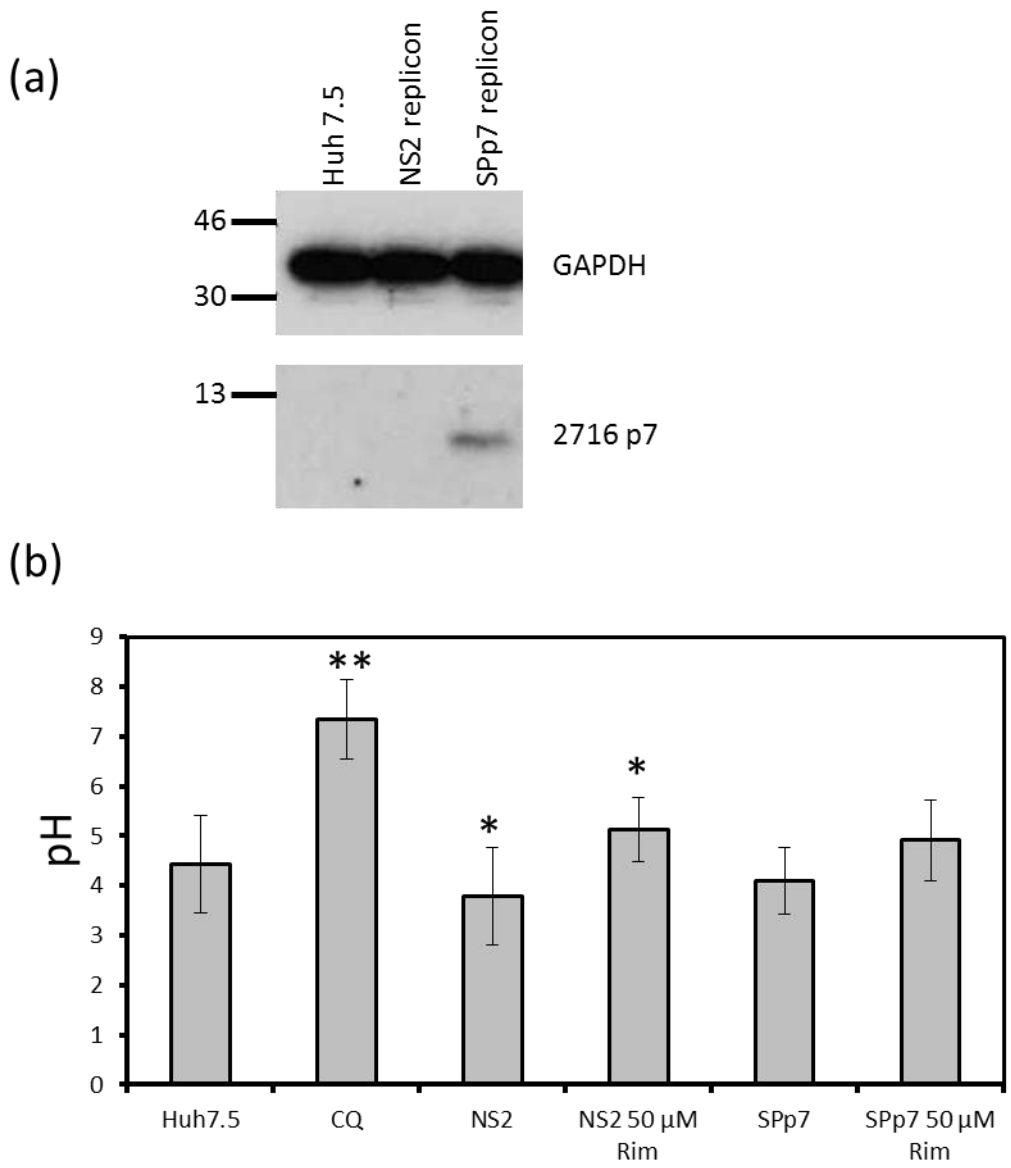

Figure 5.6 Vesicular pH in JFH1 SPp7 replicon cells

Panel (a): Western blots for GAPDH and p7, for Huh 7.5 cells, and Huh 7.5 cells harbouring the JFH1 NS2-5B and SPp7-5B replicons. p7 was run on 10% Tris-tricine gels and probed with the 2716 p7 antibody. GAPDH was run on 12% Tris-glycine. Panel (b): pH values generated by the green/blue Lysosensor Y/B ratios for each cell line, with and without 50 µM rimantadine. Lysosensor Y/B was incubated at 5 µM for 30 minutes prior to imaging. Fluorescence intensity was measured using ImageJ and data processed using Microsoft Excel. N = 20 cells for each data-point. A Student T test was used to compare each value with that of the Huh 7.5 cells, * = p≤ 0.05, ** = p≤ 0.01

5.2.2.4 Bicistronic SPp7-IRES-mCherry

A number of mammalian cell p7 expression constructs, containing a variety of epitope tags, have previously been generated. The majority of these constructs were epitope insertions that allowed visualisation of p7 by fixed-cell immunofluorescence. For live cell imaging experiments, bicistronic constructs expressing both p7 and the red fluorescent protein mCherry were cloned. These were based on previously characterised constructs containing IAV M2 and mCherry. Previous work had shown that the inclusion of the preceding signal-peptide sequence of E2 (SP) improved the expression of p7. The pLXV-M2-IRES-mCherry construct proved difficult to clone, and so PCR was used to amplify the region containing the IRES and mCherry sequences, allowing successful cloning into the mammalian expression construct pCDNA3.1+. The p7 sequence was then cloned into the pCDNA3-IRES-mCherry constructs and p7 expression assessed by Western blot analysis, shown in Fig. 5.7 (a).

Huh 7 cells were transfected with the pCDNA3-SPp7-IRES-mCherry (SPp7 ImC) construct and incubated for 24 hours. Images showing red fluorescent cells were analysed for the effect of p7 expression on the Lysosensor Y/B ratio. Analysis of the Lysosensor Y/B ratio for non-transfected cells showed a mean pH of 3.3, which increased to 5.9 when the cells were treated with 20 μM chloroquine. The cells expressing SPp7 ImC showed a mean pH of 3.0, which was slightly lower than the non-transfected cells, but showed no statistically significant difference. Thus, while p7 expression in cells has been shown with this construct, no effects of p7 on vesicular pH in this system were observed.

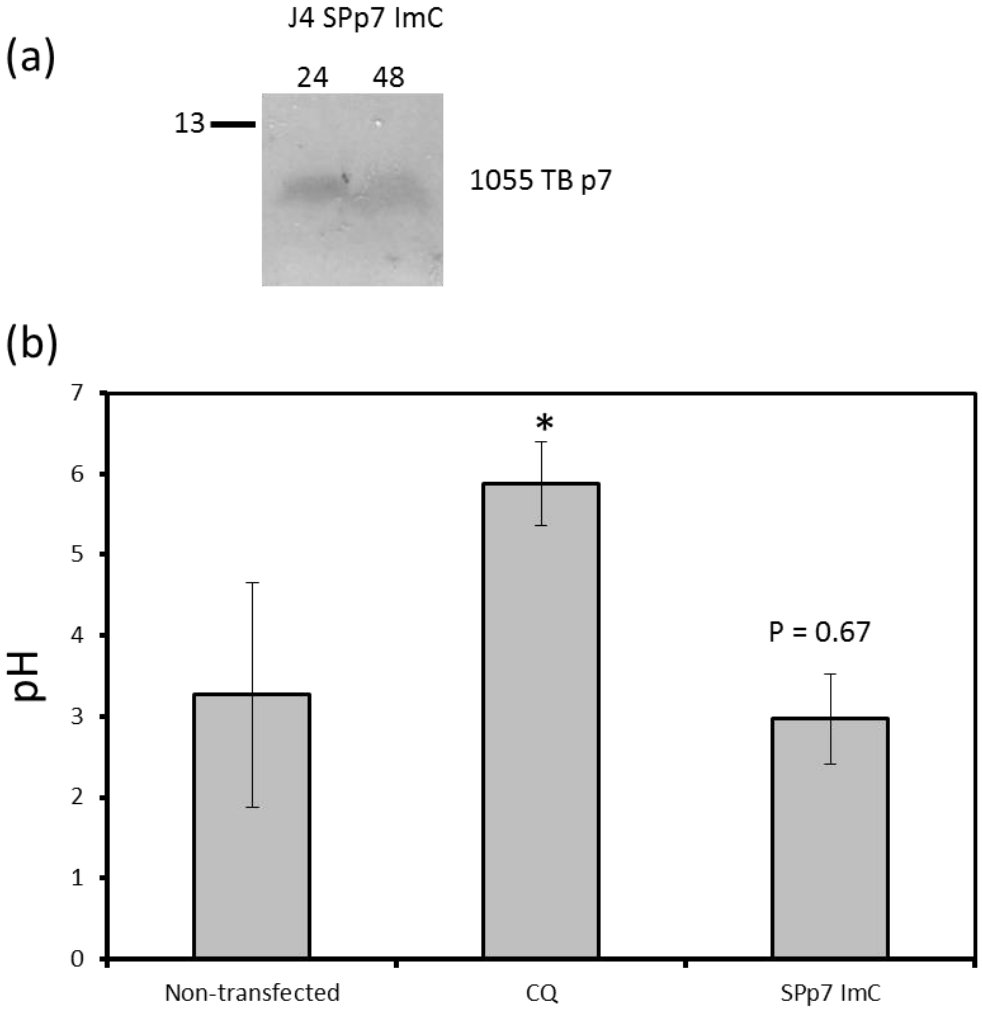

Figure 5.7 Vesicular pH in Huh7 cells transfected with SPp7-ImC

Huh 7 cells were transfected with pCDNA3-SPp7-IRES-mCherry (SPp7-ImC). Panel (a): transfected cells were harvested at 24 and 48 hours post-transfection and analysed by western blot. Samples were run on 10% Tris-tricine gel and probed with 1055 TB p7 antibody. Panel (b): vesicular pH values generated by the green/blue Lysosensor Y/B ratios. Transfected cells were incubated with Lysosensor Y/B as before and imaged. N = 15 cells, pH values were compared with Huh7 cells using Student T test, * = p≤ 0.05

5.2.3 Ratiometric pHluorin

5.2.3.1 The effects of FCCP treatment on endosomal pH

In collaboration with Dr. Jonathan Lippiat, who had previously used the VAMP2-pHluorin construct to measure endosomal pH (Smith & Lippiat, 2010), initial control experiments were performed in HEK 293T cells transfected for 24 hrs with the construct. Cells were viewed on a confocal microscope with excitation at 488 nm, and a buffer flow system that continuously flushed the glass-bottomed dish with HEPES cell buffer was constructed. Under this system, the protonophore FCCP – an ionophore that allows protons to cross lipid bilayers – could be transiently added to the cells and washed away, with any perturbation to the endosomal pH shown by a reduction, followed by recovery of the green emission signal. Only one emission wavelength could be read during the timecourse, but this was sufficient to qualitatively measure the changes in endosomal pH.

Initial control experiments showed promising results (Fig. 5.8 (a)), with a 40% decrease of pHluorin fluorescence emission following an influx of FCCP at the 3 minute timepoint, and a recovery of the signal following the removal of FCCP at the 8 minute timepoint recorded. However, 6 subsequent experiments failed to show any response to FCCP. A representative example of one of these experiments is shown in Fig. 5.8 (b).

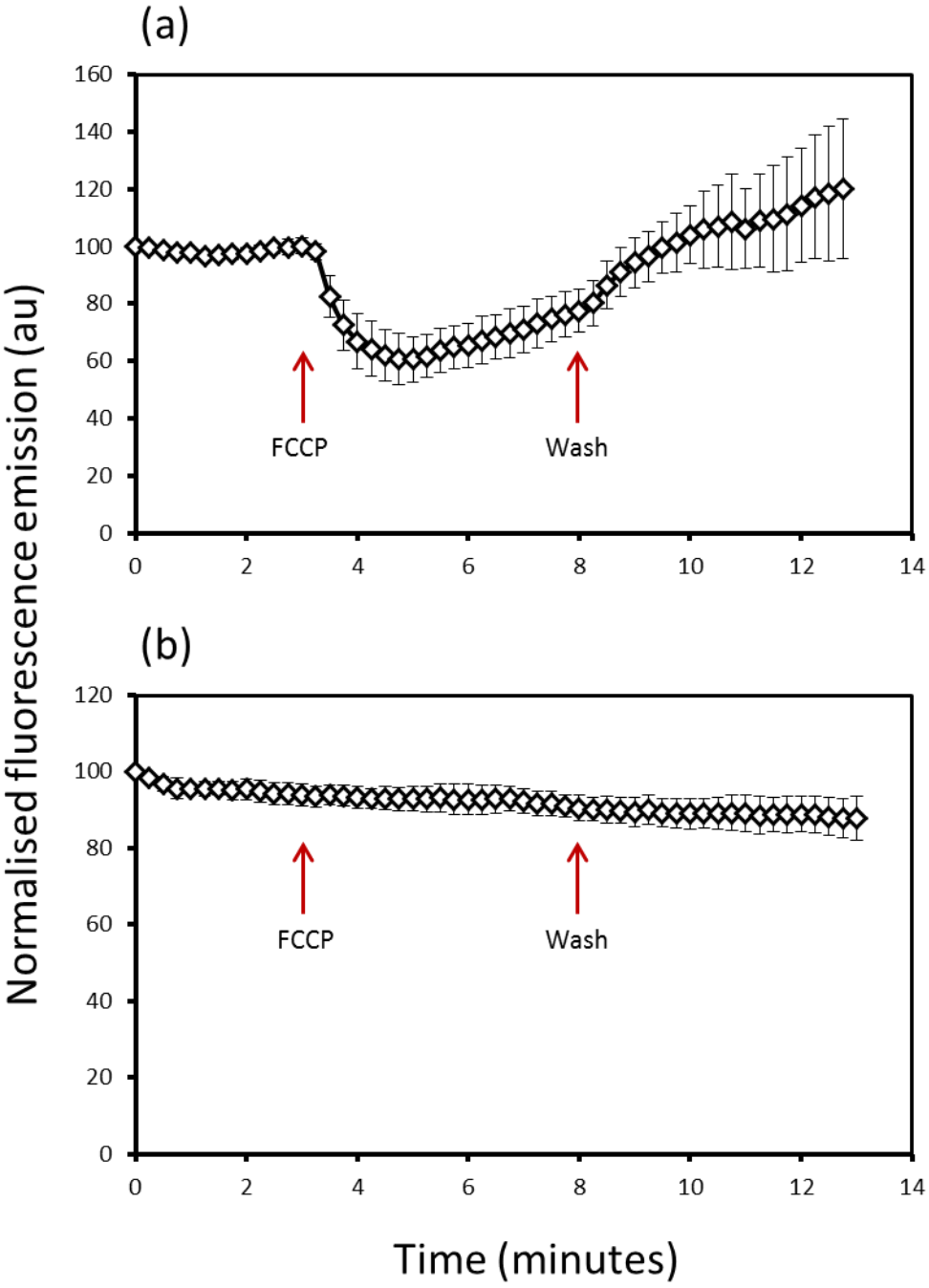

Figure 5.8 Real-time drop in pHluorin signal in response to FCCP at pH 7.4 in 293T cells

HEK293T cells were plated onto glass-bottomed dishes and transfected with VAMP2-pHluorin. 24 hrs post-transfection cells were bathed in HEPES cell buffer under a gentle flow rate. pHluorin was imaged every 15 seconds at 530 nm with 488nm excitation. After 3 minutes, the ionophore FCCP (4 μM) was washed into the cell dish, and after 8 minutes was removed. Panel (a) shows the results of an initial experiment. N = 5 cells. Panel (b) is a representative example of 6 experiments performed to repeat the experiment shown in Panel (a). N= 6 cells. Error bars = SD

5.2.3.2 Whole-cell fluorescence microscopy

The whole-cell fluorescence microscope set up for Lysosensor Y/B could also be utilised to measure ratiometric pHluorin. However, 293T cells were not suitable for use in this system due to their rounded shape, resulting in images of poor resolution. Huh7 cells were utilised as the most physiologically relevant cell line for HCV studies, particularly for comparison to virus/replicon harbouring cells. Cos7 cells were also selected due to their flat and defined nature, and the high expression levels of this cell line following transfection.

Control experiments were carried out to generate the pH-response curve of the ratio of green: blue excitation, and to determine if the external pH buffer affects endosomal pH. Immediately prior to imaging, the cell media was replaced with HEPES cell buffer titrated to the pH points shown, in the absence or presence of the protonophore FCCP to equalise the endosomal pH with the external buffer. The results are shown in Fig. 5.9. Both Huh7 and Cos7 cells displayed identical pH response curves in the presence and absence of FCCP. For Huh7 cells at pH 7.4, the green/blue excitation ratio was 1.1, and at pH 5.1 the ratios were 2.5 for untreated cells, and 2.4 for FCCP treated cells. For Cos7 cells, at pH 7.4 the ratios were 1.2 for untreated and 1.0 for FCCP treated, and at pH 5.2 the ratios were 1.9 for untreated and 2.2 for FCCP treated. This indicates that, even without the presence of a protonophore to facilitate the transport of hydrogen ions across cell membranes, the endosomal pH of the cells is equilibrating with the external buffer pH. Thus, the VAMP2-pHluorin construct was deemed unsuitable as a measure of the ability of p7 to increase endosomal pH.

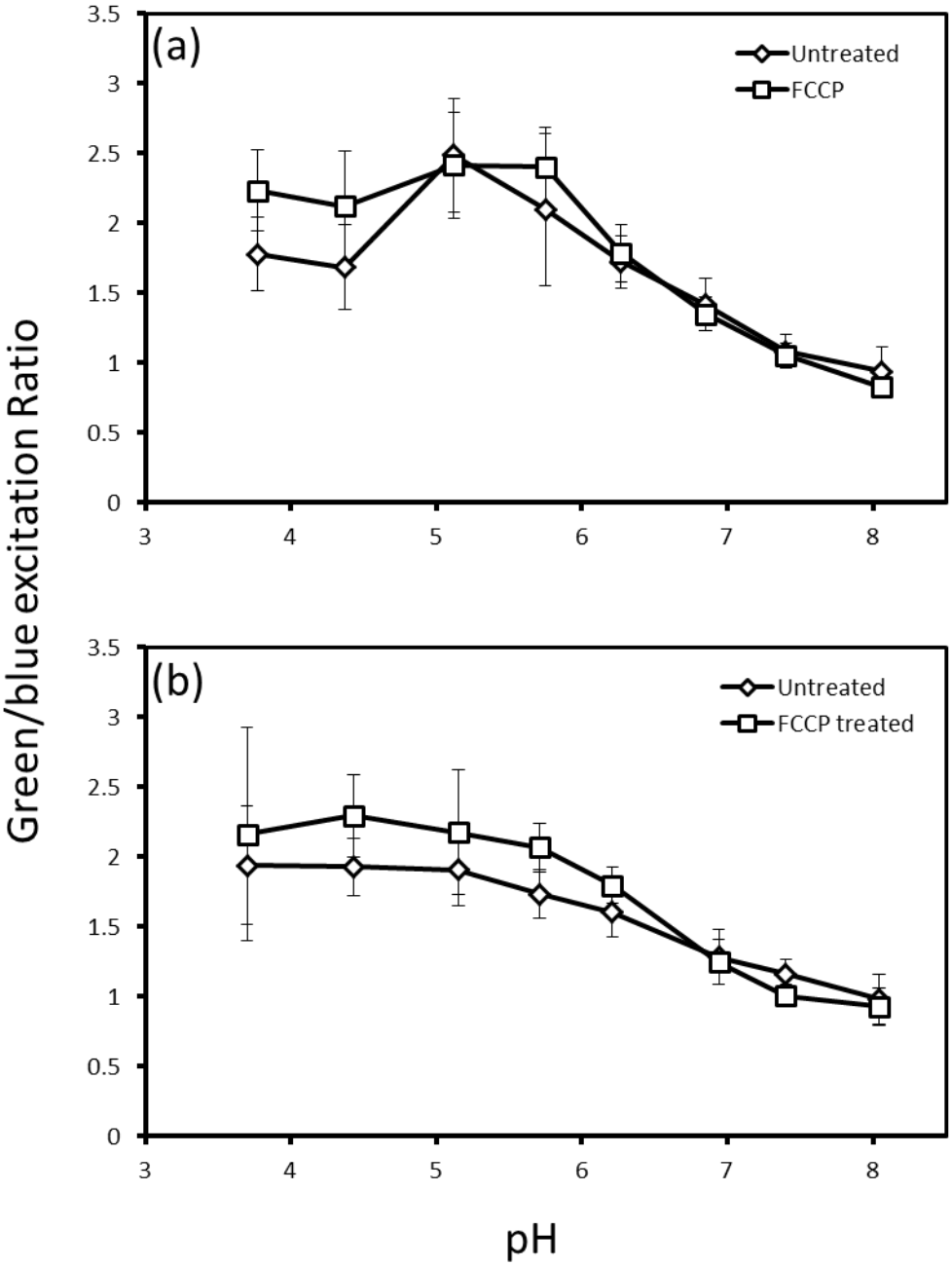

Figure 5.9 Control experiments of pHluorin in Huh7/Cos7 cells over the pH range, with and without FCCP

Huh7 and Cos7 cells were transfected with the VAMP2-pHluorin construct in 8-well microcroscopy slides and imaged 16 hrs post-transfection. Cells were imaged in HEPES cell buffer titrated to the indicated pH points ± FCCP (4 μM). Panel (a) Huh7 cells, Panel (b) Cos7 cells. Each data-point represents the mean from 10-30 cells. Error bars = SD

5.2.4 Xenopus oocyte two-electrode voltage clamp

In collaboration with Dr. Jonathan Lippiat, attempts were made to use the Xenopus oocyte system to measure p7 activity. *Xenopus laevis* oocytes can be injected with mRNA encoding the protein of interest, with the protein typically trafficked at high levels to the plasma membrane, where its activity can be measured using two electrode voltage clamp recordings. This system has been frequently utilised for the high throughput assessment of the function of mammalian cell ion channel activity.

To allow Xenopus oocyte expression of p7, the J4 FLAG-p7 sequence was cloned into the vector pBF+, and capped mRNA synthesised using an SP7 transcription kit (Ambion). The mRNA was then micro-injected into prepared oocytes and incubated for 24 hrs to allow protein expression prior to patch clamp recordings. When recordings were performed at pH 7.4, no channel activity was detectable above that of the mock-injected (water) controls, suggesting no functional p7 activity was present (Fig 5.10 (b)). However, when the pH of the oocyte bathing solution was reduced to pH 6.2 a voltage dependent increase in the currents was observed, that peaked at ~3 μA at 100 mV. No currents above those of endogenous channels were observed in the mock-injected oocytes.

Attempts to repeat this work, however, were unsuccessful as the health of the oocytes consistently deteriorated during the 24 hour incubation period post-microinjection. This was attributed to the poor-quality oocytes which were also observed in similar experiments in the laboratory. Within the scope of this PhD it was not possible to repeat this work.

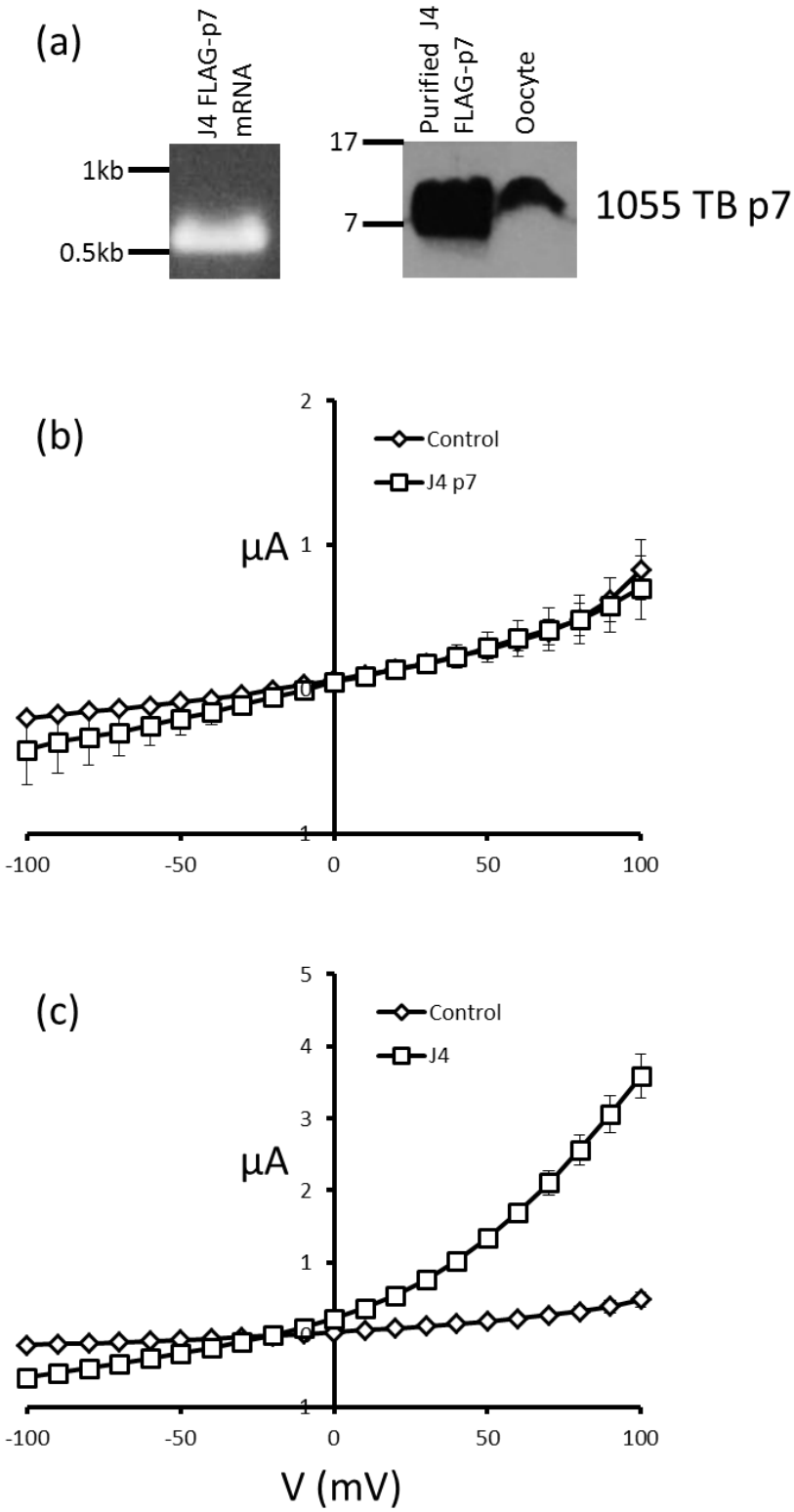

Figure 5.10 Electrophysiology analysis of J4 FLAG-p7 expressed in *Xenopus laevis* oocytes

mRNA transcribed from the pBF+ vector containing the J4 FLAG-p7 sequence was injected into prepared *Xenopus laevis* oocytes as described in section 2.10. After 24 hrs to allow protein expression, patch clamp recordings were performed. Panel (a) shows the mRNA and p7 western blot, Panel (b) shows the ion channel activity of mock injected and J4 p7 mRNA injected oocytes at pH 7.4, Panel (c) shows the ion channel activity of mock injected and J4 p7 mRNA injected oocytes at pH 6.2. N = 6 oocytes. Error bars = SEM. All electrophysiology experiments were performed by Dr. Jonathan Lippiat.

5.3 Discussion

5.3.1 Lysosensor Y/B

Previous studies that used Lysosensor Y/B to measure the effect of p7 on vesicular pH used a full-length H77 replicon system (Wozniak *et al.*, 2010), and confocal microscopy with dual-excitation wavelengths. It was not possible to replicate these conditions as the use of the full-length virus would have required the use of a confocal microscope in a CL3 facility. Thus, attempts were made to replicate both the microscopy conditions and a suitable p7 expression system for CL2 analysis. The control experiments show that it was possible to measure the vesicular pH of Huh7/7.5 cells using this system. In addition, the lysomotropic drug chloroquine was able to raise endosomal pH in a statistically significant manner. However, in contrast to previously published data, the ability of the ability of p7 to raise vesicular pH in these systems was not observed.

5.3.2 Ratiometric pHluorin

The lack of response of VAMP2-pHluorin to alterations in the external pH was unlikely to be due to incorrect distribution of the protein, as cells showed a punctate, cytoplasmic VAMP-2 like distribution consistent with an endosomal distribution.

The limitations found with pHluorin may have been overcome with extensive testing in other tumour derived cell lines. As HCV has been shown only to replicate in hepatocyte derived cell lines and cell lines of neuronal lineage, the physiological representation of p7 activity in non-permissive cells would have been questionable. The single working control experiment with VAMP2-pHluorin in 293T cells where FCCP showed a transient effect showed some potential, but the lack of reproducibility made it unsuitable as an experimental method.

5.3.3 *Xenopus laevis* oocyte two-electrode voltage clamp

The *Xenopus laevis* oocyte experiments showed the highest potential of all the methods tested in this chapter, and indeed this method has been used in recent

published studies with GT2A p7 (OuYang *et al.*, 2013). IAV M2 viroporin activity, with its pH gating and directionality of proton flux has been well characterised in this system, with M2 activity shown in the positive voltage range, with no detectable currents in the negative voltage range. The measured J4 p7 activity at pH 6.2 provides further evidence for low-pH activation of this channel, and recent studies manipulating this system have demonstrated reduced function for inhibitory p7 mutations (OuYang *et al.*, 2013). Further assessment of p7 activity using non-functional mutants, the inclusion of p7 inhibitors to block measured p7 currents, and comparison of the functionality of p7 across genotypes will be further required to verify the Xenopus system as a more physiological assay for p7 activity than previously described liposome assays.

Expression of native p7 in bacteria is known to be toxic to bacterial cells, but the lack of current above control levels shown at pH 7.4 means that for J4 FLAG-p7, the channel is unlikely to be active during the 24 hr expression period prior to readings, therefore p7 activity is unlikely to be killing the cells during this period. If this was the case, other p7 isolates that do not display a low-pH activation profile and are thus more active at pH 7.4 may prove more toxic, and it can be speculated that the addition of p7 inhibitors to the bathing media during this time period may improve cell survival.

5.4 Conclusions

Attempts to develop a cell-based assay for the effects of p7 on endosomal pH using Lysosensor Y/B and ratiometric pHluorin were unsuccessful. Xenopus oocyte electrophysiology showed strong potential as a technique to analyse p7 channel function, but was not reproducible within the scope of this project.

Chapter 6 – General discussion and future perspectives

This study demonstrates that the natural HCV quasispecies sequence variation that occurs within patients is capable of generating significant changes in the behaviour of the HCV viroporin p7 protein *in vitro.* According with the known roles of p7 in the HCV lifecycle, these sequence variations also lead to changes in the production and secretion of infectious virus and the response to p7 inhibitors (Chapter 4). p7 is a potential target for direct-acting antiviral drugs (Griffin, 2010). Understanding how changes in the p7 sequence affect both the function of the protein, and its sensitivity to characterised p7 inhibitors, will aid in the development of new anti-HCV compounds. Current HCV therapy includes only one type of direct acting anti-viral that targets the NS3-4A viral protease (Lange *et al.*, 2010). Further drugs targeting other viral proteins and stages in the virus life cycle may significantly increase the efficacy of treatment, as is the case with HIV. A number of p7 structural studies have now been published (Foster *et al.*, 2014; Cook *et al.*, 2013), including an NMR structure of a GT5a p7 oligomer (OuYang *et al.*, 2013), and these structures could allow much more accurate modelling of how changes in the amino acid sequence of the protein affect the function and inhibitor sensitivity.

The use of patient isolate sequences has advantages over previous studies that performed targeted mutagenesis of p7 residues predicted to be important for normal p7 activity. By definition, the p7 sequences investigated in this study came from functional viruses that were able to replicate, assemble and release infectious progeny within human patients. Thus, it is less likely that any of these patient mutations would lead to protein processing defects that can occur with targeted mutagenesis. The observed phenotypes for the Seattle isolate p7 proteins, either *in vitro* or in virus did, however, fail to show any correlation to the disease severity of the patients (Chapters 3 and 4). This may argue against the level of p7 functionality directly contributing to the levels of disease pathogenesis in an *in vivo* system.

In this study, the p7 inhibitor assays and pH responsiveness of the Seattle isolate virions were only performed with 3 out of the 6 isolates under investigation (section 4.6.2). Continuation of this work to determine if the reduced sensitivity of Seattle isolate virions compared with the parental H77 virions is consistent across more than one experiment and for all 6 isolates may determine whether p7 is involved in a glycoprotein maturation process that renders secreted virus insensitive to transient reductions in pH, as is the case with JFH1 (Wozniak *et al.*, 2010). This may provide insight into further roles of p7 during assembly and egress of the virions, in addition to its prevention of endosomal acidification. S3-1 and S3-2 would make an interesting comparison in this case, as it can be speculated that the reduced p7 expression levels observed in S3-2 could may hinder such a maturation process and produce virions that are sensitive to transient exposure to reduced pH, as with the H77 chimera.

The other possible reason for the observed change in virion pH sensitivity could be due to the presence of p7 in the virion, where it may serve to mediate virion uncoating during acid-dependent membrane fusion during virus entry, as previously demonstrated for M2 in influenza (Shimbo *et al.*, 1996). Large-scale bulk preparation of secreted virus and p7 analysis by western blot or mass spectrometry could finally identify if indeed this is the case and p7 is present in the virion, in previously undetectable levels.

Of the cell-based assays developed to study p7 function, *Xenopus laevis* oocyte electrophysiology showed the most potential for the detailed study of p7 function, and was recently used to confirm p7 viroporin activity in an NMR structural study (OuYang *et al*., 2013). Further work to standardise the *Xenopus* oocyte system, with known non-functional mutants and the application of known p7 activators/inhibitors are currently under investigation in the laboratory. This will further develop this system as a reliable and high throughput method to study p7 functionality.

The calibration and controls for Lysosensor Y/B showed that this system was able to measure changes in vesicular pH, but its use is limited by the lack of a suitable cell-based p7 expression system for CL2 facilities. Future studies applying this method in the context of virus infected cells imaged under CL3 conditions, now possible with the recent acquisition of a confocal microscope in the CL3 facility, would allow p7 function to be studied in the context of the fully infectious virus system. This would allow a full temporal investigation into the role of p7 during the full course of HCV infection.

Recently, a number of new HCV infectious clones have been developed. These include another GT 2A clone designated JFH2 (Date *et al*., 2012), three GT 2B clones (Ramirez *et al*., 2014) and a GT 1A clone that produces much higher titres than the previous H77 clone (Li *et al*., 2012b). The development of a wider range of HCV constructs that can be cultured as infectious virus will allow further investigation of the role of p7 in the whole virus lifecycle, and how changes in p7 structure between different genotypes affect the production of infectious virus.

Recent further evidence of the role of p7 in assembly and release of infectious extracellular virus has been shown by studies of cell-cell transmission of HCV, where the p7 inhibitors BIT225, *N*NDNJ and Rimantadine caused a 50% reduction in transmission, while a GT 5A/JFH1 chimeric virus showed no effect of p7 inhibitors on reducing cell-cell virus transmission (Meredith *et al*., 2013). This raises the intriguing possibility that p7 may be involved in cell-cell transmission of the virus in some HCV isolates but not others, and is worth further investigation.

The structural studies that have been published since this work was completed may also provide new avenues of investigation for the study of p7. As well as the NMR structure of the J4 monomer in methanol, a second monomer structure of the monomer in detergent micelles has also been published (Cook *et al*., 2013). This second monomer structure shows some differences with the methanol structure, the

slight kink in TMD1 is more pronounced, and the N-terminus without the FLAG-tag sequence does not form an α-helix. A further study used a GT 5A p7 to generate an NMR structure of the oligomer in detergent micelles (OuYang *et al*., 2013), and showed a more complex structure than previous computer models of the p7 oligomer structure had suggested. Each monomer is spread out, so that it not only interacts with its two immediate neighbours but also comes into contact with a further two monomers. The most constricted part of the channel is at the lumenal rather than the cytosolic side of the pore, with proposed channel gating residues at I6 and N9. However, the sequence of GT 5A shows low conservation with the previously-studied p7s, with only 25 residues out of 63 shared with J4 p7, so more work will be required to determine if this structure is applicable to other HCV isolates. It is noted in the oligomer study that this HCV isolate was chosen due to its ability to produce high-quality NMR data unlike all other isolates that were tested, and this may perhaps be due to this isolate solely forming hexamers, whereas a mixture of hexamers and heptamers could explain why attempts to determine the oligomer structure of J4 p7 have not been successful (T. Foster, unpublished observations).

A possible adamantane binding site was also identified in the GT 5A oligomer structure which includes residue 20, which work in J4 p7 has previously shown to map to adamantane resistance when this residue was mutated (Foster *et al*., 2011). Thus, while there are substantial amino acid sequence differences between GT 5A and J4 p7 that may result in significant structural differences, there may also be common elements between the structures that can potentially be targeted by p7 inhibitors. Further structural work on p7 isolates from across the genotypes could show why there is such a wide variation in inhibitor sensitivities, and potentially use any common structures as better inhibitor targets. This structural work can also be used as a starting point for further targeted mutagenesis of p7 in other genotypes to investigate how the channel gating mechanism may change as the p7 protein sequence evolves.

In conclusion, there are many further avenues of investigation that can be pursued from this work and from the work of others. This work, if continued, may lead to viable p7 inhibitors joining the ranks of the newly-developed directly-targeted drugs against HCV.

Bibliography

Acharya, R., Carnevale, V., Fiorin, G., Levine, B. G., Polishchuk, A. L., Balannik, V., Samish, I., Lamb, R. a, Pinto, L. H., DeGrado, W. F. & Klein, M. L. (2010). Structure and Mechanism of Proton Transport through the Transmembrane Tetrameric M2 Protein Bundle of the Influenza A Virus. *Proceedings of the National Academy of Sciences of the United States of America*, 107(34), 15075–80.

Agirre, A., Barco, A., Carrasco, L. & Nieva, J. L. (2002). Viroporin-Mediated Membrane Permeabilization. Pore Formation by Nonstructural Poliovirus 2B Protein. *The Journal of Biological Chemistry*, 277(43), 40434–41.

Aizaki, H., Saito, S., Ogino, T., Miyajima, N., Harada, T., Matsuura, Y., Miyamura, T. & Kohase, M. (2000). Suppression of Interferon-Induced Antiviral Activity in Cells Expressing Hepatitis C Virus Proteins. *Journal of Interferon & Cytokine Research : The Official Journal of the International Society for Interferon and Cytokine Research*, 20(12), 1111–20.

Akari, H., Bour, S., Kao, S., Adachi, A. & Strebel, K. (2001). The Human Immunodeficiency Virus Type 1 Accessory Protein Vpu Induces Apoptosis by Suppressing the Nuclear Factor κB–dependent Expression of Antiapoptotic Factors. *The Journal of Experimental Medicine*, 194(9), 1299–312.

Aldabe, R., Barco, A. & Carrasco, L. (1996). Membrane Permeabilization by Poliovirus Proteins 2B and 2BC. *Journal of Biological Chemistry*, 271(38), 23134–7.

Alter, H., Holland, P., Purcell, R. & Popper, H. (1978). Transmissible Agent in Non-A, Non-B Hepatitis. *The Lancet*, 311(8062), 459–63.

Alter, M. J. (2006). Epidemiology of Viral Hepatitis and HIV Co-Infection. *Journal of Hepatology*, 44(1 Suppl), S6–9.

Barco, A. & Carrasco, L. (1998). Identification of Regions of Poliovirus 2BC Protein That Are Involved in Cytotoxicity. *Journal of Virology*, 72(5), 3560–70.

Bartenschlager, R., Ahlborn-Laake, L., Mous, J. & Jacobsen, H. (1994). Kinetic and Structural Analyses of Hepatitis C Virus Polyprotein Processing. *Journal of Virology*, 68(8), 5045–55.

Bartenschlager, R. & Lohmann, V. (2000). Replication of Hepatitis C Virus. *The Journal of General Virology*, 81(Pt 7), 1631–48.

Bartosch, B., Bukh, J., Meunier, J.-C., Granier, C., Engle, R. E., Blackwelder, W. C., Emerson, S. U., Cosset, F.-L. & Purcell, R. H. (2003a). In Vitro Assay for Neutralizing Antibody to Hepatitis C Virus: Evidence for Broadly Conserved Neutralization Epitopes. *Proceedings of the National Academy of Sciences of the United States of America*, 100(24), 14199–204.

Bartosch, B., Dubuisson, J. & Cosset, F.-L. (2003b). Infectious Hepatitis C Virus Pseudo-Particles Containing Functional E1-E2 Envelope Protein Complexes. *Journal of Experimental Medicine*, 197(5), 633–42.

Bartosch, B., Vitelli, A., Granier, C., Goujon, C., Dubuisson, J., Pascale, S., Scarselli, E., Cortese, R., Nicosia, A. & Cosset, F.-L. (2003c). Cell Entry of Hepatitis C Virus Requires a Set of Co-Receptors That Include the CD81 Tetraspanin and the SR-B1 Scavenger Receptor. *The Journal of Biological Chemistry*, 278(43), 41624–30.

Baumert, T. F., Ito, S., Wong, D. T., Liang, T. J. & Jake, T. (1998). Hepatitis C Virus Structural Proteins Assemble into Viruslike Particles in Insect Cells. *Journal of Virology*, 72(5), 3827–36.

De Beeck, A. O., Montserret, R., Duvet, S., Cocquerel, L., Cacan, R., Barberot, B., Le Maire, M., Penin, F., Dubuisson, J., Beeck, A. Op De & Maire, M. Le. (2000). The Transmembrane Domains of Hepatitis C Virus Envelope Glycoproteins E1 and E2 Play a Major Role in Heterodimerization. *Journal of Biological Chemistry*, 275(40), 31428–37.

Beran, R. K. F., Lindenbach, B. D. & Pyle, A. M. (2009). The NS4A Protein of Hepatitis C Virus Promotes RNA-Coupled ATP Hydrolysis by the NS3 Helicase. *Journal of Virology*, 83(7), 3268–75.

Bissig, K., Wieland, S. & Tran, P. (2010). Human Liver Chimeric Mice Provide a Model for Hepatitis B and C Virus Infection and Treatment. *The Journal of Clinical Investigation*, 120(3), 924–30.

Blight, K. J., Kolykhalov, A. A. & Rice, C. M. (2000). Efficient Initiation of HCV RNA Replication in Cell Culture. *Science*, 290(5498), 1972–74.

Blight, K. J., McKeating, J. A., Marcotrigiano, J. & Rice, C. M. (2003). Efficient Replication of Hepatitis C Virus Genotype 1a RNAs in Cell Culture. *Journal of Virology*, 77(5), 3181–90.

Blight, K. J., McKeating, J. A. & Rice, C. M. (2002). Highly Permissive Cell Lines for Subgenomic and Genomic Hepatitis C Virus RNA Replication. *Journal of Virology*, 76(24), 13001–14.

Boo, I., teWierik, K., Douam, F., Lavillette, D., Poumbourios, P. & Drummer, H. E. (2012). Distinct Roles in Folding, CD81 Receptor Binding and Viral Entry for Conserved Histidine Residues of Hepatitis C Virus Glycoprotein E1 and E2. *The Biochemical Journal*, 443(1), 85–94.

Boson, B., Granio, O., Bartenschlager, R. & Cosset, F.-L. (2011). A Concerted Action of Hepatitis C Virus p7 and Nonstructural Protein 2 Regulates Core Localization at the Endoplasmic Reticulum and Virus Assembly. *PLoS Pathogens*, 7(7), e1002144.

Boulant, S., Douglas, M. W., Moody, L., Budkowska, A., Targett-Adams, P. & McLauchlan, J. (2008). Hepatitis C Virus Core Protein Induces Lipid Droplet Redistribution in a Microtubule- and Dynein-Dependent Manner. *Traffic (Copenhagen, Denmark)*, 9(8), 1268–82.

Boulant, S., Montserret, R., Hope, R. G., Ratinier, M., Targett-Adams, P., Lavergne, J.-P., Penin, F. & McLauchlan, J. (2006). Structural Determinants That Target the Hepatitis C Virus Core Protein to Lipid Droplets. *The Journal of Biological Chemistry*, 281(31), 22236–47.

Boulant, S., Vanbelle, C., Ebel, C., Penin, F. & Lavergne, J.-P. (2005). Hepatitis C Virus Core Protein Is a Dimeric Alpha-Helical Protein Exhibiting Membrane Protein Features. *Journal of Virology*, 79(17), 11353–65.

Bour, S., Perrin, C., Akari, H. & Strebel, K. (2001). The Human Immunodeficiency Virus Type 1 Vpu Protein Inhibits NF-Kappa B Activation by Interfering with Beta TrCP-Mediated Degradation of Ikappa B. *The Journal of Biological Chemistry*, 276(19), 15920–8.

Brass, V., Berke, J. M., Montserret, R., Blum, H. E., Penin, F. & Moradpour, D. (2008). Structural Determinants for Membrane Association and Dynamic Organization of the Hepatitis C Virus NS3-4A Complex. *Proceedings of the National Academy of Sciences of the United States of America*, 105(38), 14545–50.

Brass, V., Bieck, E., Montserret, R., Wölk, B., Hellings, J. A., Blum, H. E., Penin, F. & Moradpour, D. (2002). An Amino-Terminal Amphipathic Alpha-Helix Mediates Membrane Association of the Hepatitis C Virus Nonstructural Protein 5A. *The Journal of Biological Chemistry*, 277(10), 8130–9.

Breiman, A., Grandvaux, N., Lin, R., Ottone, C., Akira, S., Yoneyama, M., Fujita, T., Hiscott, J. & Meurs, E. F. (2005). Inhibition of RIG-I-Dependent Signaling to the Interferon Pathway during Hepatitis C Virus Expression and Restoration of Signaling by IKKε. *Journal of Virology*, 79(7), 3969–78.

Brillet, R., Penin, F., Hezode, C., Chouteau, P., Dhumeaux, D. & Pawlotsky, J.-M. (2007). The Nonstructural 5A Protein of Hepatitis C Virus Genotype 1b Does Not Contain an Interferon Sensitivity-Determining Region. *The Journal of Infectious Diseases*, 195(3), 432–41.

Bukh, J., Pietschmann, T., Lohmann, V., Krieger, N., Faulk, K., Engle, R. E., Govindarajan, S., Shapiro, M., St Claire, M. & Bartenschlager, R. (2002). Mutations That Permit Efficient Replication of Hepatitis C Virus RNA in Huh-7 Cells Prevent Productive Replication in Chimpanzees. *Proceedings of the National Academy of Sciences of the United States of America*, 99(22), 14416–21.

Bukh, J., Purcell, R. H. & Miller, R. H. (1992). Sequence Analysis of the 5' Noncoding Region of Hepatitis C Virus. *Proceedings of the National Academy of Sciences of the United States of America*, 89(11), 4942–6.

Bukreyev, A., Whitehead, S. S., Murphy, B. R. & Collins, P. L. (1997). Recombinant Respiratory Syncytial Virus from Which the Entire SH Gene Has Been Deleted Grows Efficiently in Cell Culture and Exhibits Site-Specific Attenuation in the Respiratory Tract of the Mouse. *Journal of Virology*, 71(12), 8973–82.

Burbelo, P. D., Dubovi, E. J., Simmonds, P., Medina, J. L., Henriquez, J. a, Mishra, N., Wagner, J., Tokarz, R., Cullen, J. M., Iadarola, M. J., Rice, C. M., Lipkin, W. I. & Kapoor, A. (2012). Serology-Enabled Discovery of Genetically Diverse Hepaciviruses in a New Host. *Journal of Virology*, 86(11), 6171–8.

Cady, S. D., Schmidt-Rohr, K., Wang, J., Soto, C. S., Degrado, W. F. & Hong, M. (2010). Structure of the Amantadine Binding Site of Influenza M2 Proton Channels in Lipid Bilayers. *Nature*, 463(7281), 689–92.

Carrère-Kremer, S., Montpellier-Pala, C., Cocquerel, L., Wychowski, C., Penin, F. & Dubuisson, J. (2002). Subcellular Localization and Topology of the p7 Polypeptide of Hepatitis C Virus. *Journal of Virology*, 76(8), 3720–30.

Carter, S. D., Dent, K. C., Atkins, E., Foster, T. L., Verow, M., Gorny, P., Harris, M., Hiscox, J. A., Ranson, N. A., Griffin, S. & Barr, J. N. (2010). Direct Visualization of the Small Hydrophobic Protein of Human Respiratory Syncytial Virus Reveals the Structural Basis for Membrane Permeability. *FEBS Letters*, 584(13), 2786–90.

Castrucci, M. R., Hughes, M., Calzoletti, L., Donatelli, I., Wells, K., Takada, a & Kawaoka, Y. (1997). The Cysteine Residues of the M2 Protein Are Not Required for Influenza A Virus Replication. *Virology*, 238(1), 128–34.

Chandler, D. E., Penin, F., Schulten, K. & Chipot, C. (2012). The p7 Protein of Hepatitis C Virus Forms Structurally Plastic, Minimalist Ion Channels. *PLoS Computational Biology*, 8(9), e1002702.

Chew, C. F., Vijayan, R., Chang, J., Zitzmann, N. & Biggin, P. C. (2009). Determination of Pore-Lining Residues in the Hepatitis C Virus p7 Protein. *Biophysical Journal*, 96(2), L10–2.

Choo, Q. L., Kuo, G., Weiner, A. J., Overby, L. R., Bradley, D. W. & Houghton, M. (1989). Isolation of a cDNA Clone Derived from a Blood-Borne Non-A, Non-B Viral Hepatitis Genome. *Science*, 244(4902), 359–62.

Choukhi, A., Ung, S., Wychowski, C. & Dubuisson, J. (1998). Involvement of Endoplasmic Reticulum Chaperones in the Folding of Hepatitis C Virus Glycoproteins. *Journal of Virology*, 72(5), 3851–58.

Ciampor, F., Bayley, P. M., Nermut, M. V, Hirst, E. M., Sugrue, R. J. & Hay, a J. (1992). Evidence That the Amantadine-Induced, M2-Mediated Conversion of Influenza A Virus Hemagglutinin to the Low pH Conformation Occurs in an Acidic Trans Golgi Compartment. *Virology*, 188(1), 14–24.

Clarke, A. & Kulasegaram, R. (2006). Hepatitis C Transmission -- Where Are We Now? *International Journal of STD & AIDS*, 17(2), 74–80;

Clarke, D., Griffin, S., Beales, L., Gelais, C. S., Burgess, S., Harris, M. & Rowlands, D. (2006). Evidence for the Formation of a Heptameric Ion Channel Complex by the Hepatitis C Virus p7 Protein in Vitro. *The Journal of Biological Chemistry*, 281(48), 37057–68.

Cocquerel, L., Op de Beeck, A., Lambot, M., Roussel, J., Delgrange, D., Pillez, A., Wychowski, C., Penin, F. & Dubuisson, J. (2002). Topological Changes in the Transmembrane Domains of Hepatitis C Virus Envelope Glycoproteins. *The EMBO Journal*, 21(12), 2893–902.

Cohen, E. A., Terwilliger, E. F., Sodroski, J. G. & Haseltine, W. A. (1988). Identification of a Protein Encoded by the Vpu Gene of HIV-1. *Nature*, 334(6182), 532–4.

Cook, G. a & Opella, S. J. (2010). NMR Studies of p7 Protein from Hepatitis C Virus. *European Biophysics Journal : EBJ*, 39(7), 1097–104.

Cook, G. a & Opella, S. J. (2011). Secondary Structure, Dynamics, and Architecture of the p7 Membrane Protein from Hepatitis C Virus by NMR Spectroscopy. *Biochimica et Biophysica Acta*, 1808(6), 1448–53.

Cook, G., Dawson, L., Tian, Y. & Opella, S. J. (2013). Three-Dimensional Structure and Interaction Studies of Hepatitis C Virus p7 in 1,2-Dihexanoyl-Sn-Glycero-3-Phosphocholine by Solution Nuclear Magnetic Resonance. *Biochemistry*.

Corless, L., Crump, C. M., Griffin, S. D. C. & Harris, M. (2010). Vps4 and the ESCRT-III Complex Are Required for the Release of Infectious Hepatitis C Virus Particles. *The Journal of General Virology*, 91(Pt 2), 362–72.

Cormier, E. G., Tsamis, F., Kajumo, F., Durso, R. J., Gardner, J. P. & Dragic, T. (2004). CD81 Is an Entry Coreceptor for Hepatitis C Virus. *Proceedings of the National Academy of Sciences of the United States of America*, 101(19), 7270–4.

Costa-Mattioli, M., Svitkin, Y., Sonenberg, N. & Costa-mattioli, M. (2004). La Autoantigen Is Necessary for Optimal Function of the Poliovirus and Hepatitis C Virus Internal Ribosome Entry Site in Vivo and in Vitro. *Molecular and Cellular Biology*, 24(15), 6861–70.

Dalagiorgou, G., Vassilaki, N., Foka, P., Boumlic, a, Kakkanas, a, Kochlios, E., Khalili, S., Aslanoglou, E., Veletza, S., Orfanoudakis, G., Vassilopoulos, D., Hadziyannis, S. J., Koskinas, J. & Mavromara, P. (2011). High Levels of HCV core+1 Antibodies in HCV Patients with Hepatocellular Carcinoma. *The Journal of General Virology*, 92(Pt 6), 1343–51.

Date, T., Kato, T., Kato, J., Takahashi, H., Morikawa, K., Akazawa, D., Murayama, A., Tanaka-Kaneko, K., Sata, T., Tanaka, Y., Mizokami, M. & Wakita, T. (2012). Novel Cell Culture-Adapted Genotype 2a Hepatitis C Virus Infectious Clone. *Journal of Virology*, 86(19), 10805–20.

Davis, M., Sagan, S. M., Pezacki, J. P., Evans, D. J. & Simmonds, P. (2008). Bioinformatic and Physical Characterizations of Genome-Scale Ordered RNA Structure in Mammalian RNA Viruses. *Journal of Virology*, 82(23), 11824–36.

Deleersnyder, V., Pillez, A., Wychowski, C., Blight, K., Xu, J., Hahn, Y. S., Rice, C. M. & Dubuisson, J. (1997). Formation of Native Hepatitis C Virus Glycoprotein Complexes. *Journal of Virology*, 71(1), 697–704.

Dentzer, T. G., Lorenz, I. C., Evans, M. J. & Rice, C. M. (2009). Determinants of the Hepatitis C Virus Nonstructural Protein 2 Protease Domain Required for Production of Infectious Virus. *Journal of Virology*, 83(24), 12702–13.

Dijkstra, J., Van Galen, M. & Scherphof, G. L. (1984). Effects of Ammonium Chloride and Chloroquine on Endocytic Uptake of Liposomes by Kupffer Cells in Vitro. *Biochimica et Biophysica Acta (BBA) - Molecular Cell Research*, 804(1), 58–67.

Dorner, M., Horwitz, J. a, Robbins, J. B., Barry, W. T., Feng, Q., Mu, K., Jones, C. T., Schoggins, J. W., Catanese, M. T., Burton, D. R., Law, M., Rice, C. M. & Ploss, A. (2011). A Genetically Humanized Mouse Model for Hepatitis C Virus Infection. *Nature*, 474(7350), 208–11.

Dumont, S., Cheng, W., Serebrov, V., Beran, R. K., Tinoco, I., Pyle, A. M. & Bustamante, C. (2006). RNA Translocation and Unwinding Mechanism of HCV NS3 Helicase and Its Coordination by ATP. *Nature*, 439(7072), 105–8.

Eckart, M. R., Selby, M., Masiarz, F., Lee, C., Berger, K., Crawford, K., Kuo, C., Kuo, G., Houghton, M. & Choo, Q. L. (1993). The Hepatitis C Virus Encodes a Serine Protease Involved in Processing of the Putative Nonstructural Proteins from the Viral Polyprotein Precursor. *Biochemical and Biophysical Research Communications*, 192(2), 399–406.

Egger, D., Wölk, B., Gosert, R., Bianchi, L., Blum, H. E., Moradpour, D. & Bienz, K. (2002). Expression of Hepatitis C Virus Proteins Induces Distinct Membrane Alterations Including a Candidate Viral Replication Complex. *Journal of Virology*, 76(12), 5974–84.

Elazar, M., Cheong, K. H., Liu, P., Greenberg, H. B., Rice, C. M. & Glenn, J. S. (2003). Amphipathic Helix-Dependent Localization of NS5A Mediates Hepatitis C Virus RNA Replication. *Journal of Virology*, 77(10), 6055–61.

Enomoto, N., Sakuma, I., Asahina, Y., Kurosaki, M., Murakami, T., Yamamoto, C., Izumi, N., Marumo, F. & Sato, C. (1995). Comparison of Full-Length Sequences of Interferon-Sensitive and Resistant Hepatitis C Virus 1b. Sensitivity to Interferon Is Conferred by Amino Acid Substitutions in the NS5A Region. *Journal of Clinical Investigation*, 96(1), 224.

Enomoto, N., Sakuma, I., Asahina, Y., Kurosaki, M., Murakami, T., Yamamoto, C., Ogura, Y., Izumi, N., Marumo, F. & Sato, C. (1996). Mutations in the Nonstructural Protein 5A Gene and Response to Interferon in Patients with Chronic Hepatitis C Virus 1b Infection. *The New England Journal of Medicine*, 334(2), 77–81.

Evans, M. J., von Hahn, T., Tscherne, D. M., Syder, A. J., Panis, M., Wölk, B., Hatziioannou, T., McKeating, J. a, Bieniasz, P. D. & Rice, C. M. (2007). Claudin-1 Is a Hepatitis C Virus Co-Receptor Required for a Late Step in Entry. *Nature*, 446(7137), 801–5.

Ewart, G. D., Sutherland, T., Gage, P. W. & Cox, G. B. (1996). The Vpu Protein of Human Immunodeficiency Virus Type 1 Forms Cation-Selective Ion Channels. *Journal of Virology*, 70(10).

Ewart, G., Mills, K., Cox, G. & Gage, P. (2002). Amiloride Derivatives Block Ion Channel Activity and Enhancement of Virus-like Particle Budding Caused by HIV-1 Protein Vpu. *European Biophysics Journal*, 31(1), 26–35.

Ferrari, E., Wright-Minogue, J., Fang, J. W. S., Baroudy, B. M., Lau, J. Y. N. & Hong, Z. (1999). Characterization of Soluble Hepatitis C Virus RNA-Dependent RNA Polymerase Expressed in Escherichia Coli. *Journal of Virology*, 73(2), 1649–54.

Foster, T. L., Belyaeva, T., Stonehouse, N. J., Pearson, A. R. & Harris, M. (2010). All Three Domains of the Hepatitis C Virus Nonstructural NS5A Protein Contribute to RNA Binding. *Journal of Virology*, 84(18), 9267–77.

Foster, T. L., Thompson, G. S., Kalverda, A. P., Kankanala, J., Bentham, M., Wetherill, L. F., Thompson, J., Barker, A. M., Clarke, D., Noerenberg, M., Pearson, A. R., Rowlands, D. J., Homans, S. W., Harris, M., Foster, R. & Griffin, S. (2014). Structure-Guided Design Affirms Inhibitors of Hepatitis C Virus p7 as a Viable Class of Antivirals Targeting Virion Release. *Hepatology (Baltimore, Md.)*, 59(2), 408–22.

Foster, T. L., Verow, M., Wozniak, A. L., Bentham, M. J., Thompson, J., Atkins, E., Weinman, S. A., Fishwick, C., Foster, R., Harris, M. & Griffin, S. (2011). Resistance Mutations Define Specific Antiviral Effects for Inhibitors of the Hepatitis C Virus p7 Ion Channel. *Hepatology*, 54(1), 79–90.

Franck, N., Le Seyec, J., Guguen-guillouzo, C., Erdtmann, L. & Seyec, J. Le. (2005). Hepatitis C Virus NS2 Protein Is Phosphorylated by the Protein Kinase CK2 and Targeted for Degradation to the Proteasome. *Journal of Virology*, 79(5), 2700–8.

Frick, D. N., Banik, S. & Rypma, R. S. (2007). Role of Divalent Metal Cations in ATP Hydrolysis Catalyzed by the Hepatitis C Virus NS3 Helicase: Magnesium Provides a Bridge for ATP to Fuel Unwinding. *Journal of Molecular Biology*, 365(4), 1017–32.

Friebe, P. & Bartenschlager, R. (2002). Genetic Analysis of Sequences in the 3′ Nontranslated Region of Hepatitis C Virus That Are Important for RNA Replication. *Journal of Virology*, 76(11), 5326–38.

Friebe, P., Lohmann, V., Krieger, N. & Bartenschlager, R. (2001). Sequences in the 5′ Nontranslated Region of Hepatitis C Virus Required for RNA Replication. *Journal of Virology*, 75(24), 12047–57.

Fuentes, S., Tran, K. C., Luthra, P., Teng, M. N. & He, B. (2007). Function of the Respiratory Syncytial Virus Small Hydrophobic Protein. *Journal of Virology*, 81(15), 8361–6.

Gan, S., Ng, L., Lin, X., Gong, X. & Torres, J. (2008). Structure and Ion Channel Activity of the Human Respiratory Syncytial Virus (hRSV) Small Hydrophobic Protein Transmembrane Domain. *Protein Science*, 17, 813–20.

Gan, S.-W., Tan, E., Lin, X., Yu, D., Wang, J., Tan, G. M.-Y., Vararattanavech, A., Yeo, C. Y., Soon, C. H., Soong, T. W., Pervushin, K. & Torres, J. (2012). The Small Hydrophobic Protein of the Human Respiratory Syncytial Virus Forms Pentameric Ion Channels. *The Journal of Biological Chemistry*, 287(29), 24671–89.

Gao, M., Nettles, R. E., Belema, M., Snyder, L. B., Nguyen, V. N., Fridell, R. A., Serrano-Wu, M. H., Langley, D. R., Sun, J.-H., O'Boyle II, D. R., Lemm, J. A.,

Wang, C., Knipe, J. O., Chien, C., Colonno, R. J., Grasela, D. M., Meanwell, N. A. & Hamann, L. G. (2010). Chemical Genetics Strategy Identifies an HCV NS5A Inhibitor with a Potent Clinical Effect. *Nature*, 465(7294), 96–100.

Gerold, G. & Rice, C. M. (2011). Locking out Hepatitis C. *Nature Medicine*, 17(5), 542–4.

Ghany, M. G., Strader, D. B., Thomas, D. L. & Seeff, L. B. (2009). Diagnosis, Management, and Treatment of Hepatitis C: An Update. *Hepatology (Baltimore, Md.)*, 49(4), 1335–74.

Gieswein, C. E., Sharom, F. J. & Wildeman, A. G. (2003). Oligomerization of the E5 Protein of Human Papillomavirus Type 16 Occurs through Multiple Hydrophobic Regions. *Virology*, 313(2), 415–426.

Giordano, T. P., Kramer, J. R., Souchek, J., Richardson, P. & El-Serag, H. B. (2004). Cirrhosis and Hepatocellular Carcinoma in HIV-Infected Veterans with and without the Hepatitis C Virus: A Cohort Study, 1992-2001. *Archives of Internal Medicine*, 164(21), 2349.

Goh, P.-Y., Tan, Y.-J., Lim, S. P., Tan, Y. H., Lim, S. G., Fuller-Pace, F. & Hong, W. (2004). Cellular RNA Helicase p68 Relocalization and Interaction with the Hepatitis C Virus (HCV) NS5B Protein and the Potential Role of p68 in HCV RNA Replication. *Journal of Virology*, 78(10), 5288–98.

Gonzalez, M. E. & Carrasco, L. (1998). The Human Immunodeficiency Virus Type 1 Vpu Protein Enhances Membrane Permeability. *Biochemistry*, 2960(29), 13710–19.

Gosert, R., Egger, D., Lohmann, V., Bartenschlager, R., Blum, H. E., Bienz, K. & Moradpour, D. (2003). Identification of the Hepatitis C Virus RNA Replication Complex in Huh-7 Cells Harboring Subgenomic Replicons. *Journal of Virology*, 77(9), 5487–92.

Gouttenoire, J., Montserret, R., Kennel, A., Penin, F. & Moradpour, D. (2009). An Amphipathic Alpha-Helix at the C Terminus of Hepatitis C Virus Nonstructural Protein 4B Mediates Membrane Association. *Journal of Virology*, 83(21), 11378–84.

Gouttenoire, J., Penin, F., Moradpour, D. & Iew, R. E. V. (2010a). Hepatitis C Virus Nonstructural Protein 4B: A Journey into Unexplored Territory. *Reviews in Medical Virology*, 20(2), 117–29.

Gouttenoire, J., Roingeard, P., Penin, F. & Moradpour, D. (2010b). Amphipathic Alpha-Helix AH2 Is a Major Determinant for the Oligomerization of Hepatitis C Virus Nonstructural Protein 4B. *Journal of Virology*, 84(24), 12529–37.

Grakoui, A., Wychowski, C., Lin, C., Feinstone, S. M. & Rice, C. M. (1993). Expression and Identification of Hepatitis C Virus Polyprotein Cleavage Products. *Journal of Virology*, 67(3), 1385–95.

Grantham, M. L., Wu, W.-H., Lalime, E. N., Lorenzo, M. E., Klein, S. L. & Pekosz, A. (2009). Palmitoylation of the Influenza A Virus M2 Protein Is Not Required for

Virus Replication in Vitro but Contributes to Virus Virulence. *Journal of Virology*, 83(17), 8655–61.

Griffin, S. (2010). Inhibition of HCV p7 as a Therapeutic Target. *Current Opinion in Investigational Drugs*, 11(2), 175.

Griffin, S., Clarke, D. & McCormick, C. (2005). Signal Peptide Cleavage and Internal Targeting Signals Direct the Hepatitis C Virus p7 Protein to Distinct Intracellular Membranes. *Journal of Virology*, 79(24), 15525–36.

Griffin, S. D. C., Beales, L. P., Clarke, D. S., Worsfold, O., Evans, S. D., Jaeger, J., Harris, M. P. G. & Rowlands, D. J. (2003). The p7 Protein of Hepatitis C Virus Forms an Ion Channel That Is Blocked by the Antiviral Drug, Amantadine. *FEBS Letters*, 535(10), 34–38.

Griffin, S. D. C., Harvey, R., Clarke, D. S., Barclay, W. S., Harris, M. & Rowlands, D. J. (2004). A Conserved Basic Loop in Hepatitis C Virus p7 Protein Is Required for Amantadine-Sensitive Ion Channel Activity in Mammalian Cells but Is Dispensable for Localization to Mitochondria. *The Journal of General Virology*, 85(Pt 2), 451–61.

Griffin, S., StGelais, C., Owsianka, A. M., Patel, A. H., Rowlands, D. & Harris, M. (2008). Genotype-Dependent Sensitivity of Hepatitis C Virus to Inhibitors of the p7 Ion Channel. *Hepatology (Baltimore, Md.)*, 48(6), 1779–90.

Gwack, Y., Kim, D. W., Han, J. H. & Choe, J. (1996). Characterization of RNA Binding Activity and RNA Helicase Activity of the Hepatitis C Virus NS3 Protein. *Biochemical and Biophysical Research Communications*, 225(2), 654–59.

Hahm, B., Han, D. A. E. S., Back, S. H., Song, O.-K., Cho, M.-J., Kim, C.-J., Shimotohno, K. & Jang, S. K. (1995). NS3-4A of Hepatitis C Virus Is a Chymotrypsin-like Protease. *Journal of Virology*, 69(4), 2534–39.

Halbert, C. L. & Galloway, D. A. (1988). Identification of the E5 Open Reading Frame of Human Papillomavirus Type 16. *Journal of Virology*, 62(3), 1071–75.

Han, J. H., Shyamala, V., Richman, K. H., Brauer, M. J., Irvine, B., Urdea, M. S., Tekamp-Olson, P., Kuo, G., Choo, Q. L. & Houghton, M. (1991). Characterization of the Terminal Regions of Hepatitis C Viral RNA: Identification of Conserved Sequences in the 5’ Untranslated Region and poly(A) Tails at the 3' End. *Proceedings of the National Academy of Sciences of the United States of America*, 88(5), 1711–5.

Hanoulle, X. & Verdegem, D. (2009). Domain 3 of Non-Structural Protein 5A from Hepatitis C Virus Is Natively Unfolded. *Biochemical and Biophysical Research Communications*, 381(4), 634–38.

Haqshenas, G., Dong, X., Ewart, G., Bowden, S. & Gowans, E. J. (2007a). A 2a/1b Full-Length p7 Inter-Genotypic Chimeric Genome of Hepatitis C Virus Is Infectious in Vitro. *Virology*, 360(1), 17–26.

Haqshenas, G., Mackenzie, J. M., Dong, X. & Gowans, E. J. (2007b). Hepatitis C Virus p7 Protein Is Localized in the Endoplasmic Reticulum When It Is Encoded

by a Replication-Competent Genome. *The Journal of General Virology*, 88(Pt 1), 134–42.

Hay, A. J., Wolstenholme, A. J., Skehel, J. J. & Smith, M. H. (1985). The Molecular Basis of the Specific Anti-Influenza Action of Amantadine. *The EMBO Journal*, 4(11), 3021–4.

Hollinger, F. B. & Liang, T. J. (2001). Hepatitis B Virus. *Fields Virology, 4th Ed. Philadelphia, Lippincott Williams & Wilkins*, 2971–3036.

Holsinger, L. J., Shaughnessy, M. A., Micko, A., Pinto, L. H. & Lamb, R. A. (1995). Analysis of the Posttranslational Modifications of the Influenza Virus M2 Protein. *Journal of Virology*, 69(2), 1219–25.

Homewood, C. A., Warhurst, D. C., Peters, W. & Baggaley, V. C. (1972). Lysosomes, pH and the Anti-Malarial Action of Chloroquine. *Nature*, 235, 50–52.

Honda, M., Beard, M. R., Ping, L. & Lemon, S. M. (1999). A Phylogenetically Conserved Stem-Loop Structure at the 5′ Border of the Internal Ribosome Entry Site of Hepatitis C Virus Is Required for Cap-Independent Viral Translation. *Journal of Virology*, 73(2), 1165–74.

Hong, Z., Cameron, C. E., Walker, M. P., Castro, C., Yao, N., Lau, J. Y. & Zhong, W. (2001). A Novel Mechanism to Ensure Terminal Initiation by Hepatitis C Virus NS5B Polymerase. *Virology*, 285(1), 6–11.

Hoofnagle, J. H. (2002). Course and Outcome of Hepatitis C. *Hepatology (Baltimore, Md.)*, 36(5 Suppl 1), S21–9.

Hope, V. D., Judd, a, Hickman, M., Lamagni, T., Hunter, G., Stimson, G. V, Jones, S., Donovan, L., Parry, J. V & Gill, O. N. (2001). Prevalence of Hepatitis C among Injection Drug Users in England and Wales: Is Harm Reduction Working? *American Journal of Public Health*, 91(1), 38–42.

Horner, S. M., Park, H. S. & Gale, M. (2012). Control of Innate Immune Signaling and Membrane Targeting by the Hepatitis C Virus NS3/4A Protease Are Governed by the NS3 Helix α0. *Journal of Virology*, 86(6), 3112–20.

Hsu, M., Zhang, J., Flint, M., Logvinoff, C., Cheng-Mayer, C., Rice, C. M. & McKeating, J. a. (2003). Hepatitis C Virus Glycoproteins Mediate pH-Dependent Cell Entry of Pseudotyped Retroviral Particles. *Proceedings of the National Academy of Sciences of the United States of America*, 100(12), 7271–6.

Hu, F., Luo, W. & Hong, M. (2010). Mechanisms of Proton Conduction and Gating in Influenza M2 Proton Channels from Solid-State NMR. *Science*, 330(October), 505–8.

Huang, L., Hwang, J., Sharma, S. D., Hargittai, M. R. S., Chen, Y., Arnold, J. J., Raney, K. D. & Cameron, C. E. (2005). Hepatitis C Virus Nonstructural Protein 5A (NS5A) Is an RNA-Binding Protein. *The Journal of Biological Chemistry*, 280(43), 36417–28.

Huang, R.-B., Du, Q.-S., Wang, C.-H. & Chou, K.-C. (2008). An in-Depth Analysis of the Biological Functional Studies Based on the NMR M2 Channel Structure of Influenza A Virus. *Biochemical and Biophysical Research Communications*, 377(4), 1243–7.

Hughes, M., Griffin, S. & Harris, M. (2009). Domain III of NS5A Contributes to Both RNA Replication and Assembly of Hepatitis C Virus Particles. *Journal of General Virology*, 90(6), 1329–34.

Hügle, T., Fehrmann, F., Bieck, E., Kohara, M., Kräusslich, H. G., Rice, C. M., Blum, H. E. & Moradpour, D. (2001). The Hepatitis C Virus Nonstructural Protein 4B Is an Integral Endoplasmic Reticulum Membrane Protein. *Virology*, 284(1), 70–81.

Isherwood, B. J. & Patel, A. H. (2005). Analysis of the Processing and Transmembrane Topology of the E2p7 Protein of Hepatitis C Virus. *The Journal of General Virology*, 86(Pt 3), 667–76.

Ito, T. & Lai, M. M. (1997). Determination of the Secondary Structure of and Cellular Protein Binding to the 3'-Untranslated Region of the Hepatitis C Virus RNA Genome. *Journal of Virology*, 71(11), 8698–706.

Ivashkina, N., Wölk, B., Lohmann, V., Bartenschlager, R., Blum, H. E., Penin, F. & Moradpour, D. (2002). The Hepatitis C Virus RNA-Dependent RNA Polymerase Membrane Insertion Sequence Is a Transmembrane Segment. *Journal of Virology*, 76(24), 13088–93.

Jacobson, I. M., McHutchison, J. G., Dusheiko, G., Di Bisceglie, A. M., Reddy, K. R., Bzowej, N. H., Marcellin, P., Muir, A. J., Ferenci, P., Flisiak, R., George, J., Rizzetto, M., Shouval, D., Sola, R., Terg, R. a, Yoshida, E. M., Adda, N., Bengtsson, L., Sankoh, A. J., Kieffer, T. L., George, S., Kauffman, R. S. & Zeuzem, S. (2011). Telaprevir for Previously Untreated Chronic Hepatitis C Virus Infection. *The New England Journal of Medicine*, 364(25), 2405–16.

Ji, H., Fraser, C. S., Yu, Y., Leary, J. & Doudna, J. a. (2004). Coordinated Assembly of Human Translation Initiation Complexes by the Hepatitis C Virus Internal Ribosome Entry Site RNA. *Proceedings of the National Academy of Sciences of the United States of America*, 101(49), 16990–5.

Jin, H., Zhou, H., Cheng, X., Tang, R., Munoz, M. & Nguyen, N. (2000). Recombinant Respiratory Syncytial Viruses with Deletions in the NS1, NS2, SH, and M2-2 Genes Are Attenuated in Vitro and in Vivo. *Virology*, 273(1), 210–8.

Jirasko, V., Montserret, R., Lee, J. Y., Gouttenoire, J., Moradpour, D., Penin, F. & Bartenschlager, R. (2010). Structural and Functional Studies of Nonstructural Protein 2 of the Hepatitis C Virus Reveal Its Key Role as Organizer of Virion Assembly. *PLoS Pathogens*, 6(12), e1001233.

Jones, C. T., Murray, C. L., Eastman, D. K., Tassello, J. & Rice, C. M. (2007). Hepatitis C Virus p7 and NS2 Proteins Are Essential for Production of Infectious Virus. *Journal of Virology*, 81(16), 8374–83.

De Jong, A. S., Melchers, W. J. G., Glaudemans, D. H. R. F., Willems, P. H. G. M. & van Kuppeveld, F. J. M. (2004). Mutational Analysis of Different Regions in the

Coxsackievirus 2B Protein: Requirements for Homo-Multimerization, Membrane Permeabilization, Subcellular Localization, and Virus Replication. *The Journal of Biological Chemistry*, 279(19), 19924–35.

De Jong, A. S., Wessels, E., Dijkman, H. B. P. M., Galama, J. M. D., Melchers, W. J. G., Willems, P. H. G. M. & van Kuppeveld, F. J. M. (2003). Determinants for Membrane Association and Permeabilization of the Coxsackievirus 2B Protein and the Identification of the Golgi Complex as the Target Organelle. *The Journal of Biological Chemistry*, 278(2), 1012–21.

Jopling, C. L., Yi, M., Lancaster, A. M., Lemon, S. M. & Sarnow, P. (2005). Modulation of Hepatitis C Virus RNA Abundance by a Liver-Specific MicroRNA. *Science Signalling*, 309(5740), 1577.

Kapoor, A., Simmonds, P., Gerold, G., Qaisar, N., Jain, K., Henriquez, J. a, Firth, C., Hirschberg, D. L., Rice, C. M., Shields, S. & Lipkin, W. I. (2011). Characterization of a Canine Homolog of Hepatitis C Virus. *Proceedings of the National Academy of Sciences of the United States of America*, 108(28), 11608–13.

Karayiannis, P., Petrovic, L. M., Fry, M., Moore, D., Enticott, M., McGarvey, M. J., Scheuer, P. J. & Thomas, H. C. (1989). Studies of GB Hepatitis Agent in Tamarins. *Hepatology (Baltimore, Md.)*, 9(2), 186–92.

Kass, I. & Arkin, I. T. (2005). How pH Opens a H+ Channel: The Gating Mechanism of Influenza A M2. *Structure (London, England : 1993)*, 13(12), 1789–98.

Kato, T., Choi, Y., Elmowalid, G., Sapp, R. K., Barth, H., Furusaka, A., Mishiro, S., Wakita, T., Krawczynski, K. & Liang, T. J. (2008). Hepatitis C Virus JFH-1 Strain Infection in Chimpanzees Is Associated with Low Pathogenicity and Emergence of an Adaptive Mutation. *Hepatology (Baltimore, Md.)*, 48(3), 732–40.

Kato, T., Date, T., Miyamoto, M., Furusaka, A., Tokushige, K., Mizokami, M. & Wakita, T. (2003). Efficient Replication of the Genotype 2a Hepatitis C Virus Subgenomic Replicon. *Gastroenterology*, 125(6), 1808–17.

Kaukinen, P., Sillanpää, M., Kotenko, S., Lin, R., Hiscott, J., Melén, K. & Julkunen, I. (2006). Hepatitis C Virus NS2 and NS3/4A Proteins Are Potent Inhibitors of Host Cell Cytokine/chemokine Gene Expression. *Virology Journal*, 3, 66.

Keeffe, E. B. (2001). Liver Transplantation: Current Status and Novel Approaches to Liver Replacement. *Gastroenterology*, 120(3), 749–62.

Kell, B., Jewers, R. J., Cason, J., Pakarian, F., Kaye, J. N. & Best, J. M. (1994). Detection of E5 Oncoprotein in Human Papillomavirus Type 16-Positive Cervical Scrapes Using Antibodies Raised to Synthetic Peptides. *Journal of General Virology*, 75, 2451–56.

Kerkau, B. T., Bacik, I., Bennink, J. R., Yewdell, J. W., Hünig, T. & Schimpl, A. (1997). Protein Interferes with an Early Step in the Biosynthesis of Major Histocompatibility Complex (MHC) Class I Molecules. *The Journal of Experimental Medicine*, 185(7).

Kim, D. W., Gwack, Y., Han, J. H. & Choe, J. (1995). C-Terminal Domain of the Hepatitis C Virus NS3 Protein Contains an RNA Helicase Activity. *Biochemical and Biophysical Research Communications*, 215(1), 160–66.

Kim, J. L., Morgenstern, K. a, Griffith, J. P., Dwyer, M. D., Thomson, J. a, Murcko, M. a, Lin, C. & Caron, P. R. (1998). Hepatitis C Virus NS3 RNA Helicase Domain with a Bound Oligonucleotide: The Crystal Structure Provides Insights into the Mode of Unwinding. *Structure (London, England : 1993)*, 6(1), 89–100.

Kim, J. L., Morgenstern, K. a, Lin, C., Fox, T., Dwyer, M. D., Landro, J. a, Chambers, S. P., Markland, W., Lepre, C. a, O'Malley, E. T., Harbeson, S. L., Rice, C. M., Murcko, M. a, Caron, P. R. & Thomson, J. a. (1996). Crystal Structure of the Hepatitis C Virus NS3 Protease Domain Complexed with a Synthetic NS4A Cofactor Peptide. *Cell*, 87(2), 343–55.

Kim, Y. K., Kim, C. S., Lee, S. H. & Jang, S. K. (2002). Domains I and II in the 5' Nontranslated Region of the HCV Genome Are Required for RNA Replication. *Biochemical and Biophysical Research Communications*, 290(1), 105–12.

Kolykhalov, A. A., Feinstone, S. M. & Rice, C. M. (1996). Identification of a Highly Conserved Sequence Element at the 3'terminus of Hepatitis C Virus Genome RNA. *Journal of Virology*, 70(6), 3363–71.

Komurian-Pradel, F., Rajoharison, A., Berland, J., Khouri, V., Perret, M., Van Roosmalen, M., Pol, S., Negro, F., Paranhos-Baccalà, G., November, R. & Paranhos-raccala, G. (2004). Antigenic Relevance of F Protein in Chronic Hepatitis C Virus Infection. *Hepatology*, 40(4), 900–9.

Koutsoudakis, G., Kaul, A., Steinmann, E., Kallis, S., Lohmann, V., Pietschmann, T. & Bartenschlager, R. (2006). Characterization of the Early Steps of Hepatitis C Virus Infection by Using Luciferase Reporter Viruses. *Journal of Virology*, 80(11), 5308–20.

Krajden, M. (2000). Hepatitis C Virus Diagnosis and Testing. *Canadian Journal of Public Health. Revue Canadienne de Santé Publique*, 91 Suppl 1, S34–S39.

Krawczyk, E., Suprynowicz, F. a, Sudarshan, S. R. & Schlegel, R. (2010). Membrane Orientation of the Human Papillomavirus Type 16 E5 Oncoprotein. *Journal of Virology*, 84(4), 1696–703.

Krawczynski, K. (1993). Hepatitis E. *Hepatology*, 17(5), 932–41.

Krieger, N., Lohmann, V. & Bartenschlager, R. (2001). Enhancement of Hepatitis C Virus RNA Replication by Cell Culture-Adaptive Mutations. *Journal of Virology*, 75(10), 4614–24.

Kukol, a & Arkin, I. T. (1999). Vpu Transmembrane Peptide Structure Obtained By Site-Specific Fourier Transform Infrared Dichroism and Global Molecular Dynamics Searching. *Biophysical Journal*, 77(3), 1594–601.

Kumar, D., Farrell, G. C., Fung, C. & George, J. (2002). Hepatitis C Virus Genotype 3 Is Cytopathic to Hepatocytes: Reversal of Hepatic Steatosis after Sustained Therapeutic Response. *Hepatology (Baltimore, Md.)*, 36(5), 1266–72.

Van Kuppeveld, F. J., Galama, J. M., Zoll, J., Van den Hurk, P. J. & Melchers, W. J. (1996). Coxsackie B3 Virus Protein 2B Contains Cationic Amphipathic Helix That Is Required for Viral RNA Replication. *Journal of Virology*, 70(6), 3876–86.

Van Kuppeveld, F. J., Hoenderop, J. G., Smeets, R. L., Willems, P. H., Dijkman, H. B., Galama, J. M. & Melchers, W. J. (1997). Coxsackievirus Protein 2B Modifies Endoplasmic Reticulum Membrane and Plasma Membrane Permeability and Facilitates Virus Release. *The EMBO Journal*, 16(12), 3519–32.

Kyono, K., Miyashiro, M. & Taguchi, I. (2002). Human Eukaryotic Initiation Factor 4AII Associates with Hepatitis C Virus NS5B Protein in Vitro. *Biochemical and Biophysical Research Communications*, 292(3), 659–66.

Kyte, J. & Doolittle, R. F. (1982). A Simple Method for Displaying the Hydropathic Character of a Protein. *Journal of Molecular Biology*, 157(1), 105–32.

Lai, C.-K., Jeng, K.-S., Machida, K., Cheng, Y.-S. & Lai, M. M. C. (2008). Hepatitis C Virus NS3/4A Protein Interacts with ATM, Impairs DNA Repair and Enhances Sensitivity to Ionizing Radiation. *Virology*, 370(2), 295–309.

Lama, J. & Carrasco, L. (1992). Expression of Poliovirus Nonstructural Proteins in Escherichia Coli Cells. , 267(22), 15932–37.

Lamb, R. A., Zebedee, S. L. & Richardson, C. D. (1985). Influenza Virus M2 Protein Is an Integral Membrane Protein Expressed on the Infected-Cell Surface. *Cell*, 40(3), 627–33.

Lanford, R. E., Bigger, C., Bassett, S. & Klimpel, G. (2001). The Chimpanzee Model of Hepatitis C Virus Infections. *ILAR Journal / National Research Council, Institute of Laboratory Animal Resources*, 42(2), 117–26.

Lange, C. M., Sarrazin, C. & Zeuzem, S. (2010). Review Article: Specifically Targeted Anti-Viral Therapy for Hepatitis C - a New Era in Therapy. *Alimentary Pharmacology & Therapeutics*, 32(1), 14–28.

Large, M. K., Kittlesen, D. J. & Hahn, Y. S. (1999). Suppression of Host Immune Response by the Core Protein of Hepatitis C Virus: Possible Implications for Hepatitis C Virus Persistence. *Journal of Immunology (Baltimore, Md. : 1950)*, 162(2), 931–8.

Lau, J. Y. N., Tam, R. C., Liang, T. J. & Hong, Z. (2002). Mechanism of Action of Ribavirin in the Combination Treatment of Chronic HCV Infection. *Hepatology (Baltimore, Md.)*, 35(5), 1002–9.

Lavanchy, D. (2009). The Global Burden of Hepatitis C. *Liver International : Official Journal of the International Association for the Study of the Liver*, 29 Suppl 1, 74–81.

Leary, T. P., Muerhoff, S., Simons, J. N., Pilot-Matias, T. J., Erker, J. C., Chalmers, M. L., Schalauder, G. G., Dawson, G. J., Desai, S. M. & Mushahwar, I. K. (1996). Sequence and Genomic Organization of GBV-C: A Novel Member of the Flaviviridae Associated with Human Non-A-E Hepatitis. *Journal of Medical Virology*, 48(1), 60–67.

Legrand-Abravanel, F., Nicot, F. & Izopet, J. (2010). New NS5B Polymerase Inhibitors for Hepatitis C. *Expert Opinion on Investigational Drugs*, 19(8), 963–75.

Lemaitre, V., Ali, R., Kim, C. G., Watts, a & Fischer, W. B. (2004). Interaction of Amiloride and One of Its Derivatives with Vpu from HIV-1: A Molecular Dynamics Simulation. *FEBS Letters*, 563(1-3), 75–81.

Lesburg, C. A., Cable, M. B., Ferrari, E., Hong, Z., Mannarino, A. F. & Weber, P. C. (1999). Crystal Structure of the RNA-Dependent RNA Polymerase from Hepatitis C Virus Reveals a Fully Encircled Active Site. *Nature Structural & Molecular Biology*, 6(10), 937–43.

Lewis, C., Baro, M. F., Marques, M., Grüner, M., Alonso, A. & Bravo, I. G. (2008). The First Hydrophobic Region of the HPV16 E5 Protein Determines Protein Cellular Location and Facilitates Anchorage-Independent Growth. *Virology Journal*, 5, 30.

Li, H., Atkins, E., Bruckner, J., McArdle, S., Qiu, W. C., Thomassen, L. V, Scott, J., Shuhart, M. C., Livingston, S., Townshend-Bulson, L., McMahon, B. J., Harris, M., Griffin, S. & Gretch, D. R. (2012a). Genetic and Functional Heterogeneity of the Hepatitis C Virus p7 Ion Channel during Natural Chronic Infection. *Virology*, 423(1), 30–37.

Li, H., Hughes, A. L., Bano, N., McArdle, S., Livingston, S., Deubner, H., McMahon, B. J., Townshend-Bulson, L., McMahan, R., Rosen, H. R. & Gretch, D. R. (2011). Genetic Diversity of near Genome-Wide Hepatitis C Virus Sequences during Chronic Infection: Evidence for Protein Structural Conservation over Time. *PloS One*, 6(5), e19562.

Li, K., Foy, E., Ferreon, J. C., Nakamura, M., Ferreon, A. C. M., Ikeda, M., Ray, S. C., Gale, M. & Lemon, S. M. (2005). Immune Evasion by Hepatitis C Virus NS3/4A Protease-Mediated Cleavage of the Toll-like Receptor 3 Adaptor Protein TRIF. *Proceedings of the National Academy of Sciences of the United States of America*, 102(8), 2992–7.

Li, Y.-P., Ramirez, S., Jensen, S. B., Purcell, R. H., Gottwein, J. M. & Bukh, J. (2012b). Highly Efficient Full-Length Hepatitis C Virus Genotype 1 (strain TN) Infectious Culture System. *Proceedings of the National Academy of Sciences of the United States of America*, 109(48), 19757–62.

Liang, Y., Ye, H., Kang, C. B. & Yoon, H. S. (2007). Domain 2 of Nonstructural Protein 5A (NS5A) of Hepatitis C Virus Is Natively Unfolded. *Biochemistry*, 46(41), 11550–8.

Liaw, Y.-F. & Chu, C.-M. (2009). Hepatitis B Virus Infection. *Lancet*, 373(9663), 582–92.

Liljeström, P., Lusa, S., Huylebroeck, D., Garoff, H. & Liljestrom, P. (1991). In Vitro Mutagenesis of a Full-Length cDNA Clone of Semliki Forest Virus: The Small 6,000-Molecular-Weight Membrane Protein Modulates Virus Release. *Journal of Virology*, 65(8), 4107–13.

Lin, C., Lindenbach, B. D., Prágai, B. M., McCourt, D. W. & Rice, C. M. (1994). Processing in the Hepatitis C Virus E2-NS2 Region: Identification of p7 and Two

Distinct E2-Specific Products with Different C Termini. *Journal of Virology*, 68(8), 5063–73.

Lin, C., Thomson, J. A. & Rice, C. M. (1995). A Central Region in the Hepatitis C Virus NS4A Protein Allows Formation of an Active NS3-NS4A Serine Proteinase Complex in Vivo and in Vitro. *Journal of Virology*, 69(7), 4373–80.

Lindenbach, B. D., Evans, M. J., Syder, A. J., Wölk, B., Tellinghuisen, T. L., Liu, C. C., Maruyama, T., Hynes, R. O., Burton, D. R., McKeating, J. A. & Rice, C. M. (2005). Complete Replication of Hepatitis C Virus in Cell Culture. *Science*, 309(5734), 623–26.

Lindenbach, B. D., Prágai, B. M., Montserret, R., Beran, R. K. F., Pyle, A. M., Penin, F. & Rice, C. M. (2007). The C Terminus of Hepatitis C Virus NS4A Encodes an Electrostatic Switch That Regulates NS5A Hyperphosphorylation and Viral Replication. *Journal of Virology*, 81(17), 8905–18.

Lindenbach, B. D. & Rice, C. M. (2001). Flaviviridae: The Viruses and Their Replication, in: *Fields Virology*, (pp. 991–1041).

Lo, S.-Y., Selby, M., Tong, M. & Ou, J.-H. (1994). Comparative Studies of the Core Gene Products of Two Different Hepatitis C Virus Isolates: Two Alternative Forms Determined by a Single Amino Acid Substitution. *Virology*, 199(1), 124–31.

Loewy, A., Smyth, J., Von Bonsdorff, C. H., Liljeström, P. & Schlesinger, M. J. (1995). The 6-Kilodalton Membrane Protein of Semliki Forest Virus Is Involved in the Budding Process. *Journal of Virology*, 69(1), 469–75.

Lohmann, V., Korner, F., Koch, J., Herian, U., Theilmann, L. & Bartenschlager, R. (1999). Replication of Subgenomic Hepatitis C Virus RNAs in a Hepatoma Cell Line. *Science*, 285(5424), 110–3.

Lorenz, I. C., Marcotrigiano, J., Dentzer, T. G. & Rice, C. M. (2006). Structure of the Catalytic Domain of the Hepatitis C Virus NS2-3 Protease. *Nature*, 442(7104), 831–5.

Love, R. a, Brodsky, O., Hickey, M. J., Wells, P. a & Cronin, C. N. (2009). Crystal Structure of a Novel Dimeric Form of NS5A Domain I Protein from Hepatitis C Virus. *Journal of Virology*, 83(9), 4395–403.

Love, R. A., Parge, H. E., Wickersham, J. A., Hostomsky, Z., Habuka, N., Moomaw, E. W., Adachi, T. & Hostomska, Z. (1996). The Crystal Structure of Hepatitis C Virus NS3 Proteinase Reveals a Trypsin-like Fold and a Structural Zinc Binding Site. *Cell*, 87(2), 331–42.

Lozach, P.-Y., Amara, A., Bartosch, B., Virelizier, J.-L., Arenzana-Seisdedos, F., Cosset, F.-L. & Altmeyer, R. (2004). C-Type Lectins L-SIGN and DC-SIGN Capture and Transmit Infectious Hepatitis C Virus Pseudotype Particles. *The Journal of Biological Chemistry*, 279(31), 32035–45.

Lu, W. & Ou, J. (2002). Phosphorylation of Hepatitis C Virus Core Protein by Protein Kinase A and Protein Kinase C. *Virology*, 300(1), 20–30.

Luik, P., Chew, C., Aittoniemi, J., Chang, J., Wentworth, P., Dwek, R. a, Biggin, P. C., Vénien-Bryan, C. & Zitzmann, N. (2009). The 3-Dimensional Structure of a Hepatitis C Virus p7 Ion Channel by Electron Microscopy. *Proceedings of the National Academy of Sciences of the United States of America*, 106(31), 12712–6.

Lundin, M., Lindström, H., Grönwall, C. & Persson, M. a a. (2006). Dual Topology of the Processed Hepatitis C Virus Protein NS4B Is Influenced by the NS5A Protein. *The Journal of General Virology*, 87(Pt 11), 3263–72.

Lundin, M., Monné, M., Widell, A., Von Heijne, G. & Persson, M. A. A. (2003). Topology of the Membrane-Associated Hepatitis C Virus Protein NS4B. *Journal of Virology*, 77(9), 5428–38.

Lupberger, J., Zeisel, M. B., Xiao, F., Thumann, C., Fofana, I., Zona, L., Davis, C., Mee, C. J., Turek, M., Gorke, S., Royer, C., Fischer, B., Zahid, M. N., Lavillette, D., Fresquet, J., Cosset, F.-L., Rothenberg, S. M., Pietschmann, T., Patel, A. H., Pessaux, P., Doffoël, M., Raffelsberger, W., Poch, O., McKeating, J. a, Brino, L. & Baumert, T. F. (2011). EGFR and EphA2 Are Host Factors for Hepatitis C Virus Entry and Possible Targets for Antiviral Therapy. *Nature Medicine*, 17(5), 589–95.

Lusa, S., Garoff, H. & Liueström, P. (1991). Fate of the 6K Membrane Protein of Semliki Forest Virus during Virus Assembly. *Virology*, 185(2), 843–46.

Luscombe, C. A., Huang, Z., Murray, M. G., Miller, M., Wilkinson, J. & Ewart, G. D. (2010). A Novel Hepatitis C Virus p7 Ion Channel Inhibitor, BIT225, Inhibits Bovine Viral Diarrhea Virus in Vitro and Shows Synergism with Recombinant Interferon-Alpha-2b and Nucleoside Analogues. *Antiviral Research*, 86(2), 144–53.

Ma, C., Marassi, F. & Jones, D. (2002). Expression, Purification, and Activities of Full-Length and Truncated Versions of the Integral Membrane Protein Vpu from HIV-1. *Protein Science*, 11, 546–57.

Ma, C., Polishchuk, A. L., Ohigashi, Y., Stouffer, A. L., Schön, A., Magavern, E., Jing, X., Lear, J. D., Freire, E., Lamb, R. a, DeGrado, W. F. & Pinto, L. H. (2009). Identification of the Functional Core of the Influenza A Virus A/M2 Proton-Selective Ion Channel. *Proceedings of the National Academy of Sciences of the United States of America*, 106(30), 12283–8.

Ma, Y., Anantpadma, M., Timpe, J. M., Shanmugam, S., Singh, S. M., Lemon, S. M. & Yi, M. (2011). Hepatitis C Virus NS2 Protein Serves as a Scaffold for Virus Assembly by Interacting with Both Structural and Nonstructural Proteins. *Journal of Virology*, 85(1), 86–97.

Macdonald, A., Chan, J. K. Y. & Harris, M. (2005). Perturbation of Epidermal Growth Factor Receptor Complex Formation and Ras Signalling in Cells Harbouring the Hepatitis C Virus Subgenomic Replicon. *The Journal of General Virology*, 86(Pt 4), 1027–33.

Macdonald, A. & Harris, M. (2004). Hepatitis C Virus NS5A: Tales of a Promiscuous Protein. *The Journal of General Virology*, 85(Pt 9), 2485–502.

Madan, V., Castelló, A. & Carrasco, L. (2008). Viroporins from RNA Viruses Induce Caspase-Dependent Apoptosis. *Cellular Microbiology*, 10(2), 437–51.

Maheshwari, A., Ray, S. & Thuluvath, P. J. (2008). Acute Hepatitis C. *Lancet*, 372(9635), 321–32.

Maldarelli, F., Chen, M. Y., Willey, R. L. & Strebel, K. (1993). Human Immunodeficiency Virus Type 1 Vpu Protein Is an Oligomeric Type I Integral Membrane Protein. *Journal of Virology*, 67(8), 5056–61.

Mandell, G., Dolin, R., Bennett, J., Mandell, G. L. & Bennett, J. E. (2009). *Mandell, Douglas, and Bennett's Principles and Practice of Infectious Diseases.* Elsevier.

Mankouri, J., Dallas, M. L., Hughes, M. E., Griffin, S. D. C., Macdonald, A., Peers, C. & Harris, M. (2009). Suppression of a pro-Apoptotic K+ Channel as a Mechanism for Hepatitis C Virus Persistence. *Proceedings of the National Academy of Sciences of the United States of America*, 106(37), 15903–8.

Manor, J., Mukherjee, P., Lin, Y.-S., Leonov, H., Skinner, J. L., Zanni, M. T. & Arkin, I. T. (2009). Gating Mechanism of the Influenza A M2 Channel Revealed by 1D and 2D IR Spectroscopies. *Structure (London, England : 1993)*, 17(2), 247–54.

Martin, A. & Lemon, S. M. (2006). Hepatitis A Virus: From Discovery to Vaccines. *Hepatology (Baltimore, Md.)*, 43(2 Suppl 1), S164–72.

Martínez-Gil, L., Bañó-Polo, M., Redondo, N., Sánchez-Martínez, S., Nieva, J. L., Carrasco, L. & Mingarro, I. (2011). Membrane Integration of Poliovirus 2B Viroporin. *Journal of Virology*, 85(21), 11315–24.

Mazumdar, B., Banerjee, A., Meyer, K. & Ray, R. (2011). Hepatitis C Virus E1 Envelope Glycoprotein Interacts with Apolipoproteins in Facilitating Entry into Hepatocytes. *Hepatology (Baltimore, Md.)*, 54(4), 1149–56.

McCown, M. F. & Pekosz, A. (2006). Distinct Domains of the Influenza a Virus M2 Protein Cytoplasmic Tail Mediate Binding to the M1 Protein and Facilitate Infectious Virus Production. *Journal of Virology*, 80(16), 8178–89.

McLauchlan, J. (2000). Properties of the Hepatitis C Virus Core Protein: A Structural Protein That Modulates Cellular Processes. *Journal of Viral Hepatitis*, 7(1), 2–14.

Melton, J. V, Ewart, G. D., Weir, R. C., Board, P. G., Lee, E. & Gage, P. W. (2002). Alphavirus 6K Proteins Form Ion Channels. *The Journal of Biological Chemistry*, 277(49), 46923–31.

Mercer, D. F., Schiller, D. E., Elliott, J. F., Douglas, D. N., Hao, C., Rinfret, a, Addison, W. R., Fischer, K. P., Churchill, T. a, Lakey, J. R., Tyrrell, D. L. & Kneteman, N. M. (2001). Hepatitis C Virus Replication in Mice with Chimeric Human Livers. *Nature Medicine*, 7(8), 927–33.

Meredith, L. W., Zitzmann, N. & McKeating, J. a. (2013). Differential Effect of p7 Inhibitors on Hepatitis C Virus Cell-to-Cell Transmission. *Antiviral Research*, 100(3), 636–39.

Merican, I., Sherlock, S., McIntyre, N. & Dusheiko, G. M. (1993). Clinical, Biochemical and Histological Features in 102 Patients with Chronic Hepatitis C Virus Infection. *The Quarterly Journal of Medicine*, 86(2), 119–25.

Meshkat, Z., Audsley, M., Beyer, C., Gowans, E. J. & Haqshenas, G. (2009). Reverse Genetic Analysis of a Putative, Influenza Virus M2 HXXXW-like Motif in the p7 Protein of Hepatitis C Virus. *Journal of Viral Hepatitis*, 16(3), 187–94.

Michalak, J. P., Wychowski, C., Choukhi, a, Meunier, J. C., Ung, S., Rice, C. M. & Dubuisson, J. (1997). Characterization of Truncated Forms of Hepatitis C Virus Glycoproteins. *The Journal of General Virology*, 78 (Pt 9), 2299–306.

Miesenbock, G., De Angelis, D. A. & Rothman, J. E. (1998). Visualizing Secretion and Synaptic Transmission with pH-Sensitive Green Fluorescent Proteins. *Nature*, 394(6689), 192–95.

Mihm, U., Grigorian, N., Welsch, C., Herrmann, E., Kronenberger, B., Teuber, G., von Wagner, M., Hofmann, W.-P., Albrecht, M., Lengauer, T., Zeuzem, S. & Sarrazin, C. (2006). Amino Acid Variations in Hepatitis C Virus p7 and Sensitivity to Antiviral Combination Therapy with Amantadine in Chronic Hepatitis C. *Antiviral Therapy*, 11(4), 507–19.

Mizushima, H., Hijikata, M., Asabe, S., Hirota, M., Kimura, K. & Shimotohno, K. (1994). Two Hepatitis C Virus Glycoprotein E2 Products with Different C Termini. *Journal of Virology*, 68(10), 6215–22.

Mondelli, M. U., Cerino, A. & Cividini, A. (2005). Acute Hepatitis C: Diagnosis and Management. *Journal of Hepatology*, 42 Suppl(1), S108–14.

Montal, M. (2003). Structure–function Correlates of Vpu, a Membrane Protein of HIV-1. *FEBS Letters*, 552(1), 47–53.

Montserret, R., Saint, N., Vanbelle, C., Salvay, A. G., Simorre, J.-P., Ebel, C., Sapay, N., Renisio, J.-G., Böckmann, A., Steinmann, E., Pietschmann, T., Dubuisson, J., Chipot, C. & Penin, F. (2010). NMR Structure and Ion Channel Activity of the p7 Protein from Hepatitis C Virus. *The Journal of Biological Chemistry*, 285(41), 31446–61.

Moreno-Sánchez, R., Rodríguez-Enríquez, S., Marín-Hernández, A. & Saavedra, E. (2007). Energy Metabolism in Tumor Cells. *The FEBS Journal*, 274(6), 1393–418.

Morice, Y., Ratinier, M., Miladi, A., Chevaliez, S., Germanidis, G., Wedemeyer, H., Laperche, S., Lavergne, J.-P. & Pawlotsky, J.-M. (2009). Seroconversion to Hepatitis C Virus Alternate Reading Frame Protein during Acute Infection. *Hepatology (Baltimore, Md.)*, 49(5), 1449–59.

Morikawa, K., Zhao, Z., Miyamoto, M., Murayama, A., Akazawa, D., Tanabe, J., Sone, S. & Wakita, T. (2007). The Roles of CD81 and Glycosaminoglycans in the Adsorption and Uptake of Infectious HCV Particles. *Journal of Medical Virology*, 79(6), 714–23.

Murphy, D., Chamberland, J., Dandavino, R. & Sablon, E. (2007). A New Genotype of Hepatitis C Virus Originating from Central Africa, in: *Hepatology*, (p. 623A). JOHN WILEY & SONS INC 111 RIVER ST, HOBOKEN, NJ 07030 USA.

Narbus, C. M., Israelow, B., Sourisseau, M., Michta, M. L., Hopcraft, S. E., Zeiner, G. M. & Evans, M. J. (2011). HepG2 Cells Expressing microRNA miR-122 Support the Entire Hepatitis C Virus Life Cycle. *Journal of Virology*, 85(22), 12087–92.

Negro, F. & Alberti, A. (2011). The Global Health Burden of Hepatitis C Virus Infection. *Liver International : Official Journal of the International Association for the Study of the Liver*, 31 Suppl 2(July), 1–3.

Nieva, J. L., Madan, V. & Carrasco, L. (2012). Viroporins: Structure and Biological Functions. *Nature Reviews. Microbiology*, 10(8), 563–74.

Nkontchou, G., Ziol, M., Aout, M., Lhabadie, M., Baazia, Y., Mahmoudi, a, Roulot, D., Ganne-Carrie, N., Grando-Lemaire, V., Trinchet, J.-C., Gordien, E., Vicaut, E., Baghad, I. & Beaugrand, M. (2011). HCV Genotype 3 Is Associated with a Higher Hepatocellular Carcinoma Incidence in Patients with Ongoing Viral C Cirrhosis. *Journal of Viral Hepatitis*, 18(10), e516–22.

Nomura-Takigawa, Y., Nagano-Fujii, M., Deng, L., Kitazawa, S., Ishido, S., Sada, K. & Hotta, H. (2006). Non-Structural Protein 4A of Hepatitis C Virus Accumulates on Mitochondria and Renders the Cells Prone to Undergoing Mitochondria-Mediated Apoptosis. *The Journal of General Virology*, 87(Pt 7), 1935–45.

Okada, a, Miura, T. & Takeuchi, H. (2001). Protonation of Histidine and Histidine-Tryptophan Interaction in the Activation of the M2 Ion Channel from Influenza a Virus. *Biochemistry*, 40(20), 6053–60.

OuYang, B., Xie, S., Berardi, M. J., Zhao, X., Dev, J., Yu, W., Sun, B. & Chou, J. J. (2013). Unusual Architecture of the p7 Channel from Hepatitis C Virus. *Nature*.

Owsianka, A., Tarr, A. W., Juttla, V. S., Lavillette, D., Bartosch, B., Cosset, F., Ball, J. K., Patel, A. H. & Ball, K. (2005). Monoclonal Antibody AP33 Defines a Broadly Neutralizing Epitope on the Hepatitis C Virus E2 Envelope Glycoprotein. *Journal of Virology*, 79(17), 11095–104.

Pallaoro, M., Lahm, A., Biasiol, G., Brunetti, M., Nardella, C., Orsatti, L., Bonelli, F., Orrù, S., Narjes, F. & Steinkühler, C. (2001). Characterization of the Hepatitis C Virus NS2/3 Processing Reaction by Using a Purified Precursor Protein. *Journal of Virology*, 75(20), 9939–46.

Pappalardo, B. L. (2003). Influence of Maternal Human Immunodeficiency Virus (HIV) Co-Infection on Vertical Transmission of Hepatitis C Virus (HCV): A Meta-Analysis. *International Journal of Epidemiology*, 32(5), 727–34.

Park, E. K., Castrucci, M. R., Portner, A. & Kawaoka, Y. (1998). The M2 Ectodomain Is Important for Its Incorporation into Influenza A Virions. *Journal of Virology*, 72(3), 2449–55.

Patargias, G., Zitzmann, N., Dwek, R. & Fischer, W. B. (2006). Protein-Protein Interactions: Modeling the Hepatitis C Virus Ion Channel p7. *Journal of Medicinal Chemistry*, 49(2), 648–55.

Paul, M. & Jabbar, M. a. (1997). Phosphorylation of Both Phosphoacceptor Sites in the HIV-1 Vpu Cytoplasmic Domain Is Essential for Vpu-Mediated ER Degradation of CD4. *Virology*, 232(1), 207–16.

Pavlović, D., Neville, D. C. a, Argaud, O., Blumberg, B., Dwek, R. a, Fischer, W. B. & Zitzmann, N. (2003). The Hepatitis C Virus p7 Protein Forms an Ion Channel That Is Inhibited by Long-Alkyl-Chain Iminosugar Derivatives. *Proceedings of the National Academy of Sciences of the United States of America*, 100(10), 6104–8.

Pawlotsky, J.-M. (2006). Therapy of Hepatitis C: From Empiricism to Eradication. *Hepatology (Baltimore, Md.)*, 43(2 Suppl 1), S207–20.

Perez, M., García-Barreno, B., Melero, J. a, Carrasco, L. & Guinea, R. (1997). Membrane Permeability Changes Induced in Escherichia Coli by the SH Protein of Human Respiratory Syncytial Virus. *Virology*, 235(2), 342–51.

Pérez-Berná, A. J., Guillén, J., Moreno, M. R., Bernabeu, A., Pabst, G., Laggner, P. & Villalaín, J. (2008). Identification of the Membrane-Active Regions of Hepatitis C Virus p7 Protein: Biophysical Characterization of the Loop Region. *The Journal of Biological Chemistry*, 283(13), 8089–101.

Pestova, T. V., Shatsky, I. N., Fletcher, S. P., Jackson, R. J. & Hellen, C. U. T. (1998). A Prokaryotic-like Mode of Cytoplasmic Eukaryotic Ribosome Binding to the Initiation Codon during Internal Translation Initation of Hepatitis C and Classical Swine Fever Virus RNAs. *Genes & Development*, 12(1), 67–83.

Piccininni, S., Varaklioti, A., Nardelli, M., Dave, B., Raney, K. D. & McCarthy, J. E. G. (2002). Modulation of the Hepatitis C Virus RNA-Dependent RNA Polymerase Activity by the Non-Structural (NS) 3 Helicase and the NS4B Membrane Protein. *The Journal of Biological Chemistry*, 277(47), 45670–9.

Pieroni, L., Santolini, E., Fipaldini, C., Pacini, L., Migliaccio, G., La Monica, N., Monica, L., Monica, N. L. A. & Ricerche, I. R. B. M. (1997). In Vitro Study of the NS2-3 Protease of Hepatitis C Virus. *Journal of Virology*, 71(9), 6373–80.

Pietschmann, T., Kaul, A., Koutsoudakis, G., Shavinskaya, A., Kallis, S., Steinmann, E., Abid, K., Negro, F., Dreux, M., Cosset, F.-L. & Bartenschlager, R. (2006). Construction and Characterization of Infectious Intragenotypic and Intergenotypic Hepatitis C Virus Chimeras. *Proceedings of the National Academy of Sciences of the United States of America*, 103(19), 7408–13.

Pileri, P., Uematsu, Y., Campagnoli, S., Galli, G., Falugi, F., Petracca, R., Weiner, A. J., Houghton, M., Rosa, D. & Grandi, G. (1998). Binding of Hepatitis C Virus to CD81. *Science*, 282(5390), 938–41.

Pinto, L. H. & Lamb, R. a. (2006). Influenza Virus Proton Channels. *Photochemical & Photobiological Sciences : Official Journal of the European Photochemistry Association and the European Society for Photobiology*, 5(6), 629–32.

Ploss, A., Evans, M. J., Gaysinskaya, V. a, Panis, M., You, H., de Jong, Y. P. & Rice, C. M. (2009). Human Occludin Is a Hepatitis C Virus Entry Factor Required for Infection of Mouse Cells. *Nature*, 457(7231), 882–6.

Polish, L. B., Gallagher, M., Fields, H. A. & Hadler, S. C. (1993). Delta Hepatitis: Molecular Biology and Clinical and Epidemiological Features. *Clinical Microbiology Reviews*, 6(3), 211–29.

Poordad, F., McCone, J., Bacon, B. R., Bruno, S., Manns, M. P., Sulkowski, M. S., Jacobson, I. M., Reddy, K. R., Goodman, Z. D., Boparai, N., DiNubile, M. J., Sniukiene, V., Brass, C. A., Albrecht, J. K. & Bronowicki, J.-P. (2011). Boceprevir for Untreated Chronic HCV Genotype 1 Infection. *New England Journal of Medicine*, 364(13), 1195–206.

Popescu, C.-I., Callens, N., Trinel, D., Roingeard, P., Moradpour, D., Descamps, V., Duverlie, G., Penin, F., Héliot, L., Rouillé, Y. & Dubuisson, J. (2011). NS2 Protein of Hepatitis C Virus Interacts with Structural and Non-Structural Proteins towards Virus Assembly. *PLoS Pathogens*, 7(2), e1001278.

Post, J. J., Pan, Y., Freeman, A. J., Harvey, C. E., White, P. a, Palladinetti, P., Haber, P. S., Marinos, G., Levy, M. H., Kaldor, J. M., Dolan, K. a, Ffrench, R. a, Lloyd, A. R. & Rawlinson, W. D. (2004). Clearance of Hepatitis C Viremia Associated with Cellular Immunity in the Absence of Seroconversion in the Hepatitis C Incidence and Transmission in Prisons Study Cohort. *The Journal of Infectious Diseases*, 189(10), 1846–55.

Premkumar, A., Wilson, L., Ewart, G. D. & Gage, P. W. (2004). Cation-Selective Ion Channels Formed by p7 of Hepatitis C Virus Are Blocked by Hexamethylene Amiloride. *FEBS Letters*, 557(1-3), 99–103.

Quinkert, D., Bartenschlager, R. & Lohmann, V. (2005). Quantitative Analysis of the Hepatitis C Virus Replication Complex. *Journal of Virology*, 79(21), 13594–605.

Ramirez, S., Li, Y.-P., Jensen, S. B., Pedersen, J., Gottwein, J. M. & Bukh, J. (2014). Highly Efficient Infectious Cell Culture of Three Hepatitis C Virus Genotype 2b Strains and Sensitivity to Lead Protease, Nonstructural Protein 5A, and Polymerase Inhibitors. *Hepatology (Baltimore, Md.)*, 59(2), 395–407.

Ray, R. B., Steele, R., Meyer, K. & Ray, R. (1997). Transcriptional Repression of p53 Promoter by Hepatitis C Virus Core Protein. *The Journal of Biological Chemistry*, 272(17), 10983–6.

Rex, S. & Schwarz, G. (1998). Quantitative Studies on the Melittin-Induced Leakage Mechanism of Lipid Vesicles. *Biochemistry*, 37(8), 2336–45.

Reynolds, J. E., Kaminski, a, Kettinen, H. J., Grace, K., Clarke, B. E., Carroll, a R., Rowlands, D. J. & Jackson, R. J. (1995). Unique Features of Internal Initiation of Hepatitis C Virus RNA Translation. *The EMBO Journal*, 14(23), 6010–20.

Rosenberg, M. & Casarotto, M. (2010). Coexistence of Two Adamantane Binding Sites in the Influenza A M2 Ion Channel. *Proceedings of the National Academy of Sciences*, 107(31), 13866–71.

Rossman, J. S., Jing, X., Leser, G. P. & Lamb, R. a. (2010). Influenza Virus M2 Protein Mediates ESCRT-Independent Membrane Scission. *Cell*, 142(6), 902–13.

Roussel, J., Pillez, A., Montpellier, C., Duverlie, G., Cahour, A., Dubuisson, J. & Wychowski, C. (2003). Characterization of the Expression of the Hepatitis C Virus F Protein. *Journal of General Virology*, 84(7), 1751–59.

Sakai, A., Claire, M. S., Faulk, K., Govindarajan, S., Emerson, S. U., Purcell, R. H. & Bukh, J. (2003). The p7 Polypeptide of Hepatitis C Virus Is Critical for Infectivity and Contains Functionally Important Genotype-Specific Sequences. *Proceedings of the National Academy of Sciences of the United States of America*, 100(20), 11646–51.

Sambrook, J., Fritsch, E. F. & Maniatis, T. (1989). *Molecular Cloning*. Cold Spring Harbor Laboratory Press, New York.

Sandoval, I. I. V & Carrasco, L. (1997). Poliovirus Infection and Expression of the Poliovirus Protein 2B Provoke the Disassembly of the Golgi Complex, the Organelle Target for the Antipoliovirus Drug Ro-090179. *Journal of Virology*, 71(6), 4679–93.

Santolini, E., Migliaccio, G., Monica, N. L. A., Molecolare, B., Pomezia, P. A. & La Monica, N. (1994). Biosynthesis and Biochemical Properties of the Hepatitis C Virus Core Protein. *Journal of Virology*, 68(6), 3631–41.

Santolini, E., Pacini, L., Fipaldini, C., Migliaccio, G. & Monica, N. L. A. (1995). The NS2 Protein of Hepatitis C Virus Is a Transmembrane Polypeptide. *Journal of Virology*, 69(12), 7461–71.

Sanz, M. A., Pérez, L. & Carrasco, L. (1994). Semliki Forest Virus 6K Protein Modifies Membrane Permeability after Inducible Expression in Escherichia Coli Cells. *Journal of Biological Chemistry*, 269(16), 12106–10.

Scarselli, E., Ansuini, H., Cerino, R., Roccasecca, R. M., Acali, S., Filocamo, G., Traboni, C., Nicosia, A., Cortese, R. & Vitelli, A. (2002). The Human Scavenger Receptor Class B Type I Is a Novel Candidate Receptor for the Hepatitis C Virus. *The EMBO Journal*, 21(19), 5017–25.

Schlauder, G. G., Dawson, G. J., Simons, J. N., Pilot-Matias, T. J., Gutierrez, R. A., Heynen, C. A., Knigge, M. F., Kurpiewski, G. S., Buijk, S. L. & Leary, T. P. (1995). Molecular and Serologic Analysis in the Transmission of the GB Hepatitis Agents. *Journal of Medical Virology*, 46(1), 81–90.

Schlesinger, M. J., London, S. D. & Ryan, C. (1993). An in-Frame Insertion into the Sindbis Virus 6K Gene Leads to Defective Proteolytic Processing of the Virus Glycoproteins, a Trans-Dominant Negative Inhibition of Normal Virus Formation, and Interference in Virus Shut off of Host-Cell Protein Synthesis. *Virology*, 193(1), 424–32.

Schmidt-Mende, J., Bieck, E., Hugle, T., Penin, F., Rice, C. M., Blum, H. E. & Moradpour, D. (2001). Determinants for Membrane Association of the Hepatitis C

Virus RNA-Dependent RNA Polymerase. *The Journal of Biological Chemistry*, 276(47), 44052–63.

Schnell, J. R. & Chou, J. J. (2008). Structure and Mechanism of the M2 Proton Channel of Influenza A Virus. *Nature*, 451(7178), 591–5.

Schregel, V., Jacobi, S., Penin, F. & Tautz, N. (2009). Hepatitis C Virus NS2 Is a Protease Stimulated by Cofactor Domains in NS3. *Proceedings of the National Academy of Sciences of the United States of America*, 106(13), 5342–7.

Schubert, U., Bour, S., Ferrer-Montiel, A. V, Montal, M., Maldarell, F. & Strebel, K. (1996). The Two Biological Activities of Human Immunodeficiency Virus Type 1 Vpu Protein Involve Two Separable Structural Domains. *Journal of Virology*, 70(2), 809–19.

Schubert, U. & Ferrer-Montiel, A. (1996). Identification of an Ion Channel Activity of the Vpu Transmembrane Domain and Its Involvement in the Regulation of Virus Release from HIV-1-Infected Cells. *FEBS Letters*, 398, 12–18.

Schwer, B., Ren, S., Pietschmann, T., Kartenbeck, J., Kaehlcke, K., Bartenschlager, R., Yen, T. S. B. & Ott, M. (2004). Targeting of Hepatitis C Virus Core Protein to Mitochondria through a Novel C-Terminal Localization Motif. *Journal of Virology*, 78(15), 7958–68.

Seeff, L. B. (2002). Natural History of Chronic Hepatitis C. *Hepatology*, 36(S1), S35–S46.

Serebrov, V. & Pyle, A. (2004). Periodic Cycles of RNA Unwinding and Pausing by Hepatitis C Virus NS3 Helicase. *Nature*, 430(July), 476–80.

Shepard, C. W., Finelli, L. & Alter, M. J. (2005). Global Epidemiology of Hepatitis C Virus Infection. *The Lancet Infectious Diseases*, 5(9), 558–67.

Shi, S. T., Polyak, S. J., Tu, H., Taylor, D. R., Gretch, D. R. & Lai, M. M. C. (2002). Hepatitis C Virus NS5A Colocalizes with the Core Protein on Lipid Droplets and Interacts with Apolipoproteins. *Virology*, 292(2), 198–210.

Shimakami, T., Hijikata, M., Luo, H., Ma, Y. Y., Kaneko, S., Shimotohno, K. & Murakami, S. (2004). Effect of Interaction between Hepatitis C Virus NS5A and NS5B on Hepatitis C Virus RNA Replication with the Hepatitis C Virus Replicon. *Journal of Virology*, 78(6), 2738–48.

Shimbo, K., Brassard, D. L., Lamb, R. A. & Pinto, L. H. (1996). Ion Selectivity and Activation of the M2 Ion Channel of Influenza Virus. *Biophysical Journal*, 70(3), 1335–46.

Shimizu, Y. K., Feinstone, S. M., Purcell, R. H., Alter, H. J. & London, W. T. (1979). Non-A, Non-B Hepatitis: Ultrastructural Evidence for Two Agents in Experimentally Infected Chimpanzees. *Science*, 205(4402), 197–200.

Simmonds, P. (2004). Genetic Diversity and Evolution of Hepatitis C Virus--15 Years On. *The Journal of General Virology*, 85(Pt 11), 3173–88.

Simmonds, P., Holmes, E. C., Cha, T. -a., Chan, S.-W., McOmish, F., Irvine, B., Beall, E., Yap, P. L., Kolberg, J. & Urdea, M. S. (1993). Classification of Hepatitis C Virus into Six Major Genotypes and a Series of Subtypes by Phylogenetic Analysis of the NS-5 Region. *Journal of General Virology*, 74(11), 2391–9.

Smith, A. J. & Lippiat, J. D. (2010). Direct Endosomal Acidification by the Outwardly Rectifying CLC-5 Cl−/H+ Exchanger. *The Journal of Physiology*, 588(12), 2033–45.

Song, H., Li, J., Shi, S., Yan, L., Zhuang, H. & Li, K. (2010). Thermal Stability and Inactivation of Hepatitis C Virus Grown in Cell Culture. *Virology Journal*, 7, 40.

Soto, B., Sánchez-Quijano, A., Rodrigo, L., Olmo, J. A. del, García-Bengoechea, M., Hernández-Quero, J., Rey, C., Abad, M. A., Rodríguez, M., Sales Gilabert, M., González, F., Mirón, P., Caruz, A., Relimpio, F., Torronteras, R., Leal, M. & Lissen, E. (1997). Human Immunodeficiency Virus Infection Modified the Natural History of Chronic Parenterally-Acquired Hepatitis C with an Unusually Rapid Progression to Cirrhosis. *Journal of Hepatology*, 26(1), 1–5.

Stapleton, J. T., Foung, S., Muerhoff, a S., Bukh, J. & Simmonds, P. (2011). The GB Viruses: A Review and Proposed Classification of GBV-A, GBV-C (HGV), and GBV-D in Genus Pegivirus within the Family Flaviviridae. *The Journal of General Virology*, 92(Pt 2), 233–46.

Stapleton, J. T., Williams, C. F. & Xiang, J. (2004). GB Virus Type C: A Beneficial Infection? *Journal of Clinical Microbiology*, 42(9), 3915–19.

Starr, D. (2000). *Blood: An Epic History of Medicine and Commerce*. HarperCollins.

Steinmann, E., Penin, F., Kallis, S., Patel, A. H., Bartenschlager, R. & Pietschmann, T. (2007). Hepatitis C Virus p7 Protein Is Crucial for Assembly and Release of Infectious Virions. *PLoS Pathogens*, 3(7), e103.

StGelais, C. (2008). Development and Utilisation of an In Vitro Assay for Functional Analysis of the Hepatitis C Virus p7 Protein.

StGelais, C., Foster, T. L., Verow, M., Atkins, E., Fishwick, C. W. G., Rowlands, D., Harris, M. & Griffin, S. (2009). Determinants of Hepatitis C Virus p7 Ion Channel Function and Drug Sensitivity Identified in Vitro. *Journal of Virology*, 83(16), 7970–81.

StGelais, C., Tuthill, T. J., Clarke, D. S., Rowlands, D. J., Harris, M. & Griffin, S. (2007). Inhibition of Hepatitis C Virus p7 Membrane Channels in a Liposome-Based Assay System. *Antiviral Research*, 76(1), 48–58.

Stouffer, A. L., Acharya, R., Salom, D., Levine, A. S., Di Costanzo, L., Soto, C. S., Tereshko, V., Nanda, V., Stayrook, S. & DeGrado, W. F. (2008). Structural Basis for the Function and Inhibition of an Influenza Virus Proton Channel. *Nature*, 451(7178), 596–9.

Straight, S. W., Herman, B. & McCance, D. J. (1995). The E5 Oncoprotein of Human Papillomavirus Type 16 Inhibits the Acidification of Endosomes in Human Keratinocytes. *Journal of Virology*, 69(5), 3185–92.

Strebel, K., Klimkait, T. & Martin, M. A. (1988). A Novel Gene of HIV-1, Vpu, and Its 16-Kilodalton Product. *Science*, 241(4870), 1221–23.

Strickland, G. T., Elhefni, H., Salman, T., Waked, I., Abdel-Hamid, M., Mikhail, N. N., Esmat, G. & Fix, A. (2002). Role of Hepatitis C Infection in Chronic Liver Disease in Egypt. *The American Journal of Tropical Medicine and Hygiene*, 67(4), 436–42.

Sugrue, R. J. & Hay, a J. (1991). Structural Characteristics of the M2 Protein of Influenza A Viruses: Evidence That It Forms a Tetrameric Channel. *Virology*, 180(2), 617–24.

Suprynowicz, F., Krawczyk, E., Hebert, J. D., Sudarshan, S. R., Simic, V., Kamonjoh, C. M. & Schlegel, R. (2010). The Human Papillomavirus Type 16 E5 Oncoprotein Inhibits Epidermal Growth Factor Trafficking Independently of Endosome Acidification. *Journal of Virology*, 84(20), 10619–29.

Susser, S., Vermehren, J., Forestier, N., Welker, M. W., Grigorian, N., Füller, C., Perner, D., Zeuzem, S. & Sarrazin, C. (2011). Analysis of Long-Term Persistence of Resistance Mutations within the Hepatitis C Virus NS3 Protease after Treatment with Telaprevir or Boceprevir. *Journal of Clinical Virology*, 52(4), 321–27.

Suzuki, H., Saito, R., Masuda, H., Oshitani, H., Sato, M. & Sato, I. (2003). Emergence of Amantadine-Resistant Influenza A Viruses: Epidemiological Study. *Journal of Infection and Chemotherapy : Official Journal of the Japan Society of Chemotherapy*, 9(3), 195–200.

Tabor, E., Drucker, J., Hoofnagle, J., April, M., Gerety, R., Seeff, L., Jackson, D., Barker, L. & Pineda-Tamondong, G. (1978). Transmission of Non-A, Non-B Hepatitis from Man to Chimpanzee. *The Lancet*, 311(8062), 463–6.

Tang, Y., Zaitseva, F., Lamb, R. a & Pinto, L. H. (2002). The Gate of the Influenza Virus M2 Proton Channel Is Formed by a Single Tryptophan Residue. *The Journal of Biological Chemistry*, 277(42), 39880–6.

Targett-Adams, P., Hope, G., Boulant, S. & McLauchlan, J. (2008). Maturation of Hepatitis C Virus Core Protein by Signal Peptide Peptidase Is Required for Virus Production. *The Journal of Biological Chemistry*, 283(24), 16850–9.

Targett-Adams, P. & McLauchlan, J. (2005). Development and Characterization of a Transient-Replication Assay for the Genotype 2a Hepatitis C Virus Subgenomic Replicon. *The Journal of General Virology*, 86(Pt 11), 3075–80.

Tedbury, P., Welbourn, S., Pause, A., King, B., Griffin, S. & Harris, M. (2011). The Subcellular Localization of the Hepatitis C Virus Non-Structural Protein NS2 Is Regulated by an Ion Channel-Independent Function of the p7 Protein. *The Journal of General Virology*, 92(Pt 4), 819–30.

Tellinghuisen, T. L., Foss, K. L. & Treadaway, J. (2008). Regulation of Hepatitis C Virion Production via Phosphorylation of the NS5A Protein. *PLoS Pathogens*, 4(3), e1000032.

Tellinghuisen, T. L., Marcotrigiano, J., Gorbalenya, A. E. & Rice, C. M. (2004). The NS5A Protein of Hepatitis C Virus Is a Zinc Metalloprotein. *The Journal of Biological Chemistry*, 279(47), 48576–87.

Tellinghuisen, T. L., Marcotrigiano, J. & Rice, C. M. (2005). Structure of the Zinc-Binding Domain of an Essential Component of the Hepatitis C Virus Replicase. *Nature*, 435(7040), 374–9.

Terwilliger, E. F., Cohen, E. a, Lu, Y. C., Sodroski, J. G. & Haseltine, W. a. (1989). Functional Role of Human Immunodeficiency Virus Type 1 Vpu. *Proceedings of the National Academy of Sciences of the United States of America*, 86(13), 5163–7.

Thibeault, D., Maurice, R., Pilote, L., Lamarre, D. & Pause, a. (2001). In Vitro Characterization of a Purified NS2/3 Protease Variant of Hepatitis C Virus. *The Journal of Biological Chemistry*, 276(49), 46678–84.

Thomas, J. M., Stevens, M. P., Percy, N. & Barclay, W. S. (1998a). Phosphorylation of the M2 Protein of Influenza A Virus Is Not Essential for Virus Viability. *Virology*, 252(1), 54–64.

Thomas, S. L., Newell, M. L., Peckham, C. S., Ades, a E. & Hall, a J. (1998b). A Review of Hepatitis C Virus (HCV) Vertical Transmission: Risks of Transmission to Infants Born to Mothers with and without HCV Viraemia or Human Immunodeficiency Virus Infection. *International Journal of Epidemiology*, 27(1), 108–17.

Thorley, J. a, McKeating, J. a & Rappoport, J. Z. (2010). Mechanisms of Viral Entry: Sneaking in the Front Door. *Protoplasma*, 244(1-4), 15–24.

Tobler, L. H. & Busch, M. P. (1997). History of Posttransfusion Hepatitis. *Clinical Chemistry*, 43(8 Pt 2), 1487–93.

Tohme, R. a & Holmberg, S. D. (2010). Is Sexual Contact a Major Mode of Hepatitis C Virus Transmission? *Hepatology (Baltimore, Md.)*, 52(4), 1497–505.

Tohme, R. a & Holmberg, S. D. (2012). Transmission of Hepatitis C Virus Infection through Tattooing and Piercing: A Critical Review. *Clinical Infectious Diseases : An Official Publication of the Infectious Diseases Society of America*, 54(8), 1167–78.

Tomei, L., Failla, C., Santolini, E., De Francesco, R., La Monica, N., Francesco, R. D. E., Monica, N. L. A. & Molecolare, B. (1993). NS3 Is a Serine Protease Required for Processing of Hepatitis C Virus Polyprotein. *Journal of Virology*, 67(7), 4017–26.

Tomei, L., Failla, C., Vitale, R. L., Bianchi, E. & De Francesco, R. (1996). A Central Hydrophobic Domain of the Hepatitis C Virus NS4A Protein Is Necessary and Sufficient for the Activation of the NS3 Protease. *The Journal of General Virology*, 77 (Pt 5), 1065–70.

Vandelli, C., Renzo, F., Romanò, L., Tisminetzky, S., De Palma, M., Stroffolini, T., Ventura, E. & Zanetti, A. (2004). Lack of Evidence of Sexual Transmission of

Hepatitis C among Monogamous Couples: Results of a 10-Year Prospective Follow-up Study. *The American Journal of Gastroenterology*, 99(5), 855–9.

Verdegem, D., Badillo, A., Wieruszeski, J.-M., Landrieu, I., Leroy, A., Bartenschlager, R., Penin, F., Lippens, G. & Hanoulle, X. (2011). Domain 3 of NS5A Protein from the Hepatitis C Virus Has Intrinsic Alpha-Helical Propensity and Is a Substrate of Cyclophilin A. *The Journal of Biological Chemistry*, 286(23), 20441–54.

Vieyres, G., Brohm, C., Friesland, M., Gentzsch, J., Wölk, B., Roingeard, P., Steinmann, E. & Pietschmann, T. (2013). Subcellular Localization and Function of an Epitope-Tagged p7 Viroporin in Hepatitis C Virus-Producing Cells. *Journal of Virology*, 87(3), 1664–78.

Vogel, M. & Rockstroh, J. K. (2010). Treatment of Acute Hepatitis C in HIV Infection. *The Journal of Antimicrobial Chemotherapy*, 65(1), 4–9.

Wahid, A., Helle, F., Descamps, V., Duverlie, G., Penin, F. & Dubuisson, J. (2013). Disulfide Bonds in Hepatitis C Virus Glycoprotein e1 Control the Assembly and Entry Functions of e2 Glycoprotein. *Journal of Virology*, 87(3), 1605–17.

Wakita, T., Pietschmann, T., Kato, T., Date, T., Miyamoto, M., Zhao, Z., Murthy, K., Habermann, A., Krausslich, H.-G., Mizokami, M., Bartenschlager, R. & Liang, T. J. (2005). Production of Infectious Hepatitis C Virus in Tissue Culture from a Cloned Viral Genome. *Nature Medicine*, 11(7), 791–6.

Walewski, J. L. J. L., Keller, T. R., Stump, D. D. & Branch, A. D. (2001). Evidence for a New Hepatitis C Virus Antigen Encoded in an Overlapping Reading Frame. *Rna*, 7(5), 710–21.

Wang, C., Lamb, R. A. & Pinto, L. H. (1995). Activation of the M2 Ion Channel of Influenza Virus: A Role for the Transmembrane Domain Histidine Residue. *Biophysical Journal*, 69(4), 1363–71.

Wang, J.-F., Wei, D.-Q. & Chou, K.-C. (2009). Insights from Investigating the Interactions of Adamantane-Based Drugs with the M2 Proton Channel from the H1N1 Swine Virus. *Biochemical and Biophysical Research Communications*, 388(2), 413–7.

Wang, T., Cady, S. D. & Hong, M. (2012). NMR Determination of Protein Partitioning into Membrane Domains with Different Curvatures and Application to the Influenza M2 Peptide. *Biophysical Journal*, 102(4), 787–94.

Washburn, M. L., Bility, M. T., Zhang, L., Kovalev, G. I., Buntzman, A., Frelinger, J. a, Barry, W., Ploss, A., Rice, C. M. & Su, L. (2011). A Humanized Mouse Model to Study Hepatitis C Virus Infection, Immune Response, and Liver Disease. *Gastroenterology*, 140(4), 1334–44.

Weinstock, D. M. & Zuccotti, G. (2006). Adamantane Resistance in Influenza A. *JAMA : The Journal of the American Medical Association*, 295(8), 934–6.

Wetherill, L. F., Holmes, K. K., Verow, M., Müller, M., Howell, G., Harris, M., Fishwick, C., Stonehouse, N., Foster, R., Blair, G. E., Griffin, S. & Macdonald, A. (2012). High-Risk Human Papillomavirus E5 Oncoprotein Displays Channel-Forming

Activity Sensitive to Small-Molecule Inhibitors. *Journal of Virology*, 86(9), 5341–51.

Whitehead, S. S., Bukreyev, A., Teng, M. N., Firestone, C.-Y., Claire, M. S., Elkins, W. R., Collins, P. L. & Murphy, B. R. (1999). Recombinant Respiratory Syncytial Virus Bearing a Deletion of Either the NS2 or SH Gene Is Attenuated in Chimpanzees. *Journal of Virology*, 73(4), 3438–42.

Whitfield, T., Miles, A. J., Scheinost, J. C., Offer, J., Wentworth, P., Dwek, R. a, Wallace, B. a, Biggin, P. C. & Zitzmann, N. (2011). The Influence of Different Lipid Environments on the Structure and Function of the Hepatitis C Virus p7 Ion Channel Protein. *Molecular Membrane Biology*, 28(5), 254–64.

Williams, J. K., Zhang, Y., Schmidt-Rohr, K. & Hong, M. (2013). pH-Dependent Conformation, Dynamics, and Aromatic Interaction of the Gating Tryptophan Residue of the Influenza M2 Proton Channel from Solid-State NMR. *Biophysical Journal*, 104(8), 1698–708.

Wingfield, W. L., Pollack, D. & Grunert, R. R. (1969). Therapeutic Efficacy of Amantadine HCl and Rimantadine HCl in Naturally Occurring Influenza A2 Respiratory Illness in Man. *The New England Journal of Medicine*, 281(11), 579.

Wozniak, A. L., Griffin, S., Rowlands, D., Harris, M., Yi, M., Lemon, S. M. & Weinman, S. a. (2010). Intracellular Proton Conductance of the Hepatitis C Virus p7 Protein and Its Contribution to Infectious Virus Production. *PLoS Pathogens*, 6(9), e1001087.

Xu, Z., Choi, J., Yen, T. S., Lu, W., Strohecker, a, Govindarajan, S., Chien, D., Selby, M. J. & Ou, J. (2001). Synthesis of a Novel Hepatitis C Virus Protein by Ribosomal Frameshift. *The EMBO Journal*, 20(14), 3840–8.

Yamashita, T., Kaneko, S., Shirota, Y., Qin, W., Nomura, T., Kobayashi, K. & Murakami, S. (1998). RNA-Dependent RNA Polymerase Activity of the Soluble Recombinant Hepatitis C Virus NS5B Protein Truncated at the C-Terminal Region. *The Journal of Biological Chemistry*, 273(25), 15479–86.

Yao, J. S., Strauss, E. G. & Strauss, J. H. (1996). Interactions between PE2, E1, and 6K Required for Assembly of Alphaviruses Studied with Chimeric Viruses. *Journal of Virology*, 70(11), 7910–20.

Yasui, K., Wakita, T., Tsukiyama-Kohara, K., Funahashi, S.-I., Ichikawa, M., Kajita, T., Wands, J. R., Kohara, M. & Moradpour, D. (1998). The Native Form and Maturation Process of Hepatitis C Virus Core Protein. *Journal of Virology*, 72(7), 6048–55.

Yi, M., Ma, Y., Yates, J. & Lemon, S. M. (2007). Compensatory Mutations in E1, p7, NS2, and NS3 Enhance Yields of Cell Culture-Infectious Intergenotypic Chimeric Hepatitis C Virus. *Journal of Virology*, 81(2), 629–38.

Yi, M., Ma, Y., Yates, J. & Lemon, S. M. (2009). Trans-Complementation of an NS2 Defect in a Late Step in Hepatitis C Virus (HCV) Particle Assembly and Maturation. *PLoS Pathogens*, 5(5), e1000403.

Yi, M., Villanueva, R. a, Thomas, D. L., Wakita, T. & Lemon, S. M. (2006). Production of Infectious Genotype 1a Hepatitis C Virus (Hutchinson Strain) in Cultured Human Hepatoma Cells. *Proceedings of the National Academy of Sciences of the United States of America*, 103(7), 2310–5.

Yokosuka, O., Kojima, H., Imazeki, F., Tagawa, M., Saisho, H., Tamatsukuri, S. & Omata, M. (1999). Spontaneous Negativation of Serum Hepatitis C Virus RNA Is a Rare Event in Type C Chronic Liver Diseases: Analysis of HCV RNA in 320 Patients Who Were Followed for More than 3 Years. *Journal of Hepatology*, 31(3), 394–99.

Zebedee, S. L. & Lamb, R. A. (1988). Influenza A Virus M2 Protein: Monoclonal Antibody Restriction of Virus Growth and Detection of M2 in Virions. *Journal of Virology*, 62(8), 2762–72.

Zhong, J., Gastaminza, P., Cheng, G., Kapadia, S., Kato, T., Burton, D. R., Wieland, S. F., Uprichard, S. L., Wakita, T. & Chisari, F. V. (2005). Robust Hepatitis C Virus Infection in Vitro. *Proceedings of the National Academy of Sciences of the United States of America*, 102(26), 9294–99.

Zhong, W., Ferrari, E., Lesburg, C. A., Maag, D., Ghosh, S. K. B., Cameron, C. E., Lau, J. Y. N. & Hong, Z. (2000a). Template/primer Requirements and Single Nucleotide Incorporation by Hepatitis C Virus Nonstructural Protein 5B Polymerase. *Journal of Virology*, 74(19), 9134–43.

Zhong, W., Uss, A. S., Ferrari, E., Lau, J. Y. N. & Hong, Z. (2000b). De Novo Initiation of RNA Synthesis by Hepatitis C Virus Nonstructural Protein 5B Polymerase. *Journal of Virology*, 74(4), 2017–22.

Appendix 1 – PCR oligonucleotides

GST-FLAG-p7 cloning

H77_EcoRI_FLAGp7for:

ATATATGAATTCGCGGCCATGGATTACAAGGATGACGACGATAAGGCTTTGGAG

AACCTCGTAATACTCAATGCAGC

H77_p7_NotIrev: ATATATACTGCAGGCGGCCGCTGCGTATGCCCGCTGAGGC

S235_EcoRI_FLAGp7for:

ATATATGAATTCGCGGCCATGGATTACAAGGATGACGACGATAAGGCTTTGGAAA

ACCTTGTATTGCTTAATGCGGC

S235_p7_NotIrev: ATATATACTGCAGGCGGCCGCCGCGTATGCCCGTTGGGGC

Virus cloning

Seattle_long_for:

GCAGACGCGCGCGTCTGCTCCTGCTTGTGGATGATGTTACTCATATCCCAAGCG

GAGGCGGCTTTGGAGAACCTCGT

Seattle_short_for: GACGCGCGCGTCTGCTCCTGCTTGTGGATGATGTTACtc

Seattle_short_rev: CCATAAGCACCAGCTGATATAGCGCTTG

Seattle_chim_for: GCCTCAGCGGGCATACGCACTGGACACGGAGGTGGCCGCG

Seattle_chim_rev: CGCGGCCACCTCCGTGTCCAGTGCGTATGCCCGCTGAGGC

IRES-mCherry cloning

IRES_mCherryXhoI_for: ATATATCTCGAGCCTAACGTTACTGGCCGAAGC

IRES_mCherryXbaI_rev: TAGATATCTAGAGGTTGATTGTTCCAGACGC

EcoRI_SPp7_J4_for:

ATATATGAATTCGCGGCCATGGATTACAAGGATGACGACGATAAGGCGCGCGTG

TGTGCCTGCTTGTGG

BamHI_STOP_J4p7_rev:

ATATATCCTAGGTTATTAGGCGTAAGCTCGTGGTGGTAACG

pBF+ cloning

EcoRI_FLAG-J4p7-fwd:

ATATATGAATTCGCGGCCATGGATTACAAGGATGACGACGATAAGGCCTTAGAG

AACTTGGTGGTCC

EcoRI_J4p7_rev: ATATATGAATTCTTAGGCGTAAGCTCGTGGTGGTAACGCC

Appendix 2 – ImageJ macro

```
rename("Image1");

run("Duplicate...", "title=Image1-1");

run("Gaussian Blur...", "sigma=2");

run("Find Maxima...", "noise=10 output=[Single Points]");

run("Dilate");

run("Dilate");

run("Invert");

selectWindow("Image1-1");

setAutoThreshold("RenyiEntropy");

run("Convert to Mask");

imageCalculator("AND create", "Image1-1","Image1-1 Maxima");

selectWindow("Result of Image1-1");

run("Analyze Particles...", "size=3-Infinity circularity=0.00-
1.00 show=Outlines exclude add");

selectWindow("Image1");

roiManager("Show All");

roiManager("Measure");

run("Tile");
```